QUARTERLY REPORT 8

PROJECT A-798

# AN ANALYTICAL AND EXPERIMENTAL STUDY OF BED RIPPLES UNDER WATER WAVES (A DIFFERENT INTERPRETATION OF INCIPIENT MOTION)

M. R. CARSTENS

Contract No. DA-49-055-CIVENG-65-1

1 April 1966 to 30 June 1966

Prepared for
Department of the Army
Coastal Engineering Research Center
Washington, D. C.


Engineering Experiment Station
GEORGIA INSTITUTE OF TECHNOLOGY
Atlanta, Georgia

GEORGIA INSTITUTE OF TECHNOLOGY
School of Civil Engineering
Atlanta, Georgia



QUARTERLY REPORT 8

PROJECT A-798

# A DIFFERENT INTERPRETATION OF INCIPIENT MOTION

By

M. R. CARSTENS

CONTRACT NO. DA-49-055-CIVENG-65-1

1 April 1966 to 30 June 1966

Prepared for
DEPARTMENT OF THE ARMY
COASTAL ENGINEERING RESEARCH CENTER
WASHINGTON, D. C.

ABSTRACT

Two different concepts of incipient motion on the surface of a bed of particles are discussed. The prevalent concept is that of particles moving on a flat bed. The other concept is that of propagation of a dune system over the bed. Preference is stated for the latter concept, that is, a deformed-bed, incipient-motion condition because the duned bed is the natural condition and because a lesser flow velocity is required to form a duned bed than is required to move surface grains on a flat bed. The results of an experiment are given in which the minimum velocity to form a duned bed is less than one half that required to move surface grains on a flat bed.

Key words: incipient motion, dunes, sediment transport

# A DIFFERENT INTERPRETATION OF INCIPIENT MOTION

By Marion R. Carstens,[1] M.ASCE

## INTRODUCTION

One of the most interesting and least understood multi-phase flows is that involving fluid flow over a bed of particles. The surface of the bed is the interface between the phases. Of special interest is the flow of water over a sand bed. Exchange of water across the interface is limited to seepage flow through the voids between the sand grains. Exchange of sand grains across the interface occurs when the lift and drag forces on the surface grains are sufficient to roll them over the bed or to lift them into the fluid stream. The lower limiting condition of multi-phase flow is that of no movement of the surface particles at the interface. This limiting condition is properly called incipient motion.

The practice has developed and appears to be widely accepted that the definition of incipient motion should be construed to apply over a flat bed (flat-bed, incipient-motion condition). The writer believes that incipient motion should be construed as the lowest flow condition at which perturbations of the interface, dunes, will propagate over the bed (deformed-bed, incipient-motion condition). The deformed-bed, incipient-motion condition is preferred for two reasons. First, dunes will propagate at a lesser flow condition than surface grains will move on a flat bed. Second, a rippled interface is a natural condition whereas a flat bed is a contrived laboratory condition.

---

[1]Professor of Civil Engineering, Georgia Inst. of Tech., Atlanta, Georgia.

## CONDITIONS FOR PARTICLE MOVEMENT

The flow conditions under which surface particles can be moved are analyzed considering that the principal forces involved are hydrodynamic forces of lift and drag and gravity forces.

First consider a simpler case in which surface particles are at the incipient-motion condition as the result of gravity forces only. If a bed of particles is inclined to the angle or repose, $\varphi$, some of the surface particles will roll down the bed. As shown in Fig. 1, instability occurs at the condition when

$$\tan \varphi = \sum F_{11} / \sum F_{\perp} \qquad (1)$$

in which $\sum F_{11}$ and $\sum F_{\perp}$ are the summation of the forces on the particle which are parallel and perpendicular to the bed, respectively. The angle of repose, $\varphi$, is an experimentally determined variable which, in part, depends on the angularity of the particles.[2] Even though the force in this case is a body force, the same relation, Eq. (1), can be expected to be a close approximation when the force system is more complex, including surface forces.

The more complex situation is illustrated in Fig. 2 in which $F_D$ and $F_L$ are the hydrodynamic drag and lift forces, respectively, W is the submerged weight, and $\alpha$ is the angle of inclination of the bed from the horizontal. Substituting into Eq. (1)

$$\tan \varphi = \frac{F_D - W \sin \alpha}{W \cos \alpha - F_L} \qquad (2)$$

The drag and lift forces can be written in the conventional form

$$F_D = C_D k_1 D^2 g \frac{\rho u^2}{2} \qquad (3)$$

---

[2] Simons, Daryl B., and Maurice L. Albertson, "Uniform Water Conveyance Channels in Alluvial Material", Transactions, ASCE, Vol. 128 (1963), Part I, Fig. 12, p. 97.

and $$F_L = C_L k_2 D_g^2 \frac{\rho u^2}{2} \tag{4}$$

in which $C_D$ and $C_L$ are coefficients of lift and drag, respectively, $k_1$ and $k_2$ are particle-shape coefficients, $D_g$ is mean size of particle, $\rho$ is fluid density, and u is the fluid velocity at bed level. The submerged weight W can be written

$$W = k_3 (\gamma_s - \gamma) D_g^3 \tag{5}$$

in which $\gamma_s$ and $\gamma$ are the specific weights at the sediment and fluid, respectively, and $k_3$ is another particle-shape coefficient.

Substituting Eqs. (3), (4) and (5) into Eq. (2) and rearranging,

$$\frac{N_s^2}{(\tan \varphi \cos \alpha + \sin \alpha)} = \frac{2k_3}{C_D k_1 + C_L k_2 \tan \varphi} \tag{6}$$

in which $N_s$ is $u/\sqrt{(s-1)gD_g}$ in which s is $\gamma_s/\gamma$. The parameter, $N_s$, resembles a Froude number and will be referred to as a sediment number, hereafter. The terms on the right side of Eq. (6) are primarily functions of particle shape provided that the Reynolds number of the flow past the projecting particle is sufficiently high for $C_D$ and $C_L$ to be independent of the Reynolds number. A reasonable expectation is that at incipient motion the left side of Eq. (6) should be nearly a constant for sand provided that $N_s$ is evaluated using the local velocity, u, in the vicinity of the particle.

Martin[3] analyzed a great amount of published data on incipient motion and concluded that

$$N_s / \sqrt{\tan \varphi \cos \alpha + \sin \alpha} \approx 1.9 \tag{7}$$

In deriving the approximation, Eq. (7), Martin utilized flat-bed incipient motion data in which the interface surface would be classified as hydraulically rough.

---

[3]Martin, Charles S., "The Role of a Permeable Bed in Incipient Motion", thesis presented to the Georgia Institute of Technology at Atlanta, Georgia in 1964 in partial fulfillment of the requirements for the degree, Doctor of Philosophy.

In analyzing various data, Martin took the theoretical wall to be 0.2 $D_g$ below the plane tangent to the top of the particles and he evaluated the velocity, u, at a distance of 0.35 $D_g$ above the theoretical wall. In other words, the velocity was evaluated at 0.15 $D_g$ above the plane tangent to the top of the particles.

## INCIPIENT MOTION UNDER OSCILLATORY FLOW

The deformed bed which develops under oscillatory flow can be approximated as a repeated pattern of circular arcs with the junctions of the arcs being the crests of the dunes and with the horizontal tangents midway between the extremities being the troughs.[4] The flow pattern is schematically shown in Fig. 3 with the flow being from left to right during the one-half cycle being considered. The flow separates from the crests forming vortices in the lee of the crests. The flow reattaches to the interface at the troughs. The converging flow along the upstream face of the dune has two important results--(a) the boundary layer reforms at the stagnation point in each trough and remains thin in the accelerating flow along the upstream face of each dune, and (b) the local velocity, $u_c$, at the crests is larger than the velocity, U, in the flow above the interface. Because of the accelerating flow from the stagnation point, the expectation is that the upstream face of the dune is a hydraulically rough boundary.

With the conditions as described above, Eq. (7) should be suitable criterion to determine whether a perturbation of the interface will propagate. A reasonable value for the angle of inclination, $\alpha$, at the crest is 30 degrees. Furthermore a reasonable value of the angle of repose, $\varphi$, for well-rounded beach sands is also 30 degrees[2]. Taking both $\alpha$ and $\varphi$ as 30 degrees, the term $\tan \varphi + \sin \alpha$, is unity.

---

[4] Bagnold, R. A., "Motion of Waves in Shallow Water--Interaction between Waves and Sand Bottoms", Proceedings, Royal Society, A, Vol. 187, October 8, 1946, pp. 1-18.

Thus particles at the crest would tend to move whenever the sediment number at the crest exceeds 1.9. By constructing a flow net of the flow pattern illustrated in Fig. 3, the velocity at the crest, $u_c$, is found to be about 1.2 times the velocity, U, in the main flow. Expressing Eq. (7) in terms of the main stream velocity,

$$N_{sm} = \frac{U_m}{\sqrt{(s-1)gD_g}} \approx 1.6 \qquad (8)$$

in which the maximum velocity, $U_m$, is used to compute the maximum sediment number, $N_{sm}$. Equation (8) is the deformed-bed, incipient-motion condition for oscillatory flow.

The difference between incipient motion based upon movement of surface particles on a flat bed and the propagation of a perturbation along the interface has been experimentally demonstrated in an oscillating-flow water tunnel located in the Hydraulics Laboratory of the Georgia Institute of Technology. The water tunnel is a large U-tube with the test section being located in the horizontal bottom. Water oscillates in the U-tube at resonant frequency. Energy is added to maintain equilibrium amplitude by timed pulsing of the air pressure above the water surface in one of the vertical legs of the U-tube. Devices are included by which initial and final transients can be eliminated. The test section is 10 ft. long by 4 ft. wide by 1 ft. high. The central 6 ft. of the test section are depressed 4 in. to form a container for the sand.

Incipient-motion tests on a flat bed were executed by visual observation of movement through the transparent roof and sidewalls of the test section. The bed was screeded to form a flat bed. Amplitude of the water motion was increased in small increments until motion of the surface particles was observed. The earliest motion consisted of the unstable perched particles toppling over into adjacent recesses. After this initial adjustment a further increase in water-motion amplitude was required to obtain further motion.

Flat-bed incipient motion was judged to be when 10 per cent of the surface particles were in motion. For glass beads having a mean diameter of 0.297 mm, flat-bed incipient-motion occurred when $N_{sm}$ was 3.77. For Ottawa sand having a mean diameter of 0.585 mm, flat-bed incipient motion occurred when $N_{sm}$ was 3.02. A calculated value utilizing the maximum boundary-shear stress for laminar motion and the Shield's diagram was in good agreement with the experimentally determined incipient-motion value for the 0.297 mm glass beads. Because of boundary-layer transition no value could be calculated for the 0.585 mm sand.

Incipient-motion tests with a perturbation were executed by observation of the movement of deformation of the interface. A perturbation of the flow was induced by placing a 1/2-in. diameter, half-round, brass rod on the surface of the flat bed. The interface deformed progressively outward from the disturbance. First a dune would be scoured on each side of the rod. When the first pair of dunes reached an observable amplitude another pair of dunes would begin to scour. Each new pair of dunes started with a finite wave length but with an infinitely small amplitude. The formation of a new dune was heralded by an in-phase movement of surface grains some distance ahead of the previously formed dune. The movement increased with the grains piling up into a definable crest at this location. The initial wave length of a dune appeared to be about 1/3 the wave length of the equilibrium wave length. Hence two processes contribute to the propagation of an interfacial deformation--(a) formation of new dunes beyond the previously formed dunes, and (b) an increasing wave length of the dunes as scour continues.

The mean celerity, c, at which the interfacial deformation moved from the disturbance element was determined in eleven runs with the 0.297-mm glass beads and in six runs with the 0.585 mm Ottawa sand. A complete description of these experiments and of the results is given elsewhere.[5]

---

[5] Carstens, M. R. and F. M. Neilson, "An Analytical and Experimental Study of Bed Ripples under Water Waves (Evolution of a Duned Bed Under Oscillatory Flow)", Quarterly Report 7, Project A 798, Engineering Experiment Station, Georgia Institute of Technology, Atlanta, Georgia, March 1966.

In regard to incipient motion, the most significant run is Run 62 in which the amplitude of the simple-harmonic motion the water was 3.20 in.; the period was 3.55 sec.; and the bed material was the Ottawa sand. The duration of Run 62 was 27 hours. At the end of the run, the leading crests were only 2.18 ft. and 2.70 ft. from the disturbance. Because of the negligible celerity of dune propagation, this run can be considered as the deformed-bed incipient-motion condition. The sediment number, $N_{sm}$, was 1.49 for Run 62. The experimentally determined deformed-bed, incipient-motion condition, that is, $N_{sm}$ of 1.49 is sufficiently close to the value 1.6 as given in Eq. (8) to be considered as verification of the analysis which culminated in Eq. (8).

## CONCLUSION

The conclusion is reached that the definition of incipient motion should be the flow condition at which interfacial deformations begin to propagate over the bed rather than the flow condition at which surface grains begin to move on a flat bed. Inasmuch as the beds of rivers, lakes and oceans are littered with debris from which dune systems will be generated, the flat-bed concept is an unrealistic laboratory condition. A dune system will progagate over the bed at a lesser flow condition than surface grains will roll over a flat bed for two reasons. (A) the flow is non uniform over a dune with a fluid velocity at the crest in excess of that which would prevail at the same elevation above a flat bed. (B) the flow being non uniform over the dunes results in negligible boundary layers in the areas of active scour on the upstream face of the dune; whereas, with uniform flow over a flat bed the surface particles can be submerged in a laminar sublayer. Experimental results were presented in oscillatory flow in which velocities were over twice as large for flat-bed incipient motion as for deformed-bed incipient motion.

ACKNOWLEDGMENTS

The experimental results with oscillatory flow were obtained in a study supported by the Coastal Engineering Research Center, Department of the Army, under contract DA-49-055-CIVENG-65-1. Permission to publish the results is gratefully acknowledged.

---

## APPENDIX - NOTATION

The following symbols have been used:

$C$ = mean celerity of propagation of a dune system;

$C_D$ = coefficient of drag;

$C_L$ = coefficient of lift;

$D_g$ = mean diameter of particles;

$F_D$ = drag force on a typical particle on the bed surface;

$F_L$ = lift force on a typical particle on the bed surface;

$F_{ll}$ = component of forces on a particle, parallel to the bed;

$F_{\perp}$ = component of forces on a particle, perpendicular to the bed;

$g$ = acceleration of gravity;

$k_1$ = particle shape coefficient, area;

$k_2$ = particle shape coefficient, area;

$k_3$ = particle shape coefficient, volume;

$N_s = u/\sqrt{(s-1)gD_g}$, sediment number;

$N_{sm}$ = sediment number using maximum freestream velocity of oscillatory flow;

$s$ = specific-weight ratio, $\gamma_s/\gamma$;

$u$ = local fluid velocity at the bed;

$u_c$ = fluid velocity at dune crest;

$U$ = velocity of oscillatory flow;

$U_m$ = maximum velocity of oscillatory flow;

$W$ = submerged weight of a typical particle;

$\alpha$ = angle of inclination of the bed from horizontal;

$\gamma$ = fluid specific weight;

$\gamma_s$ = particle specific weight;

$\rho$ = fluid mass density; and

$\varphi$ = angle of repose.

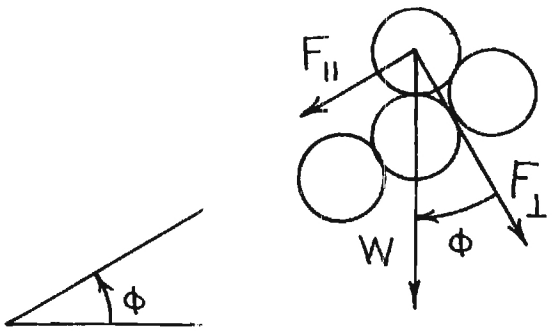


FIG. 1 - GRAVITY FORCE ON BED PARTICLES

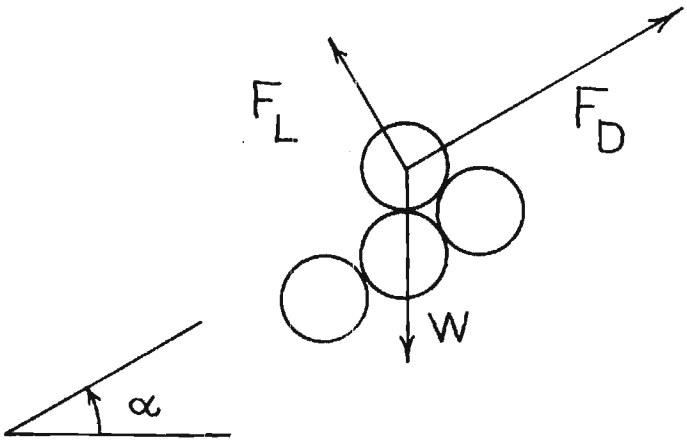


FIG. 2 - FORCES ON A BED PARTICLES

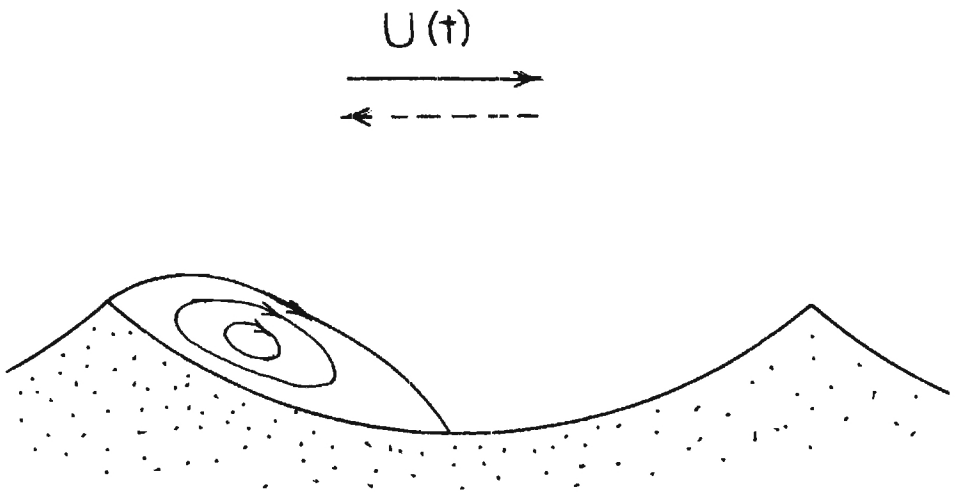


FIG. 3 - INTERFACE UNDER OSCILLATORY FLOW

11-170



QUARTERLY REPORT 9

PROJECT A-798

# AN ANALYTICAL AND EXPERIMENTAL STUDY OF BED RIPPLES UNDER WATER WAVES (INITIATION OF MOTION OF SEDIMENT PARTICLES)

M. R. CARSTENS

Contract No. DA-49-055-CIVENG-65-1

1 July to 30 September 1966

Prepared for
Department of the Army
Coastal Engineering Research Center
Washington, D. C.

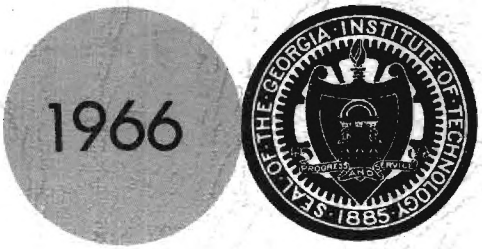


School of Civil Engineering
GEORGIA INSTITUTE OF TECHNOLOGY
Atlanta, Georgia

GEORGIA INSTITUTE OF TECHNOLOGY
School of Civil Engineering
Atlanta, Georgia

QUARTERLY REPORT 9

PROJECT A-798

# AN ANALYTICAL AND EXPERIMENTAL STUDY OF BED RIPPLES UNDER WATER WAVES (INITIATION OF MOTION OF SEDIMENT PARTICLES)

By

M. R. CARSTENS

CONTRACT NO. DA-49-055-CIVENG-65-1

1 JULY to 30 SEPTEMBER 1966

Prepared for
DEPARTMENT OF THE ARMY
COASTAL ENGINEERING RESEARCH CENTER
WASHINGTON, D. C.

ABSTRACT

Initial motion of particles lying on a "fully rough" boundary is analyzed by considering the forces on a protruding particle. The resulting function for the initial-motion fluid velocity is found to involve one constant which was evaluated using experimental results obtained with oscillatory flow. Values of the initial-motion bottom velocity are computed for oscillatory flow over a bed, for unidirectional flow over a bed, for uniform flow along a sloping bank, and for flow along a sloping bank located on the outer bank of a bend.

Key words.-- incipient motion, sediment transport, bottom velocity, local scour, and canal-bank stability.

TABLE OF CONTENTS

LIST OF FIGURES

## LIST OF TABLES

# INITIATION OF MOTION OF SEDIMENT PARTICLES

By Marion R. Carstens[1], M. ASCE

## SYNOPSIS

Initiation of motion of protruding surface particles is analyzed by considering the gravity force and the hydrodynamic surface force (lift and drag) on a typical particle. For protruding particles lying on a "fully rough" or "hydraulically rough" boundary, the velocity of flow at particle level as a function of particle diameter, particle density, fluid density, angle of repose, bed inclination, and coefficient of drag of a particle falling in an infinite fluid is derived. In the derivation, a single constant is obtained. Since this constant involves only particle-shape coefficients and a proportionality factor between the coefficient of drag of a protruding particle and a particle in an infinite fluid, the constant is independent of the orientation of the gravity force. The numerical value of the constant is determined from experimental results obtained with oscillatory flow. Derived initial-motion velocities are presented for unidirectional flow over a bed, for uniform flow along a bank, and finally for flow on the outer bank of a bend.

## INTRODUCTION

The flow condition for initial motion of surface particles can be formulated by considering the forces on a protruding surface particle, that is,

---

1 Prof. of Civil Engrg, Georgia Inst. of Tech, Atlanta, Ga.

the hydrodynamic force ( resolved into lift and drag) and the gravity force. Furthermore, a "fully rough" flow condition is presumed over the sand bed at that location where the initial motion occurs.

"Fully rough" flow occurs along the upstream face of dunes by virtue of nonuniform flow over the dunes. The flow separates at the crest of a dune with a vortex in the lee of the crest. The main flow rejoins the bed at the trough. From the stagnation point at the trough the flow is accelerated along the upstream face of the dune to a maximum velocity at the crest. This flow condition results in the formation of a boundary layer of negligible thickness at each crest. In other words, the boundary on the upstream face of the dune would be classified as a "fully rough" boundary even with fine sand. The initial movement of sand grains with increasing velocity or the final movement with decreasing velocity will occur at the crest of the dune where the velocity is a maximum. In these circumstances, there is no physical mechanism to erase previously formed dunes as the velocity is decreased. Hence on a natural stream bed, initial motion of bed particles will occur at the crests of a residual dune system remaining from the previous flow condition during which bed-load movement occurred.

Even if the bed were initially flat, a dune system will propagate downstream from a flow disturbance in unidirectional flow or will propagate away from the flow disturbance in oscillatory flow (1)[2]. Objects such as rocks, beer cans, or marine animals are sufficient flow disturbances from

---

2 Numerals in parenthesis refer to corresponding items in APPENDIX B.

which to start a self-propagating dune system. Most of the initial motion data for fine and medium sands obtained in the laboratory is quite unrepresentative of natural conditions since care had to have been exercised in order to avoid a dune system by flattening the bed and to avoid flow disturbances on the bed.

With larger diameter bed material (coarse sand or larger) the boundary would be "fully rough" by virtue of the size of the bed material.

## FORCE ANALYSIS

The simplest case of incipient motion is illustrated in Fig. 1 in which submerged weight is the only force other than adjacent particle reactions. If the bed is inclined at the angle of repose, $\phi$, some of the protruding surface particles will be at the incipient-motion condition. As shown in Fig. 1, the instability limit is

$$\tan \phi = F_T/F_N \tag{1}$$

in which $F_T$ and $F_N$ are the summation of the external forces on the particle which are tangential and normal to the bed, respectively. The angle of repose, $\phi$, can be determined in the laboratory. The angle of repose, $\phi$, is a function of particle size, angularity, and porosity. Typical values of $\phi$ are given by Simons and Albertson (2) showing the relationship between $\phi$, particle size, and angularity for an unspecified porosity.

A more complex force system is illustrated in Fig. 2 in which $F_D$ and $F_L$ are hydrodynamic drag and lift forces, respectively, W is the submerged weight, and $\alpha$ is the inclination of the bed from horizontal. Substituting the forces shown in Fig. 2 into Eq. 1,

$$\tan \phi = \frac{F_D - W \sin \alpha}{W \cos\alpha - F_L} \tag{2}$$

The drag and lift forces can be written in the conventional form

$$F_D = C_D k_1 D_g^2 \frac{\rho u^2}{2} \tag{3}$$

and

$$F_L = C_L k_2 D_g^2 \frac{\rho u^2}{2} \tag{4}$$

in which $C_D$ and $C_L$ are coefficients of drag and lift, respectively, $k_1$ and $k_2$ are particle-shape coefficients, $D_g$ is mean size of particle, $\rho$ is fluid density, and u is fluid velocity at the level of the protruding particle. The submerged weight, W, can be written as

$$W = k_3 (\gamma_s - \gamma) D_g^3 \tag{5}$$

in which $\gamma_s$ and $\gamma$ are the specific weights of the bed particles and the fluid, respectively, and $k_3$ is another particle-shape coefficient. Substituting Eqs. 3, 4, and 5 into Eq. 2,

$$\frac{u_i^2}{(s-1)g D_g} = \left[\frac{2k_3 (\tan \phi \cos \alpha + \sin \alpha)}{k_1 + k_2 (C_L/C_D) \tan\phi}\right]\left[\frac{1}{C_D}\right] \tag{6}$$

in which s is the specific-weight ratio, $\gamma_s/\gamma$, and $u_i$ is the initial-motion value of the bottom velocity. Chepil (3) measured the lift and drag on a hemisphere placed on a plane boundary. He found that $C_L$ was about 0.8 $C_D$. The protruding particles under consideration probably protrude further from the bed than the hemisphere The pressure condition under a protruding particle is unknown and variable depending upon the configuration of the flow passages under the

particle. In view of these uncertainties, a value of unity for the ratio, $C_L/C_D$, is taken as a reasonable average value. In addition, the assumption is made that the particle-shape coefficients, $k_1$ and $k_2$, are equal. Furthermore, the coefficient of drag, $C_D$, on a protruding particle in "fully rough" flow will be of the same order of magnitude as the coefficient of drag, $C_D^1$, of a geometrically similar particle falling in an infinite quiescent fluid at the same particle Reynolds number. In the succeeding analysis, the value of $C_D$ for the protruding particle is assumed to be proportional to $C_D^1$ for the freely falling particle, that is,

$$C_D = k_4 C_D^1 \tag{7}$$

Values of $C_D^1$ for sand grains with a shape factor of 0.7 are given by Albertson, Barton, and Simons (4).

Substituting the above simplifications into Eq. 6,

$$\frac{u_i^2}{(s-1)gD_g} = \left[\frac{\tan\phi\cos\alpha + \sin\alpha}{1 + \tan\phi}\right]\left[\frac{k}{C_D^1}\right] \tag{8}$$

in which k is equal to $2k_3/k_1k_4$. Since the constant, k, involves only particle-shape coefficients and a proportionality factor relating $C_D$ and $C_D^1$, the constant, k, is independent of the orientation of the gravity force.

Oscillatory Flow.-- For the past two years, experiments have been conducted in the Hydraulics Laboratory at Georgia Institute of Technology about various features of bed forms which occur under oscillatory flow. Water is oscillated through the horizontal test section with simple harmonic motion over a sand bed which is 6 ft. in length and 4 ft. wide. The horizontal test section is 10 ft. long, 1 ft. high, and 4 ft. wide. The water mass is oscillated within the large U-tube at resonance thereby insuring a constant

period during a run. Amplitude of oscillation is a controlled variable. Auxiliary equipment has been incorporated to eliminate the initial and final transients. The U-tube water tunnel is completely described elsewhere (5).

Dune systems have been observed to develop and to propagate away from a flow disturbance placed on the bed with water-motion amplitudes considerably less than amplitudes at which a dune system will spontaneously form on an initially flat bed (1). Run 62 was made for the purpose of determining the lowest water-motion amplitude at which a dune system would develop and would propagate away from the $\frac{1}{2}$-in. diameter, half-round bar used as the flow disturber. The duration of Run 62 was 27 hours. At the end of the run, the leading crests were only 2.18 ft. and 2.70 ft. from the flow disturbance. At the time the run was terminated, nine dune crests appeared to be fully developed, that is, four on each side of the central crest which covered the bar. Both of the fourth crests from the central dune were 1.48 ft. from the crest of the central dune. Five partially developed dunes extended beyond the fourth crest on one side and three partially developed dunes extended beyond the fourth crest on the other. The only sand-grain movement appeared to be over the fourth crests. On the basis of the above observations, the water-motion amplitude of Run 62 was taken to be the lowest water-motion amplitude at which a dune system would develop and would propagate.

The pertinent physical quantities during Run 62 are as follows: water-motion amplitude, 3.20 in; period, 3.55 sec; water temperature, 81°F; sand, Ottawa "Flint Shot"; geometric mean diameter, $D_g$, 0.585 mm; geometric standard deviation, $\sigma_g$, 1.16; and specific gravity, s, 2.62.

Flow over a dune under oscillatory flow is illustrated in Fig. 3. The water motion at the instant of illustration is from left to right in

Fig. 3. The flow separates from the bed at the dune crest forming a vortex in the lee of the crest. The flow reattaches to the bed in the trough. The velocity at protruded particle height is zero in the trough and increases continuously up the face of the dune to attain a maximum value at the crest. Sand grains experiencing bed-load movement are rolled along the upstream face of the dune and are dumped into the vortex in the lee of the crest. By virtue of the directions of the velocity, the angle of the bed $\alpha$ at the crest tends to be less than $\phi$ on the upstream face and to be greater than $\phi$ on the downstream face. The magnitude of the periodic fluctuations of $\alpha$ to values greater than $\phi$ and to values less than $\phi$ are proportional to the quantity of bed material moved over the crest in one half cycle. Since the quantity of material moved over the crest is negligible at the initial-motion condition,

$$\alpha\,(\text{crest}) \approx \phi \tag{9}$$

Substituting Eq. 9 into Eq. 8 for the particular situation of oscillatory flow over a dune crest results in an equation involving only one constant, k, which can be evaluated using the data of Run 62.

$$\frac{u_i^2}{(s-1)gD_g} = \left[\frac{2\sin\phi}{1+\tan\phi}\right]\left[\frac{k}{C_D^1}\right] \tag{10}$$

Using the data of Run 62 the maximum velocity in the flow above the bed is 0.473 fps. The velocity at the crest is found to be 1.2 times the velocity of the main stream by construction of the irrotational flow pattern over the dune. Hence for Run 62, the value of $u_i$ is 0.567 fps. The value of $\phi$ for the 0.585-mm Ottawa Sand was taken as being 29.4 degrees in accordance with the value for very-rounded non-cohesive material as recommended

by Simons and Albertson (2). The 29.4-degree value for $\phi$ appeared to be quite reasonable from dune slopes as measured from photographs. The value of $C_D^1$ was determined to be 1.6(4) by using the value of $u_i$ to compute the Reynolds number. Substituting the values, $u_i$ of 0.567 fps, $\phi$ of 29.4 degrees, $D_g$ of 1.92 $(10^{-3})$ ft, s of 2.62, g of 32.14 $fps^2$, and $C_D^1$ of 1.6 into Eq. 10, the value of k is found to be 8.2.

Since k involves only particle-shape coefficients and a proportionality constant relating the drag on a protruding particle, to the drag on a sand grain in an infinite fluid, the value of k should be universal for "fully rough" flow over sand beds regardless of the orientation of the gravity force. Rewriting Eq. 8.

$$\frac{u_i^2}{(s-1)gD_g} = \left[\frac{\tan\phi\cos\alpha + \sin\alpha}{1 + \tan\phi}\right] \frac{8.2}{C_D^1} \qquad (11)$$

Initial-motion values computed from Eq. 11 of $u_i/\sqrt{(s-1)gD_g}$ and $u_i$ for oscillatory flow are shown by curve A in Figs. 4 and 5 as a function of $D_g$. The values of other physical quantities used in the computation are given in Table 1.

Unidirectional Flow along the Bed.-- The preceding analysis leading to Eq.11 can be utilized directly to evaluate initial-motion conditions over the crest of a dune in unidirectional flow as illustrated in Fig. 6. The angle of inclination of the bed, $\alpha$, at the crest is quite small. For small angles, $\cos\alpha \approx 1$ and $\sin\alpha \approx 0$. Initial-motion values computed from Eq. 11 of $u_i/\sqrt{(s-1)gD_g}$ and $u_i$ for unidirectional flow are shown by curves B and C in Figs. 4 and 5 as functions of $D_g$. The values of other physical quantities used in the computation are given in Table 1.

TABLE 1.

EXPLANTORY DATA FOR FIGURES 4, 5, AND 7.

| Curve | Flow | Inclination of botton velocity from the horizontal $\alpha$, | Bank slope $\phi$, | Particle shape factor | Particle roundness | $s = \gamma_s/\gamma$ | Water temperature °F |
|---|---|---|---|---|---|---|---|
| A | Oscillatory | $\phi$ | horizontal | 0.7 | rounded | 2.58 | 60 |
| B | Unidirectional | 0 | horizontal | 0.7 | angular | 2.65 | 60 |
| C | Unidirectional | 0 | horizontal | 0.7 | rounded | 2.65 | 60 |
| D | Unidirectional | 0 | 1 (V):3(H) | 0.7 | angular | 2.65 | 60 |
| E | Unidirectional | 0 | 1 (V):3(H) | 0.7 | rounded | 2.65 | 60 |
| F | Unidirectional | 0 | 1 (V):2(H) | 0.7 | angular | 2.65 | 60 |
| G | Unidirectional | 0 | 1 (V):2(H) | 0.7 | rounded | 2.65 | 60 |
| H | Unidirectional | 0 | 1 (V):1½(H) | 0.7 | angular | 2.65 | 60 |
| I | Unidirectional | 0 | 1 (V):1½(H) | 0.7 | rounded | 2.65 | 60 |
| J* | Unidirectional | 0 | horizontal | --- | --- | 2.65 | -- |
| K** | Unidirectional | 0 | horizontal | --- | --- | 2.65 | -- |

* Mavis and Laushey (6)

** Based on logarithmic velocity distribution above a flat, "fully rough" bed with $\tau/\gamma(s-1)\ D_g$ equal to 0.06.

In order to compare the initial-motion bed velocities as computed from Eq. 11 with existing information, Fig. 7 has been prepared. Curve B values were computed using Eq. 11 for very angular materials using $\phi$ values as given by Simons and Albertson (2). Similarly curve C values were computed for very rounded materials. The initial-motion bed velocity for very angular material is never more than 9 per cent greater than for very rounded material in the size range from 1 mm to 100 mm. Curve J values were computed from the empirical relation of Mavis and Laushey (6,7).

$$\frac{u_i^2}{(s-1)gD_g} = 2.36\, D_g^{-1/9} \tag{12}$$

The diameter, $D_g$, on the right side of Eq. 12 is in mm. The left side of Eq. 12 is dimensionless. Curve K values were computed using a value of 0.06 for the Shield's parameter (7), $\tau_c/\gamma(s-1)D_g$, in which $\tau_c$ is the critical shear stress. The velocity, $u_i$, was evaluated at a distance $D_g$ from the boundary using logarithmic velocity distribution over a "fully rough" boundary resulting in

$$\frac{u_i^2}{(s-1)gD_g} = 4.34 \tag{13}$$

Flow along a Sloping Bank.-- The force-analysis method can also be applied to evaluate initial-motion conditions of particles which lie on a bank of a channel as illustrated in Fig. 8. The additional complexity is that the drag force, $F_D$, lift force, $F_L$, and submerged weight, W, on a protruding particle are

not coplanar. As a result, the summation of the tangential forces (tangential to the bank), $F_T$, is not in the same direction as the drag force, $F_D$, as shown in Fig. 8. Referring to the force diagram Fig. 8,

$$F_T = \sqrt{F_D^2 + W^2 \sin^2\theta} \tag{14}$$

in which $\theta$ is the angle between the bank and the horizontal. Referring to the other force diagram in Fig. 8,

$$F_N = W \cos \theta - F_L \tag{15}$$

Substituting Eqs. 14, 15, 3, 4, 5, and 7, into Eq. 1 and rearranging

$$\frac{u_i^2}{(s-1)gD_g} = \left[\frac{-\cos\theta \tan^2\phi + \sqrt{\tan^2\phi - \sin^2\theta}}{1 - \tan^2\phi}\right]\left[\frac{8.2}{C_D^{\frac{1}{2}}}\right] \tag{16}$$

Initial-motion values computed from Eq. 16 for $u_i / \sqrt{(s-1)gD_g}$ and $u_i$ are shown in Figs. 4 and 5 as functions of $D_g$ for bank slopes of 1 on $1\frac{1}{2}$, 1 on 2, and 1 on 3. The values of the other physical quantities used in the computation are given in Table 1.

In the above analysis, the velocity, u, and the drag force were assumed to be horizontal, that is, the velocity along the bank was assumed to be parallel to the bed as in uniform flow. A more critical situation occurs on the outer bank of a channel bend where the velocity has a component down the bank. In this case the drag force, $F_D$, which is collinear with the velocity, will be directed down and along the bank as shown in Fig. 9. The angle, $\beta$, is the angle between the velocity and a horizontal line. The angle, $\beta$, is measured in the plane of the bank. Referring to the force diagram on the right side of Fig. 9,

$$F_T = \sqrt{(F_D \cos \beta)^2 + (W \sin \theta + F_D \sin \beta)^2} \tag{17}$$

The normal force, $F_N$, is the same as before as given in Eq. 15. Substituting Eqs. 17, 15, 3, 4, 5, and 7 into Eq. 1 and rearranging

$$\frac{u_i^2}{(s-1)gD_g} = \left[ -\frac{(\cos \theta \tan^2 \phi + \sin \theta \sin \beta)}{1 - \tan^2 \phi} \right. \tag{18}$$

$$\left. + \frac{\sqrt{\tan^2 \phi \, (1 + \sin 2\theta \sin \beta) - \sin^2 \theta \cos^2 \beta}}{1 - \tan^2 \phi} \right] \left[ \frac{8.2}{C_D^{\frac{1}{1}}} \right]$$

Initial-motion values computed from Eq. 18 for $u_i$ are shown in Fig. 10 for values of $\beta$ of 0, 10, and 20 degrees on a bank with a side slope of 1 (V) on 2 (H)

## CONCLUSIONS

Initial motion of protruding particles lying on a "fully rough" boundary was analyzed by considering the forces acting on these particles. The resulting function for bottom velocity involves a single constant which is a function of particle shape and positioning on the bed. The value of the constant was determined from an oscillatory-flow experiment. Other flows were then analyzed. Values of the initial-motion bottom velocity were computed for unidirectional flow over a bed, for uniform flow along a sloping bank, and for flow along a sloping bank located on the outer bank of a bend.

The principal virtue of the rational analysis based upon forces is that effects of particle roundness, of bank slope, and of direction of velocity can be evaluated. The force-analysis method is superior to the widely used tractive-force method in that the direction of the velocity is accounted for.

This superiority is largely nullified by the lack of quantitative information concerning the direction of the velocity in zones of local scour such as on the outer bank of a canal bend.

## ACKNOWLEDGMENTS

The experimental results with oscillatory flow were obtained in study supported by the Coastal Engineering Research Center, Department of the Army, under contract DA- 49-055-CIVENG 65-1. Permission to publish the results is gratefully acknowledged. The extended experimental run, utilized in the analysis, was performed by Messrs. F. M. Neilson and H. Majumdar, graduate students at the Georgia Institute of Technology. Another graduate student, H. D. Altinbilek, was most helpful in preparing the manuscript.

## APPENDIX A -- NOTATION

The following symbols are used in this paper:

$C_D$ = coefficient of the drag on a particle protruding from the bed;

$C_D^1$ = coefficient of drag of a sand grain falling in a still fluid;

$C_L$ = coefficient of lift on a particle protruding from the bed;

$D_g$ = geometric mean diameter of bed material;

$F_D$ = drag force on a particle protruding from the bed;

$F_L$ = lift force on a particle protruding from the bed;

$F_N$ = summation of the forces normal to the bed;

$F_T$ = summation of the forces tangential to the bed;

$g$ = acceleration of gravity;

$k_1$ = particle-shape coefficient (area);

$k_2$ = particle-shape coefficient (area);

$k_3$ = particle-shape coefficient (volume);

$k_4 = C_D/C_D^1$ ;

$k = 2k_3/k_1k_4$ ;

$s$ = specific-weight ratio, $\gamma_s/\gamma$ ;

s.f.= particle-shape factor;

$u$ = fluid velocity at particle level;

$u_i$ = initial-motion fluid velocity at particle level;

$W$ = weight of protruding particle;

$\alpha$ = inclination of bed from horizontal in the direction of flow;

$\beta$ = inclination of velocity down the bank;

$\gamma$ = specific weight of fluid;

$\gamma_s$ = specific weight of bed-material;

$\theta$ = inclination of bank from horizontal;

$\rho$ = fluid density (mass);

$\sigma_g$ = geometric standard deviation (size) of bed material;

$\tau_c$ = critical boundary-shear stress; and

$\phi$ = angle of repose.

## APPENDIX B -- BIBLIOGRAPHY ON INITIAL MOTION OF PARTICLES


1. "Evolution of a Duned Bed Under Oscillatory Flow," by M. R. Carstens and F. M. Neilson, Quarterly Report 7, Project A-798, Engineering Experiment Station, Georgia Institute of Technology, Atlanta, Georgia, March, 1966.

2. "Uniform Water Conveyance Channels in Alluvial Material," by Daryl B. Simons and Maurice L. Albertson, Transactions, ASCE, Vol. 128, 1963, Fig. 12, p. 97.

3. "Use of Evenly Spaced Hemispheres to Evaluate Aerodynamic Forces on a Soil Surface," by W. S. Chepil, Transactions, AGU, Vol. 39, No. 3, June, 1958, pp. 397-404.

4. "Fluid Mechanics for Engineers," by Maurice L. Albertson, James R. Barton, and Daryl B. Simons, Prentice-Hall, Inc., Englewood Cliffs, New Jersey, 1960, Fig. 9-2, p. 399.

5. "The Effect of Dunes upon Localized Scour," by M. R. Carstens, Final Report, Part I, Project A-770, Engineering Experiment Station, Georgia Institute of Technology, Atlanta, Georgia, December, 1965, APPENDIX C.

6. "Formula for Velocity at Beginning of Bed-Load Movement is Reappraised," by F. T. Mavis and L. M. Laushey, Civil Engineering, Vol. 19, No. 1, January, 1949, pp. 38-39 and 72.

7. "Sediment Transportation Mechanics: Initiation of Motion," by Vito A. Vanoni, Journal of the Hydraulics Division, ASCE, Vol. 92, No. HY2, March, 1966, pp. 291-314.

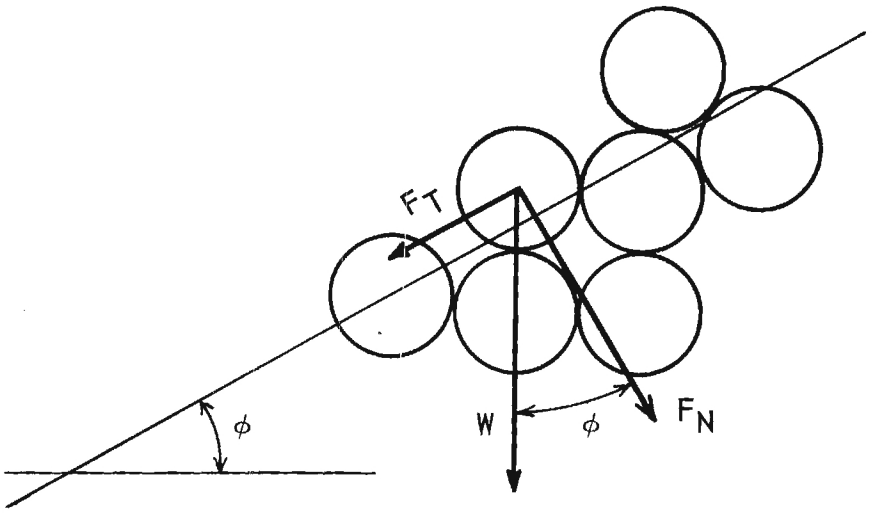


Figure 1. Gravity Forces on Bed Particles.

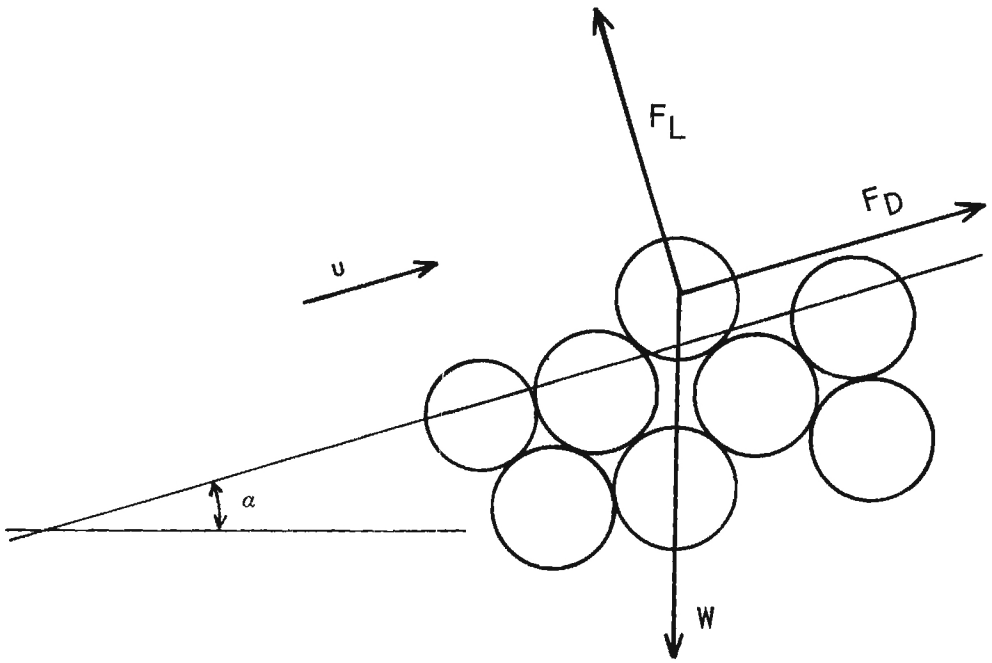


Figure 2. Forces on a Bed Particle.

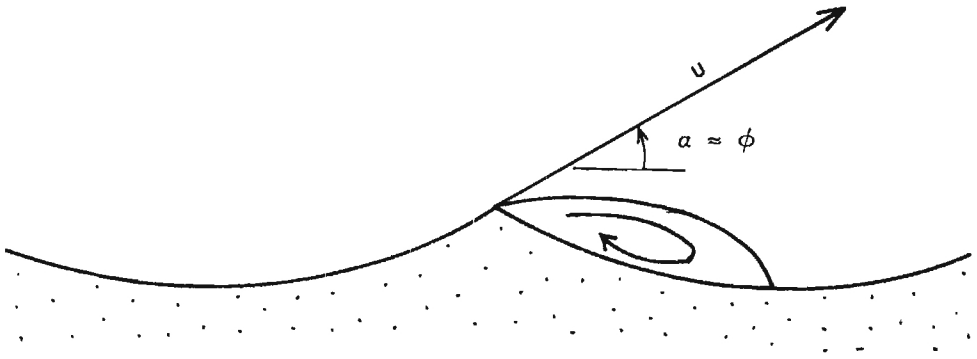


Figure 3. Velocity at the Crest of a Dune in Oscillatory Flow.

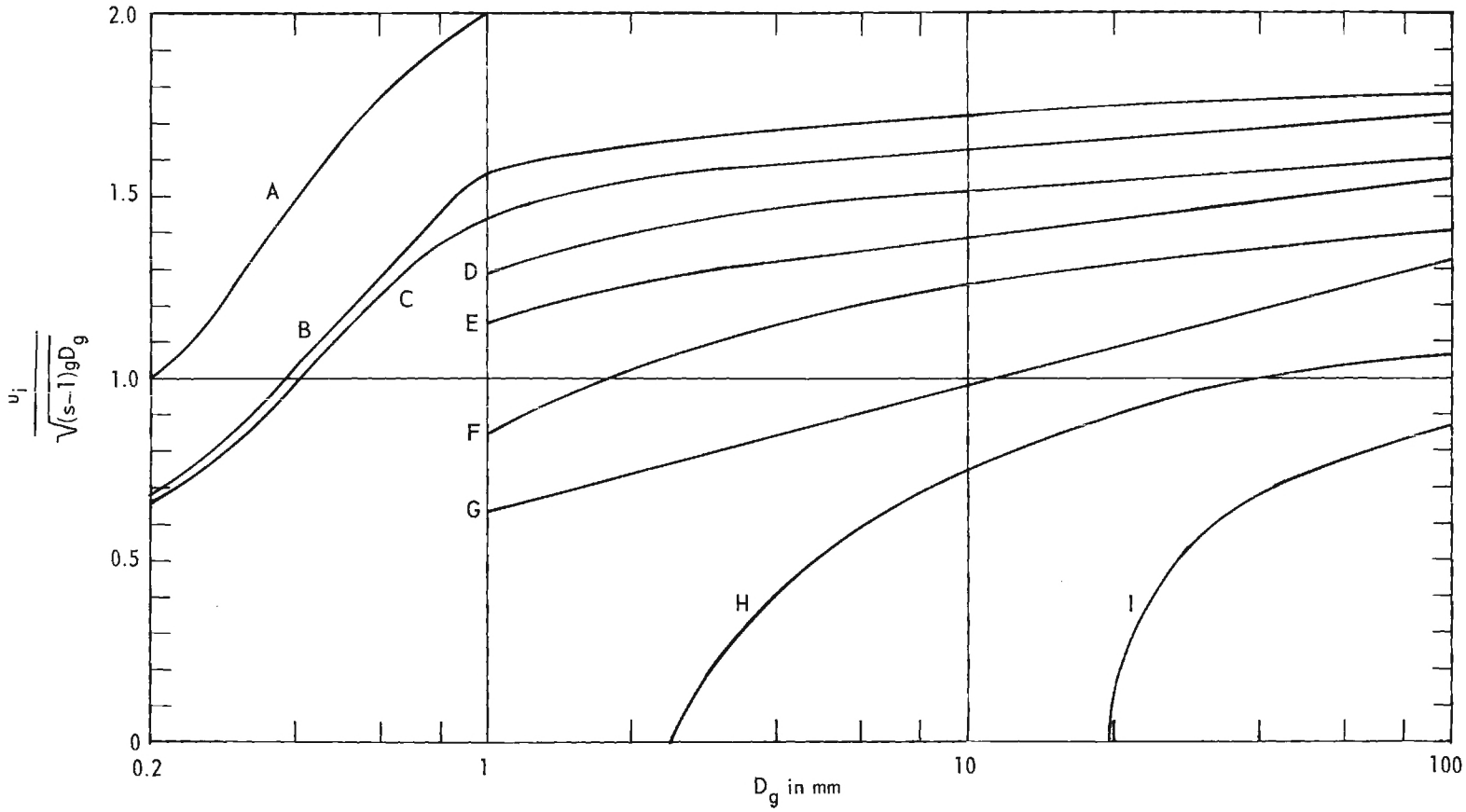


Figure 4. Initial-Motion Values of $u_i / \sqrt{(s-1)gD_g}$.

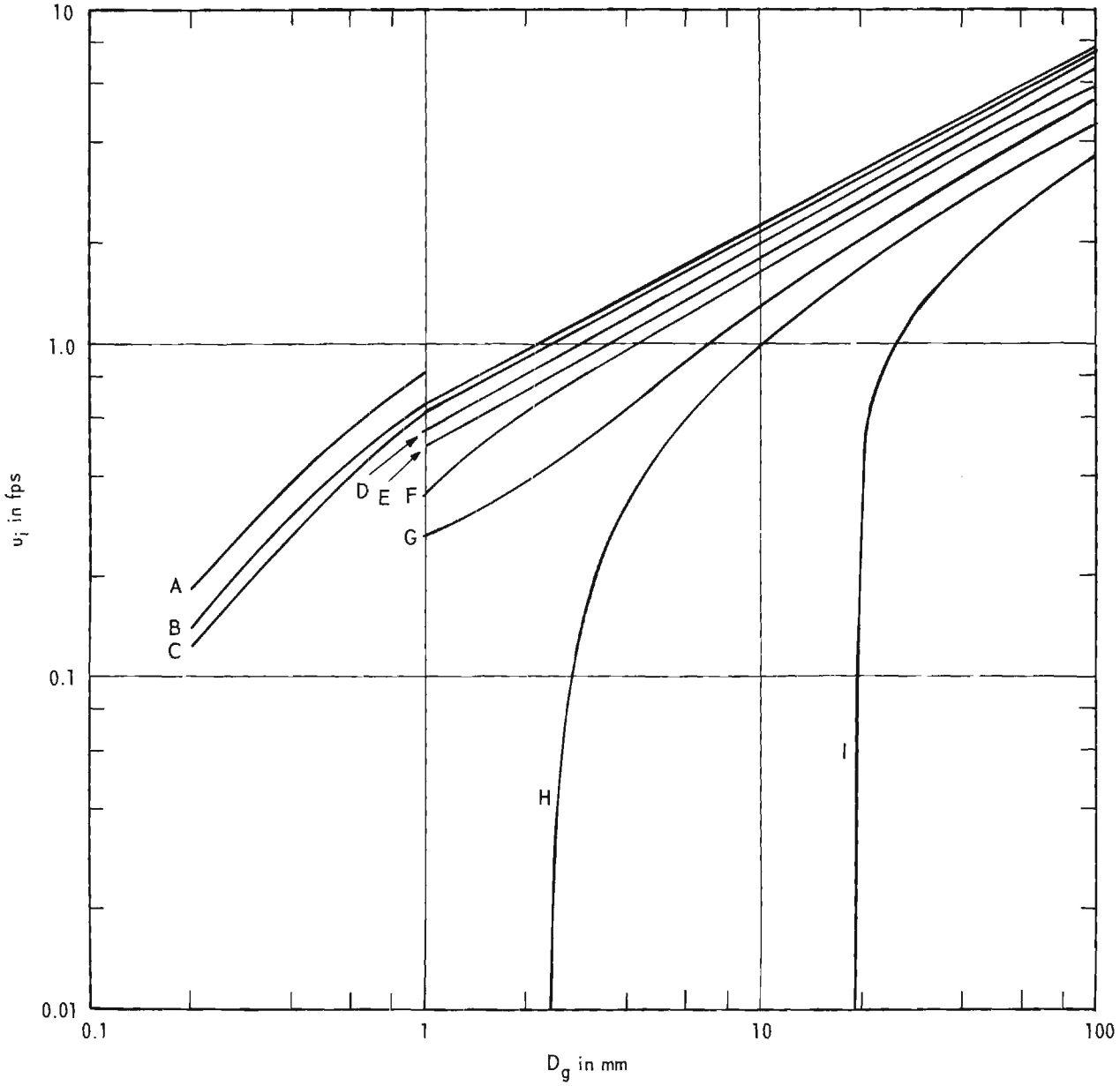


Figure 5. Initial-Motion Values of $u_i$.

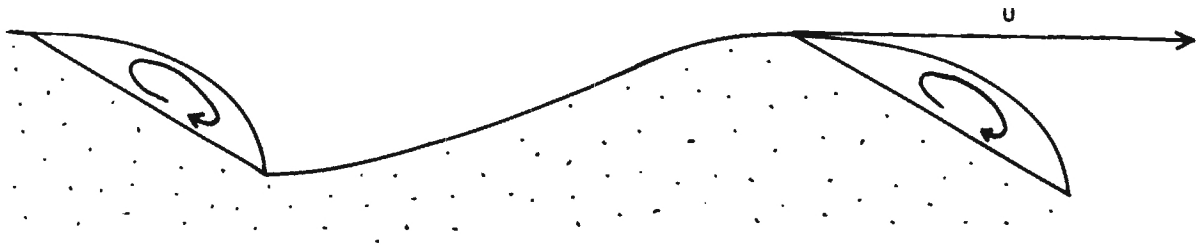


Figure 6. Velocity at the Crest of a Dune in Unidirectional Flow.

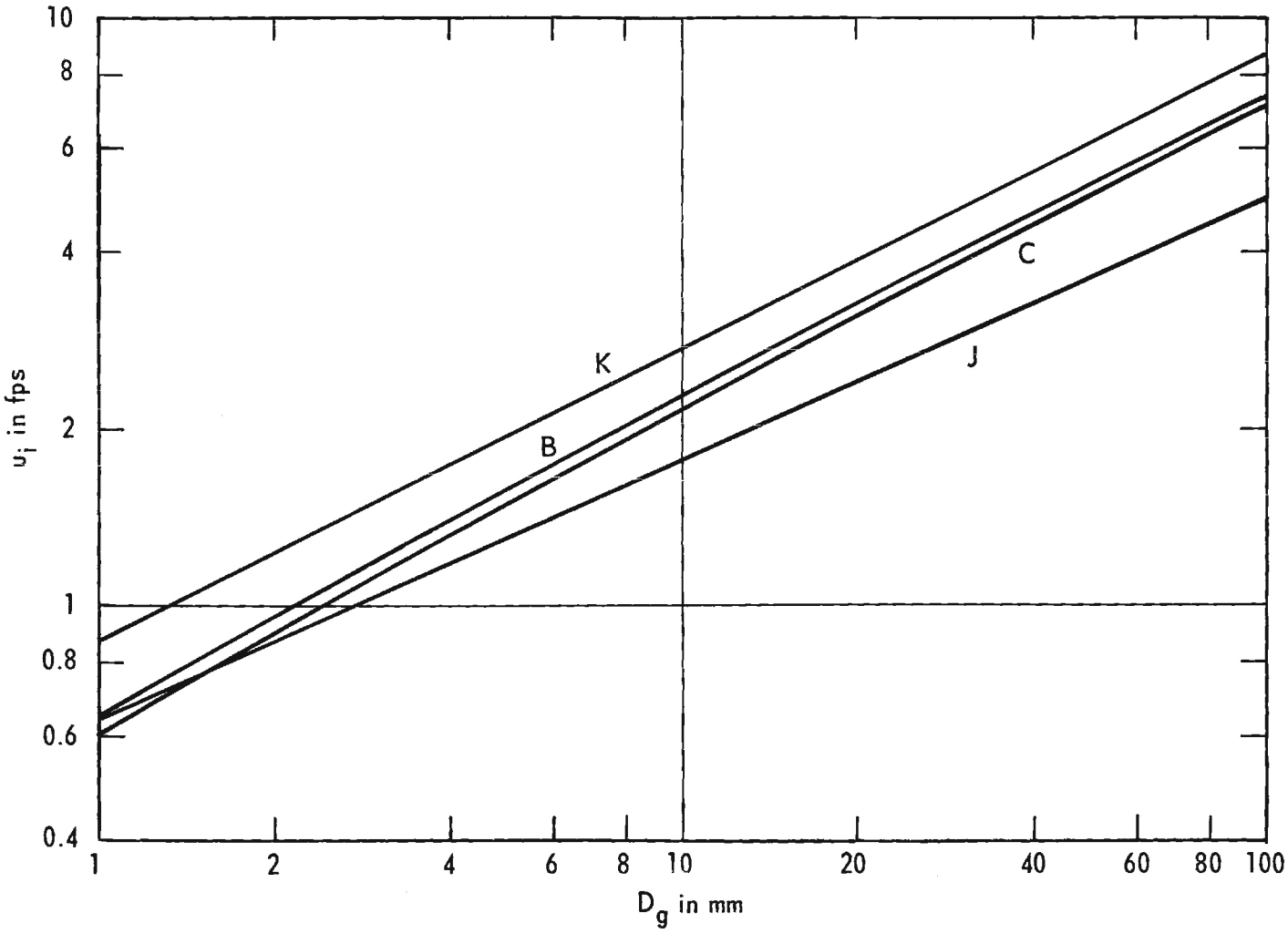


Figure 7. Comparison of Predicted, Initial-Motion, Bottom Velocities.

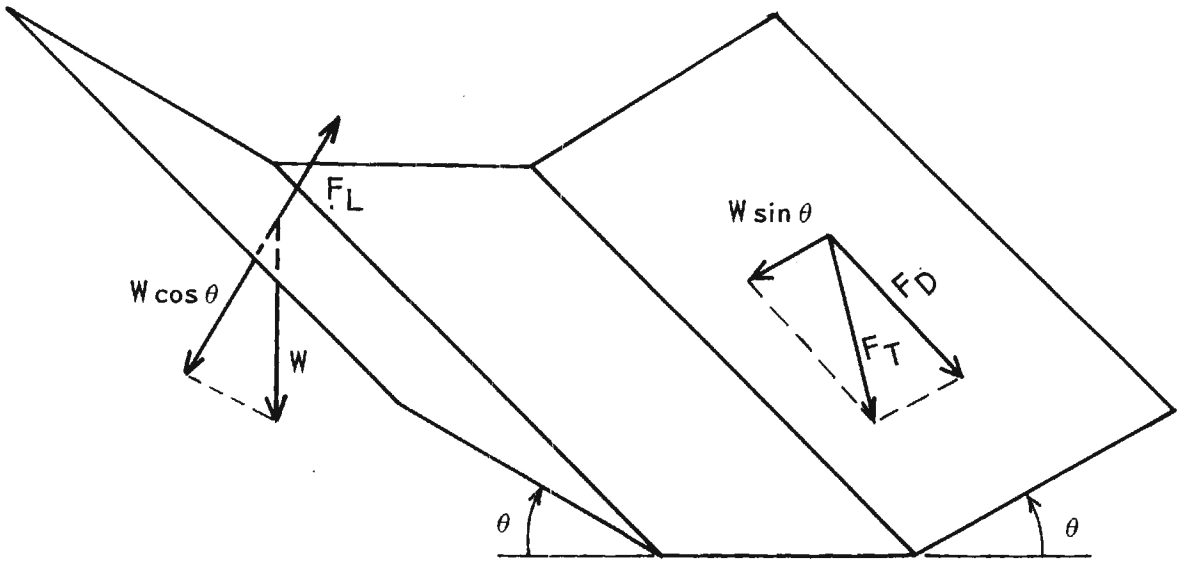


Figure 8. Forces on a Particle Lying on a Bank.

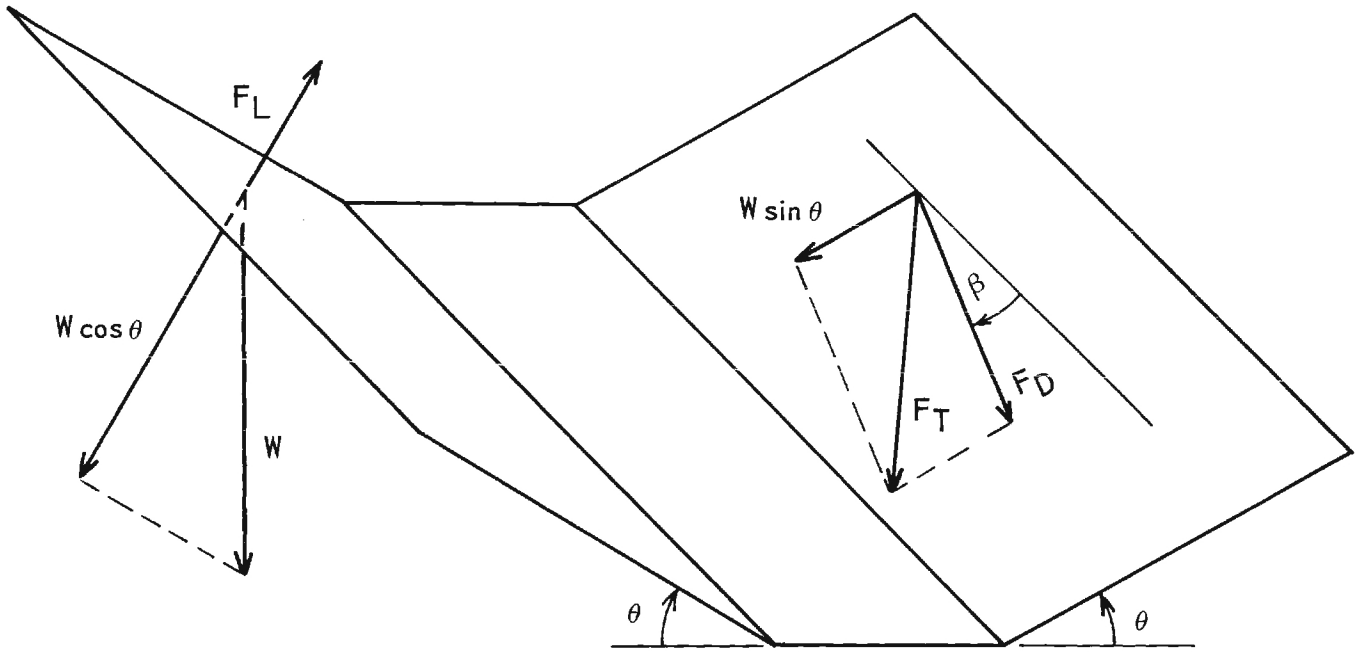


Figure 9. Forces on a Particle Lying on the Outer Bank of a Bend.

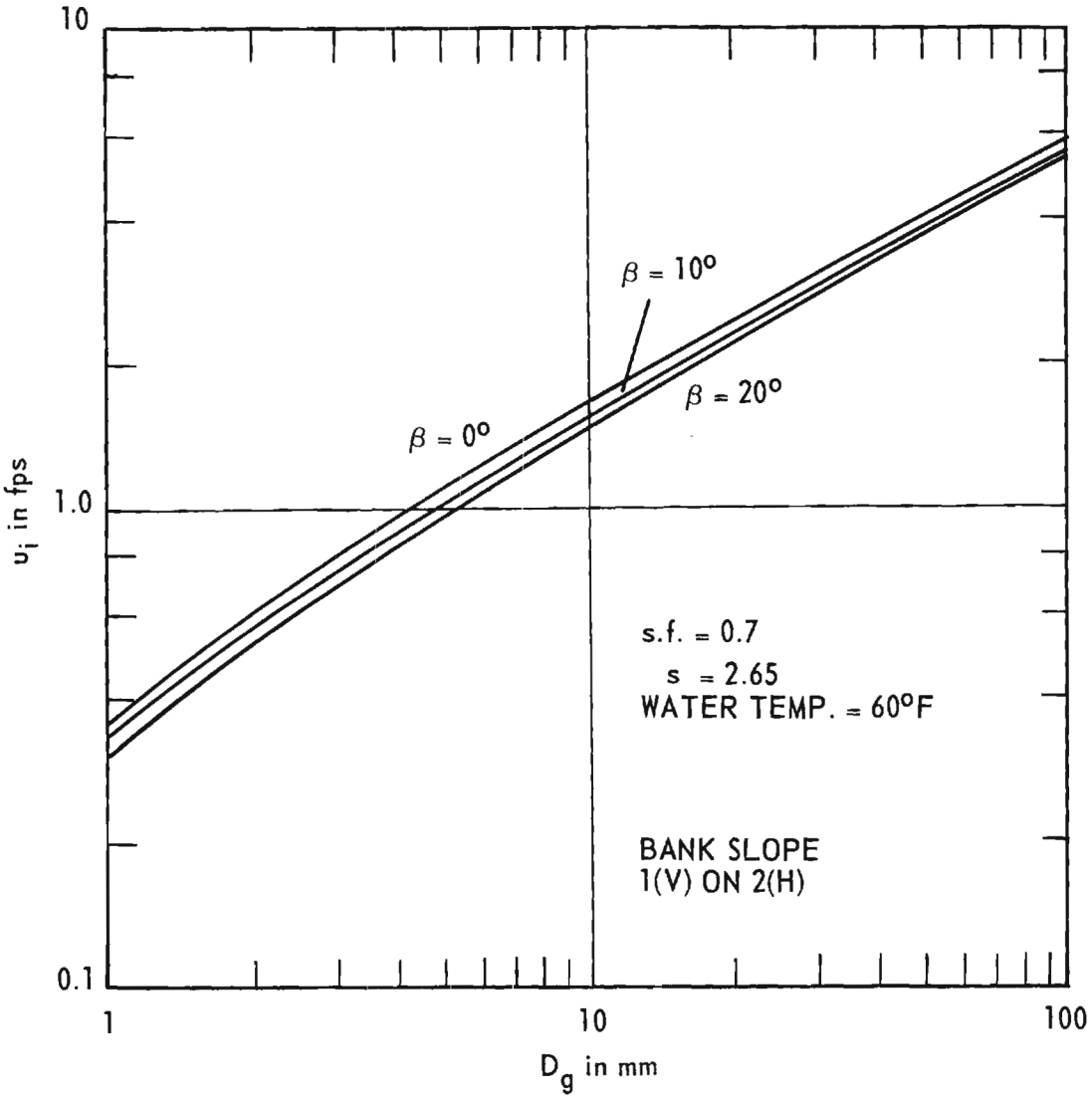


Figure 10. Initial-Motion Values of $u_i$ for Particles Lying on the Outer Bank of a Bend.

A-798



QUARTERLY REPORT 10

PROJECT A798

# AN ANALYTICAL AND EXPERIMENTAL STUDY OF BED FORMS UNDER WATER WAVES (MEASURED ENERGY DISSIPATION)

M. R. CARSTENS

Contract No. DA-49-055-CIVENG-65-1

1 October 1966 to 1 January 1967

Prepared for
Department of the Army
Coastal Engineering Research Center
Washington, D. C.

1967

Engineering Experiment Station
GEORGIA INSTITUTE OF TECHNOLOGY
Atlanta, Georgia

GEORGIA INSTITUTE OF TECHNOLOGY
School of Civil Engineering
Atlanta, Georgia

QUARTERLY REPORT 10

PROJECT A798

# AN ANALYTICAL AND EXPERIMENTAL STUDY OF BED FORMS UNDER WATER WAVES (MEASURED ENERGY DISSIPATION)

By

M. R. CARSTENS

CONTRACT NO. DA-49-055-CIVENG-65-1

1 OCTOBER 1966 to 1 JANUARY 1967

Prepared for
DEPARTMENT OF THE ARMY
COASTAL ENGINEERING RESEARCH CENTER
WASHINGTON, D. C.

# FOREWORD

This report summarizes the experimental work in regard to energy dissipation in oscillatory flow over a sand bed for experiments with the 0.297 mm glass beads and with the 0.585 mm Ottawa sand. Quarterly Report 6 issued in January 1966 summarized the experimental work in regard to dune geometry.

Essentially the same experimental program is currently being done with 0.190 mm Ottawa sand. The current program is more extensive in that contour maps of the bed of each run are being prepared and in that pressure gradients are being measured within the test section over the sand bed. Quarterly Report 11 will be a partial report of the experiments with the 0.190 mm sand.

ABSTRACT

This report is a summary on the energy dissipation in oscillatory flow over a sand bed as determined from experimental measurements. Energy dissipation is obtained by determining the work input into the oscillating-flow water tunnel. Work-input was determined with a smooth immobile boundary through a range of maximum velocities. Work input was also determined with equilibrium bed forms on a sand bed throughout a range of maximum velocities. The difference in the work input determined from experimental measurements is the additional work input required for flow over the duned bed as compared with a smooth immobile bed. The additional work input is obviously equal to the additional energy dissipation resulting from the deformed bed. Some work-input determinations were also made with flow over a flat sand bed prior to the development of dunes. Results are tabulated as additional energy dissipation per cycle per unit area of bed. The results are analyzed in terms of boundary-drag coefficients.
Key words: Energy dissipation, dunes, oscillatory flow, boundary drag.

TABLE OF CONTENTS

LIST OF FIGURES

LIST OF TABLES

# GLOSSARY

| Symbol | Definition | Units |
|---|---|---|
| $A$ | cross sectional area of water tunnel | $ft^2$ |
| $B$ | width of tunnel test section | ft |
| $C$ | height of tunnel test section | ft |
| $c_f$ | boundary drag coefficient | — |
| $\bar{c}_{fa}$ | mean boundary drag coefficient (smooth bed) | — |
| $\bar{c}_{fb}$ | mean boundary drag coefficient (flat sand bed) | — |
| $\bar{c}_{fc}$ | mean boundary drag coefficient (duned bed) | — |
| $D_g$ | geometric mean diameter of bed material | mm |
| $E$ | energy | ft-lb |
| $F$ | force | lb |
| $f$ | total boundary-drag coefficient | — |
| $f'$ | boundary-drag coefficient of immobile sand bed | — |
| $f''$ | form drag coefficient ($f - f'$) | — |
| $g$ | magnitude of the acceleration of gravity | $ft/sec^2$ |
| $L$ | length of sand-bed test section | ft |
| $N_s$ | sediment number, $U_m/\sqrt{(s-1)g\ D_g}$ | |
| $P$ | power | ft-lb/sec |
| $p$ | pressure | $lb/ft^2$ |
| PE | potential energy | ft-lb |
| $Q$ | discharge | $ft^3/sec$ |
| $R$ | hydraulic radius | ft |
| $s$ | ratio of density of bed material to fluid | — |
| $T$ | period of oscillation | sec |

GLOSSARY (Continued)

| Symbol | Definition | Units |
|---|---|---|
| $t$ | time | sec |
| $U$ | mean velocity in test section | ft/sec |
| $U_m$ | maximum value of mean velocity | ft/sec |
| $u$ | velocity in test section | ft/sec |
| $V$ | mean velocity in unidirectional open-channel flow | ft/sec |
| $\forall$ | volume | $ft^3$ |
| $v$ | velocity in vertical leg of water tunnel | ft/sec |
| WI | work-input into tunnel per cycle | ft-lb |
| $x$ | coordinate direction along axis of test section | ft |
| $2z_o$ | total water-motion amplitude in test section | ft or in |
| $\gamma$ | specific weight of water | $lb/ft^3$ |
| $\Delta$ | difference in value | |
| $\lambda$ | wave length of dunes | ft |
| $\eta$ | amplitude of dunes, trough to crest | ft |
| $\nu$ | kinematic viscosity | $ft^2/sec$ |
| $\rho$ | density | $slugs/ft^3$ or $lb\text{-}sec^2/ft^4$ |
| $\sigma_g$ | geometric standard deviation | |
| $\tau_{ob}$ | boundary shear stress, bed | $lb/ft^2$ |
| $\tau_{ow}$ | boundary shear stress, wall | $lb/ft^2$ |
| $\tau_{or}$ | boundary shear stress, roof | $lb/ft^2$ |
| $\phi$ | angle of repose of bed material | degrees |

# INTRODUCTION

This report is a summary on the energy dissipation in oscillatory flow over a sand bed as determined from experimental measurements. Energy dissipation is obtained by calculating the work input into the oscillating-flow water tunnel. Work input into the tunnel was evaluated for flow over (a) a smooth immobile boundary, (b) a flat sand bed, and (c) a deformed sand bed. Work-input determinations were made throughout a range of velocities for bed conditions (a), (b), and (c). The difference in the calculated work input at identical velocities with bed conditions (b) and (a) is the additional energy dissipation in the flow due to the roughened boundary. Similarly, the difference in the calculated work input at identical velocities with bed conditions (c) and (a) is the additional energy dissipation in the flow due to the deformed boundary.

The results on energy dissipation have been partially reported in prior reports, Quarterly Reports 1, 2, 3, 4. For the sake of completeness, all of the results reported previously are repeated in this report.

## A. The water tunnel, instrumentation, and procedure

A complete description of the water tunnel, instrumentation, and procedures employed during a run are included in the appendix. Measurements used in the calculation of the work input are briefly explained in pages 4 and 5 and are illustrated in figure 3 of the appendix. These measurements are displacement of the water as a function of time and pressure in the west leg of the U-tube as a function of time.

Work-input is evaluated from the work input on the water surface in the west leg of the U-tube. All of the external work to the oscillating

tunnel required to maintain oscillation is pressure work applied to the free-water surface in the west leg of the U-tube. The work input per cycle in the west leg is

$$WI = \int_{-T/2}^{T/2} P \, dt \tag{1}$$

in which WI is the work input per cycle, T is the period of oscillation, P is power, and t is time. By definition

$$P = F \, v \tag{2}$$

in which F is the pressure force on the water surface and v is the velocity of the water surface. Further

$$F = p \, A \tag{3}$$

in which p is the measured pressure in the air above the water surface and A is the area of the water surface in the west leg of the U-tube. Since the water motion within the water tunnel is simple harmonic

$$v = \frac{2\pi}{T} z_o \cos \frac{2\pi t}{T} \tag{4}$$

in which $2z_o$ is the total amplitude of the water motion in the west leg of the U-tube and T is the period of the motion. Because the cross sectional area of the west leg, test section, and east leg are equal (1 ft by 4 ft in dimensions), the value of $2z_o$ which is measured in the east leg is equal to the total water-motion amplitude in the west leg. As a further consequence of the equality of cross sectional areas the maximum mean velocity in the test section, $U_m$, is simply $(2z_o)(\pi/T)$. Combining equations 1, 2, 3, and 4,

$$WI = A\, z_o \int_{-\pi}^{\pi} p \cos \frac{2\pi t}{T} \; d\left(\frac{2\pi t}{T}\right) \qquad (5)$$

Work input to maintain oscillation was evaluated by numerical integration of equation 5. The water-motion record (upper trace in figure 3 in the appendix) was used to establish the relation between the measured value of p (middle trace in figure 3 in the appendix) and $2\pi t/T$. Values of the pressure were determined at every millimeter along the strip chart. The complete cycle in figure 3 in the appendix is 87 mm in length of chart. Using the trapezoidal rule for numerical integration of equation 5, the total integral would be approximated by the summation 86 equal-width trapezoids in figure 3 in the appendix. The numerical computations were done by means of an electronic computer from punched-card data.

Equation 5 is the work input into the water tunnel. The work input is equal to the energy dissipation provided that the total water-motion amplitude, $2z_o$, is constant. On the other hand if the amplitude, $2z_o$, is increasing, part of the work input is used to increase the energy of the oscillating water mass. In this case, energy dissipation per cycle would be the work input per cycle minus the energy increase per cycle. Conversely if the amplitude, $2z_o$, is decreasing, energy dissipation is the sum of the work input and the energy decrease per cycle. The energy of the oscillating water mass can be conveniently evaluated either when the kinetic energy is a maximum and the potential energy is zero or when the potential energy is a maximum and the kinetic energy is zero. When the kinetic energy is zero, the potential energy, PE, is as follows

$$PE_{max} = \gamma A z_o^2 \tag{6}$$

in which $\gamma$ is the specific weight of the water. The change in energy, E, of the oscillating mass between cycle, i + 1, and cycle, i, is as follows

$$E_{i+1} - E_i = \gamma A \left( z^2_{o(i+1)} - z^2_{o(i)} \right) \approx \frac{\gamma A}{2} (2z_o)(\Delta 2z_o) \tag{7}$$

in which $\Delta 2z_o$ is the change in total water-motion amplitude per cycle. A convenient method of determining $\Delta 2z_o$ is to plot $2z_o$ versus the integer, i, and then to determine the slope graphically at the value of i of interest.

B. Bed materials

Three different bed materials were used in the testing program. The properties of the bed materials are shown in table I.

TABLE I

BED-MATERIAL PROPERTIES

| Property | Bed Material | | |
|---|---|---|---|
| | Al Sheet | Glass Beads | Ottawa Sand |
| Geometric Mean Diameter, $D_g$, in mm | 0 | 0.297 | 0.585 |
| Geometric Standard Deviation, $\sigma_g$ | 1.00 | 1.06 | 1.16 |
| Specific gravity, s | — | 2.47 | 2.62 |
| Angle of repose, $\phi$, in degrees* | — | 2.4 | 32.5 |

*Approximate value since $\phi$ is also a function of porosity.

The smooth immobile boundary was formed by a sheet of 18 ga. aluminum placed over the depression in the bed of the test section. Prior to placement of the aluminum sheet, sand was placed in the bed-material container in the floor of the test section. The sand bed was smoothed and levelled to the elevation of the floor of the test section. Next the 4 ft by 8 ft sheet of 18 ga. aluminum was placed on the floor of the test section. Two extruded aluminum angles, 1 in by 1 in by 1/16 in, were then placed in the corners with one exterior surface of each angle in contact with the aluminum sheet and the other exterior surface in contact with the sidewall of the test section. The angles were held in position with lengths of 2 in wide duct tape. To insure that the aluminum sheet was pulled down firmly onto the underlying sand, a negative pressure of about -3 ft of water was created in the sand during the immobile-smooth-bed runs.

In addition to the properties listed in table I, the two sands were composed of well-rounded grains. The glass beads are nearly spherical as evidenced by the small angle of repose, $\phi$.

C. Bed condition

Measurements from which work input and energy dissipation could be computed were made with three different bed conditions as follows: (a) smooth, flat, immobile bed, (b) flat sand bed, and (c) deformed sand bed throughout a range of velocities in the test section. Obviously the runs with bed condition (a) were made with the aluminum sheet covering the bed-material container. In order to obtain the work input with bed condition (b), measurements were recorded early in the run prior to the time that the bed became deformed. Every run was begun with a flat bed. A run was continued

a sufficient length of time for the dune system to have reached equilibrium before the work-input measurements were taken for bed condition (c). The existence of an equilibrium duned bed was determined by observing the bed and by referring to the amplitude-time record. As the duned bed develops, resistance to the oscillatory flow in the tunnel increases. The effect of increasing resistance is to decrease the amplitude of oscillation. When the amplitude of oscillation reaches equilibrium, the frictional resistance is constant from cycle to cycle which is indicative that the bed forms are no longer changing.

## II. RESULTS

### A. Smooth, flat, immobile bed -- bed condition (a)

The results determined from experimental measurements are listed in table II. The columns of table 2 contain the following information.

Column 1. Run number

Column 2. Water temperature in degrees Fahrenheit

Column 3. Period in seconds

Column 4. Total water-motion amplitude, $2z_o$, in inches

Column 5. Work input to tunnel per cycle in ft-lb/cycle

Column 6. Energy increase per cycle in ft-lb/cycle

Column 7. Energy dissipation per cycle in ft-lb/cycle

The results are graphically shown in figure 1 in which energy dissipation per cycle for the entire water mass (col. 7, table II) is plotted as a function of total water-motion amplitude, $2z_o$, (col. 4, table II). The straight-line functions were visually fitted to the measured points.

TABLE II

RESULTS WITH SMOOTH IMMOBILE BED
BED CONDITION (a)

| 1 | 2 | 3 | 4 | 5 | 6 | 7 |
|---|---|---|---|---|---|---|
| | (°F) | (sec) | (in) | (ft-lb/cycle) | (ft-lb/cycle) | (ft-lb/cycle) |
| 13 A | 79 | 3.565 | 6.21 | 1.85 | 0 | 1.85 |
| B | 79 | 3.552 | 8.05 | 2.81 | 0 | 2.81 |
| C | 79 | 3.550 | 11.12 | 4.20 | 0 | 4.20 |
| D | 79 | 3.549 | 12.97 | 5.90 | 0 | 5.90 |
| E | 79 | 3.549 | 15.31 | 7.44 | 0 | 7.44 |
| 14 A | 80 | 3.554 | 5.52 | 1.63 | 0 | 1.63 |
| B | 80 | 3.562 | 6.28 | 2.23 | 0 | 2.23 |
| C | 80 | 3.564 | 7.29 | 2.83 | 0 | 2.83 |
| D | 80 | 3.554 | 8.92 | 3.41 | 0 | 3.41 |
| E | 80 | 3.557 | 10.61 | 4.39 | 0 | 4.39 |
| 15 A | 80 | 3.538 | 8.99 | 4.40 | 0 | 4.40 |
| B | 80 | 3.553 | 10.48 | 5.59 | 0 | 5.59 |
| C | 80 | 3.557 | 13.28 | 7.41 | 0 | 7.41 |
| D | 80 | 3.558 | 14.87 | 8.74 | 0 | 8.74 |
| 16 A | 79 | 3.551 | 12.86 | 7.96 | 0 | 7.96 |
| B | 79 | 3.553 | 16.32 | 9.72 | 0 | 9.72 |
| C | 79 | 3.552 | 19.92 | 13.4 | 0 | 13.4 |
| E | 79 | 3.548 | 22.72 | 14.5 | 0 | 14.5 |
| F | 79 | 3.548 | 21.23 | 13.5 | 0 | 13.5 |
| 17 A | 80 | 3.55 | 12.17 | 5.66 | 0 | 5.66 |
| B | 80 | 3.553 | 16.34 | 8.69 | 0 | 8.69 |
| C | 80 | 3.551 | 23.33 | 14.8 | 0 | 14.8 |
| D | 80 | 3.548 | 26.33 | 20.8 | 0 | 20.8 |
| E | 80 | 3.540 | 28.78 | 27.5 | 0 | 27.5 |
| 18 A | 80.2 | 3.55 | 18.78 | 13.2 | 0 | 13.2 |
| B | 80.2 | 3.546 | 26.35 | 23.1 | 0 | 23.1 |

(Continued)

TABLE II (Continued)

RESULTS WITH SMOOTH IMMOBILE BED
BED CONDITION (a)

| 1 | 2 | 3 | 4 | 5 | 6 | 7 |
|---|---|---|---|---|---|---|
| | (°F) | (sec) | (in) | (ft-lb/cycle) | (ft-lb/cycle) | (ft-lb/cycle) |
| C | 80.2 | 3.539 | 32.00 | 35.0 | 0 | 35.0 |
| D | 80.2 | 3.534 | 36.16 | 49.0 | 0 | 49.0 |
| 19 A | 80.2 | 3.555 | 3.60 | 0.639 | 0 | 0.639 |
| B | 80.2 | 3.559 | 4.94 | 0.870 | 0 | 0.870 |
| C | 80.2 | 3.560 | 5.87 | 1.40 | 0 | 1.40 |

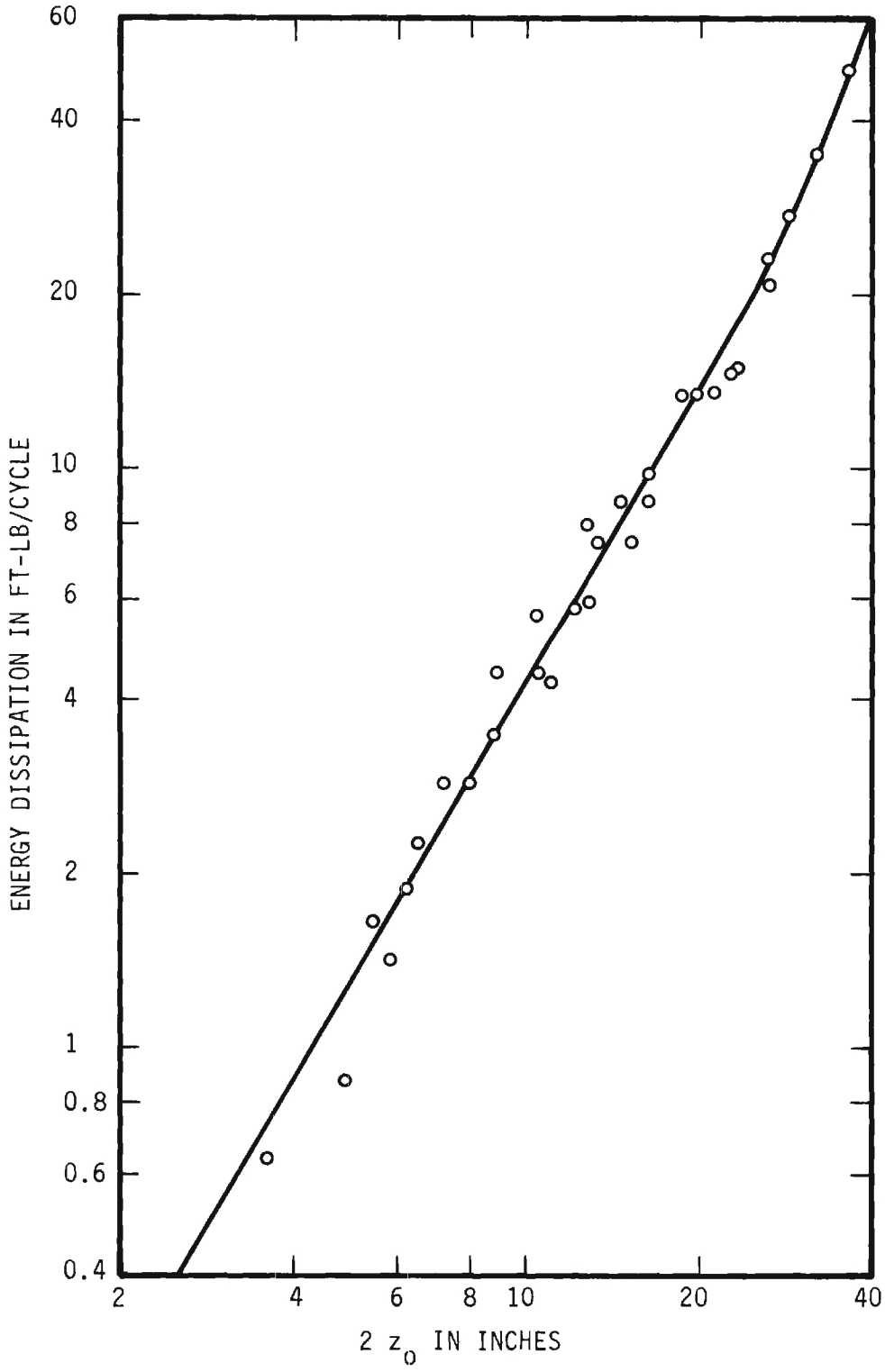


Figure 1. Energy Dissipation in the Water Tunnel with a Smooth Flat Immobile Bed.

B. Flat sand bed -- bed condition (b)

The results determined from experimental measurements are listed in table III. The columns of table III contain the following information.

Column 1. Run number

Column 2. Geometric mean diameter, $D_g$, of bed material in mm

Column 3. Water temperature in degrees Fahrenheit

Column 4. Period in seconds

Column 5. Total water-motion amplitude, $2z_o$, in inches

Column 6. Sediment number, $N_s = U_m / \sqrt{(s-1)g\, D_g}$

Column 7. Work input to tunnel per cycle in ft-lb/cycle

Column 8. Energy increase per cycle in ft-lb/cycle

Column 9. Energy dissipation per cycle in ft-lb/cycle

Column 10. Energy dissipation per cycle in ft-lb/cycle with bed condition (a) at the same value of $2z_o$ as determined from figure 1

Column 11. Difference in energy dissipation per cycle between bed condition (b) and bed condition (a) in ft-lb/cycle, that is, col. 9 minus col. 10. Since nothing is changed in the flow passage except in a 4 ft by 6 ft section of bed, this difference is solely due to the changed bed condition over 24 $ft^2$ of bed area.

Column 12. Difference in boundary-drag coefficient, $\bar{c}_{fb} - \bar{c}_{fa}$. See III.C.

TABLE III

RESULTS WITH FLAT SAND BED
BED CONDITION (b)

| 1 | 2 | 3 | 4 | 5 | 6 | 7 | 8 | 9 | 10 | 11 | 12 |
|---|---|---|---|---|---|---|---|---|---|---|---|
| | (mm) | (°F) | (sec) | (in) | | $\left(\frac{\text{ft-lb}}{\text{cycle}}\right)$ | $\left(\frac{\text{ft-lb}}{\text{cycle}}\right)$ | $\left(\frac{\text{ft-lb}}{\text{cycle}}\right)$ | $\left(\frac{\text{ft-lb}}{\text{cycle}}\right)$ | $\left(\frac{\text{ft-lb}}{\text{cycle}}\right)$ | |
| 20 A | 0.297 | 77 | 3.555 | 3.41 | 1.17 | 0.720 | 0 | 0.720 | 0.70 | 0.02 | 0.036 |
| B | 0.297 | 77 | 3.552 | 4.62 | 1.59 | 1.15 | 0 | 1.15 | 1.16 | -0.01 | 0.007 |
| C | 0.297 | 77 | 3.555 | 6.71 | 2.30 | 2.37 | 0 | 2.37 | 2.16 | 0.21 | 0.050 |
| D | 0.297 | 77 | 3.547 | 8.31 | 2.86 | 3.33 | 0 | 3.33 | 3.12 | 0.21 | 0.026 |
| E | 0.297 | 77 | 3.549 | 9.49 | 3.27 | 4.23 | 0 | 4.23 | 3.90 | 0.33 | 0.027 |
| F | 0.297 | 77 | 3.548 | 10.51 | 3.62 | 5.22 | 0 | 5.22 | 4.65 | 0.57 | 0.035 |
| 28 | 0.297 | 69.5 | 3.510 | 21.67 | 7.53 | 26.4 | 0 | 26.4 | 16.0 | 10.4 | 0.071 |
| 30 A | 0.297 | 72 | 3.525 | 28.56 | 9.87 | 52.7 | 0 | 52.7 | 28.0 | 24.7 | 0.074 |
| 31 A | 0.297 | 72 | 3.517 | 35.41 | 12.30 | 93.9 | 0 | 93.9 | 48.0 | 45.9 | 0.073 |
| 32 A | 0.297 | 71.5 | 3.525 | 30.90 | 10.70 | 60.9 | 0 | 60.9 | 34.0 | 26.9 | 0.065 |
| 33 | 0.297 | 73.5 | 3.544 | 12.90 | 4.44 | 7.24 | -1.30 | 8.54 | 6.60 | 1.94 | 0.064 |
| 34 A | 0.297 | 73.5 | 3.555 | 11.79 | 4.05 | 9.55 | 1.71 | 7.84 | 5.60 | 2.24 | 0.096 |
| B | 0.297 | 73.5 | 3.554 | 12.41 | 4.26 | 9.61 | 1.29 | 8.32 | 6.10 | 2.22 | 0.082 |
| C | 0.297 | 73.5 | 3.546 | 12.40 | 4.27 | 9.05 | 0.90 | 8.15 | 6.10 | 2.05 | 0.076 |
| 37 | 0.297 | 68.5 | 3.552 | 7.42 | 2.55 | 2.99 | 0 | 2.99 | 2.55 | 0.44 | 0.076 |
| 38 | 0.297 | 69 | 3.546 | 8.67 | 2.99 | 4.07 | 0 | 4.07 | 3.35 | 0.72 | 0.078 |
| 39 | 0.297 | 69 | 3.548 | 10.10 | 3.48 | 5.31 | 0 | 5.31 | 4.13 | 1.18 | 0.081 |

(Continued)

TABLE III (Continued)

RESULTS WITH FLAT SAND BED
BED CONDITION (b)

| 1 | 2 | 3 | 4 | 5 | 6 | 7 | 8 | 9 | 10 | 11 | 12 |
|---|---|---|---|---|---|---|---|---|---|---|---|
| | (mm) | (°F) | (sec) | (in) | | $\left(\frac{\text{ft-lb}}{\text{cycle}}\right)$ | $\left(\frac{\text{ft-lb}}{\text{cycle}}\right)$ | $\left(\frac{\text{ft-lb}}{\text{cycle}}\right)$ | $\left(\frac{\text{ft-lb}}{\text{cycle}}\right)$ | $\left(\frac{\text{ft-lb}}{\text{cycle}}\right)$ | |
| 40 | 0.297 | 69 | 3.540 | 10.44 | 3.60 | 5.77 | 0 | 5.77 | 4.62 | 1.15 | 0.078 |
| 41 | 0.297 | 69 | 3.545 | 10.85 | 3.73 | 6.05 | 0 | 6.05 | 4.85 | 1.20 | 0.067 |
| 45 | 0.297 | 67 | 3.550 | 11.62 | 4.00 | 6.55 | 0 | 6.55 | 5.45 | 1.10 | 0.049 |
| 58 | 0.297 | 76 | 3.594 | 6.50 | 2.21 | 2.68 | 0 | 2.68 | 2.04 | 0.64 | 0.169 |

C. Deformed sand bed -- bed condition (c)

The results determined from experimental measurements are listed in table IV. The columns of table IV are identical to those of table III. The explanation of the columns is given in II.B.

TABLE IV

RESULTS WITH DEFORMED SAND BED
BED CONDITION (c)

| 1 | 2 | 3 | 4 | 5 | 6 | 7 | 8 | 9 | 10 | 11 | 12 |
|---|---|---|---|---|---|---|---|---|---|---|---|
| | (mm) | (°F) | (sec) | (in) | | $\left(\frac{\text{ft-lb}}{\text{cycle}}\right)$ | $\left(\frac{\text{ft-lb}}{\text{cycle}}\right)$ | $\left(\frac{\text{ft-lb}}{\text{cycle}}\right)$ | $\left(\frac{\text{ft-lb}}{\text{cycle}}\right)$ | $\left(\frac{\text{ft-lb}}{\text{cycle}}\right)$ | |
| 21 | 0.297 | 79 | 3.557 | 7.02 | 2.41 | 3.53 | 0 | 3.53 | 2.33 | 1.20 | 0.247 |
| 22 | 0.297 | 76 | 3.555 | 9.44 | 3.24 | 5.99 | 0 | 5.99 | 3.82 | 2.17 | 0.184 |
| 23 | 0.297 | 75 | 3.549 | 10.76 | 3.70 | 7.80 | 0 | 7.80 | 4.85 | 2.95 | 0.169 |
| 24 | 0.297 | 77 | 3.551 | 12.10 | 4.16 | 10.1 | 0 | 10.1 | 5.83 | 4.3 | 0.172 |
| 25 | 0.297 | 73 | 3.552 | 16.42 | 5.65 | 18.0 | 0 | 18.0 | 9.8 | 8.2 | 0.131 |
| 26 | 0.297 | 73 | 3.551 | 18.42 | 6.34 | 24.9 | 0 | 24.9 | 12.1 | 12.7 | 0.140 |
| 27 | 0.297 | 73 | 3.528 | 20.56 | 7.11 | 32.7 | 0 | 32.7 | 14.6 | 18.1 | 0.147 |
| 29 B | 0.297 | 73 | 3.544 | 25.50 | 8.78 | 45.5 | -0.8 | 46.3 | 21.2 | 25.1 | 0.105 |
| 30 B | 0.297 | 72 | 3.522 | 28.03 | 9.71 | 57.7 | -1.0 | 58.7 | 27.8 | 30.9 | 0.099 |
| 31 B | 0.297 | 72 | 3.521 | 35.04 | 12.18 | 89.4 | 0 | 89.4 | 46.3 | 43.1 | 0.069 |
| 32 B | 0.297 | 71.5 | 3.534 | 30.75 | 10.60 | 59.6 | 0 | 59.6 | 33.0 | 26.6 | 0.064 |
| 36 | 0.297 | 73 | 3.553 | 22.11 | 7.64 | 35.7 | 0 | 35.7 | 16.6 | 19.1 | 0.128 |
| 49 | 0.297 | 70 | 3.560 | 4.70 | 1.62 | 1.63 | 0 | 1.63 | 1.17 | 0.46 | 0.323 |
| 50 | 0.297 | 65 | 3.550 | 30.37 | 10.43 | 65.4 | 0 | 65.4 | 32.4 | 33.0 | 0.082 |
| 51 | 0.297 | 75 | 3.579 | 6.30 | 2.15 | 3.17 | 0 | 3.17 | 1.90 | 1.27 | 0.375 |
| 63 | 0.585 | 78.5 | 3.568 | 7.96 | 1.85 | 4.56 | 0 | 4.56 | 2.88 | 1.68 | 0.240 |
| 64 | 0.585 | 78 | 3.552 | 9.46 | 2.21 | 7.06 | 0 | 7.06 | 3.90 | 3.16 | 0.265 |

(Continued)

TABLE IV (Continued)

RESULTS WITH DEFORMED SAND BED
BED CONDITION (c)

| 1 | 2 | 3 | 4 | 5 | 6 | 7 | 8 | 9 | 10 | 11 | 12 |
|---|---|---|---|---|---|---|---|---|---|---|---|
| | (mm) | (°F) | (sec) | (in) | | $\left(\frac{\text{ft-lb}}{\text{cycle}}\right)$ | $\left(\frac{\text{ft-lb}}{\text{cycle}}\right)$ | $\left(\frac{\text{ft-lb}}{\text{cycle}}\right)$ | $\left(\frac{\text{ft-lb}}{\text{cycle}}\right)$ | $\left(\frac{\text{ft-lb}}{\text{cycle}}\right)$ | |
| 65 A | 0.585 | 76 | 3.543 | 10.84 | 2.54 | 10.8 | 0 | 10.8 | 4.9 | 5.9 | 0.330 |
| B | 0.585 | 76 | 3.531 | 11.12 | 2.16 | 9.12 | 0 | 9.12 | 5.15 | 3.97 | 0.202 |
| 66 | 0.585 | 75 | 3.554 | 12.65 | 2.95 | 15.1 | 0 | 15.1 | 6.3 | 8.8 | 0.308 |
| 67 | 0.585 | 77 | 3.540 | 14.60 | 3.42 | 16.8 | 0 | 16.8 | 8.0 | 8.8 | 0.202 |
| 68 | 0.585 | 76 | 3.568 | 15.47 | 3.59 | 25.2 | 0 | 25.2 | 8.9 | 16.3 | 0.310 |
| 69 | 0.585 | 77 | 3.556 | 17.60 | 4.11 | 32.8 | 0 | 32.8 | 11.1 | 21.7 | 0.282 |
| 70 | 0.585 | 77 | 3.543 | 19.05 | 4.45 | 38.8 | -0.1 | 38.9 | 12.8 | 26.1 | 0.261 |
| 71 | 0.585 | 77 | 3.530 | 19.50 | 4.58 | 40.7 | 0 | 40.7 | 13.2 | 27.5 | 0.261 |
| 72 | 0.585 | 72 | 3.532 | 20.98 | 4.92 | 47.1 | -0.1 | 47.2 | 15.1 | 32.1 | 0.244 |
| 73 | 0.585 | 73 | 3.547 | 22.90 | 5.35 | 59.4 | -0.2 | 59.6 | 17.6 | 42.0 | 0.248 |
| 74 | 0.585 | 73 | 3.560 | 24.25 | 5.65 | 68.9 | -0.1 | 69.0 | 19.4 | 49.6 | 0.248 |
| 75 | 0.585 | 73 | 3.554 | 25.73 | 6.00 | 78.0 | -0.4 | 78.4 | 22.0 | 56.4 | 0.237 |
| 76 | 0.585 | 73 | 3.531 | 27.70 | 6.50 | 91.8 | 0 | 91.8 | 26.0 | 65.8 | 0.217 |
| 77 | 0.585 | 73 | 3.545 | 29.47 | 6.89 | 109 | 0 | 109 | 30 | 79 | 0.221 |
| 78 | 0.585 | 73 | 3.474 | 30.88 | 7.38 | 118 | 0 | 118 | 34 | 84 | 0.193 |
| 79 | 0.585 | 74 | 3.555 | 33.35 | 7.78 | 141 | - | 141 | 41 | 100 | 0.190 |
| 80 A | 0.585 | 73 | 3.540 | 9.80 | 2.29 | 10.8 | 0 | 10.8 | 4.1 | 6.7 | 0.502 |
| B | 0.585 | 73 | 3.580 | 9.65 | 2.23 | 10.9 | 0 | 10.9 | 4.2 | 6.7 | 0.536 |

## III. ANALYSIS OF RESULTS

The difference in energy dissipation at identical mean velocities in the test section is solely the result of different bed conditions on the floor of the test section. This difference in a cycle is tabulated in column 11 of tables II and III and is a measure of the added energy dissipation per cycle between bed conditions (b) and (a), table II, and between bed conditions (c) and (a), table III.

The mean rate of energy dissipation per unit area of bed is primarily a function of the velocity of the water, movement of the bed material, and geometry of the bed. The following analysis is for the purpose of eliminating the velocity by determining a boundary drag coefficient for each of the runs. Since the differences are confined within the horizontal test section, the analysis is restricted to the horizontal test section.

### A. Linear-momentum

The fluid control volume for which the linear momentum equation is written is shown schematically in figure 2. The general linear momentum equation in the x direction is

$$\Sigma F_{(ex)x} = \frac{\partial}{\partial t} \iiint_{c.v.} \rho u \, d\forall + \iint_{A_2} \rho u \, dQ - \iint_{A_1} \rho u \, dQ \qquad (8)$$

in which $\Sigma F_{(ex)x}$ is the summation of the external forces on the control volume; $\rho$ is fluid density, u is the x component of velocity; t is time; $d\forall$ is a volume element; and dQ is the volume rate of flow (discharge) through an element of area dA in the cross section.

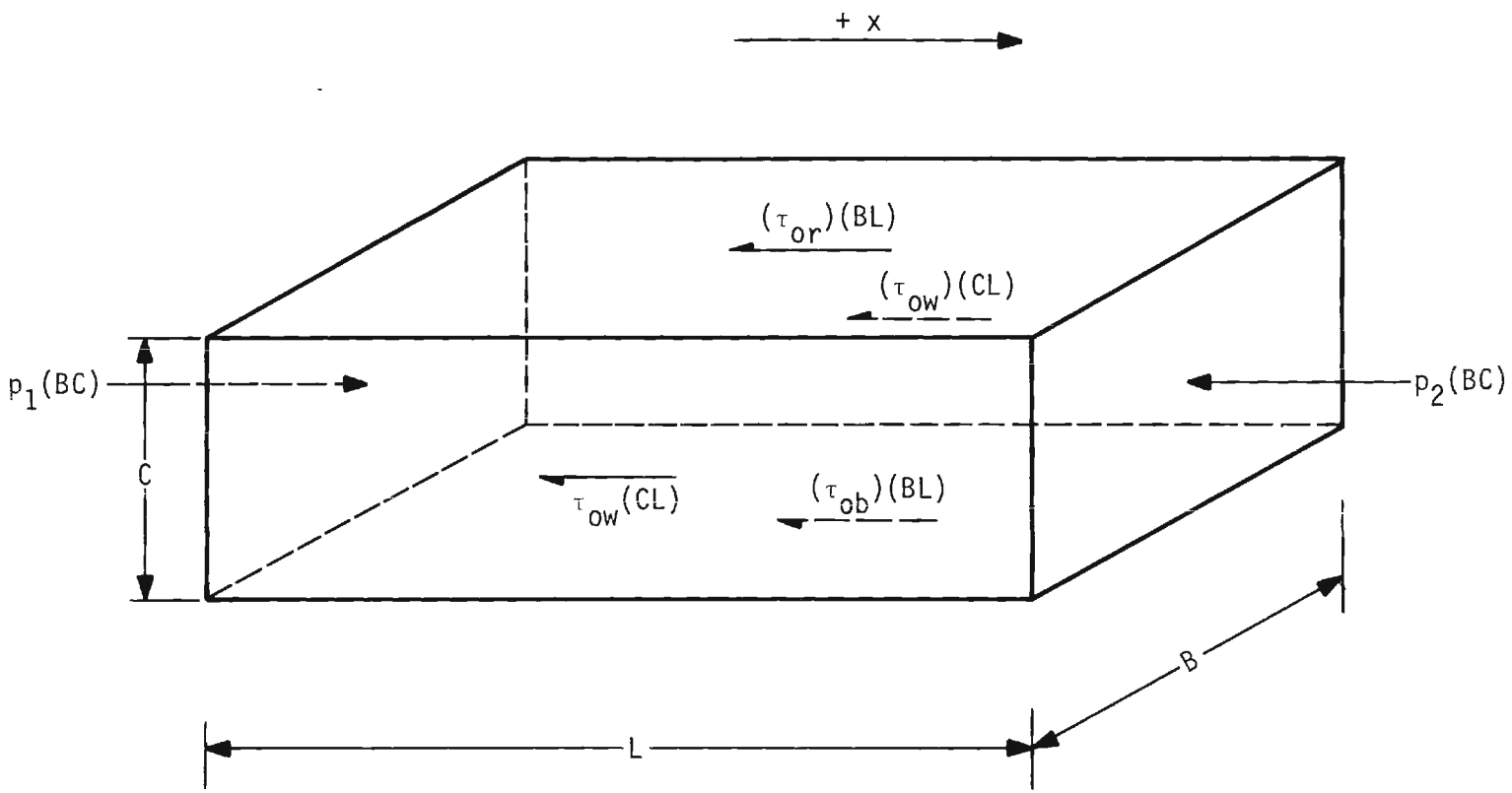


Figure 2. Control Volume.

Since the test section is a uniform flow zone and since $\rho$ is constant,

$$\iint_{A_2} \rho u \, dQ - \iint_{A_1} \rho u \, dQ = 0 \tag{9}$$

at any instant.

The term embodying the unsteadiness of the motion can be simplified by noting that $d\forall$ can be written as $LdA$. Thus

$$\frac{\partial}{\partial t} \iiint_{c.v.} \rho u \, d\forall = \rho L \frac{\partial}{\partial t} \iint_{A} u \, dA = \rho L \frac{dQ}{dt} = \rho LA \frac{dU}{dt} \tag{10}$$

in which U is the mean velocity in the test section.

The external forces are surface forces which are as follows

$$\Sigma F_{(ex)x} = + (p_1 - p_2)A - \tau_{or}(BL) - 2\tau_{ow}(CL) - \tau_{ob}(BL) \tag{11}$$

in which p is the pressure at a cross section; $\tau_{or}$ is the boundary-shear stress at the roof; $\tau_{ow}$ is the boundary-shear stress at the walls; $\tau_{ob}$ is the boundary-shear stress on the bed; and B, C, and L are the width, height, and length, respectively, of the control volume which is over the sediment container in the bed of the test section.

Substituting equations 9, 10, and 11 into equation 8 and solving for $(p_1 - p_2)A$,

$$(p_1 - p_2)A = \tau_{or}(BL) + 2\tau_{ow}(CL) + \tau_{ob}(BL) + \rho LA \frac{dU}{dt} \tag{12}$$

B. Work-energy

The work-energy equation in the power form for the horizontal control volume shown in figure 2 is as follows

$$-(\text{rate of energy dissipation}) + \iint_{A_1} p_1 \, dQ - \iint_{A_2} p_2 \, dQ$$

$$= \frac{\partial}{\partial t} \iiint_{c.v.} \left(\frac{\rho u^2}{2}\right) d\forall + \iint_{A_2} \frac{\rho u^2}{2} \, dQ - \iint_{A_1} \frac{\rho u^2}{2} \, dQ \tag{13}$$

Since the test section is a uniform flow zone and since $\rho$ is constant

$$\iint_{A_2} \frac{\rho u^2}{2} \, dQ - \iint_{A_1} \frac{\rho u^2}{2} \, dQ = 0 \tag{14}$$

Since the test section is a uniform flow zone, the pressure work terms can be simplified as follows

$$\iint_{A_1} p \, dQ - \iint_{A_2} p \, dQ = (p_1 - p_2)Q = (p_1 - p_2)A \, U \tag{15}$$

Substituting equations 14 and 15 into equation 12

$$-\left(\begin{matrix}\text{rate of energy dissipation} \\ \text{within the control volume}\end{matrix}\right) + (p_1 - p_2)A \, U = \frac{\partial}{\partial t} \iiint_{c.v.} \frac{\rho u^2}{2} \, d\forall \tag{16}$$

Since the motion within the test section is cyclic, the kinetic energy within the control volume will be identical at time interval of one period, T. Hence the term on the right side of equation 16 can be eliminated by multiplying each term of equation 16 by dt and integrating throughout a cycle giving

$$\frac{\text{energy dissipation in control volume}}{\text{cycle}} = \int_t^{t+T} (p_1 - p_2) \, A \, U \, dt \tag{17}$$

Substituting equation 12 into equation 17

$$\left(\frac{\text{energy dissipation within control volume}}{\text{cycle}}\right) = +BL \int_t^{t+T} \tau_{or} U \, dt + 2CL \int_t^{t+T} \tau_{ow} U \, dt + BL \int_t^{t+T} \tau_{ob} U \, dt + \rho LA \int_t^{t+T} U \frac{dU}{dt} \, dt \quad (18)$$

The last term of equation 18 is zero because the motion is cyclic.

The difference in energy dissipation per cycle in column 11 of tables II and III was evaluated from experimental measurements at identical values of water-motion amplitude or maximum velocity $U_m$. A reasonable assumption is that the boundary-shear stress on the smooth roof and smooth sidewalls is the same for bed conditions (a), (b), and (c) at identical values of water-motion amplitude. In other words the difference in energy dissipation is totally in the changed flow conditions at the bed. This assumption is quite reasonable because the boundary layers which form on the smooth boundaries of the roof and sidewalls reform twice each cycle and are very thin at the maximum thickness. With this assumption the value of column 11 in the tables has the following meaning from equation 18

$$\text{column 11 of table II} = \underbrace{+BL \int_t^{t+T} \tau_{ob} U \, dt}_{\text{bed condition(b)}} \underbrace{- BL \int_t^{t+T} \tau_{ob} U \, dt}_{\text{bed condition(a)}} \quad (19)$$

and

$$\text{column 11 of table III} = \underbrace{+BL \int_t^{t+T} \tau_{ob} U \, dt}_{\text{bed condition(c)}} \underbrace{- BL \int_t^{t+T} \tau_{ob} U \, dt}_{\text{bed condition(a)}} \quad (20)$$

C. Boundary-drag coefficient

A rational boundary-drag coefficient can be introduced at this stage of analysis by assuming that the boundary-shear stress is $\pi$ radians out of phase with the velocity, U, and that the magnitude of $\tau_{ob}$ is given in the usual form as follows

$$\tau_{ob} = c_f \frac{\rho |U| U}{2} \tag{21}$$

in which $c_f$ is the boundary-drag coefficient.

Substituting equation 21 into equation 19

$$\text{column 11 of table II} = BL \left\{ \int_t^{t+T} (c_{fb} - c_{fa}) \frac{\rho |U^3|}{2} \, dt \right. \tag{22}$$

and substituting equation 21 in equation 20

$$\text{column 11 of table III} = BL \int_t^{t+T} (c_{fc} - c_{fa}) \frac{\rho |U^3|}{2} \, dt \tag{23}$$

in which the subscripts on $c_f$ indicate the bed condition.

Defining a mean value of $c_f$ such that

$$\int_t^{t+T} c_f \frac{\rho |U^3|}{2} \, dt = \bar{c}_f \int_t^{t+T} \frac{\rho |U^3|}{2} \, dt \tag{24}$$

and substituting equation 24 into equations 22 and 23,

$$\text{column 11 of table II} = BL \, (\bar{c}_{fb} - \bar{c}_{fa}) \int_t^{t+T} \frac{\rho |U^3|}{2} \, dt \tag{25}$$

and

$$\text{column 11 of table III} = BL \, (\bar{c}_{fc} - \bar{c}_{fa}) \int_t^{t+T} \frac{\rho |U^3|}{2} \, dt \tag{26}$$

Since the motion is simple harmonic in the test section, equation 4, the integral in equations 25 and 26 can be evaluated in terms of measured quantities as follows

$$\int_t^{t+T} \frac{\rho |U^3|}{2}\, dt = \frac{\rho}{2}(2z_o)^3 \frac{\pi^2}{T^2} \int_{-\pi/2}^{\pi/2} \cos^3 \frac{2\pi t}{T}\, d\left(\frac{2\pi t}{T}\right) = \frac{2\pi^2}{3} \frac{\rho (2z_o)^3}{T^2} \qquad (27)$$

Substituting equation 27 into equations 25 and 26 and solving for the difference in boundary-drag coefficients

$$\bar{c}_{fb} - \bar{c}_{fa} = \left[ \frac{3}{2\pi^2} \frac{T^2}{\rho (2z_o)^3 BL} \right] [\text{col. 11, table II}] \qquad (28)$$

and

$$\bar{c}_{fc} - \bar{c}_{fa} = \left[ \frac{3}{2\pi^2} \frac{T^2}{\rho (2z_o)^3 BL} \right] [\text{col. 11, table III}] \qquad (29)$$

The computed values of the difference in boundary-drag coefficients are listed in column 12 of tables II and III. Differences in boundary-drag coefficient are also shown in figure 3 as a function of the sediment number $N_s$.

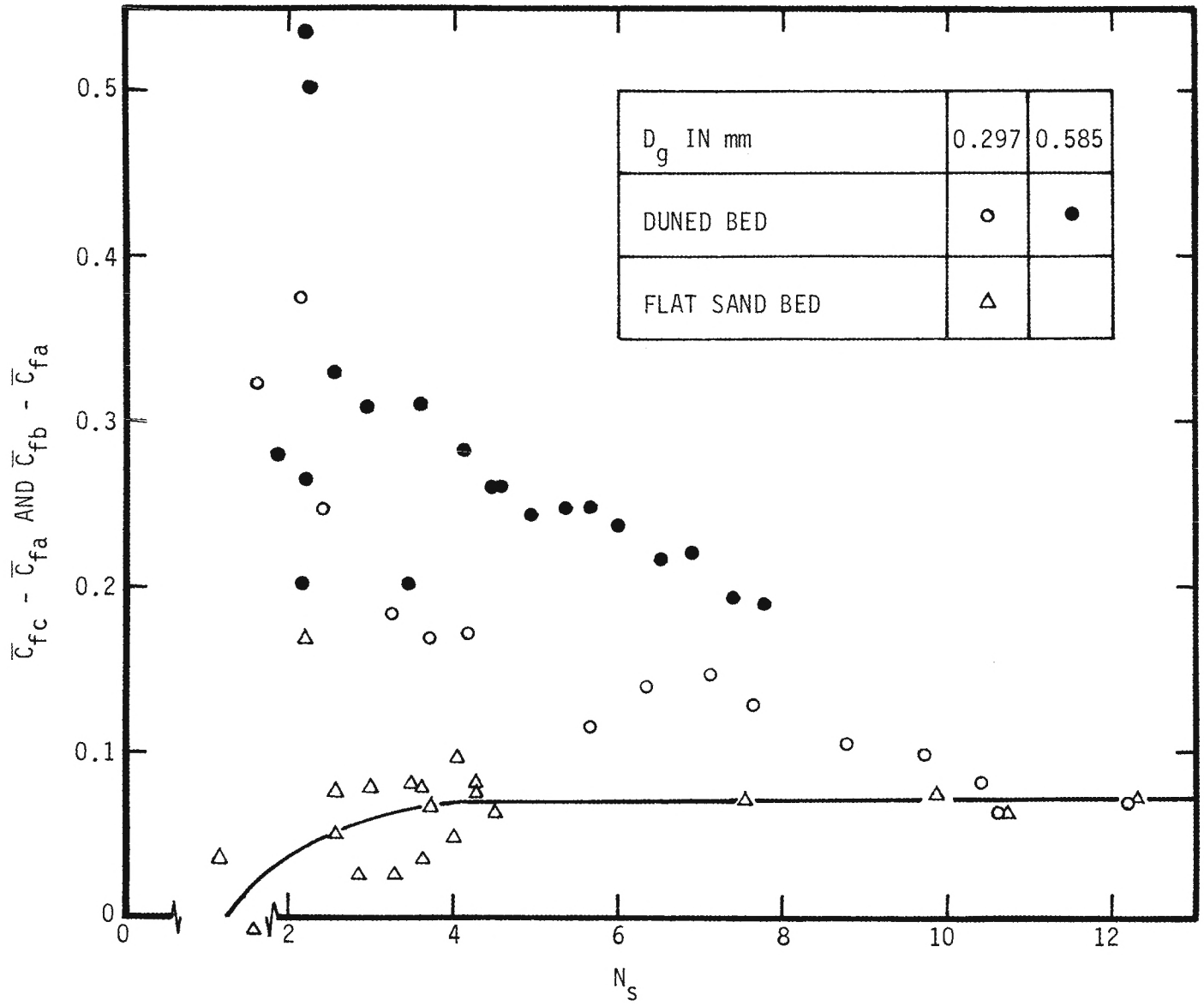


Figure 3. Boundary-drag Coefficients.

## IV. DISCUSSION OF RESULTS

Using experimental data, the difference in the value of the boundary-drag coefficient for oscillatory flow over a sand bed and for oscillatory flow over a smooth immobile bed was computed for a range of maximum bottom velocities, $U_m$. The differences in boundary drag coefficient are listed in tables II and III and are shown in figure 3. By using the smooth immobile bed as a reference, the results could be determined entirely from experimental measurements. In computing boundary-drag-coefficient difference, the assumption was made that the boundary-drag force was 180 degrees out of phase with the velocity. In addition, the boundary-drag-coefficient difference was calculated as a mean value over a cycle.

The precedent for representing the form drag of dunes as a difference of drag coefficients with and without dunes has been established by Alam, Cheyer, and Kennedy 1/ in an extensive review and reanalysis of boundary drag in unidirectional open-channel flow over sand beds. In the MIT study 1/, measured values of the physical variables from both flume experiments and natural-stream investigations were recorded on punched cards for later use as input into an electronic digital computer. Using the electronic computer, different arrangements of dimensionless variables could be readily tested to determine the significance of the variables.

The method of analysis which resulted in the best correlation of the data from a large number of studies involved subdividing the boundary-drag coefficient. The boundary-shear stress was expressed in the traditional form

$$\tau_o = \left(\frac{f}{4}\right) \frac{\rho V^2}{2} \tag{30}$$

in which V is the mean velocity of the unidirectional flow and $f/4$ is the boundary-drag coefficient comparable to $c_f$ in equation 21. The total-boundary-drag coefficient, $f/4$, was then subdivided as follows.

$$c_f = \frac{f}{4} = \frac{f' + f''}{4} \tag{31}$$

in which $f'/4$ is the boundary-drag coefficient for flow over a immobile flat sand bed and $f''/4$ is the contribution of form drag of dunes to the total drag. In analyzing various data, the form-drag contribution, $f''$, was found to be a function of $V/\sqrt{g\ D_g}$ and $R/D_g$ in which R the hydraulic radius.

The similarity of the analysis at Alam, Cheyer, and Kennedy 1/ to that employed by the writer is apparent by noting that

$$f'' = f - f' \tag{32}$$

is analogous to $\bar{c}_{fc} - \bar{c}_{fb}$ for an immobile sand bed, that is, for $N_s < 4$. A further similarity is that the sediment number is also similar to the parameter deduced in the MIT study, that is, for unidirectional flow

$$N_s = \frac{V}{\sqrt{(s-1)g\ D_g}} = \left\{ \frac{1}{\sqrt{s-1}} \right\} \frac{V}{\sqrt{g\ D_g}} \tag{33}$$

If $R/D_g$ is greater than about 1000, the value of $f''$ was found to be nearly independent of $R/D_g$.

The minor dissimilarity of analyses is that Alam, Cheyer, and Kennedy 1/ used the immobile flat sand bed as a reference, whereas, the writer used the immobile smooth bed as a reference. For unidirectional steady flow in a uniform channel the value of the drag coefficient, $f'/4$, for an immobile flat sand bed can be determined quite accurately from the well-known and

widely used Moody diagram for pipe flow using the value of $D_g$ as the roughness-length measure. With oscillatory flow, the experiments were such that the difference in drag coefficients between the deformed sand bed and the immobile smooth bed could be determined. Thus in order to obtain the total-drag coefficient, $\bar{c}_{fc}$, for oscillatory flow over a deformed bed, the drag coefficient, $\bar{c}_{fa}$, for an immobile smooth bed must be determined first. The determination of a reasonable value for $\bar{c}_{fa}$ with oscillatory flow can be determined analytically if the boundary layer is laminar. The velocity distribution can be resolved from a solution presented by Schlichting 2/. From this solution the energy dissipation per cycle per unit area of bed is found to be

$$\frac{\text{energy dissipation/cycle}}{\text{unit area of bed}} = \frac{\pi \rho z_o^2 \sqrt{\nu}}{\sqrt{2}} \left\{ \frac{2\pi}{T} \right\}^{3/2} \tag{34}$$

From the analysis presented in III

$$\frac{\text{energy dissipation/cycle}}{\text{unit area of bed}} = \bar{c}_{fa} \frac{2\pi^2}{3} \frac{\rho (2z_o)^3}{T^2} \tag{35}$$

Solving equations 34 and 35 for $\bar{c}_{fa}$ for oscillatory flow with a laminar boundary layer over an immobile smooth bed

$$\bar{c}_{fa} = \frac{3\sqrt{\pi \nu T}}{4 (2z_o)} \tag{36}$$

Determination of $\bar{c}_{fa}$ for oscillatory flow with a turbulent boundary layer over an immobile smooth boundary is certainly much more difficult and probably less accurate. The experimental studies of Kalkanis 3/ can be utilized for the determination of the coefficient of drag.

Because of the similarity of phenomena, that is, oscillatory flow over a duned bed and unidirectional flow over a duned bed, the results of the MIT study 1/ are also shown in figure 3. Even though the value of unidirectional-flow, drag-coefficient difference is greater than that determined for oscillatory flow, the trend of the results is the same.

Other comments about the experimentally determined results shown in figure 3 are given in the following. In order to interpret boundary drag in terms of bed geometry, dune amplitude as a function of $N_s$ is shown in figure 4, and the ratio of dune amplitude to dune wavelength is shown in figure 5.

The drag-coefficient difference between a mobile flat sand bed and an immobile smooth bed is nearly constant, that is, $\bar{c}_{fb} - \bar{c}_{fa} \approx 0.007$ for values of $N_s$ greater than 4. When $N_s$ is greater than 4, the particles on the surface of the bed are in motion. However, the most interesting question is unanswered -- is the boundary-drag coefficient with mobile particles greater than with immobile particles? The results of the MIT study 1/ are indicative that the boundary-drag coefficient with mobile surface particles is greater than with immobile surface particles. If $N_s$ is 13, the expectation is that the bed is essentially flat with the surface particles being in motion. Since the MIT results indicate a positive value of drag-coefficient difference when $N_s$ is 13, a mobile flat sand bed must exert a greater drag on the fluid above than an immobile flat sand bed does.

The difference between the two lower curves in figure 3 is the increase in drag coefficient because of the form drag of dunes as compared with a mobile flat sand bed. The form drag of the dunes does not exist if the

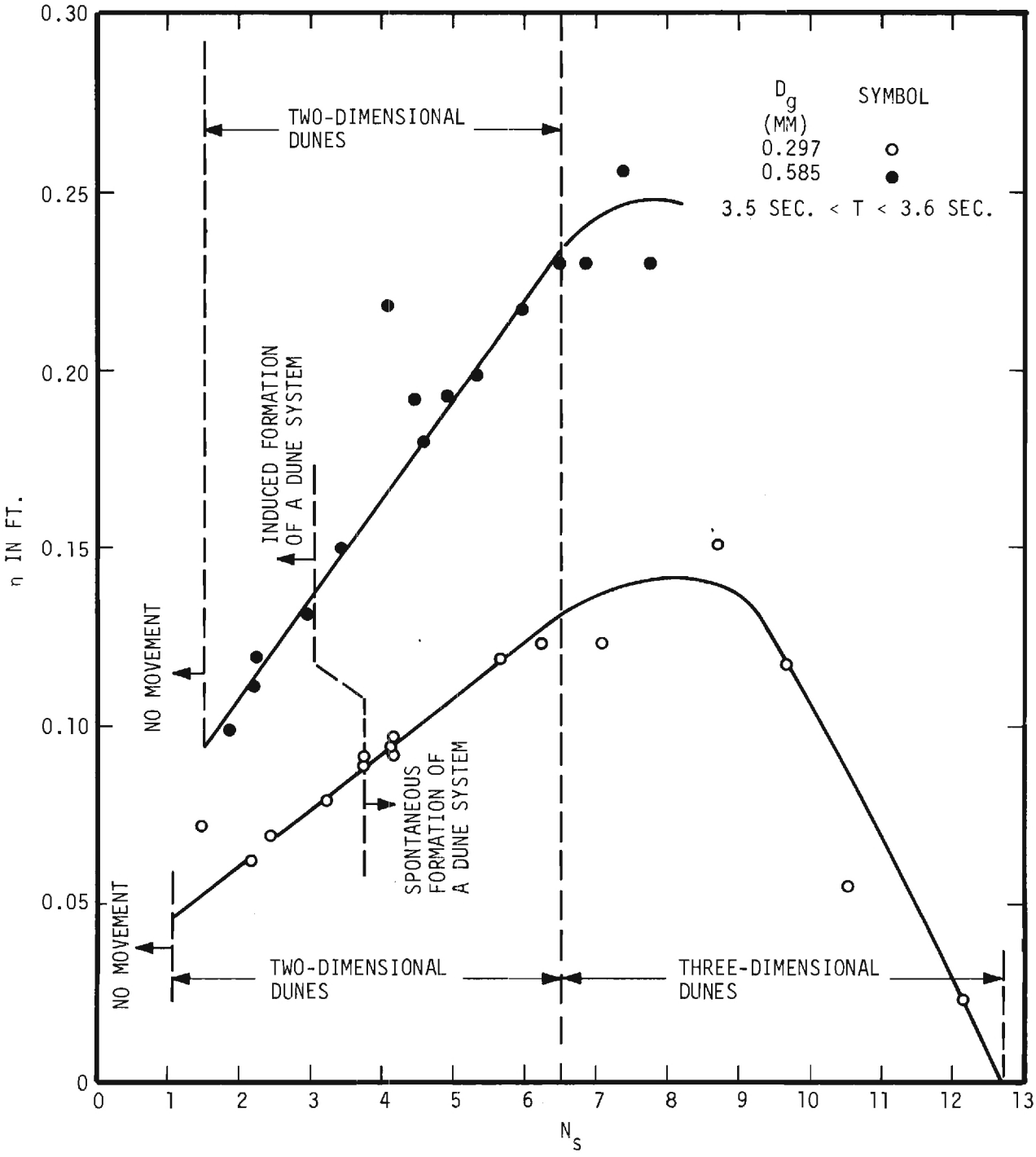


Figure 4. Dune Amplitude (Oscillatory Flow).

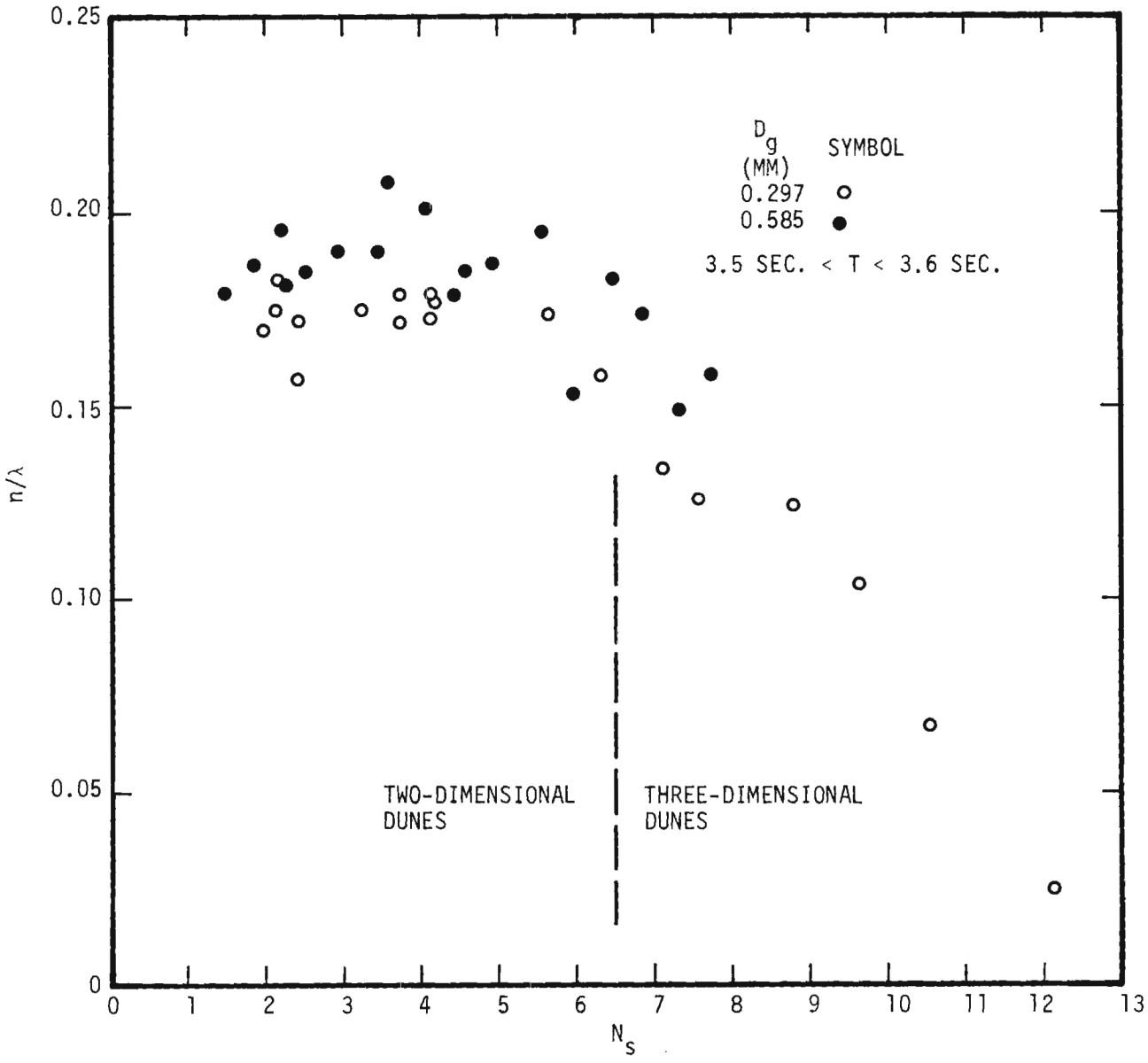


Figure 5. Ratio of Dune Amplitude to Wave Length (Oscillatory Flow).

value of $N_s$ is greater than about 11.5. The disappearance of the form drag at a value of $N_s$ of about 11.5 in figure 3 is in qualitative agreement with the disappearance of dunes at a value of $N_s$ of 12.7 as shown in figure 4.

A surprising feature of the form drag of dunes as shown in figure 3 is the lack of proportionality between form drag and dune amplitude as shown in figure 4. The maximum dune amplitude occurs at a value of $N_s$ of about 7.5. A corresponding maximum of form-drag coefficient at a value of $N_s$ of about 7.5 is not shown in figure 3. In fact, the form-drag coefficient appears to be largest at the smallest values of $N_s$. However, the scatter of the experimental results for $N_s < 4$ is too great to be conclusive on this point.

## REFERENCES


1/ A. M. Z. Alam, T. F. Cheyer, and John F. Kennedy, Friction Factors for Flow in Sand Bed Channels, Hydrodynamics Laboratory Report No. 78, Massachusetts Institute of Technology, Cambridge, Massachusetts, June 1966, 98 pages.

2/ H. Schlichting, Boundary Layer Theory, translated by J. Kestin, Pergamon Press, 1955 edition, pages 67 and 68.

3/ G. Kalkanis, Turbulent Flow near an Oscillating Wall, Beach Erosion Board Tech. Memo. No. 97, U. S. Army Corps of Engineers, July 1957, 35 pages.

# APPENDIX

## The Georgia Tech oscillating-flow water tunnel

# THE GEORGIA TECH OSCILLATING-FLOW WATER TUNNEL

M. R. CARSTENS, M. ASCE, Professor, School of Civil Engineering
Georgia Institute of Technology, Atlanta, Georgia

A water tunnel in which the water is oscillated with simple harmonic motion through the test section has been installed in the Georgia Tech Hydraulics Laboratory and has been in operation since January 1963. The principal purpose for constructing the water tunnel was to study various physical phenomena at the sea bed under a system of first-order Stokian waves. To date, the water tunnel has been used to study ripple (dune) formations and to study localized scour around objects resting upon the sea bed. Other potential uses are for the study of boundary-layer transition and for the determination of forces on submerged bodies such as piles. The only other similar water tunnel (to the writer's knowledge) is located at the Technical University of Denmark in Copenhagen.

## DESCRIPTION

The water tunnel is constructed as a large U-tube in which the bottom horizontal leg of the U is the test section as shown in Figures 1 and 2. The vertical legs of the U-tube are contained within steel tanks (A) which are 3 ft by 4 ft in cross section and are 11 ft tall. Streamlined flow passages are formed by inserts (C) fastened to the inner walls of the steel tanks. The water oscillates through the flow passage of the U-tube at the natural or resonant frequency. The free surface of the East leg, RHS of Figure 1, is utilized for water-surface-elevation measurement. The free surface of the West leg, LHS

of Figure 1, is utilized as a piston by which work is done on the oscillating system in an amount equal to the energy dissipated as the water moves back and forth through the U-tube.

The test section is 1 ft (vertical) by 4 ft (horizontal) in cross section and is 10 ft long. The roof and sidewalls are fabricated of 1/2-in transparent plastic and are framed on the exterior with steel angles and channels. A 3-ft square flush-mounted hatch is located in the center of the roof as an access into the test section. The central section of the floor is depressed in order to provide a container for erodible bed material. The depressed section is 6 ft long by 4 ft wide by 4 in deep. The entire test section rests upon three pre-fabricated steel trusses which span between the steel tanks.

The water in the U-tube is made to oscillate at the resonant frequency by applying a pressure pulse on the water surface in the West leg during the time the water surface is falling in that leg. The output of a centrifugal blower is discharged continuously in the air space above the water surface. Two 7 in diameter, pneumatically powered, poppet valves (E) in the top of the West leg are open except for a time during which the water level is falling in the West leg. The feedback mechanism by which the exhaust valves are sequentially operated is initiated by the change of direction of the water surface in the East leg. A float (F) in the East leg is attached to a steel rod (G) by means of a light flexible cable. The steel rod (G) slides easily past a permanent magnet which operates a microswitch. The combination of the steel rod, the magnet, and the switch constitute a direction-sensing switch (H). Whenever the steel rod (G) is falling the switch (H) is closed and vice versa. The closing of the switch (H) actuates a single-cycle timer. This timer makes one revolution in 2 seconds and then stops. A second microswitch is contained within the timer unit. By

means of an adjustable cam this second microswitch can be made to close during any portion of the two-second interval. Solenoid valves which control the pneumatically operated pistons on the exhaust valves are in the circuit with the timer microswitch. The timer microswitch is set such that the exhaust valves close when the timer starts and remain closed for about one-quarter cycle.

Initial and final transients of the oscillatory motion are eliminated by means of the blowdown and damping valve (I) in the East leg. The blowdown and damping valve is an 8 in diameter, pneumatically powered, poppet valve (I). In order to eliminate the initial transient, the blowdown valve (I) is closed and air is forced into the tank through (K). The water surface is forced downward to the desired equilibrium amplitude at which time the operator switches to the "run" position. As the operator switches to "run" the blowdown valve (I) opens, the air supply through air inlet (2) is stopped, and control of the tunnel reverts to the feedback mechanism described above. The terminal transient at the end of a run is eliminated by simply closing the damping valve (I). To start a run, the operator turns the masterswitch to "blowdown." When the water surface in the East leg is depressed to equilibrium amplitude, the operator turns the masterswitch to "run." To end a run, the operator turns the masterswitch to "stop."

## VARIABLES

Since the tunnel is designed to operate at the resonant frequency of the water mass, only small changes in the period of the motion are possible without altering the flow passages. The tunnel was designed to be operated at different frequencies by changing the upper inserts (C) within the steel tanks.

Up to the present time only one set of inserts has been fabricated forming flow passages in the vertical legs which are 1 ft by 4 ft in cross section. With a normal water level the period of oscillation is 3.56 sec. By filling the tunnel to higher-than-normal level a period of 3.79 sec has been attained. By filling the tunnel to lower-than-normal level a period of 3.30 sec has been attained.

Total amplitude of the motion can be varied from 0 to 36 in by adjusting the magnitude of the pressure pulse which is applied to the water surface in the West leg of the U-tube. This pressure adjustment is accomplished by control of the angular velocity of the blower. By means of a mechanically variable V-belt drive, the blower can be operated at any speed from 400 to 3600 rpm. The motor, speed changer, and blower are shown in the foreground of Figure 2.

## INSTRUMENTATION

The kinematics of the water are determined from the water-surface level in the East leg. The float-elevation sensor system consists of a small-diameter, stainless-steel cable which passes over 6-in diameter pulleys at the top and bottom of the East leg. The spring-tensioned endless cable is fastened to the wooden float (F). A three-turn potentiometer is connected to the axle of the upper pulley. The potentiometer is series connected in one leg of a Wheatstone bridge. Bridge unbalance is amplified and recorded by means of a Sanborn direct-writing oscillograph. The float-elevation sensor system is calibrated just before and just after a run by making short records at several elevations of the float. An example of the recorded motion curve is the uppermost trace in Figure 3. In addition to the continuous measurements of float-level, the maximum and minimum levels can be directly read from the position of the steel rod (G) which has a stationary scale fastened parallel to the rod.

A dual system of time measurement is provided. A timing marker in the recorder produces pips at one-second intervals as shown by the lowermost trace in Figure 3. In addition, an electrically operated digital counter is placed in the circuit with the direction-sensing switch (H). The readout of the counter is the integer number of cycles since the beginning of a run.

Work input to maintain the oscillation is calculated from the water-motion curve and the measured air pressure in the volume above the water surface in the West leg. Pressure measurement is accomplished by means of a Statham pressure transducer ($\pm$ 0.15 psid). Bridge unbalance in the transducer is amplified and recorded. The pressure measuring and recording system is calibrated just before and just after a run by making short records at several pressures applied to the transducer diaphragm. The middle trace in Figure 3 is the pressure record.

Additional measurements of phenomena within the test section have been measured and recorded by optical devices. Photographs through the transparent sidewall and coordinate grid have been used extensively for the measurement of ripple (dune) geometry. Figure 4 is a photograph of a ripple system developed in the tunnel. A cathetometer has been employed to determine and record the scour depth in localized-scour studies involving objects resting on the bed. For this purpose, the telescope of the cathetometer was attached to a traversing mechanism such that an observer can raise or lower the telescope by turning a crank. The telescope was attached to a differential transformer which served as a transducer for the recording of the elevation of the telescope axis by means of a direct-writing oscillograph.

Plans are being formulated to incorporate a force-transducer system for the measurement of forces on bodies which are submerged in the oscillatory flow.

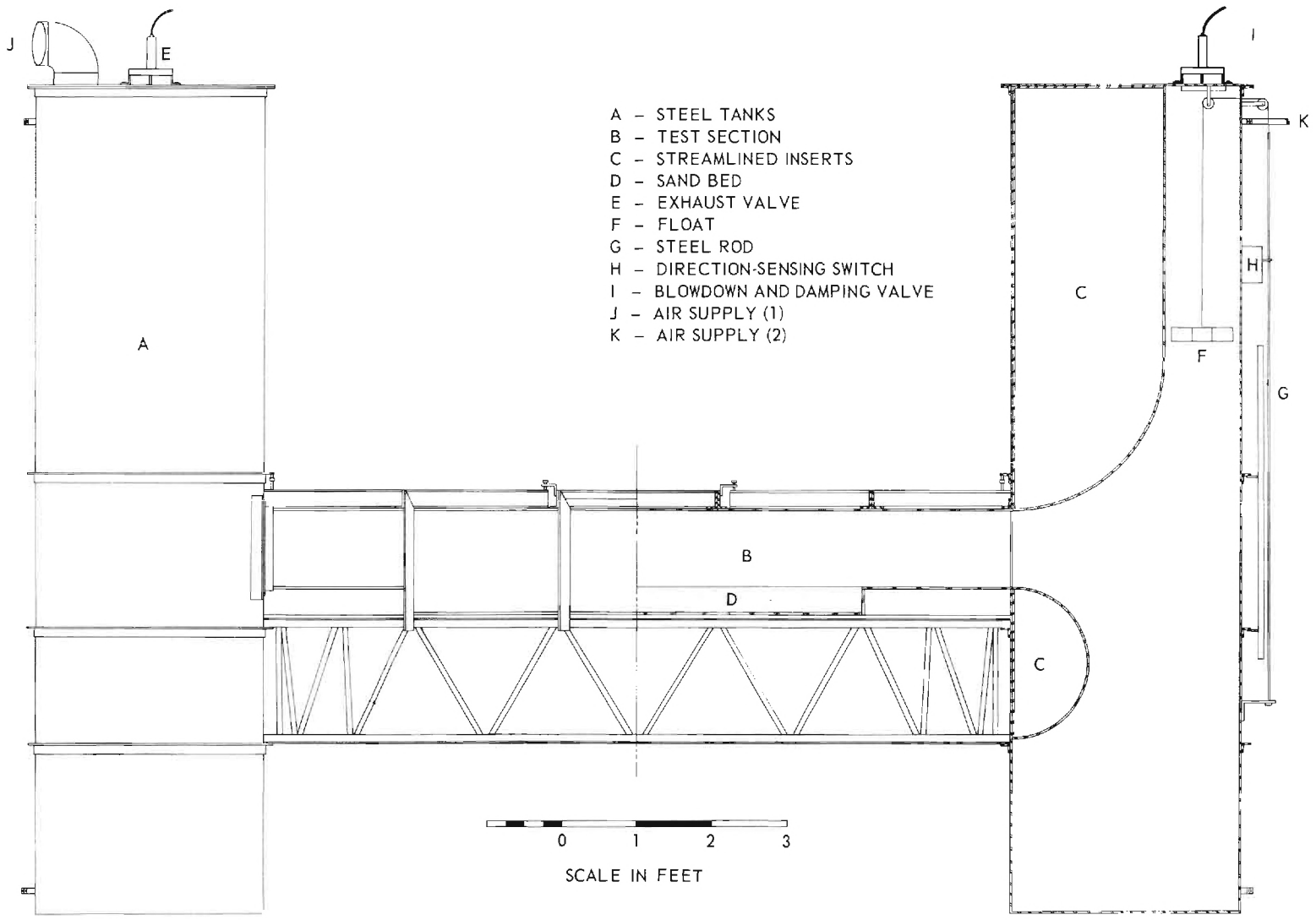


Figure 1. Side Elevation of Oscillatory-Flow Water Tunnel.

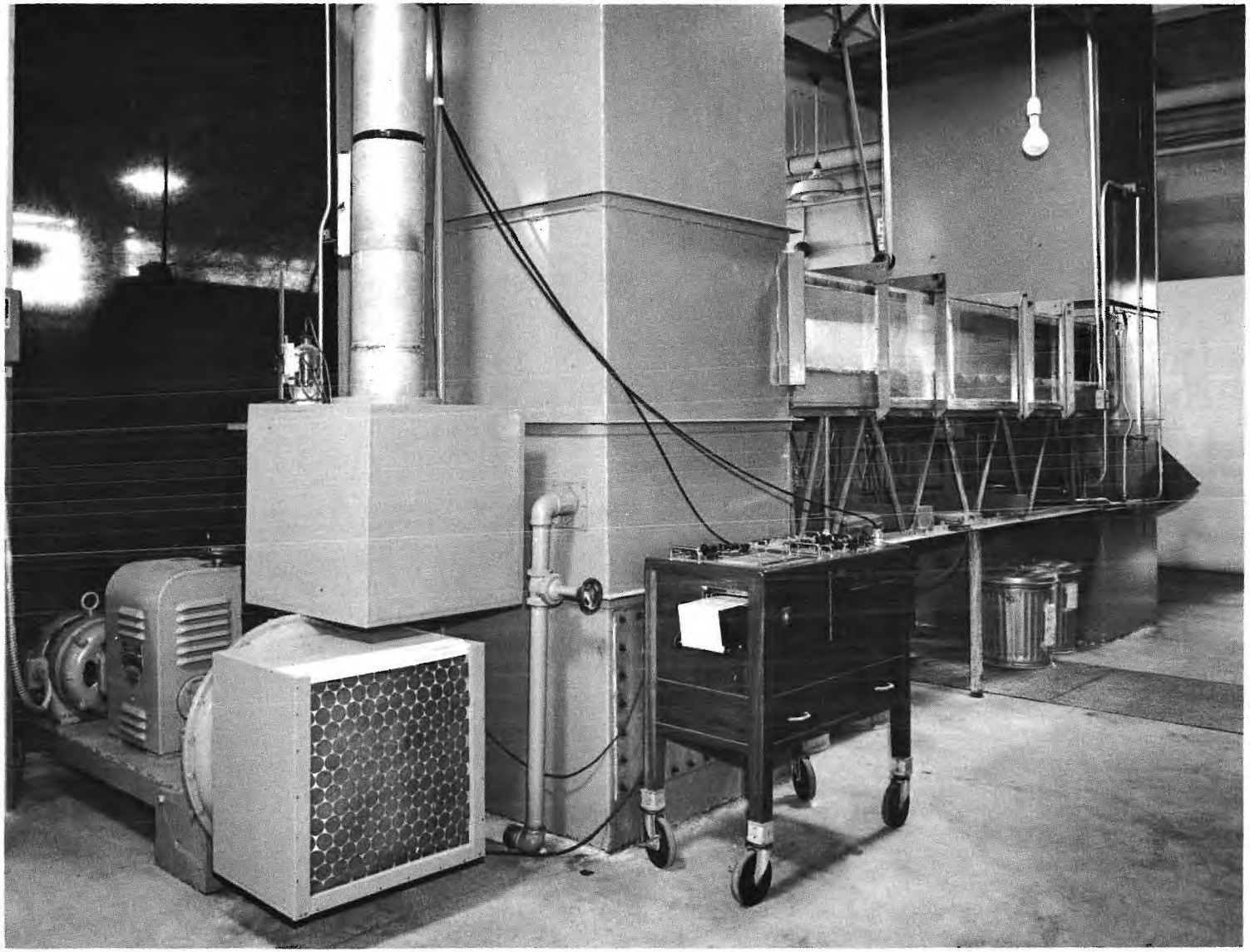

Figure 2. Photograph of Oscillatory-Flow Water Tunnel.

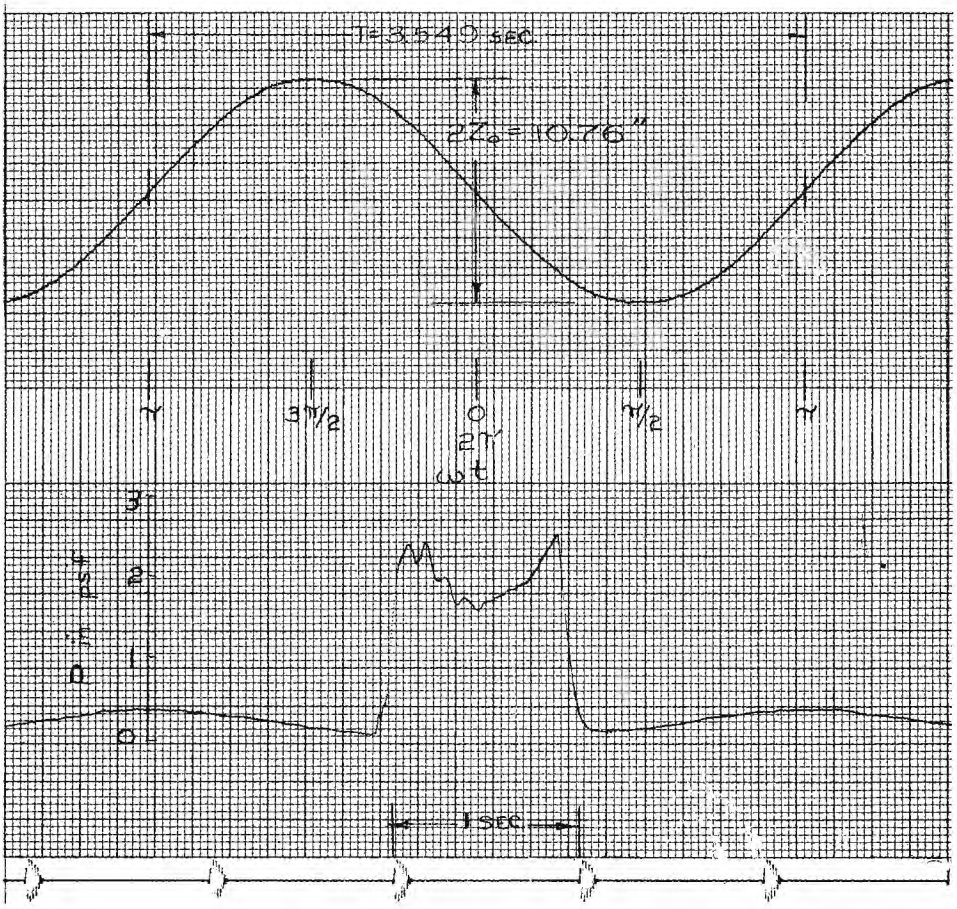


Figure 3. Record of Motion, Pressure Input, and Time.

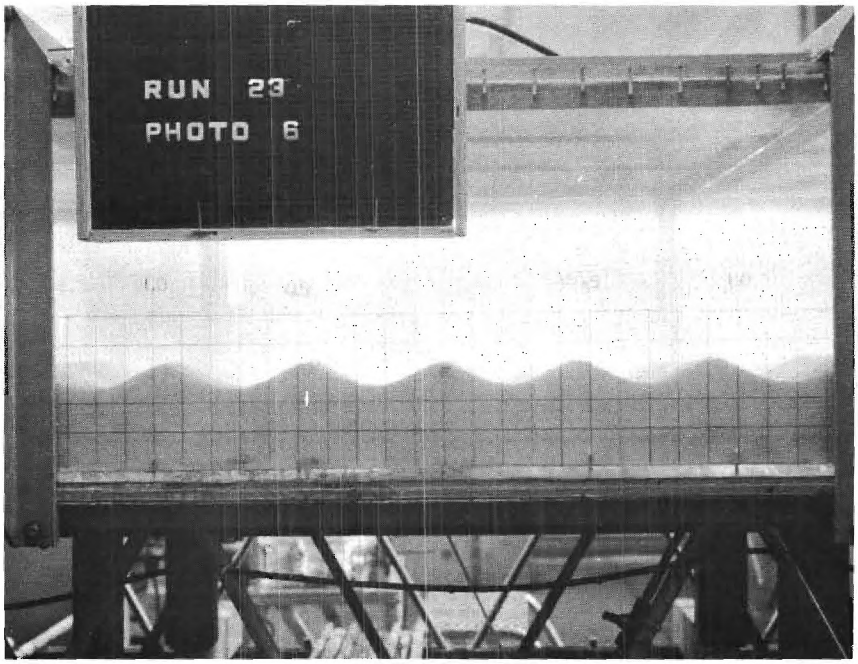


Figure 4. Dune Pattern.

QUARTERLY REPORT 11

PROJECT A-798

# AN ANALYTICAL AND EXPERIMENTAL STUDY OF BED RIPPLES UNDER WATER WAVES

M. R. CARSTENS AND H. D. ALTINBILEK

Contract No. DA-49-055-CIVENG-65-1

1 January to 31 March 1967

Prepared for
Department of the Army
Coastal Engineering Research Center
Washington, D. C.


Engineering Experiment Station
GEORGIA INSTITUTE OF TECHNOLOGY
Atlanta, Georgia

GEORGIA INSTITUTE OF TECHNOLOGY
School of Civil Engineering
Atlanta, Georgia

QUARTERLY REPORT 11

PROJECT A-798

# AN ANALYTICAL AND EXPERIMENTAL STUDY OF BED RIPPLES UNDER WATER WAVES

By

M. R. CARSTENS AND H. D. ALTINBILEK

CONTRACT NO. DA-49-055-CIVENG-65-1

1 JANUARY to 31 MARCH 1967

Prepared for
DEPARTMENT OF THE ARMY
COASTAL ENGINEERING RESEARCH CENTER
WASHINGTON, D. C.

TABLE OF CONTENTS

LIST OF FIGURES

## GLOSSARY

| Symbol | Definition | Units |
|---|---|---|
| $A$ | cross sectional area of water tunnel | $ft^2$ |
| $\bar{c}_{fb}$ | mean boundary drag coefficient (flat sand bed) | — |
| $\bar{c}_{fc}$ | mean boundary drag coefficient (duned bed) | — |
| $D_g$ | geometric mean diameter of bed material | mm |
| $E$ | energy | ft-lb |
| $L$ | length of sand-bed test section | ft |
| $N_s$ | sediment number, $U_m/\sqrt{(s-1)g\ D_g}$ | |
| $p$ | pressure | $lb/ft^2$ |
| $Q$ | discharge | $ft^3/sec$ |
| $s$ | ratio of density of bed material to fluid | — |
| $T$ | period of oscillation | sec |
| $t$ | time | sec |
| $U$ | mean velocity in test section | ft/sec |
| $U_m$ | maximum value of mean velocity | ft/sec |
| $WI$ | work-input into tunnel per cycle | ft-lb |
| $2z_o$ | total water-motion amplitude in test section | ft or in |
| $\gamma$ | specific weight of water | $lb/ft^3$ |
| $\Delta$ | difference in value | — |
| $\lambda$ | wave length of dunes | mm |
| $\eta$ | amplitude of dunes, trough to crest | mm |
| $\sigma_g$ | geometric standard deviation | — |

# I. INTRODUCTION

The more recent experiments involve three modifications of the experiments reported in Quarterly Reports 1, 6, 7, and 10. The modifications are as follows: (a) the bed material has been changed to fine sand, (b) topographic maps are being made of the duned bed, and (c) additional pressure-time measurements are being made within the test section. The modifications in the experimental program are discussed in this report.

## II. BED MATERIAL

The bed material used in the current tests is "banding sand" obtained from the Ottawa Silica Company of Ottawa, Illinois.

### A. Size

Size of the sand was determined by sieve analysis using 8-inch diameter U. S. Standard sieves following the procedures recommended by Vanoni, Brooks, and Kennedy 1/. The results of a sieve analysis of a random sample are given below

| U. S. Standard Sieve No. | Grams Retained |
|---|---|
| 40 | 0.67 |
| 50 | 0.91 |
| 70 | 6.73 |
| 100 | 9.18 |
| 140 | 3.78 |
| 200 | 0.88 |
| Pan | 0.18 |
| | total sample 22.33 gr |

The cumulative size distribution is shown in figure 1. From figure 1, the geometric-mean sieve diameter, $D_g$, is found to be 0.190 mm and the geometric standard deviation, $\sigma_g$, is found to be 1.35 2/.

### B. Specific Gravity

Specific gravity of the banding sand was determined by weighing a graduated cylinder. The weight of the graduated cylinder partially filled with distilled water was determined before and after sand was added. The measured and computed values are tabulated below

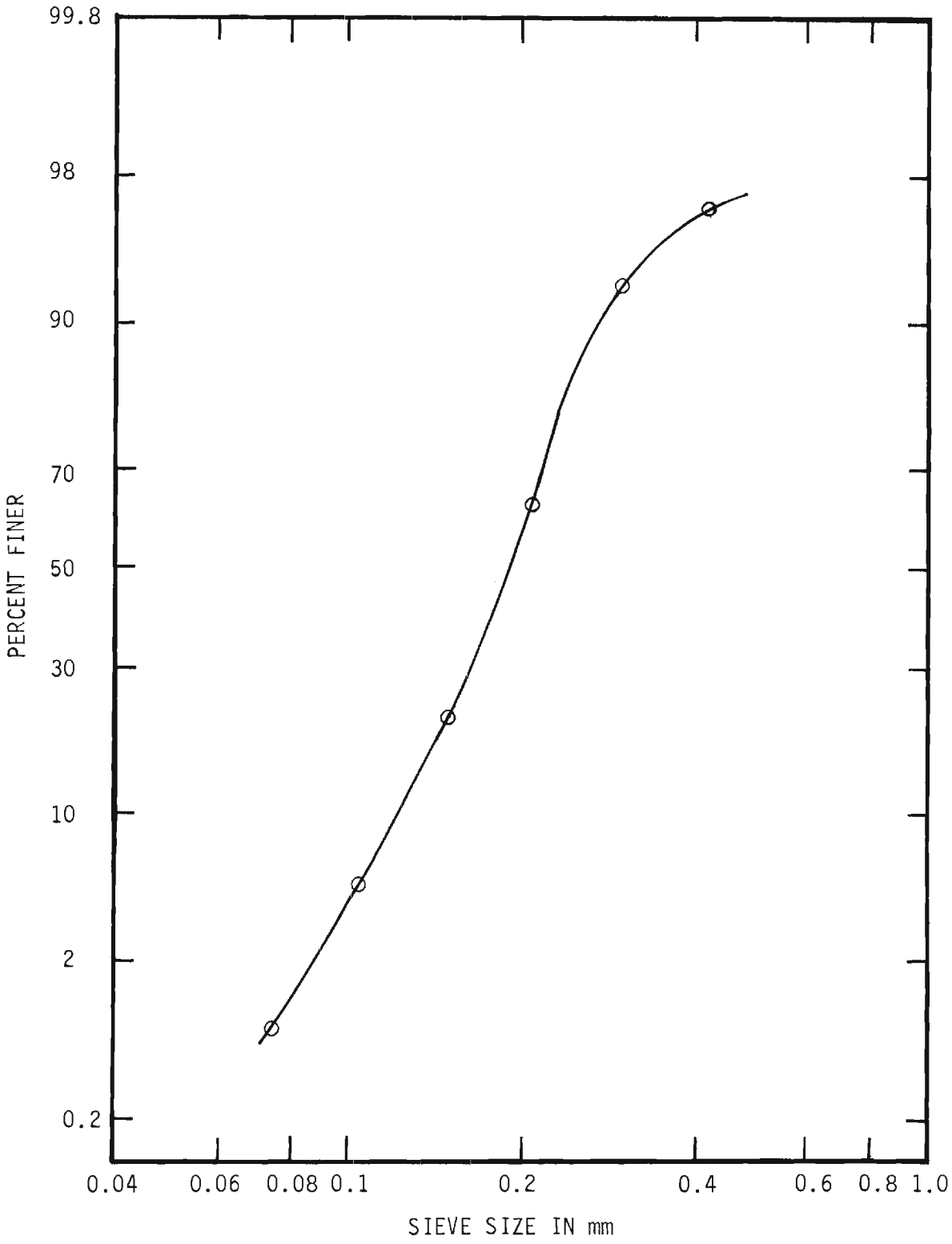


Figure 1. Cumulative Logarithmic Probability Size-frequency Distribution.

| Item | Determination 1 | 2 | 3 |
|---|---|---|---|
| Volume of water (cc) | 60.0 | 60.0 | 70.0 |
| Volume of sand and water (cc) | 81.0 | 82.0 | 94.0 |
| Wt. of cylinder and water (gr) | 100.00 | 0 | 0 |
| Wt. of cylinder, water and sand (gr) | 155.84 | 58.8 | 63.25 |
| Temperature (°C) | 25 | 25 | 25 |
| $\gamma_s$ (gr/cc) | 2.66 | 2.67 | 2.64 |
| $\gamma$ (gr/cc) | 0.996 | 0.996 | 0.996 |
| $s = \gamma_s/\gamma$ | 2.67 | 2.68 | 2.64 |

## III. TOPOGRAPHIC MAPPING OF THE BED

The amplitude, $\eta$, and the wave length, $\lambda$, of the dunes are quite satisfactory measures of bed geometry for a two-dimensional system of dunes but are an inadequate description of bed geometry for a three-dimensional system of dunes. Recognition of this inadequacy during the tests with the medium sand ($D_g = 0.297$ mm) led to the decision to prepare topographic maps of the bed during the tests with the fine sand ($D_g = 0.190$ mm).

In order to map the bed after a run, instrument rails have been mounted above the test section such that an instrument carriage can be accurately positioned in the axial direction over the 3-ft square hatch opening in the roof of the test section. An electrical point gage is mounted on the instrument carriage such that the point gage can be accurately positioned in the transverse direction. The electrical point gage gives excellent response upon contact with the moist-sand bed. Because of the careful fabrication of the instrument carriage and the careful levelling of the instrument rails (from a water surface), the belief is that all coordinate measurements can be readily determined within ±1 mm of the true value.

Figure 2 is the topographic map of the bed obtained after the cessation of Run 85. Upon cessation of Run 85 after 3500 cycles of oscillation, the water was slowly drained from the water tunnel in order to avoid any change in the dune system. The roof hatch was removed from the test section. In the interim period of six days between the end of the run and the measurement of bed coordinates, the bed was kept moist by intermittently pumping water into one corner of the bed. Elevations of the bed were determined at the grid points

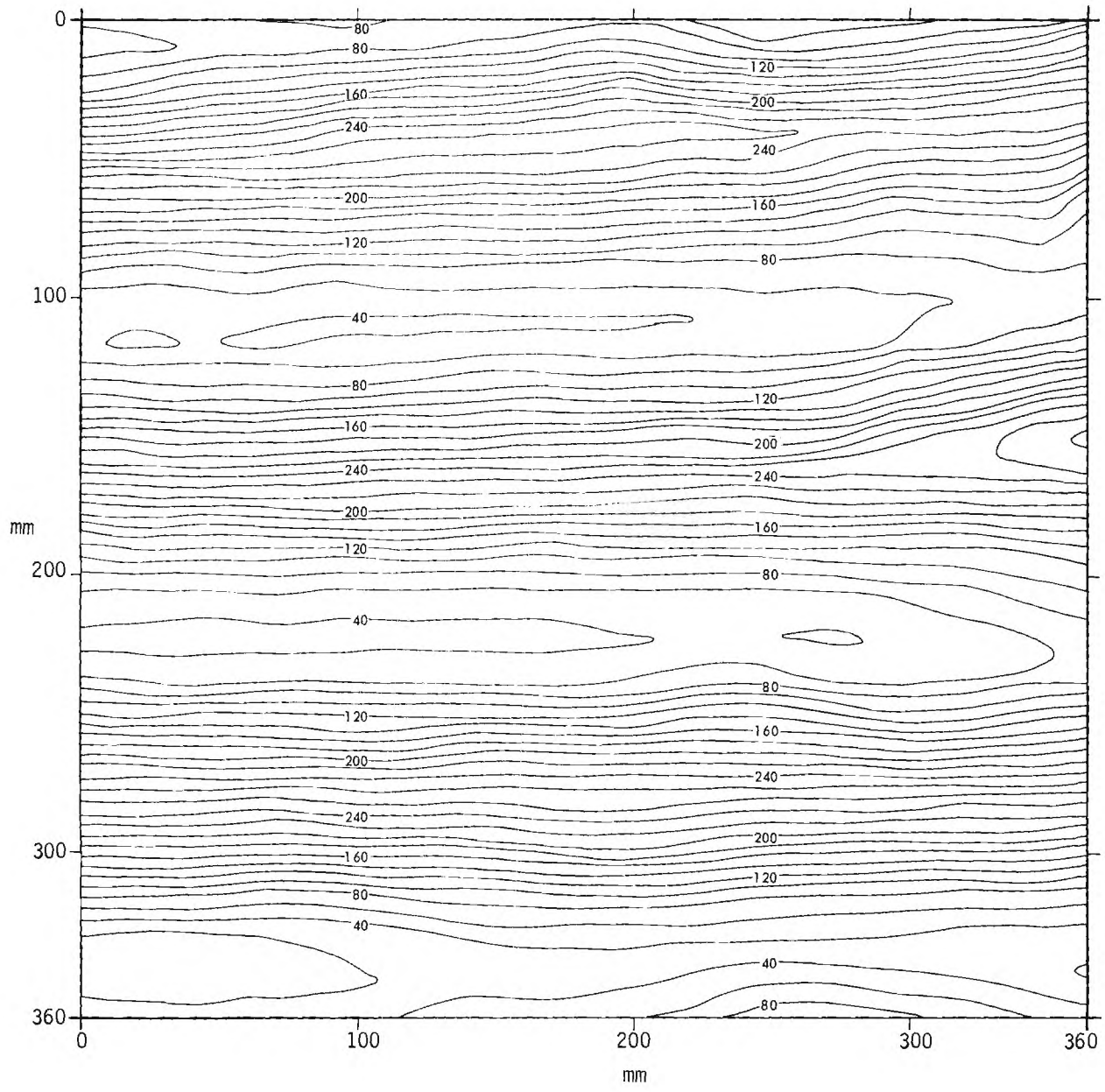


Figure 2. Topographic Map of Bed (Run 85).

of a horizontal rectangular grid. The grid lines were spaced at 1.00-in intervals across the test section and at 0.050-ft intervals along the test section.

The total amplitude of the water motion in Run 85 was maintained within a range from 6.7 in to 7.2 in by manual correction of the blower speed. In all prior tests with the medium ($D_g$ = 0.297 mm) and coarse ($D_g$ = 0.585 mm) sands, the total water-motion amplitude had been allowed to decrease as the dunes (bed resistance) developed from the initially flat bed. The period of the motion was 3.61 seconds. The sediment number, $N_s$, which has been used as a parametric index had a value of 2.8 in Run 85.

From figure 2 the mean amplitude, $\eta$, of the dunes is 21.0 mm and the mean wave length, $\lambda$, is 116 mm. The ratio, $\eta/\lambda$, is 0.181. This value of $\eta/\lambda$ compares favorably with the value of 0.19 obtained with the 0.585-mm Ottawa sand and with the value of 0.18 obtained with the 0.297-mm glass beads.

## IV. ENERGY DISSIPATION

In the earlier experiments with the coarse and medium sand, energy dissipation was evaluated by measuring the work-input into the water tunnel as explained in Quarterly Report 10. The difference in work input between the duned-bed condition and the flat-bed condition is the additional energy dissipation resulting from the dunes. The work input was measured for two flat-bed conditions, that is, a smooth flat bed of polished aluminum sheet and a mobile flat-bed of 0.297-mm glass beads. This scheme of determining energy dissipation has a serious drawback in that the energy dissipation resulting from the duned bed must be determined from the difference in two work inputs into the tunnel. Since the total energy dissipation within the tunnel includes a much greater length of flow passage than just the 6-ft length of test section of interest, the two work inputs between which the difference has to be obtained are of comparable magnitude resulting in a loss of significant figures.

In order to obtain an independent evaluation of energy dissipation, the scheme was devised to measure the pressure gradient within the test section immediately above the sand bed and to synchronize the measured pressure gradient with the water motion in the tunnel. A description of the added equipment, method of operation, and experimental results are presented.

### A. Equipment added to the tunnel

In order to measure the pressure gradient within the test section, two piezometers are installed in the north wall of the test section as shown in figure 3. The piezometers are located only 2 inches below the roof in order to avoid the local flow non-uniformities in the vicinity of the dunes. The differential pressure is sensed and transduced by means of a Pace Model KP 15

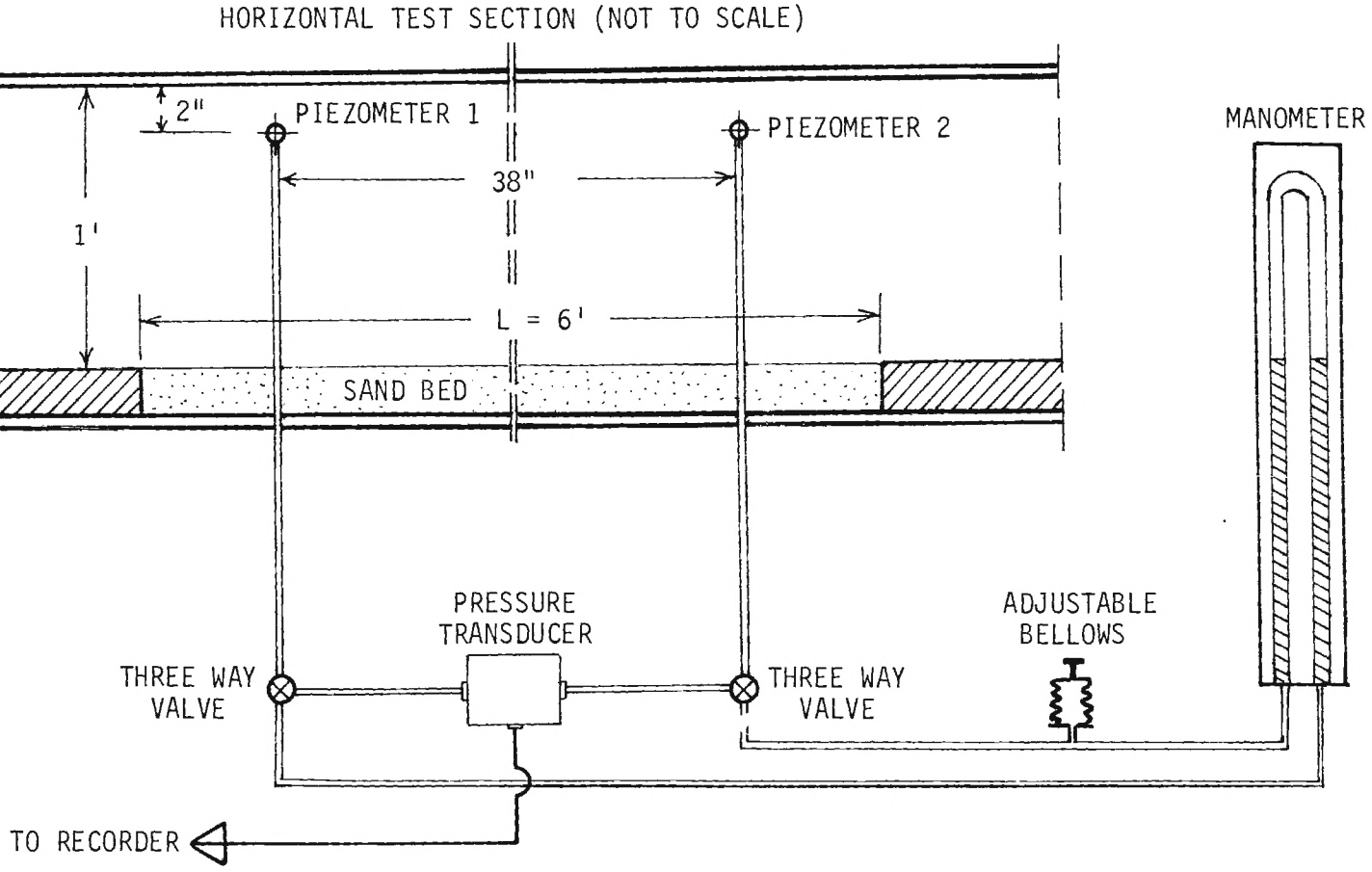


Figure 3. Arrangement for Measurement of the Pressure Gradient in the Test Section.

pressure transducer. The pressure transducer is incorporated in the circuity of one channel of a two-channel direct-writing oscillograph. The three-way valves and manometer shown in figure 3 are for calibration of the pressure-transducer circuit.

B. The data

The data for a determination of the energy dissipation within the test section consists of (a) calibration curves for the float gage in the east leg of the water tunnel and for the pressure transducer and (b) a synchronized time record of float-gage elevation, pressure difference and time.

The calibration of float-gage elevation versus recorder-stylus deflection is performed just before and just after each run as explained in Quarterly Report 1. The float-gage calibration curves of Run 95 are shown in figure 4. A positive value of float position in figure 4, is associated with a higher water level in the right leg (figure 3) than in the left leg (figure 3).

The calibration of pressure difference versus recorder-stylus deflection is also performed just before and just after each run. At the time of calibration, the tunnel is filled with water. The three-way valves are positioned to connect the pressure transducer, figure 3, with the piezometers. Then the chambers on both sides of the transducer are bled through a small opening in each chamber. The valves are then positioned to connect the manometer with the piezometers. A valve is opened at the top of the differential manometer thereby bleeding the connecting lines. Next air is forced into the top of the manometer until the water levels are about at mid-scale of the manometer. Then the valve at the top of the manometer is closed. Next both three-way valves are switched to connect the manometer with the transducer. The water-filled bellows is adjusted until the water columns in the manometer are equal in

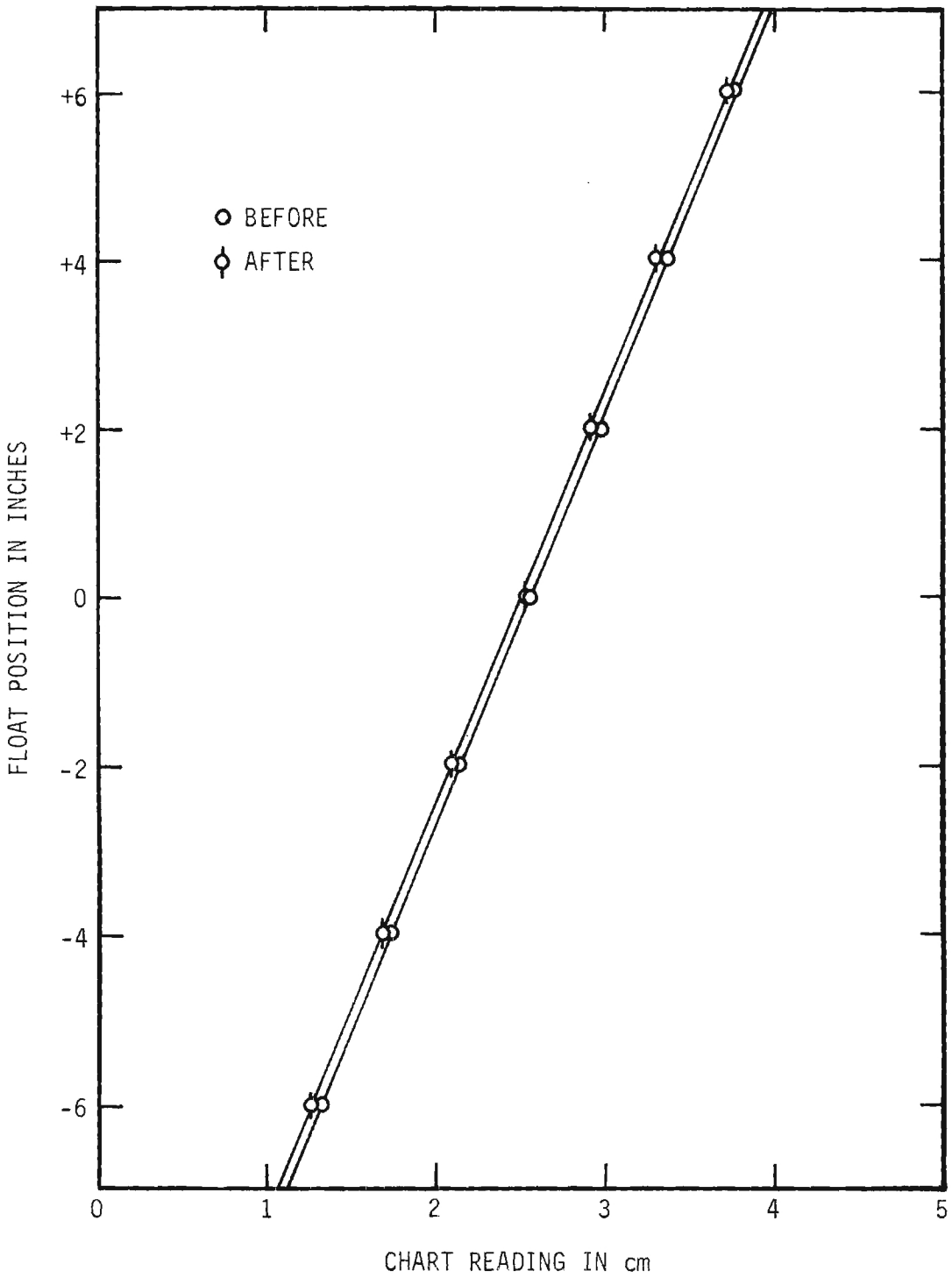


Figure 4. Calibration of the Float-position Recording System (Runs 91 - 95, incl.).

elevation. In this condition the pressure difference across the pressure transducer is zero. The transducer circuit is balanced and the recorder stylus is zeroed at approximately midposition on the recorder paper. Various pressure differences can be applied by means of the adjustable bellows. Recordings are made at numerous settings of the bellows with the pressure difference being read on the manometer. The calibration curve of Run 95 is shown in figure 5. The subscripts on the pressure terms refer to the piezometer number shown in figure 3.

A portion of the strip-chart data of Run 95 is shown in figure 6. The top trace is that of float elevation, the middle trace is that of pressure difference, and the bottom trace is time with 1-sec pip intervals.

C. Analysis of data

The flow situation within the test section can be understood through an understanding of figure 6. For clarity, the positive direction of the pressure force, $(p_1 - p_2)A$, and velocity, U, are taken to be from left to right in figure 3. The maximum velocity, $U_m$, occurs when the float gage is at midposition. The direction of $U_m$ is noted by the arrows in figure 6. The velocity lags the pressure force by nearly 90 degree or $\pi/2$ radians. In other words, the pressure force is nearly in phase with acceleration.

As derived in Quarterly Report 10, the work input per cycle into the control volume within the test section is given by

$$\int_t^{t+T} (p_1 - p_2)\, A\, U\, d\, t \qquad (1)$$

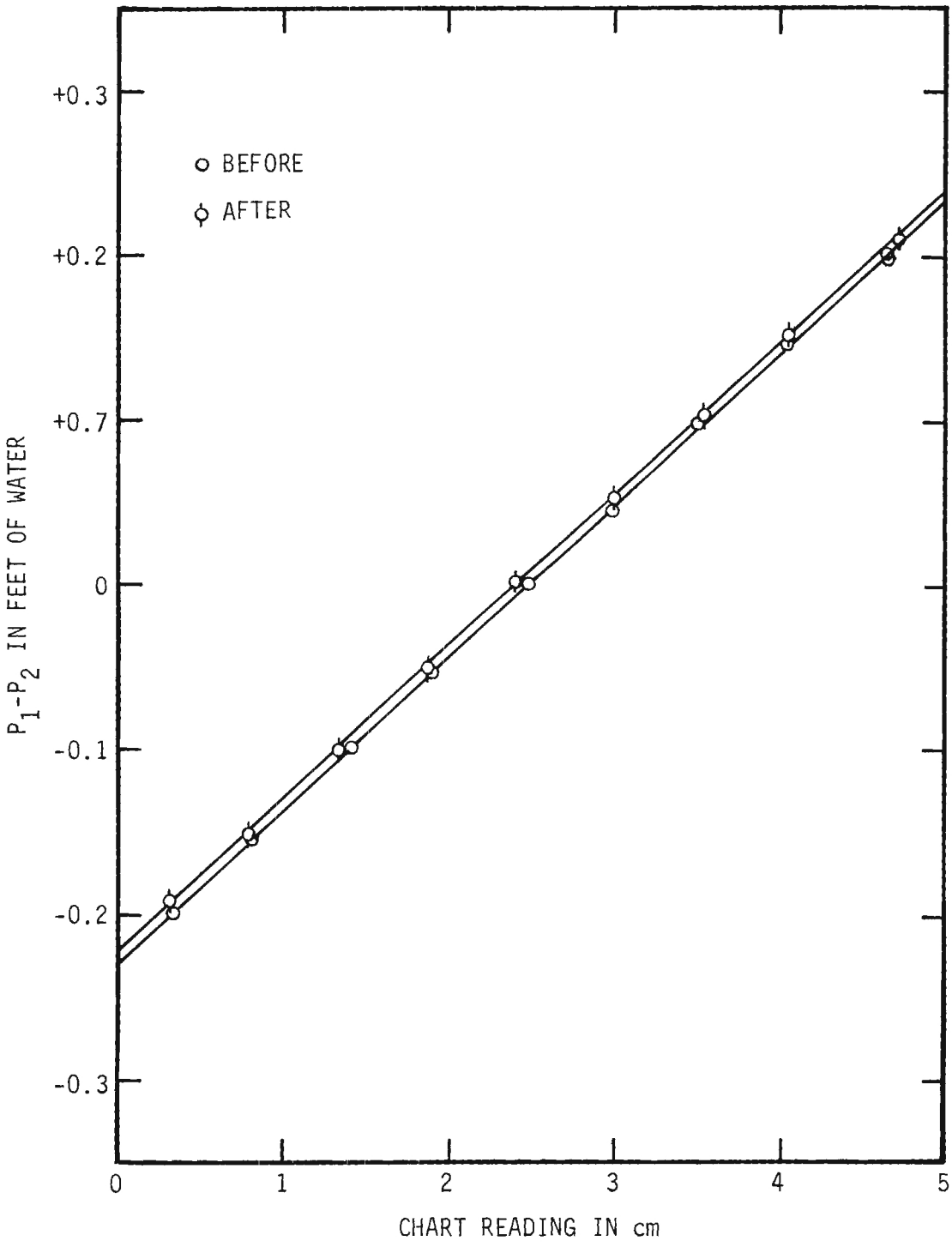


Figure 5. Calibration of the Pressure-difference Recording System (Runs 91 - 95 incl.).

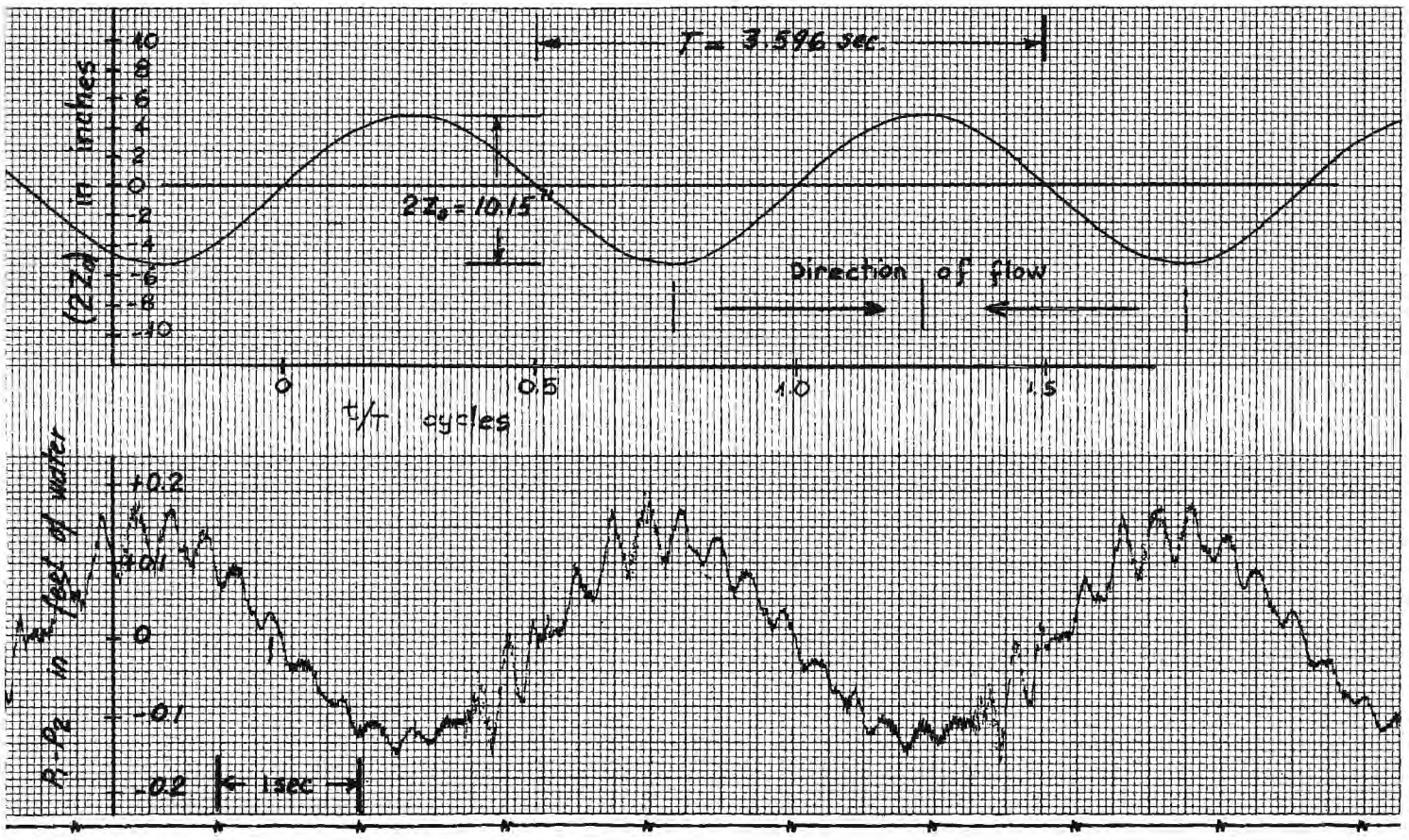


Figure 6. Strip-Chart Data (Run 95).

in which T is the period. Since the motion is simple harmonic, the work-input integral simplifies as follows

$$Az_o \int_o^{2\pi} (p_1 - p_2) \cos \frac{2\pi t}{T} \quad d\left(\frac{2\pi t}{T}\right) \qquad (2)$$

Work input per cycle was evaluated by numerical integration of the above equation. Numerical integration was by means of the trapezoidal rule using small increments of $\Delta(t/T)$. Great care has to be exercised in determining the location of $t/T = 0$ on the strip-chart record of float position, figure 6. In order to increase accuracy, actual determinations are made on longer strip chart data where 1 second interval is 100 mm long. The results are tabulated below

| Run No. | Bed Condition | $2z_o$ (in) | Temp (°F) | T (sec) | Work input/cycle (ft-lb/cycle) |
|---|---|---|---|---|---|
| 86 | Dunes (c) | 6.86 | 68.5 | 3.60 | 1.206 |
| | | | | | 1.321 |
| 88 | Flat sand (b) | 4.03 | 64.0 | 3.596 | 0.078 |
| | | | | | 0.095 |
| | | | | | 0.067 |
| 89 | Flat sand (b) | 5.48 | 64.0 | 3.590 | 0.478 |
| 90 | Flat sand (b) | 7.69 | 63.5 | 3.591 | 0.894 |
| | | | | | 0.875 |
| 91 | Flat sand (b) | 9.66 | 63.5 | 3.605 | 1.230 |
| | | | | | 1.550 |
| 93 | Flat sand (b) | 6.35 | 68.4 | 3.596 | 0.876 |
| | | | | | 0.660 |
| 95 | Flat sand (b) | 10.24 | 69.0 | 3.576 | 2.053 |

The results tabulated above are shown graphically in figure 7.

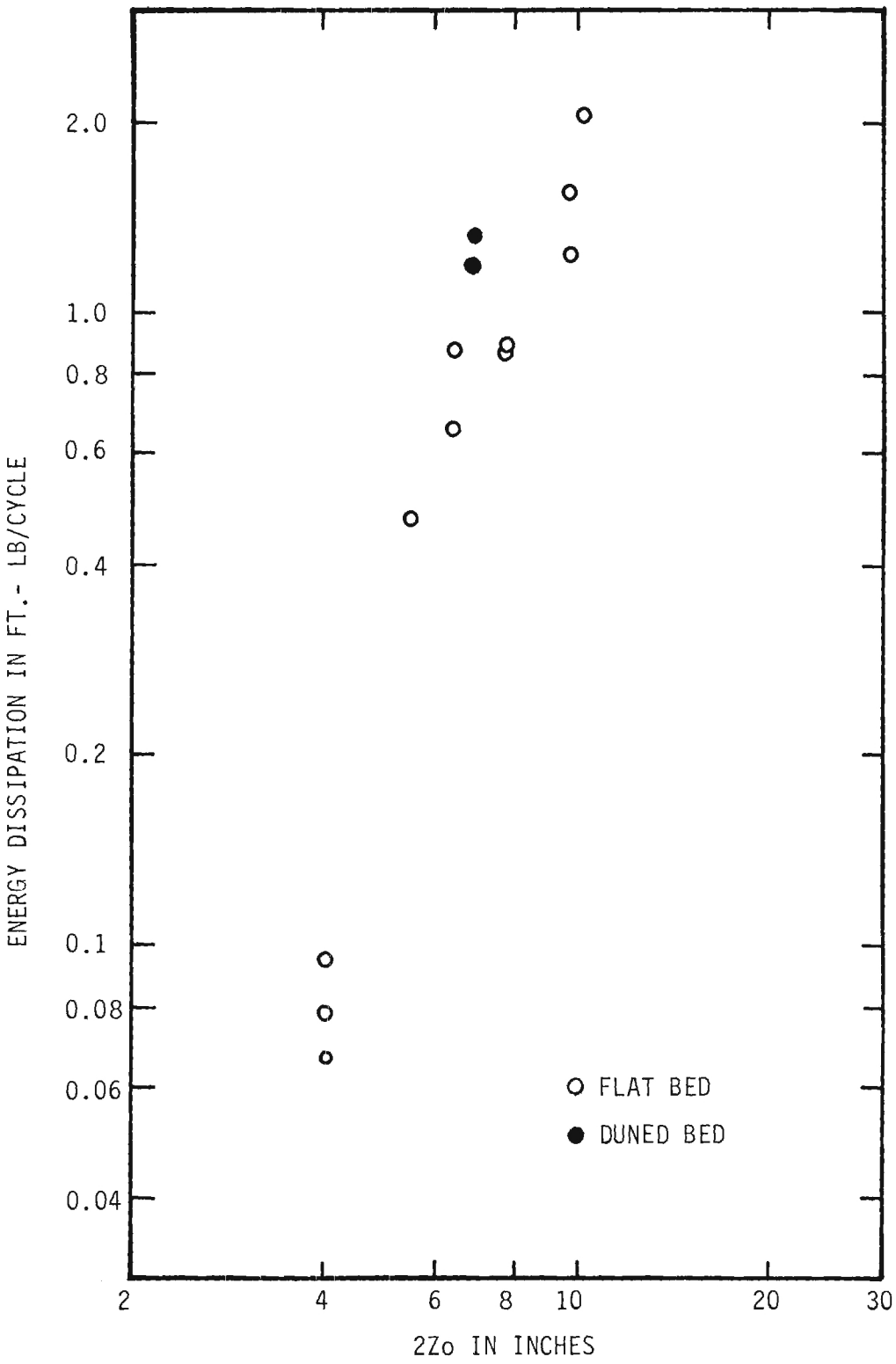


Figure 7. Energy Dissipation in Test Section (Bed Area = 12.7 ft.$^2$).

The difference in boundary-drag coefficients is formulated in Quarterly Report 10 as follows

$$\bar{c}_{fc} - \bar{c}_{fb} = \frac{3}{2\pi^2} \frac{T^2}{\rho(2z_o)^3_{BL}} [\Delta E] \qquad (3)$$

The difference in energy dissipation per cycle, $\Delta E$, between the duned bed (c) and the flat sand bed (b) is about 0.48 ft-lb/cycle in figure 7 (Run 86). The difference in the boundary-drag coefficients, $\bar{c}_{fc} - \bar{c}_{fb}$, is 0.21. This value compares favorably with that obtained with the coarse and medium sand.*

---

* A numerical error was found in Quarterly Report 10. All of the numerical values in Column 12 of TABLES III and IV should have been multiplied by 10.93. Figure 3 of Quarterly Report 10 is also in error for the same reason. Corrected copies of pages 12, 13, 15, 16, and 24 have been prepared and are being sent with this report.

## REFERENCES


1/ Vito A. Vanoni, Norman H. Brooks, and John F. Kennedy, Lecture Notes on Sediment Transportation and Channel Stability, Report No. KH-R-1, California Institute of Technology, Pasadena, California, January 1961, Appendix 3A, p. 3-20.

2/ "Sediment Transportation Mechanics: Inroduction and Properties of Sediment", Proc, ASCE, Journal of the Hydraulics Division, Vol. 88, No. HY4, July 1962, p. 98.

QUARTERLY REPORT 12

PROJECT A-798



# AN ANALYTICAL AND EXPERIMENTAL STUDY OF BED FORMS UNDER WATER WAVES

By
M. R. CARSTENS

CONTRACT NO. DA-49-055-CIVENG-65-1

Prepared for
DEPARTMENT OF THE ARMY
COASTAL ENGINEERING RESEARCH CENTER
WASHINGTON, D. C.

1967

1 April to 1 July 1967

Engineering Experiment Station
GEORGIA INSTITUTE OF TECHNOLOGY
Atlanta, Georgia

GEORGIA INSTITUTE OF TECHNOLOGY
School of Civil Engineering
Atlanta, Georgia

QUARTERLY REPORT 12

A-798

# AN ANALYTICAL AND EXPERIMENTAL STUDY OF BED FORMS UNDER WATER WAVES (SUMMARY OF RESULTS THROUGH APRIL 1967)

By

M. R. CARSTENS

CONTRACT NO. DA-49-055-CIVENG-65-1

1 April to 1 July 1967

Prepared for
DEPARTMENT OF THE ARMY
COASTAL ENGINEERING RESEARCH CENTER
WASHINGTON, D. C.

# FOREWORD

This report summarizes the results of the work accomplished under this contract concerning bed forms under oscillatory flow. Experiments with a coarse sand bed ($D_g$ = 0.585 mm) and with a medium sand bed ($D_g$ = 0.297 mm) are completed. Experiments with a fine sand bed ($D_g$ = 0.190 mm) are in progress and will be completed during the coming summer.

The major role of Frank M. Neilson and H. D. Altinbilek in performing the experimental program is gratefully acknowledged.

The writer is pleased to have been asked to present this summary to the Eighth Meeting of the Coastal Engineering Research Board.

ABSTRACT

The results of experiments with oscillatory flow of water over a bed of medium sand and of coarse sand are presented. The period of the motion was essentially constant at 3.6 seconds. The water tunnel in which the experiments were performed is described. The results include the following: (a) incipient motion, (b) evolution of a duned bed, (c) bed geometry, and (d) energy dissipation.

Key words: oscillatory flow, dunes, ripples, incipient motion, and energy dissipation.

TABLE OF CONTENTS

LIST OF FIGURES

## GLOSSARY

| | | |
|---|---|---|
| $a$ | = | half amplitude of water motion |
| $C_D$ | = | coefficient of drag |
| $\bar{C}_{fa}$ | = | boundary-drag coefficient, smooth immobile bed |
| $\bar{C}_{fb}$ | = | boundary-drag coefficient, flat sand bed |
| $\bar{C}_{fc}$ | = | boundary-drag coefficient, duned bed |
| $D_g$ | = | geometric mean diameter |
| $F_D$ | = | Drag force on a typical particle |
| $F_L$ | = | lift force on a typical particle |
| $g$ | = | magnitude of the acceleration of gravity |
| $N_s$ | = | sediment number, $U/\sqrt{(s-1)g\ D_g}$ |
| $N_{sc}$ | = | critical sediment number (at incipient motion) |
| $s$ | = | ratio of specific weights of bed material and fluid |
| s.f. | = | particle shape factor |
| $T$ | = | period of oscillation or wave |
| $t$ | = | time |
| $U$ | = | velocity of flow above the bed |
| $U_m$ | = | maximum value of U |
| $U_{mc}$ | = | value of $U_m$ at incipient motion |
| $u$ | = | velocity at particle level |
| $u_i$ | = | velocity of u at incipient motion |
| $v$ | = | Velocity of propagation of a ripple system |
| $W$ | = | submerged weight of a typical particle |

## GLOSSARY (Continued)

| | | |
|---|---|---|
| $y$ | = | distance above the bed |
| $\alpha$ | = | angle of inclination of the bed from the horizontal |
| $\eta$ | = | dune amplitude |
| $\lambda$ | = | dune wave length |
| $\nu$ | = | kinematic viscosity |
| $\sigma_g$ | = | geometric standard deviation |
| $\phi$ | = | angle of repose |

# INTRODUCTION

One of the more common and less understood multi-phase flows is that involving fluid flow over a bed of particles. Of particular interest to coastal engineers is the oscillatory flow of water over a sand bed. The surface of the bed is the interface between the liquid phase and the solid particle phase. Exchange of water across the interface is limited to seepage flow through the voids in the sand grains. Exchange of sand grains across the interface occurs when the lift and drag forces acting on the surface grains are sufficient to roll them over the bed or to lift them into the overlying water stream. Of course the removal of a sand grains from the bed results in a lowering of the interface which is called scour. Conversely deposition of sand grains onto the bed results in a raising of the interface which is called fill.

In oscillatory flow over a sand bed, a plausible hypothesis is that at a time in the cycle when the fluid velocity attains a certain magnitude, surface particles all over the bed begin to roll and lift from the bed until the maximum velocity is attained. Further, one would expect deposition to occur during the deceleration of the flow above the bed. In other words, the bed would periodically scour and fill with a flat bed remaining flat throughout the cycle and with the interface oscillating vertically. The frequency of the bed oscillation would be twice the frequency of the flow oscillation since two time intervals of scour and two time intervals of fill would occur during one cycle of flow oscillation. This behavior of the interface occurs only when the bottom velocities are quite large as during severe storms.

With lesser velocities, the conditions at the interface are much more complicated. Areas of the bed not only alternate periodically between scour

and fill during the cycle but also periodically alternate spatially between scour and fill. This complicated situation is accomplished with a duned bed. The upstream face of a dune is an area of scour as the flow is accelerated in moving toward the crest. At the crest, the flow separates from the interface forming a vortex in the separated flow region on the downstream face. Sand grains which were carried over the crest from the scour area on the upstream face are deposited on the downstream face. The separated flow rejoins the bed at the trough forming a line of stagnation along which the surface particles are at rest. Thus dune troughs and crests are the spatial boundaries of the areas of scour and fill. Furthermore these areas alternate between scour and fill once each cycle inasmuch as the upstream face of a dune becomes the downstream face of that dune after flow reversal. Just prior to flow reversal, the vortex in the separation zone above the downstream face of a dune is moved up toward the crest and out into the main flow well above the dunes.

No reasonable mathematical model has been formulated for the unsteady nonuniform oscillatory flow over a duned bed. In the absence of theoretical guidelines, (a) information concerning oscillatory flow over a bed of particles has had to be obtained by experimental methods and (b) extrapolation to other flow situations is risky. The most obvious place to obtain data about bed forms is on the sea bed. The phase lag between changes in the bed and changes in the flow complicate the problem of relating the existing bed form to the associated flow condition. In other words, history may confuse the correlation if a diver takes measurements on a day of calm sea where the existing dunes are a residual of a previous storm. A further limitation of <u>in situ</u> measurements is that a measurement of energy dissipation attributable to the bed forms is quite difficult, to say the least. A second experimental method of obtaining

experimental data is to utilize wave flumes. A principal difficulty of using wave flumes is that wave periods are necessarily quite short in order to achieve bottom velocities sufficient for sand movement in flumes of limited depth. Another disadvantage of wave flumes is that of determining the bottom velocities. Most of the experimentally determined information about bed forms, including energy dissipation, has been obtained using an oscillating tray under a still fluid. The obvious advantage of such a scheme is that the experimenter can design the equipment to achieve wave periods and bottom velocities expected on the sea bed. The principal disadvantage is that the flow situations are not dynamically similar. With a laminar boundary layer, the water motion relative to an oscillating flat plate has been shown to be kinematically similar to oscillatory flow over a stationary flat plate. The writer is not aware of the existence of a proof of kinematic similarity either with a turbulent boundary layer or with a duned bed in which vortices are generated in the lee of the crests. Intuitively, one suspects that the two motions are kinematically similar also.

In order to avoid some of the shortcomings of other experimental methods, an oscillatory-flow water tunnel was designed and was installed in the Georgia Tech Hydraulics Laboratory.

## II. THE EXPERIMENTAL PROGRAM

The geometric characteristics of bed forms, the limits between different states of bed configurations, and the energy dissipation attributable to bed deformations are being determined experimentally in the Georgia Tech oscillatory-flow water tunnel for three different bed materials--a fine sand, a medium sand, and a coarse sand. The controlled flow variable is bottom velocity which is controlled by variation of the amplitude of the oscillation of the water. The period of oscillation (wave period of 3.6 sec.) is essentially constant for all runs.

### A. The water tunnel

In order to approximate the flow condition in the vicinity of the sea bed a large U tube was designed such that water can be oscillated horizontally over a sand bed located in the bottom of the U tube as shown in figure 1. The test section (B) is 10.0 ft. long, 1.00 ft. high, and 4.00 ft. wide. The central section of the floor (D) is depressed to form a bed-material container which is 6.00 ft. long, 4.00 ft. wide, and 4.0 inches deep. The sidewalls and top of the test section are transparent plastic in order to permit visual observation of the phenomena occurring within the test section. The vertical legs of the U tube are 1.00 ft. by 4.00 ft. in a horizontal cross section. The vertical legs are joined to the horizontal legs so as to form a streamlined flow passage (C). The free surface of the water in one of the vertical legs (A) serves as a piston. Air is continuously forced into the confined volume above the water (J). Two large, solenoid-actuated, piston-operated, exhaust valves (E) are used to quickly relieve the excess pressure in the air above the water surface. The exhaust valves are closed for about one-quarter cycle during the time when

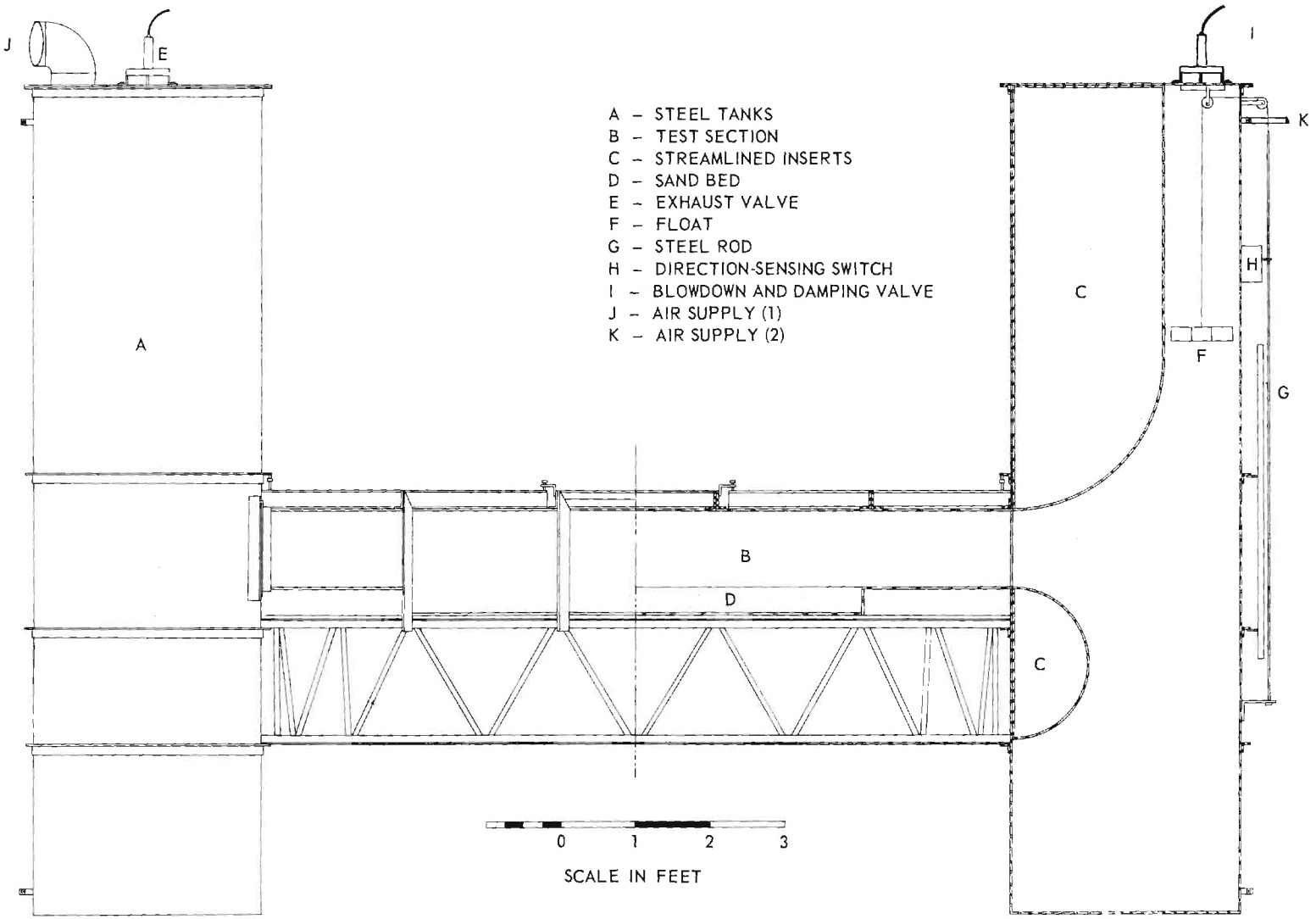


Figure 1. Oscillatory-flow Water Tunnel.

the water surface is falling in that leg. A float gage (F) in the other vertical leg is joined to a direction-sensing switch (H) which is the first element in a feedback-control system used to close and to open the exhaust valves at the proper time during the cycle.

This system oscillates the water in the U tube with simple harmonic motion at resonant frequency resulting in an almost constant period of 3.6 sec. Equilibrium amplitude can be controlled by adjustment of the air pressure. Air pressure is controlled by means of speed regulation of the blower.

Transients are eliminated by means of a separate air system (K). Initially the water levels are unbalanced to the desired equilibrium amplitude. Upon release of the initial unbalance (I), the water oscillates at equilibrium amplitude. Final transients are eliminated by closure of the valve (I) over an exhaust port.

Amplitude and period of oscillation are recorded on a direct-writing oscillograph. The float-elevation sensor system consists of an endless, small-diameter, stainless-steel cable which passes over pulleys at the top and bottom in one vertical leg of the U tube. The endless cable is fastened to a wooden float. A three-turn potentiometer, which is connected to the axle of the upper pulley, is one leg of a Wheatstone bridge. Bridge unbalance is sensed and recorded. The recorder is also equipped with a timing marker which marks pips at one- second intervals on the record. In all runs, the float elevation system is calibrated just before and immediately following a run by making short records at several elevations of the float.

A pressure transducer is attached to a piezometer in the air space above the oscillating water surface in the vertical leg (A). The output of this pressure-transducer circuit is simultaneously recorded with the water-elevation record. Using these data the work input per cycle to maintain the oscillation can be calculated.

Two piezometers are installed in one wall of the test section above the sand bed. These piezometers are located 2.0 inches below the roof and 38.0 inches apart. These piezometers are connected to a differential-pressure transducer. From the simultaneously recorded data of water motion and pressure difference, energy dissipation within the 38-inch length of test section can be calculated.

Coordinate markings on one of the transparent sidewalls of the test section are used for measurement of dune geometry. Polaroid pictures of the sidewall which show both the coordinates and the dunes are the data.

A pair of precision instrument rails have been mounted over the test section such that an instrument carriage on which a point gage is mounted can be accurately positioned anywhere over the 3-ft. square access opening located in the center of the roof of the test section. Using this instrument, topographic maps of the bed can be made of a section of the bed which is slightly less than 3-ft. square.

B. Bed material

Three different bed materials are being used having the properties listed in the table below:

| Sand | Geometric mean diameter, $D_g$ (mm) | Geometric std. deviation, $\sigma_g$ | Specific gravity, s |
|---|---|---|---|
| Ottawa (Banding) | 0.190 | 1.35 | 2.66 |
| Glass Beads | 0.297 | 1.06 | 2.47 |
| Ottawa (Flint Shot) | 0.585 | 1.16 | 2.62 |

C. Experimental method

The initial condition for all runs is a flat bed. For runs in which the maximum velocity, $U_m$, within the test section is less than that required to move the surface particles on a flat bed, a disturbance element ( a 4-ft. long, 1/2-in. diameter, half-round bar), is placed on the bed perpendicular to the flow direction in order to induce a dune system to form. All electronic circuits are calibrated just prior to starting a run.

Initial transients and final transients are eliminated by use of the blow-down and damping system as explained previously. In spite of the elimination of the initial transient, water-motion amplitude is not constant throughout a run; because, as dunes develop, resistance-to-flow increases with the result that the water-motion amplitude decreases slightly until an equilibrium duned bed is established. During the latest run, the procedure was altered by having an operator gradually increase the blower speed to maintain a constant amplitude.

After an equilibrium state of bed geometry is attained, data is taken from which to calculate work input into the tunnel and to calculate energy dissipation within the test section. The water motion is then stopped. All electronic circuits are calibrated just after cessation of a run. Photographs of the duned bed are taken. The water tunnel is drained. Topographic mapping can then be started.

## III. RESULTS

In this summary report, the results of the study are shown graphically. More complete descriptions of methods of analyzing the data and tabulations of data are contained in previous Quarterly Reports. References are limited to these Quarterly Reports.

### A. Incipient motion (Quarterly Report 9)

Incipient motion of the protruding surface particles occurs when the hydrodynamic forces on the protruding particles are sufficient to roll these surface particles over the bed. Early in the study, experiments revealed that incipient motion would occur at different values of water-motion amplitude depending upon whether the bed was flat or was deformed. Obviously the difference in the two situations is in the magnitude of the fluid velocity in the vicinity of the protruding particles. Not quite so obvious, is the desirability of formulation of an incipient-motion criterion which is in terms of the velocity in the vicinity of the protruding grains. The advantage of this kind of incipient-motion criterion is that the determination of the velocity in the vicinity of the protruding grains is a separate problem. In other words, an incipient-motion criterion which is formulated in terms of flow, fluid, and geometric variables in the vicinity of the protruding grain should be quite universal.

The experiments with a duned bed under oscillatory flow are quite ideal for the determination of a universal incipient-motion criterion since the effect of a boundary layer in the flow can be expected to be quite small for two reasons. First the boundary layer of an oscillatory flow must be reformed and grow twice each cycle. Second the pattern of separation of the flow at

the crest, reattachment in the trough, and converging flow along the upstream face are flow conditions under which boundary-layer development is suppressed even under steady flow conditions. As a further precaution to insure a negligible effect of a boundary layer, the coarse sand ($D_g$ = 0.585 mm) was used in the evaluation a universal incipient-motion criterion. The experimental run was Run 62 in which a few grains were in motion at the crest of a well-defined two-dimensional dune with a maximum mean velocity of 0.473 fps in the test section.

The analysis is based upon the hydrodynamic surface forces of drag, $F_D$, and lift, $F_L$, and the submerged weight, W, of a typical protruding particle as shown in figure 2. Additional surface forces arising from inertial reaction in the flow are not included because the surface particles at the crest were observed to move only when the velocity was near maximum, that is, when the acceleration in the flow is negligible. The flow and geometric conditions at the crest of a dune upon which particle motion has practically ceased is shown in figure 3. Using the measured physical variables of Run 62 to evaluate a numerical constant in the theoretical analysis, the following incipient-motion criterion is offered:

$$\frac{u_i}{\sqrt{(s-1)gD_g}} = \sqrt{\left(\frac{\tan\phi\cos\alpha + \sin\alpha}{1 + \tan\phi}\right)\frac{8.2}{C_D}} \qquad (1)$$

in which

$u_i$ = Fluid velocity in the vicinity of the protruding particle at the incipient-motion condition,

s = specific-weight ratio of bed material to fluid,

g = magnitude of the acceleration of gravity,

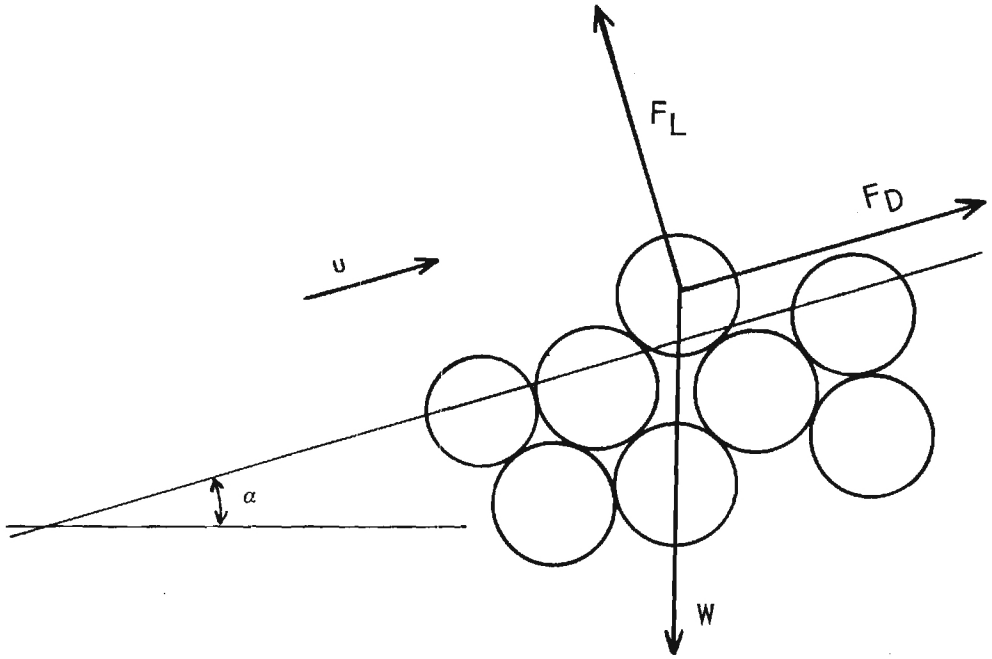


Figure 2. Forces on a Bed Particle.

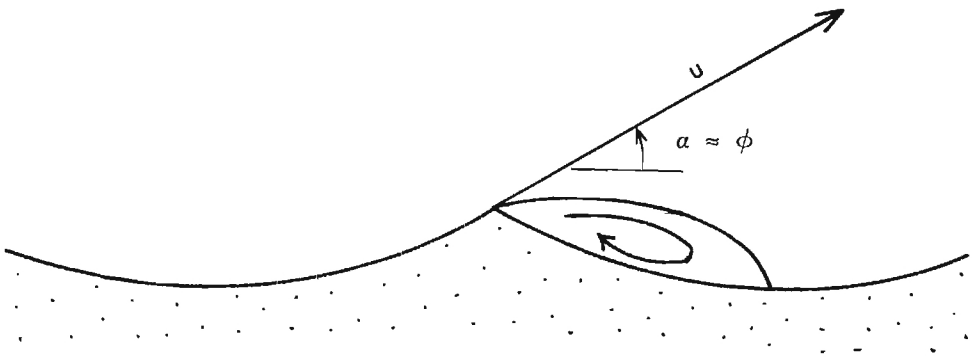


Figure 3. Velocity at the Crest of a Dune in Oscillatory Flow.

$D_g$ = geometric mean diameter of bed material,

$\phi$ = angle of repose of bed material,

$\alpha$ = inclination of the bed from the horizontal, and

$C_D$ = coefficient of drag of a particle having a length dimension of $D_g$.

There are two significant points in equation 1 which deserve to be emphasized. First, the left-hand side of equation 1 is a sediment Froude number being derived from the hydrodynamic surface forces on the sediment and the submerged weight of the sediment. Second, the coefficient of drag, $C_D$, includes a Reynolds-number effect inasmuch as the velocity, $u_i$, is used to evaluate the Reynolds number in the determination of $C_D$. The use of the parameter, settling velocity, is tenuous in any incipient-motion criterion.

The incipient-motion criterion, equation 1, is deficient for use in analyzing incipient motion of protruding surface particles in which the particles are submerged within a boundary layer. In this case the velocity gradient at particle level is large thereby requiring a more precise definition of the height, y, above the bed at which $u_i$ is to be evaluated.

Experimentally determined values of incipient motion of the three sands with a flat bed can be used to calculate the height, y, at which $u_i$ should be evaluated. The mathematical equation for the velocity distribution within a laminar boundary layer for oscillatory flow over a flat smooth bed is:

$$\frac{u}{U_m} = \sin\frac{2\pi t}{T} - e^{-y\sqrt{\pi/\nu T}} \sin\left(\frac{2\pi t}{T} - y\sqrt{\frac{\pi}{\nu T}}\right) \qquad (2)$$

in which

$u$ = fluid velocity

$U_m$ = maximum velocity above the boundary layer,

$T$ = period of the oscillatory flow,

$y$ = vertical distance above the bed, and

$\nu$ = kinematic viscosity of the oscillating fluid.

Differentiating equation 2 with respect of $2\pi t/T$ and equating the derivative to zero yields a transcendental function from which the time in the cycle at which the velocity is a maximum at various values of y can be determined. Using the measured physical variables of the incipient-motion runs (Runs 83, 55, 80, and 81) and using equations 1 and 2, the height, y, above the bed for the evaluation of $u_i$ was calculated to be $0.55D_g$, $0.60D_g$, and $0.59D_g$ for the fine, medium, and coarse sand, respectively. The reasonable values of the height, y, and the close agreement of the values for the three sand sizes is interpreted by the writer to substantiate the entire analysis based upon forces. Therefore, on the basis of this study, the writer is proposing equation 1 as a universal incipient-motion criterion with the velocity, $u_i$, being at a position $0.6D_g$ above the bed for bed materials in which the geometric standard deviation is small, say less than 1.3.

This modest theory permits the incipient-motion condition to be extrapolated to other wave periods as shown in figure 4. The lowest curve is for incipient motion either for the beginning of motion on a residual dune system or for the cessation of motion on a dune system. The upper three curves are for the incipient motion of particles on a flat bed for wave periods of 3, 6, and 9 seconds. The abscissa of figure 4 is geometric-mean diameter, $D_g$. The ordinate of figure 4 is the critical sediment number, $N_{sc}$, defined as:

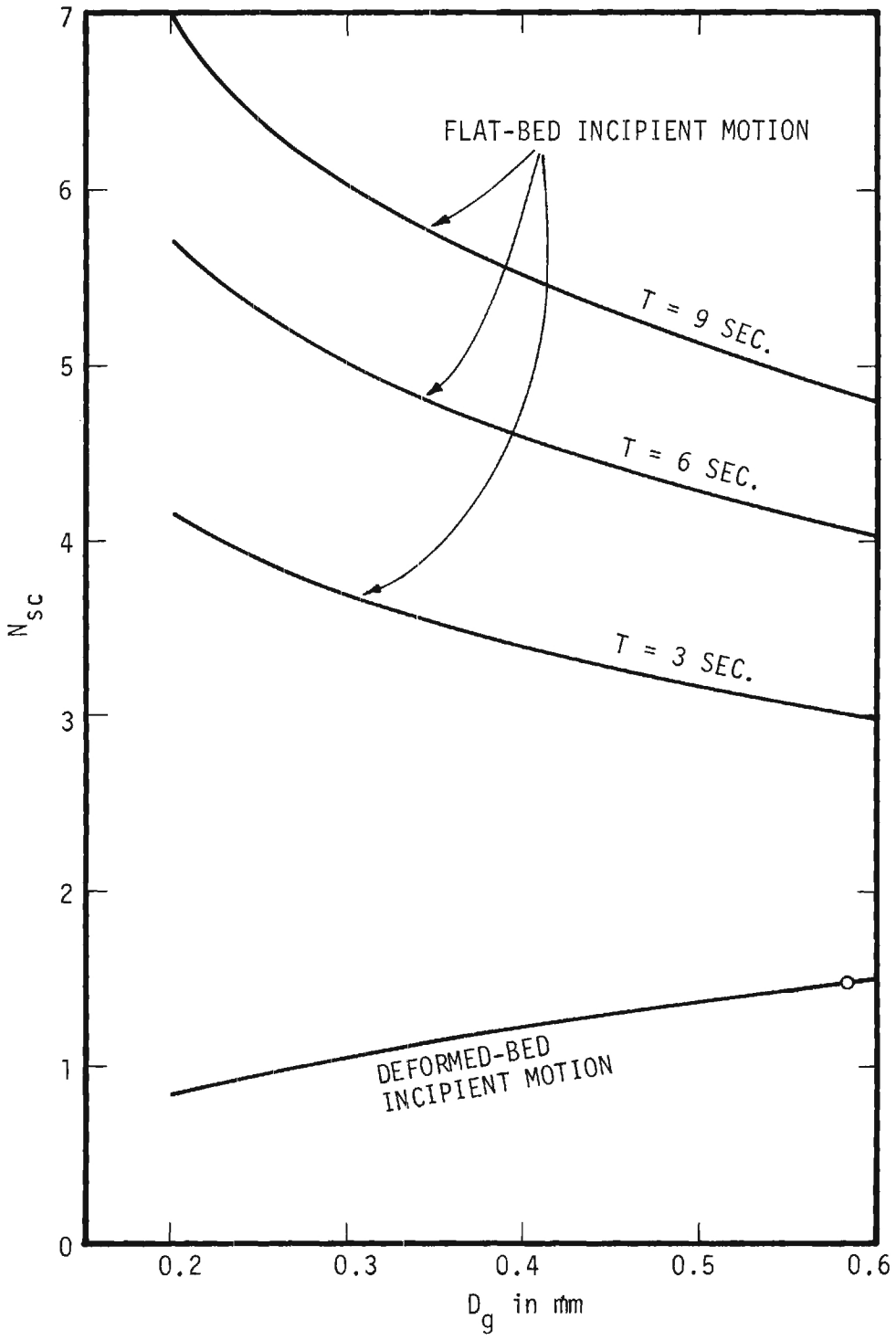


Figure 4. $N_{sc}$ at Incipient Motion for Oscillatory Flow (Water at 60°F, s.f. = 0.7).

$$N_{sc} = \frac{U_{mc}}{\sqrt{(s-1)gD_g}} \qquad (3)$$

In preparing figure 4 the bed material was assumed to have a shape factor of 0.7 for the evaluation of $C_D$ in equation 1.

B. Evolution of a duned bed (Quarterly Report 7)

Since all runs were begun with a flat bed, the evolution of a duned bed could be observed from the appearance of the first ripple, through the dune scouring process, to the final equilibrium bed. The process of dune development is different depending upon whether the sediment number, $N_s = U_m/\sqrt{(s-1)gD_g}$, is greater than or less than the critical sediment number, $N_{sc}$, for a flat bed.

If the sediment number, $N_s$, is greater than the flat-bed $N_{sc}$, some of the surface grains move back and forth practically in phase with the water motion. After a few cycles of oscillation in this manner, the motion of the surface grains is restricted to transverse bands of grains moving essentially in phase with the velocity. These bands of moving grains are separated by bands of stationary grains. The bands of moving grains become ripple crests and the stationary bands become ripple troughs. The ripple crests move back and forth nearly to the edge of the band of moving grains. With further oscillation, ripple amplitude increases until separation occurs and vortices form in the lee of the crests. From this time until an equilibrium dune system is scoured into the bed, the bed-form pattern is very irregular as the shorter wave-length ripple system is being replaced by the longer wave-length dune system. The wave length of the observed beginning ripple system was always less than one half the wave length of the equilibrium system. Since the ripple system which forms spontaneously all over the bed is transitory, experimental observations were qualitative.

If the sediment number, $N_s$, of a run is less than the flat-bed $N_{sc}$, ripples do not form spontaneously but can be induced. Ripples were induced by placing a 4-ft. long, 1/2-in. diameter, half-round bar on the bed in the center of the test section and oriented perpendicular to the flow direction. Upon starting the oscillation, ripples are formed on both sides of the bar. These ripples grow in amplitude and wave length becoming dunes. Then a new pair of ripples form. The process is repetitive. Since the wave length of each pair of dunes formed is much less than the equilibrium wave length, the wave length must increase as the dune system develops. If the sediment number is quite small the dune system will develop in an orderly manner by continuous outward movement of the more recently formed dunes as demonstrated in Run 48 during which the sediment number was 1.8. The history of dune development during Run 48 is shown in figure 5. In some runs the scouring process was so rapid that the older dunes overtook some of the newer dunes resulting in a mixed and disorderly pattern. In spite of this interim disorderliness, the dune system developed into a regular pattern at equilibrium.

The mean velocity at which induced ripples propagate over a flat bed can be determined from data plotted as in figure 5. The ratio of velocity of propagation, V, of the ripple system to the maximum velocity of the oscillatory flow, $U_m$, is shown in figure 6 as a function the sediment number, $N_s$. The data shown in figure 6 can be represented by the empirical funciton

$$\frac{V}{U_m} = 1.7\ (10^{-4})\ (N_s^2 - 1.7)^{3/2} \qquad (4)$$

From this empirical equation, equation 4, ripple progagation over a flat bed ceases when $N_s = 1.3$. Using the incipient-motion criterion, equation 1, as shown in figure 4, cessation of ripple progagation is a function of $D_g$

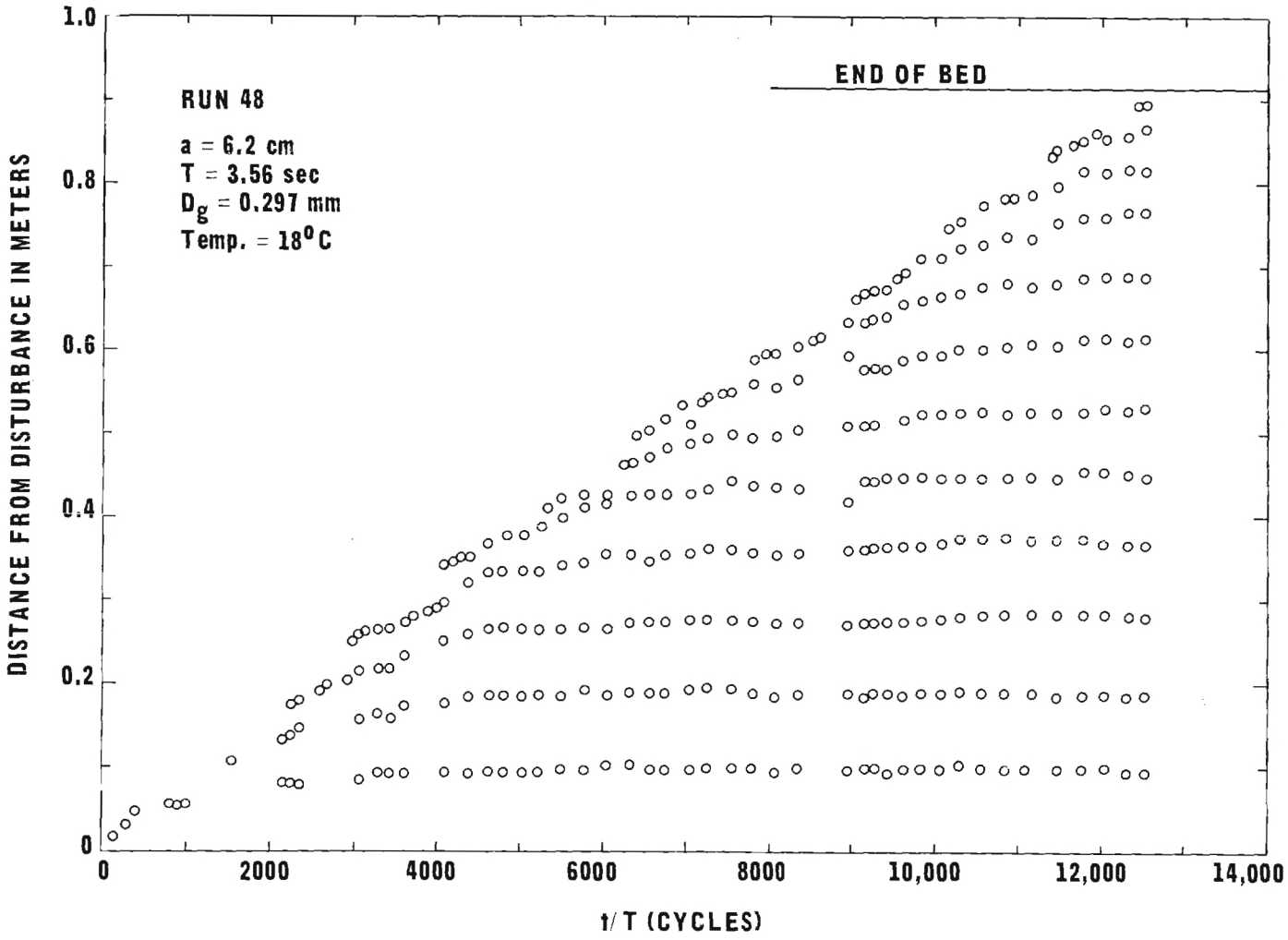


Figure 5. Dune Position as a Function of Time.

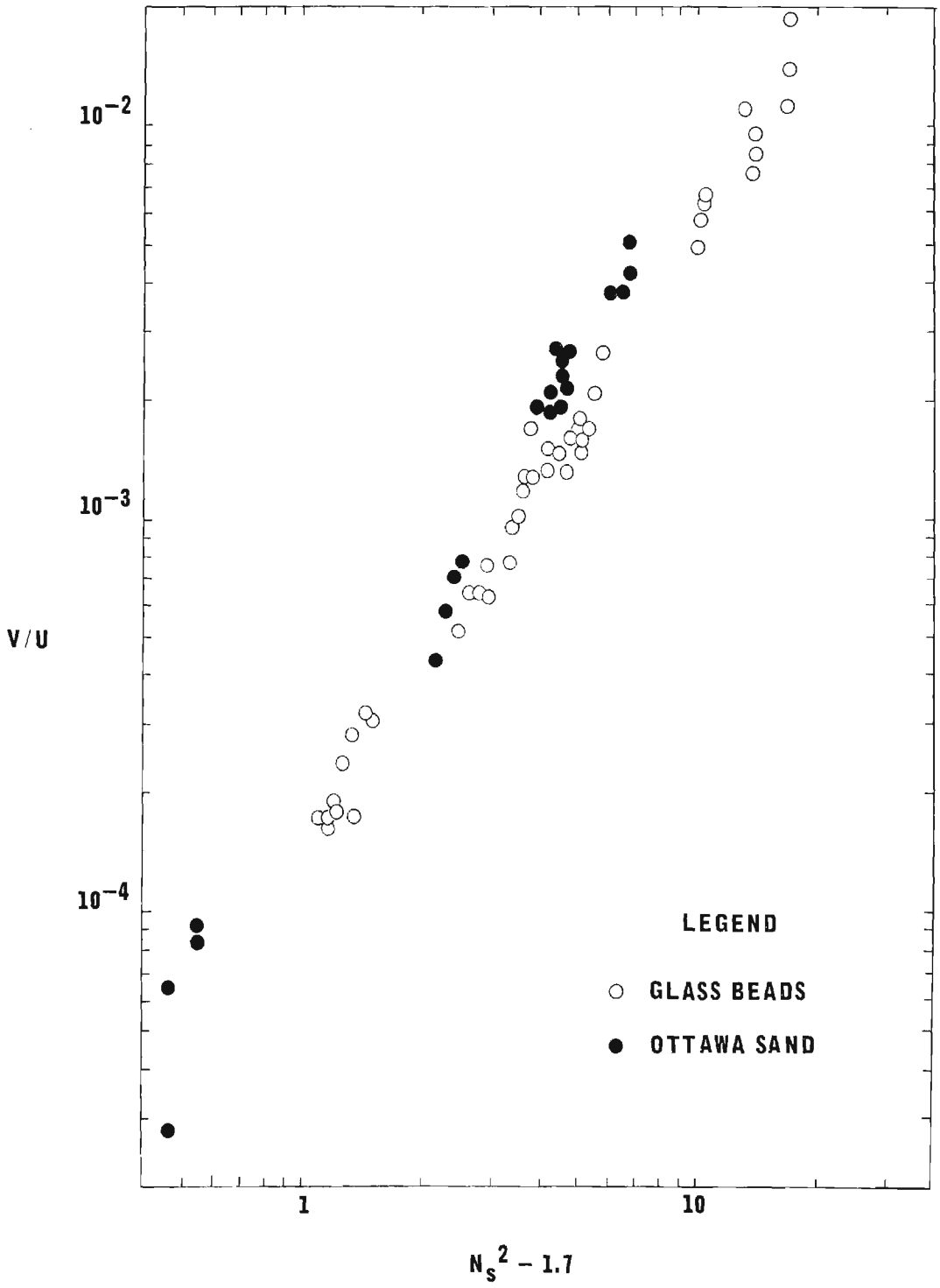


Figure 6. Rate of Ripple Propagation.

with the value of $N_{sc}$ being about 1.0 for the medium sand (glass beads) and being about 1.5 for the coarse sand (Ottawa sand). This independent determination is interpreted as a validation of the analysis which culminated in equation 1.

C. Bed geometry (Quarterly Report 6)

Geometric characteristics of the equilibrium bed forms are being determined in two ways. Except for two runs, geometric characteristics of dunes have been obtained from photographs taken through one of the transparent sidewalls of the test section. Figure 7 is a photograph taken of the equilibrium system of dunes of Run 23 during which the value of $N_s$ was 3.7 and the bed material was the medium sand. Topographic maps are now being prepared for all of the runs with fine sand. Examples of the topographic maps are shown in figure 8 and figure 9. The two-dimensional dune pattern shown in figure 8 developed during Run 85 during which the value of $N_s$ was 2.8 and the bed material was the fine sand. The three-dimensional dune pattern shown in figure 9 developed during Run 50 during which the value of $N_s$ was 10.5 and the bed material was the medium sand.

Geometric characteristics of equilibrium dunes shown in figures 10 and 11 are divided into two categories, two-dimensional and three-dimensional dunes. In figure 10 the region of two-dimensional dunes extends to a value of $N_s$ of about 6.5. Two-dimensional dunes are shown in figures 7 and 8. If the value of $N_s$ is greater than 6.5, the dune system assumes a three-dimensional form as shown in figure 9. Destruction of the two-dimensional dune system is progressive with increasing values of $N_s$. The dune system on the medium-sand bed was completely destroyed if the value of $N_s$ were 12.7 or greater.

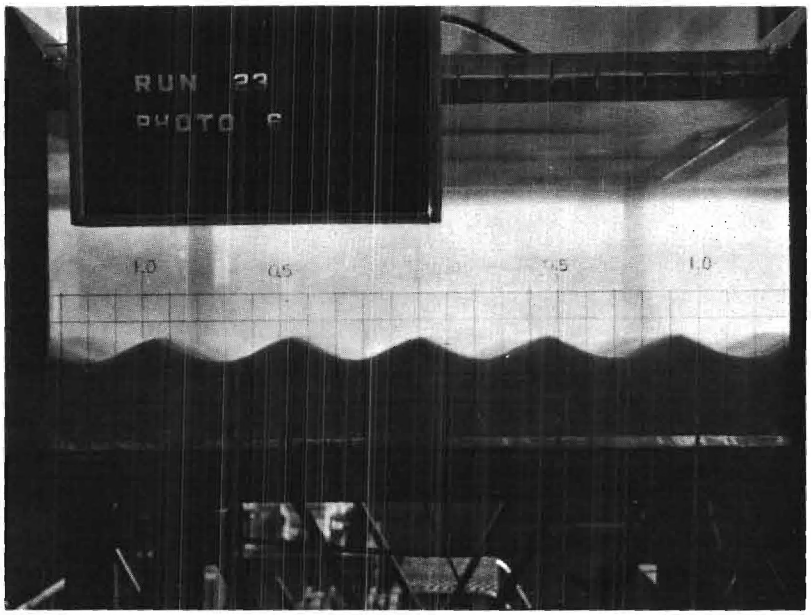


Figure 7. Photograph of Two-dimensional Dunes.

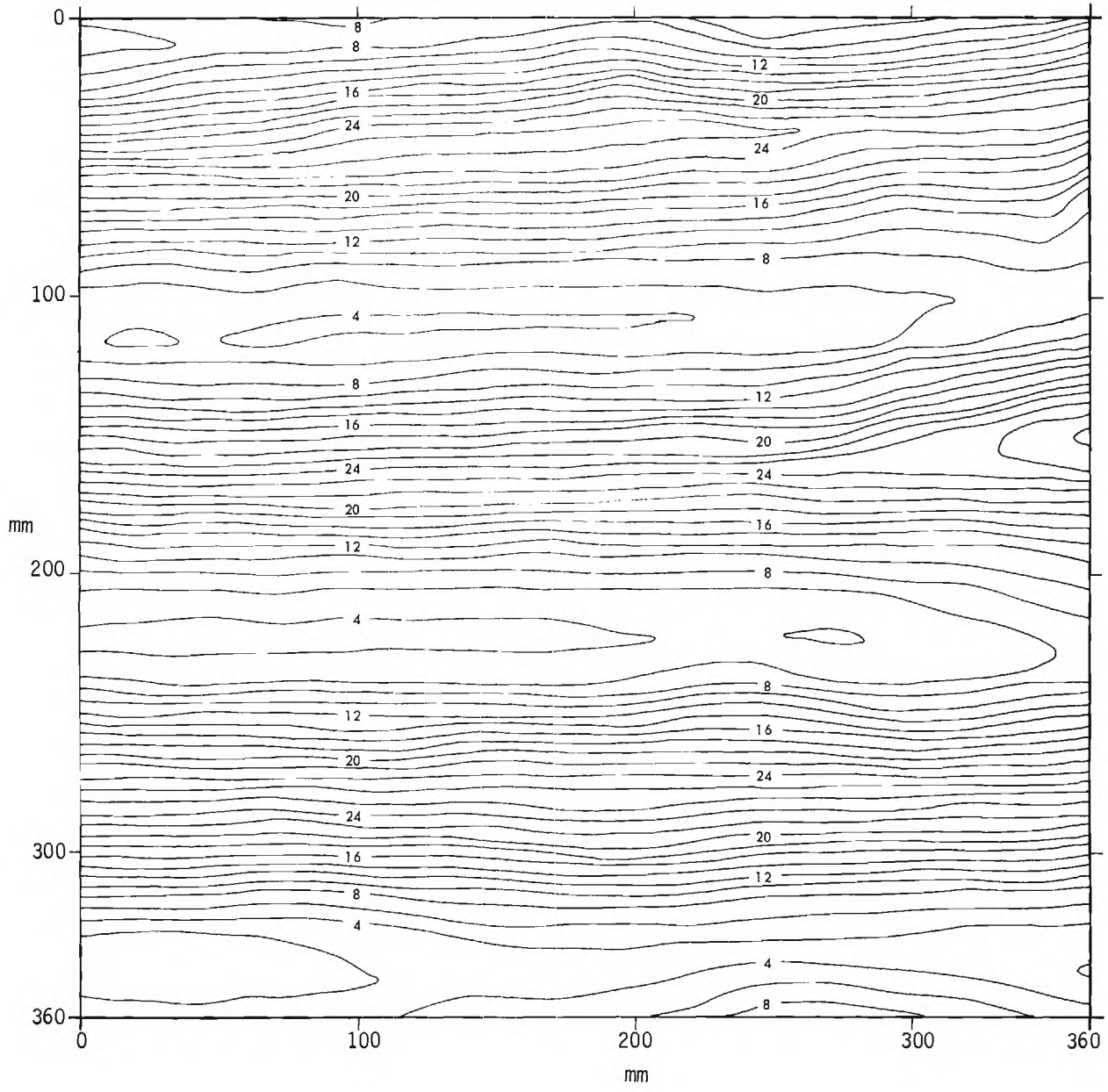


Figure 8. Topographic Map of Two-dimensional Dunes ($N_s$ = 2.8).

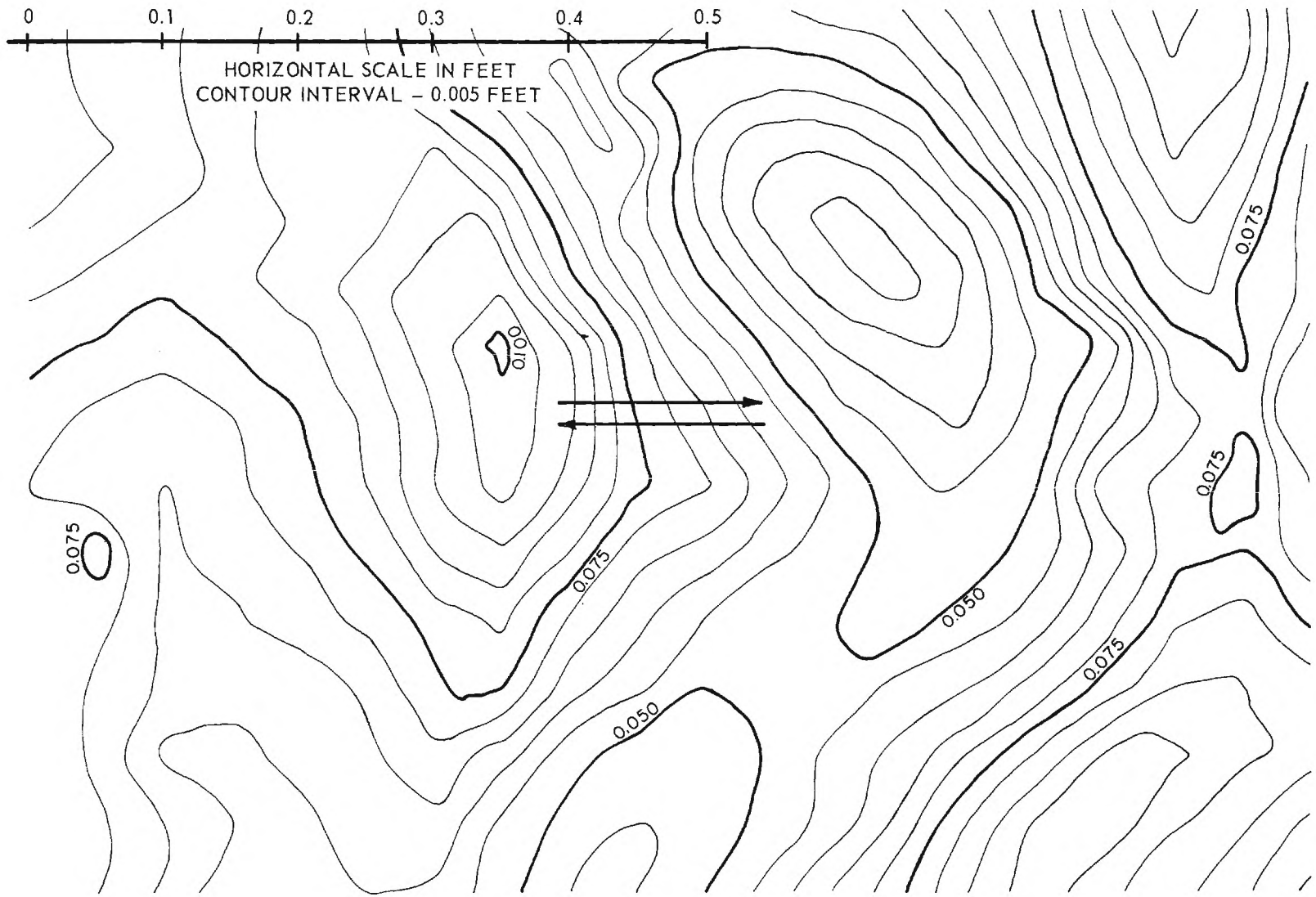


Figure 9. Topographic Map of Three-dimensional Dunes ($N_s$ = 10.5).

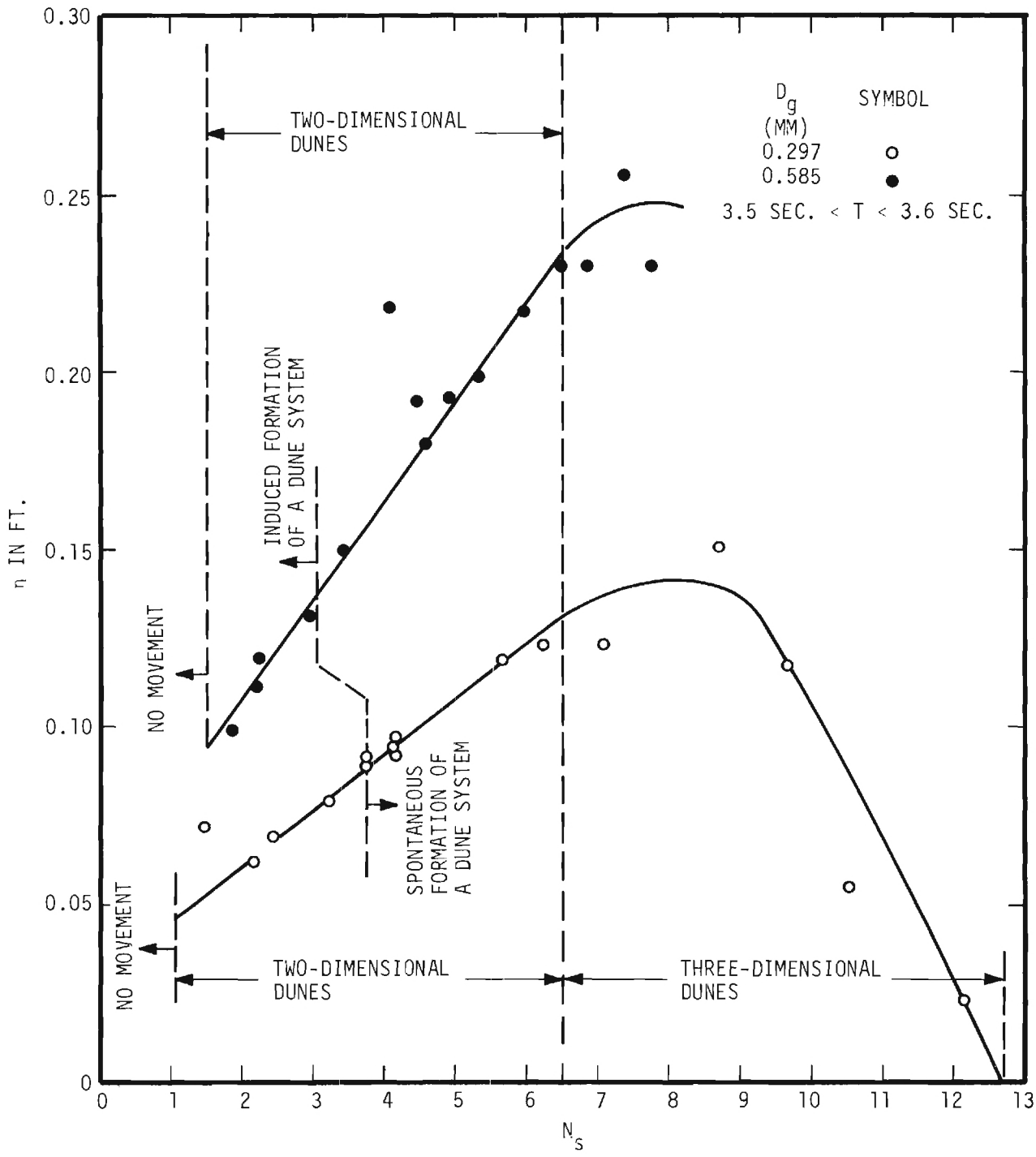


Figure 10. Dune Amplitude (Oscillatory Flow).

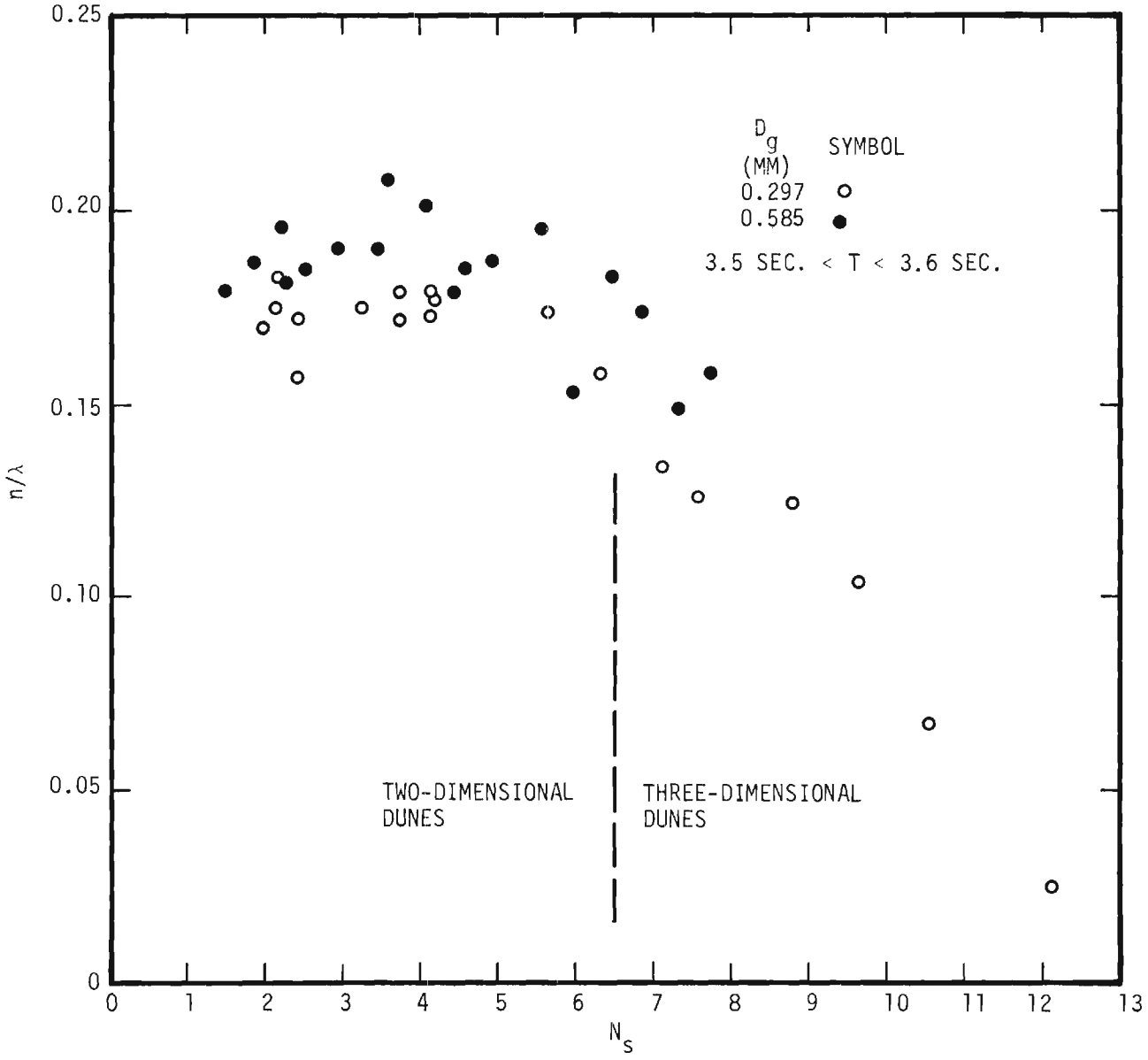


Figure 11. Ratio of Dune Amplitude to Wave Length (Oscillatory Flow).

If $N_s$ was greater than 12.7, the bed was flat with a large number of surface particles moving back and forth over the bed giving the appearance of a layer of another fluid beneath the water.

The ratio of amplitude-to-wave length, $\eta/\lambda$, of two-dimensional dunes is approximately constant as shown in figure 11. The value of $\eta/\lambda$ is about 0.18 with the medium sand and about 0.19 with the coarse sand. The difference is probably the result of the larger angle of repose, $\phi$, of the coarse sand--about 24 degrees for the medium sand and about 30 degrees for the coarse sand. The form of two-dimensional dunes is closely appproximated by circular arcs which terminate at the crests at an angle of somewhat less than $\phi$ as measured from the horizontal. For two-dimensional dunes, the ratio, $\eta/\lambda$, will probably be slightly less than 0.2 irrespective of the wave period and water temperature.

The lack of theoretical guidelines is a barrier to the extrapolation of the dune amplitude data to other wave periods. Because of this theoretical deficiency, the range of flow conditions in the sea will probably only be covered by experiments similar to the experiments reported herein except that a range of wave periods would be examined. The writer anticipated this need when the water tunnel was designed. Changes in wave period were to have been accomplished by altering the ratio of the cross-sectional area of the vertical leg to the cross sectional area of the test section by changing the inserts (C) as shown in figure 1. The difficulties in installing the original inserts have demonstrated that a more feasible scheme is to lengthen the vertical legs so that the operator of the tunnel can change the resonant frequency by simply changing the amount of water in the tunnel thereby changing the mass which is oscillating. Plans are in progress to reconstruct the Georgia Tech tunnel incorporating the longer vertical legs.

One of our graduate students, Frank M. Neilson, who made the majority of measurements reported in this study is in the process of attempting to determine valid extrapolation methods. Neilson is attempting to formulate a theoretical analysis and is also attempting to correlate all published experimental results.

Hence the next step toward the solution of the problem of predicting bed forms as a function of the flow variables is to determine the following functions

$$\frac{\eta}{D_g} \text{ and } \frac{\lambda}{D_g} = f\left[T\sqrt{\frac{(s-1)}{D_g}g}\,,\ \frac{U_m}{\sqrt{(s-1)gD_g}}\,,\ \sigma_g,\ \begin{matrix}\text{particle}\\ \text{shape}\end{matrix}\right] \quad (5)$$

Fortunately sea sands are quite uniform in shape and are quite uniformly sized at a given location. Hence the last two variables in the array, equation 5, are probably inconsequential in a practical sense. The experiments in this study are being performed throughout a range of values of the parameter, $U_m/\sqrt{(s-1)gD_g}$, at three separate levels of the parameter, $T\sqrt{(s-1)g/D_g}$.

After satisfactory solutions to the function, equation 5, are found in one way or another, the following step will be to investigate historical effects. There are probably two aspects to the effects of prior events. First is the phase lag between the changed flow condition and a change in bed form. Second is that the wave length of a dune system is so weakly dependent upon the flow parameters that the flow can be accommodated by the wrong bed! After all, two-dimensional dunes are geometrically similar regardless of wave length. In order to avoid historical effects in the current study, the bed was initially flat and transients were eliminated from the oscillatory motion.

D. Energy dissipation (Quarterly Report 10)

Dunes on the sea bed quite obviously increase the energy dissipation within the water by virtue of the generation of vortices in the lee of dune crests. Vortices are generated twice in an oscillatory cycle. These vortices are moved out and up into the main stream at about the time of flow reversal. A reasonable assumption is that energy required to produce and that energy stored within these vortices is ultimately dissipated as heat. The added energy dissipation resulting from flow over a duned bed was calculated from experimental results.

Two methods of evaluation of energy input are now being used. The first method involves determining the work input into the entire tunnel from simultaneous measurements of the pressure over and the velocity of the driving piston which is the water surface in one of the vertical legs. The second method involves determining the energy dissipation within the test section from simultaneous measurements of the pressure gradient and the mean velocity within the test section. Since the second scheme has only recently been installed and has been used during one run, Run 86, the results presented in this report are limited to those obtained by the first method.

The work input into the entire water tunnel is equal to the energy dissipated within the oscillating water mass if the mass is oscillating at a constant amplitude. Hence the difference in work input at the same amplitude is the difference in the energy dissipation within the test section since the remainder of the flow passage of the tunnel is invariant. Work input was evaluated for three bed conditions over a range of water-motion amplitudes within the test section as follows: (a) a smooth immobile bed, (b) a flat

sand bed, and (c) a duned sand bed. The smooth immobile bed, bed condition (a), was achieved by covering the flat sand bed with a sheet of polished aluminum.

The results were calculated in terms of a difference in boundary-drag coefficients such that the added energy-dissipation per unit area of bed per cycle could be recomputed. The difference in energy dissipation per unit area of bed per cycle between bed condition (c) and bed condition (a) is given by

$$(\bar{C}_{fc} - \bar{C}_{fa}) \int_{t}^{t+T} \frac{\rho |U^3|}{2} \, dt \tag{6}$$

in which T is the period of oscillation. Similarly the difference in energy dissipation per unit area of bed per cycle between bed condition (b) and bed condition (a) is given by

$$(\bar{C}_{fb} - \bar{C}_{fa}) \int_{t}^{t+T} \frac{\rho |U^3|}{2} \, dt \tag{7}$$

Values of $\bar{C}_{fc} - \bar{C}_{fa}$ and of $\bar{C}_{fb} - \bar{C}_{fc}$ are shown in figure 12.* The spread of the values of $\bar{C}_{fc} - \bar{C}_{fa}$ at low values of $N_s$ is probably not entirely attributable to the experimental method inasmuch as the same method was used to evaluate $\bar{C}_{fb} - \bar{C}_{fa}$ for which the values are much less scattered. Because the scatter of the experimental results, the decision has been made to determine the energy dissipation by two independent methods during the last eight runs.

* A numerical error was found in Quarterly Report 10. All of the numerical values in Column 12 of TABLES III and IV should have been multiplied by 10.93. Figure 3 of Quarterly Report 10 also is in error for the same reason.

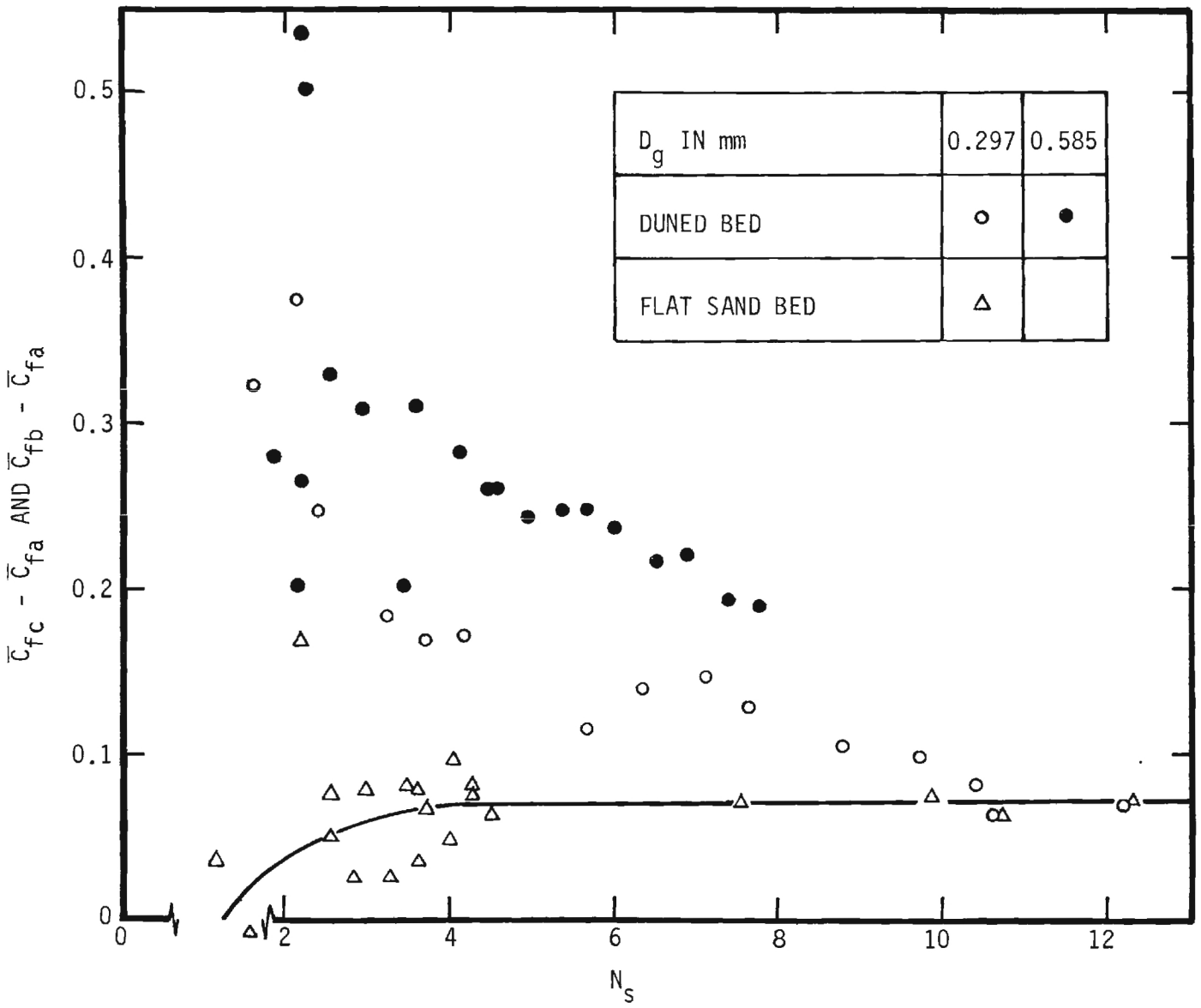


Figure 12. Boundary-drag Coefficients.

# IV. FUTURE WORK

The remaining work under the current contract consists of performing seven more runs with the fine sand and of analyzing the results in a similar manner to the results shown in this report. Also a final report is to be prepared.

The hope is that the water tunnel can be used next year in making a scour study. As a result of a previous scour study for the U. S. Navy Mine Defense Laboratory, the writer believes that the Georgia Tech Hydraulics Laboratory is now in a position to make a genuine contribution to our knowledge about and similarity laws for localized scour.

After five years of operating the oscillatory flow tunnel, the writer is quite convinced that the oscillatory-flow water tunnel is a valuable laboratory instrument for a variety of unsteady flow experiments. As a result of this five-year operating experience, several worthwhile improvements in design have been noted. The hope is that a new improved tunnel can be designed and constructed by October 1968.

FINAL REPORT

PROJECT A-798

# AN ANALYTICAL AND EXPERIMENTAL STUDY OF BED FORMS UNDER WATER WAVES

By
M. R. Carstens
F. M. Neilson
H. D. Altinbilek

Contract No. DA-49-055-CIVENG-65-1

Performed for
DEPARTMENT OF THE ARMY
COASTAL ENGINEERING RESEARCH CENTER
WASHINGTON, D. C.


September 1967

Engineering Experiment Station
GEORGIA INSTITUTE OF TECHNOLOGY
Atlanta, Georgia

GEORGIA INSTITUTE OF TECHNOLOGY
School of Civil Engineering
Atlanta, Georgia

FINAL REPORT

PROJECT A-798

# AN ANALYTICAL AND EXPERIMENTAL STUDY OF BED FORMS UNDER WATER WAVES

By

M. R. CARSTENS, F. M. NEILSON, and H. D. ALTINBILEK

CONTRACT NO. DA-49-055-CIVENG-65-1

SEPTEMBER 1967

Performed for
DEPARTMENT OF THE ARMY
COASTAL ENGINEERING RESEARCH CENTER
WASHINGTON, D. C.

ERRATA

The following are major corrections to Final Report, Project A-798.

Page xii:

$N_s$ Sediment number, $U_m / \sqrt{(s-1)g\, D_g}$

Page xiv:

s Spontaneous formation of ripples; smooth; sediment

Page 26:

In equation 8, "U" should be "$U_m$"

Page 29:

In the first line "equations 14 and 15" should be "equations 13 and 14."

Page 38:

After line 6, insert the following "...cessation of motion. The upper three curves in Figure 20 are for..."

Page 40:

In equation 38, "$u_i$" should be "$u_c$".

FOREWORD

Appreciation is expressed to the Commanding Officer of the Coastal Engineering Research Center and his staff (particularly Thorndike Saville, Jr., Chief of the Research Division) for their many kind acts throughout the project. Among these acts were permission to publish some of the findings in the following articles:

(1) "Similarity Laws for Localized Scour," Proc. ASCE, paper no. 4818, HY3, May 1966, pp. 13-36, and

(2) "Evolution of a Duned Bed under Oscillatory Flow," Journal of Geophysical Research, Vol. 72, No. 12, June 15, 1967, pp. 3053-3059.

Also permission was granted to present some of the observations orally at the ASCE, Hydraulics Division Conference held at the University of Wisconsin in August 1966 in a paper entitled "Are We Kidding Ourselves with the Concept of Incipient Motion."

## ABSTRACT

Various features of the bed forms which occur with oscillatory flow over a bed of uniform sand were studied experimentally in an oscillatory-flow water tunnel. The amplitude of the water motion was a controlled variable. Three sizes of bed material were used in otherwise duplicate experiments. The period of oscillation was essentially constant in all runs. A flat bed was the initial condition in all runs. Initial and final transients were eliminated from the water motion. The experiments were organized in order to study (a) incipient motion, (b) evolution of a duned bed, (c) geometry of equilibrium dunes, and (d) energy dissipation in the flow over a duned bed.

The incipient-motion condition was determined both on a duned bed and on a flat bed. The incipient-motion condition was analyzed by considering the lift, drag, and submerged weight forces on a typical particle on the surface of the bed. An analytical expression was derived for the critical velocity in terms of the ratio of the specific weights of bed material and fluid, mean size of particle, angle of repose of bed material, bed slope, and a coefficient of drag (the magnitude of the coefficient of drag depends upon the critical velocity, fluid viscosity, and particle size). This rational incipient-motion criterion proved to be quite satisfactory for the prediction of incipient motion under oscillatory flow both with a duned bed and flat bed. The incipient-motion criterion was applied to two-dimensional, turbulent, unidirectional flow over a flat bed with very reasonable agreement with experimental results of others. As a result of this analysis rational expressions were derived (for the first time to the writers knowledge) for the widely-used Shields diagram which is based upon experimental findings.

The manner in which an initially flat bed evolves into a duned bed was observed. A ripple system forms spontaneously all over the flat bed if the maximum velocity is greater than the critical velocity. A ripple system can be induced to form with lesser velocities by a disturbance which creates a non-uniform flow zone just above the bed. Ripples will form and grow into dunes with the earlier formed dunes being a disturbance from which a new ripple will form. Celerity of an induced dune system was determined from experimental measurements.

Geometry of equilibrium dunes was determined from side-elevation photographs and from point-gage traverses over the bed after a run. The ratio of dune amplitude to mean particle diameter and the ratio of dune amplitude to dune wave length were found to be unique functions of a single variable--ratio of water motion amplitude to mean particle diameter. If the amplitude-to-diameter ratio is less than 775, the dunes are two dimensional with essentially straight and level crests and troughs. If the amplitude-to-diameter ratio is greater than 1700 the bed is flat regardless of the initial condition. In the intermediate range from 775 to 1700 the dunes are three dimensional with ill-defined crests and troughs. Dune amplitude decreases almost linearly with increasing water-motion amplitude in the range of three-dimensional dunes.

The added energy dissipation with oscillatory flow over a duned bed as compared with oscillatory flow over a smooth flat bed was determined by measurements of the work input into the oscillatory-flow tunnel. The results were analyzed and presented in terms of the difference in boundary-drag coefficients between the duned bed and the smooth flat bed. The values of the drag-coefficients appeared to be abnormally large in comparison with

drag coefficients determined in other flow situations. The apparent discrepancy was traced to the existence of an essentially uniform velocity distribution above the bed in oscillatory flow in contrast to the non-uniform velocity distribution above the bed in unidirectional flow. The magnitude of boundary-drag coefficients computed from experimental measurements is obviously greatly influenced by the choice of a reference velocity. The conclusion is that a velocity in the vicinity of the bed deformation is a more rational reference than a velocity far from the bed such as the mean velocity in unidirectional flow.

TABLE OF CONTENTS



(Continued)

TABLE OF CONTENTS (Continued)

LIST OF FIGURES



(Continued)

LIST OF FIGURES (Concluded)

LIST OF TABLES

GLOSSARY

| Symbol | Quantity | Dimensions |
|---|---|---|
| $A$ | Area | $L^2$ |
| $a$ | Amplitude of water motion (2a is total amplitude) | $L$ |
| $B$ | Width of test section | $L$ |
| $C$ | Height of test section | $L$ |
| $C_D$ | Coefficient of drag | |
| $C_D^1$ | Coefficient of drag of particle falling in a quiescent infinite fluid | |
| $C_L$ | Coefficient of lift | |
| $c$ | Ripple-propagation celerity | $L/T$ |
| c.v. | Control volume | (descriptive) |
| $D_g$ | Geometric mean diameter of bed material | $L$ |
| $E$ | Energy | $FL$ |
| $F$ | Force | $F$ |
| $f$ | Coefficient of boundary drag | |
| $\bar{f}$ | Spatial mean value of f | |
| $\bar{\bar{f}}$ | Temporal mean value of $\bar{f}$ | |
| $g$ | Acceleration of gravity | $L/T^2$ |
| $K$ | $2k_3/k_1k_4$ | |
| $k$ | Nikuradse sand roughness height | $L$ |
| $k_1$, $k_2$ | Particle-shape coefficient (area) | |
| $k_3$ | Particle-shape coefficient (volume) | |

GLOSSARY (Continued)

| Symbol | Quantity | Dimensions |
|---|---|---|
| $k_4$ | $C_D/C_D^1$ | |
| KE | Kinetic energy | FL |
| L | Length of test section | L |
| $N_s$ | Sediment number, $U/\sqrt{(s-1)g\ D_g}$ | |
| P | Power | FL/T |
| p | Pressure | $F/L^2$ |
| Q | Volume rate of flow past a section | $L^3/T$ |
| s | Specific-weight ratio (sand to water) | |
| s.f. | Shape factor | |
| T | Period | T |
| t | Time | T |
| U | Mean velocity in the test section | L/T |
| u | Local velocity | L/T |
| ~~V~~ | Volume | $L^3$ |
| v | Velocity | L/T |
| W | Submerged weight | F |
| WI | Work input per cycle | FL |
| x | Horizontal coordinate | L |
| y | Vertical coordinate | L |
| $\alpha$ | Angle of inclination of the bed from the horizontal | |
| $\gamma$ | Specific weight | $F/L^3$ |

GLOSSARY (Continued)

| Symbol | Quantity | Dimensions |
|---|---|---|
| $\Delta$ | Difference in | (descriptive) |
| $\eta$ | Dune amplitude | L |
| $\lambda$ | Dune wave length | L |
| $\nu$ | Kinematic viscosity | $L^2/T$ |
| $\rho$ | Density | $FT^2/L^4$ |
| $\sigma_g$ | Geometric standard deviation of bed material in respect to size | |
| $\tau$ | Boundary shear stress | $F/L^2$ |
| $\phi$ | Angle of repose | |
| $\omega$ | $2\pi/T$ | $T^{-1}$ |

| Subscript | Meaning |
|---|---|
| b | Bed |
| c | Critical (incipient motion) |
| D | Drag |
| d | Duned bed |
| f | Flat bed |
| i | Integer |
| L | Lift |
| m | Maximum value |
| N | Normal to the bed |
| o | Boundary |
| r | Roof |

GLOSSARY (Concluded)

| Subscript | Meaning |
|---|---|
| s | Spontaneous formation of ripples and smooth |
| T | Tangential to the bed |
| w | Sidewall |

# I. INTRODUCTION

One of the more common and less understood multi-phase flows is that involving fluid flow over a bed of particles. Of particular interest to coastal engineers is the oscillatory flow of water over a sand bed. The surface of the bed is the interface between the liquid phase and the solid-particle phase. Exchange of water across the interface is limited to seepage flow through the voids in the sand grains. Exchange of sand grains across the interface occurs when the lift and drag forces acting on the surface grains are sufficient to roll them over the bed or to lift them into the overlying water stream. Of course the removal of sand grains from the bed results in a lowering of the interface which is called scour. Conversely deposition of sand grains onto the bed results in a raising of the interface which is called fill.

In oscillatory flow over a sand bed, a plausible hypothesis is that at a time in the cycle when the fluid velocity attains a certain magnitude, surface particles all over the bed begin to roll and lift from the bed until the maximum velocity is attained. Further, one would expect deposition to occur during the deceleration of the flow above the bed. In other words, the bed would periodically scour and fill with a flat bed remaining flat throughout the cycle and with the interface oscillating vertically. The frequency of the bed oscillation would be twice the frequency of the flow oscillation since two time intervals of scour and two time intervals of fill would occur during one cycle of flow oscillation. This behavior of the interface occurs only when the bottom velocities are quite large as during severe storms.

With lesser velocities, the conditions at the interface are much more complicated. Areas of the bed not only alternate periodically between scour

and fill during the cycle but also alternate spatially between scour and fill. This complicated situation is accomplished with a duned bed. The upstream face of a dune is an area of scour as the flow is accelerated in moving toward the crest. At the crest, the flow separates from the interface forming a vortex in the separated flow region on the downstream face. Sand grains which were carried over the crest from the scour area on the upstream face are deposited on the downstream face. The separated flow rejoins the bed at the trough forming a line of stagnation along which the surface particles are at rest. Thus dune troughs and crests are the spatial boundaries of the areas of scour and fill. Furthermore these areas alternate between scour and fill once each cycle inasmuch as the upstream face of a dune becomes the downstream face of that dune after flow reversal. Just prior to flow reversal, the vortex in the separation zone above the downstream face of a dune is moved up toward the crest and out into the main flow well above the dunes.

Because of the complexity of the physical problem involving an interface of fluid and particulate solids, a satisfactory mathematical analog for the flow situation at the interface has yet to be formulated. The best mathematical model as of this time (1967) has been formulated by Kennedy 1, 2, 3*/. The profile of the deformed bed is assumed to be represented by a moving sinusoid of varying amplitude and constant wave length. The assumed profile is quite reasonable if one considers the boundary to consist of the upstream face of a dune and

*Reference 3/ contains an excellent survey of the literature concerning bed forms under water waves. Because the writers have nothing to add to the literature survey, the reader is referred to this publication for an up-to-date summary (1967).

of the upper boundary of the separation zone in the lee of a crest. The water motion above the bed is assumed to be simple harmonic, that is, the wave length of the water waves is long in comparison to the wave length of the bed deformations. With these assumptions, the fluid velocity along the assumed boundary can be derived. The next step is to substitute the equation for velocity distribution into an empirical sediment-transport function which relates local sediment transport rate to the local fluid velocity. Mathematical functions for celerity of the bed form and for the ratio of dune amplitude to wave length are derived. The results of the analysis are not very significant primarily because of approximations required but this pioneer analysis is extremely significant in establishing the outline of an analytical approach for others to follow.

In the absence of an adequate mathematical model for the interface at the bed under oscillatory flow, characteristics of bed forms and the effect of these bed forms on the flow have had to be obtained experimentally without a sound basis for extrapolation to other flow situations. Experimental data about bed forms have been obtained (a) on the sea bed, (b) on the bed of wave flumes, and (c) on the surface of trays of sand which are oscillated under water.

A program for determining the characteristics of bed forms on the ocean bed was made at the Scripps Institution of Oceanography as reported by Inman 4/. Divers measured the bed forms while the water-wave characteristics were being measured on the surface. Even though measurements in situ are free from artificiality, there are some disadvantages. First the variables are uncontrolled in contrast to a laboratory experiment. Second, the phase lag between changes in the bed and changes in the flow complicate the problem of relating the existing bed to the associated flow condition. Third, the measurement of energy dissipation attributable to flow over the bed forms is extremely difficult.

Generation of and measurement of bed forms in wave flumes have been reported by Kennedy and Falcon 3/, by Inman and Bowen 5/, and by Yalin and Russell 6/. The principal difficulty with wave flumes of limited depth is that short-period high-amplitude waves are necessary in order to achieve bottom velocities which will move the particles on the bed. The fluid velocity at bed level under a short-period high-amplitude surface wave is difficult to compute or to measure. One method of achieving bed-material movement with lower velocities is by using lightweight particles such as coal or plastic particles. In any event, the range of the experimental variables is quite restricted in a wave flume.

The most versatile arrangement for determining the interfacial characteristics is that of oscillating a tray of sand under quiescent water. Bagnold 7/ used a curved tray as a pendulum bob. In an extensive program conducted at the University of California 8, 9/, a flat tray was oscillated horizontally near the bottom of a water-filled tank. The principal objection to the oscillating tray is that the forces which act on a surface particle in an oscillating tray are not dynamically similar to the forces which act on a surface particle under an oscillating fluid.

In order to closely approximate the flow conditions on the sea bed under dynamically similar conditions, an oscillatory-flow water tunnel was designed for and installed in the Georgia Tech Hydraulics Laboratory. The test section is the bottom horizontal leg of a large U-tube. Within the test section, the water motion is simple harmonic corresponding to the bottom velocity under small-amplitude progressive waves. The water tunnel was designed for a variety of experiments with oscillatory flow such as boundary-layer studies, scour studies around submerged bodies, and force studies on submerged bodies. The

most extensive use of the oscillatory-flow water tunnel has been that of studying the characteristics of the sand-water interface at the bed of the test section. The results of the three-year study about bed forms is contained in this report.

## II. EXPERIMENTAL PROGRAM

The geometric characteristics of bed forms, the limits between different states of bed configurations, and the energy dissipation attributable to bed deformations have been determined experimentally in the oscillatory-flow water tunnel for three different bed materials--a fine sand, a medium sand, and a coarse sand. The controlled flow variable is bottom velocity which is controlled by variation of the amplitude of the oscillation of the water. The period of oscillation (wave period of 3.6 sec.) is essentially constant for all runs.

### A. The water tunnel

In order to approximate the flow condition in the vicinity of the sea bed a large U-tube was designed so that water can be oscillated horizontally over a sand bed located in the bottom of the U-tube as shown in figure 1*. The test section, B, is 10.0 ft. long, 1.00 ft. high, and 4.00 ft. wide. The central section of the floor, D, is depressed to form a bed-material container which is 6.00 ft.-long, 4.00 ft.-wide, and 4.0-inches deep. The sidewalls and top of the test section are transparent plastic in order to permit visual observation of the phenomena occurring within the test section. The vertical legs of the U-tube are 1.00 ft. by 4.00 ft. in a horizontal cross section. The vertical legs are joined to the horizontal legs so as to form a streamlined flow passage, C. The free surface of the water in one of the vertical legs, A, serves as a piston. Air is continuously forced into the confined volume, J, above the water.

*All of the figures are contained in APPENDIX A.

Two large, solenoid-actuated, piston-operated, exhaust valves, E, are used to quickly relieve the excess pressure in the air above the water surface. The exhaust valves are closed for about one-quarter cycle during the time when the water surface is falling in that leg. A float gage, F, in the other vertical leg is joined to a direction-sensing switch, H, which is the first element in a feedback-control system used to close and to open the exhaust valves at the proper time during the cycle.

This system oscillates the water in the U-tube with simple harmonic motion at resonant frequency resulting in an almost constant period of 3.6 sec. Equilibrium amplitude can be controlled by adjustment of the air pressure at J. Air pressure at J is controlled by means of speed regulation of the blower.

Transients are eliminated by means of a separate air system, K. Initially the water levels are unbalanced to the desired equilibrium amplitude. Upon release of the initial unbalance by opening the valve, I, the water oscillates at equilibrium amplitude. Final transients are eliminated by closure of the valve, I, over an exhaust port.

Amplitude and period of oscillation are recorded on a direct-writing oscillograph. The float-elevation sensor system consists of an endless, small diameter, stainless-steel cable which passes over pulleys at the top and bottom in one vertical leg of the U-tube. The endless cable is fastened to a wooden float. A three-turn potentiometer, which is connected to the axle of the upper pulley, is one leg of a Wheatstone bridge. Bridge unbalance is sensed and recorded. The recorder is also equipped with a timing marker which marks pips at one-second intervals on the record.

A pressure transducer is attached to a piezometer in the air space above the oscillating water surface in the vertical leg, A. The output of this

pressure-transducer circuit is simultaneously recorded with the water-elevation record. Using these data the work input per cycle to maintain the oscillation can be calculated.

Two piezometers are installed in one wall of the test section above the sand bed. These piezometers are located 2.0 inches below the roof and 38.0 inches apart as shown in figure 2. These piezometers are connected to a differential-pressure transducer. From the simultaneously recorded data of water motion and pressure difference, energy dissipation within the 38-inch length of test section can be calculated.

Coordinate markings on one of the transparent sidewalls of the test section are used for measurement of dune geometry. Polaroid pictures of the sidewall which show both the coordinates and the dunes are the data.

A pair of precision instrument rails have been mounted over the test section so that an instrument carriage on which an electric point gage is mounted can be accurately positioned anywhere over the 3-ft. square access opening located in the center of the roof of the test section. Using this instrument, topographic maps of the bed can be made of a section of the bed which is slightly less than 3-ft. square.

B. Bed material

The coarse sand and fine sand were obtained from the Ottawa Silica Company and the medium sand was obtained from the Minnesota Mining and Manufacturing Comapny. Size and gradation of the sands were determined by sieve analysis following the procedures recommended by Vanoni, Brooks, and Kennedy 10/. The results were analyzed following the practice described in a committee publication of the American Society of Civil Engineers 11/. Standard techniques were

used to determine the specific-weight ratio, $\gamma_s/\gamma$ or s. The Ottawa sands are well rounded for which a shape factor of 0.7 is applicable 12/. The glass beads (medium sand) are almost spherical with a shape factor of nearly unity. The pertinent properties of the sands are listed in TABLE I.*

## C. Experimental procedure

### 1. Regular run

The following description of the procedure during a run is in chronological order.

Prior to each run, the submerged sand bed was leveled by means of a wooden screed which is long enough to bridge the bed-material container, D in figure 1. If the amplitude of the water motion were to be insufficient for a dune system to develop spontaneously, a 1/2-inch half-round bar was placed on the flat sand bed in the middle of the test section. The bar, which extended across the test section perpendicular to the water motion, is a two-dimensional disturbance from which a dune system will propagate during low-amplitude runs. The bar was not used during high-amplitude runs when the dune system would develop spontaneously all over the bed. After the bed was leveled, the roof hatch was fastened.

Prior to filling the water tunnel, the float-elevation sensor system was calibrated. Calibration consisted of clamping the float at various levels as noted on the scale which is parallel to the steel rod, G in figure 1, and making a short record on the oscillograph recorder at each level.

---

*All Tables are contained in APPENDIX B.

During the time that the water tunnel was being filled, the pressure transducer in the air space in one vertical leg, A in figure 1, was calibrated. The pressure transducer is connected to one side of a constant-displacement, precision water manometer by means of a flexible plastic tube. The pressure within the air volume between the pressure transducer and the differential manometer was adjusted by blowing into a branch and then clamping this branching tube. Calibration consisted of making short records on the oscillograph recorder at five or more pressure levels. The magnitude of the pressure head at these various levels was read on the scale of the constant-displacement manometer and was recorded directly on the strip chart beside the corresponding trace.

The water level within the tunnel was carefully adjusted to a reference level as determined by a pointer on the rod, G, which moved parallel to a scale as indicated in figure 1. By having the mass of water in the tunnel constant during each run, the period of oscillation was maintained at a nearly constant value of 3.6 sec.

Next the blower was started. The master switch for designating the operating conditions was placed in the "stop" position. In the "stop" position both of the exhaust valves, E in figure 1, are open and the damping valve, I in figure 1, is closed. With the valves in this position, the blower can be operated without oscillating the water in the tunnel. The blower speed was then adjusted so that the work input would be about that required to maintain the desired amplitude of oscillation. The requisite speed setting was determined through measurement of the stagnation pressure in the blower outlet. After

a few runs, a calibration curve of this stagnation pressure as a function of water-motion amplitude was established*.

With the blower-speed adjusted, the next step was to turn the master switch to "blowdown". In the "blowdown" position both of the exhaust valves, E in figure 1, are open, the damping valve, I in figure 1, is closed, and the solenoid valve in the high-pressure air supply line, K in figure 1, is open. Air is forced into the now-closed chamber above the water surface thereby forcing a difference in the water levels in the two vertical legs of the U-tube. When the unbalance reaches the desired amplitude, the master switch is turned to "run" which shuts off the air supply through K, opens the valve, I, and switches control of the exhaust valves, E, to the float-actuated feedback system**.

During a run one operator makes repeated readings and recordings of the maximum and minimum elevations of the float position and the elapsed number of cycles***. In addition, this operator reads and records the water temperature from a thermometer which is taped on the inside of the transparent sidewall at the end of the test section nearest to the float gage.

---

*During the runs with the coarse and medium sand, the blower speed was unchanged during a run. The amplitude of oscillation decreased somewhat as the energy dissipation over the duned bed is greater than over the flat bed which was always the initial condition. During the runs with the fine sand, an operator manually increased the blower speed as the duned bed developed in order to maintain a constant amplitude throughout a run.

**The purpose of the "blowdown" sequence is, of course, to eliminate the initial transients of the oscillatory motion. Thus the initial conditions are flat bed and an amplitude which is nearly at equilibrium.

***Because of the effort required in preparing for, in making of, and in analyzing the results of a run, duplicate records of water-motion amplitude were deemed to be worthwhile.

The other operator has various duties. During low-amplitude runs, this operator reads and records the position of the dune crests which develop and propagate away from the two-dimensional disturbance. This duty is not required for high-amplitude runs in which the dunes develop spontaneously all over the bed. He also obtains the work-input data by obtaining strip-chart records of the pressure-transducer output at the beginning of a run while the bed is still flat and near the end of a run after the equilibrium duned bed is achieved. In addition he makes and develops photographs (Polaroid prints) showing a side-elevation view of the dunes as seen through the transparent sidewalls of the test section.

The run is stopped by turning the master switch to "stop". In the "stop" position both exhaust valves, E in figure 1, are open and the damping valve, I in figure 1, is closed. By switching from "run" to "stop", final transients are eliminated except for a gradual movement to a condition of equal water levels in both vertical legs. Elimination of the final transients preserves the interfacial configuration of the sand which developed during the periodic motion.

After the oscillatory motion is stopped, the blower is turned off, the water level is lowered, and both the float-elevation sensor system and the pressure transducer system are calibrated in exactly the same way as before the run.

In each of the later runs (fine-sand runs) additional data were taken from which the energy dissipation within the test section could be calculated. The setup for these additional measurements is shown in figure 2. Prior to making this second part of the run, the Wheatstone bridge of the float-elevation sensor

system was transferred to a second 2-channel Sanborn oscillograph. The bridge circuit of the pressure transducer shown in figure 2 was also connected to this second recorder.*

The float-elevation sensor system was calibrated as described previously.

Then water was added within the tunnel until the water was again at the reference level.

Next the pressure transducer was calibrated as follows. The three-way valves are positioned to connect the pressure transducer, figure 2, with the piezometers. Then the chambers on both sides of the transducer are bled through a small opening in each chamber. The valves are then positioned to connect the manometer with the piezometers. A valve is opened at the top of the differential manometer thereby bleeding the connecting lines. Next air is forced into the top of the manometer until the water levels are about at mid-scale of the manometer. Then the value at the top of the manometer is closed. Next both three-way valves are switched to connect the manometer with the transducer. The water-filled bellows is adjusted until the water columns in the manometer are equal in elevation. In this condition the pressure difference across the pressure transducer is zero. The transducer circuit is balanced and the recorder stylus is zeroed at approximately midposition on the recorder paper. Various pressure differences can be applied by means of the adjustable bellows. Recordings are made at numerous settings of the bellows with the pressure difference being read on the manometer.

*The second part of a run was necessary because the laboratory instrumentation includes only single and dual channel oscillograph recorders.

The steps described previously to start the oscillation were repeated except that blower-speed adjustment was not required inasmuch as the oscillation was occurring over the same deformed bed and at the same amplitude as in the first part of the run.

As soon as the oscillation at equilibrium amplitude was reestablished a simultaneous record of the float position and of the pressure-transducer output was obtained.

After the data were recorded, the water oscillation was stopped, and both instrument systems were recalibrated.

For the fine-sand runs, dune geometry was recorded on topographic maps rather than on the side-elevation photographs described previously. In order to map the bed after a run, instrument rails have been mounted above the test section so that an instrument carriage can be accurately positioned in the axial direction over the 3-ft. square hatch opening in the roof of the test section. An electrical point gage is mounted on the instrument carriage so that the point gage can be accurately positioned in the transverse direction. The electrical point gage gives excellent response upon contact with the moist-sand bed. Because of the careful fabrication of the instrument carriage and the careful levelling of the instrument rails (from a water surface), the belief is that all elevations could be readily determined within $\pm 1/2$ mm of the true value and the horizontal coordinates could be readily determined within $\pm 1$ mm of the true value. Following a run, the water was slowly drained from the water tunnel in order to avoid any change in the dune system. The roof hatch was removed from the test section. In the interim period between the end of the run and the measurement of bed coordinates, the bed was kept

moist by intermittently pumping water into one corner of the bed. Elevations of the bed were determined at the grid points of a horizontal rectangular grid. The grid lines were spaced at 1.00-in. intervals across the test section and at 0.050-ft. intervals along the test section.

2. Special runs

a. Boundary-layer transition

The mechanism of boundary-layer transition was observed with three bed conditions--a plane smooth bed, a coarse-sand flat bed, and a medium-sand flat bed. For the plane smooth bed, cement-asbestos sheets were fastened in the sediment container, D in figure 1, with the surface of the sheets alined with the bottom of the test section. A red dye was forced to seep through a small hole in the sheet. Data consisted of water-motion amplitude, water temperature, and observations about the motion of the dye. The flat sand bed tests were similar except that the tip of the dye injector was slightly beneath the surface of the sand. Observations were made during steady cyclic motion. The observations were repeated at several values of water-motion amplitude--each larger than the previous value.

b. Flat-bed incipient motion

The flat-bed incipient motion tests were also with steady cyclic motion with a step increase in the value of the water-motion amplitude. Data consisted of water-motion amplitude, water temperature, and observations about the movement of the surface particles. Obviously, the bed was leveled prior to the flat-bed incipient motion tests.

c. Deformed-bed incipient motion

Run 62 was made at the lowest water-motion amplitude at which a dune system was expected to develop and to propagate away from the 1/2-inch, half-round bar which was placed at midlength of the test section. Run 62 exceeded expectations in that after 27 hours the leading crests were close but had not reached the end of the bed. Data consisted of water-motion amplitude, water temperature, and dune positions as a function of elapsed cycles.

d. Work input (smooth flat immobile bed)

In order to determine the energy dissipation attributable to the flow over a duned bed, work input into the tunnel was determined for two bed conditions--a smooth flat immobile bed and the duned beds.

The smooth immobile boundary was formed by a sheet of 18-ga. aluminum placed over the depression in the bed of the test section. Prior to placement of the aluminum sheet, sand was placed in the bed-material container in the floor of the test section. The sand bed was smoothed and levelled to the elevation of the floor of the test section. Next the 4 ft. by 8 ft. sheet of 18-ga aluminum was placed on the floor of the test section. Two extruded aluminum angles, 1 in. by 1 in. by 1/16 in., were then placed in the corners with one exterior surface of each angle in contact with the aluminum sheet and the other exterior surface in contact with the sidewall of the test section. The angles were held in position with lengths of 2 in. wide duct tape. To insure that the aluminum sheet was pulled down firmly onto the underlying sand, a negative pressure of about -3 ft. of water was created in the sand during the immobile-smooth-bed runs.

Runs with a flat smooth immobile bed were executed in a similar manner to the regular runs described previously.

D. Range and purpose of the experiments

A complete listing of all runs, the physical variables, bed conditions, and purpose is contained in TABLE II.

# III. RESULTS

## A. Special runs

The results of the special studies are summarized in TABLES III and IV.

### 1. Boundary-layer transition

The boundary-layer data in TABLE III were obtained by observation of the dye which was allowed to seep upward from the bed. The beginning of transition was judged to occur when line vortices were first formed parallel to the bed and perpendicular to the direction of the water motion. These vortices formed at about the time of flow reversal. The axes of the vortices were a small distance from the bed. This distance was estimated to be about 5 mm. The flow was laminar both above and below the visually observed row of vortices. In the beginning the vortices persisted for a very short time. With increasing amplitude, the duration of the vortices also increased. The boundary layer was called fully turbulent when the vortices persisted throughout the entire cycle. Even with the turbulent boundary layer, the main body of the flow remained laminar--really irrotational. The smallest amplitude for fully turbulent boundary layer could not be determined on the sand beds because of the rolling of the surface particles.

### 2. Flat-bed incipient motion

Flat-bed incipient motion was visually observed and was defined when approximately 10 percent of the surface particles were rolling back and forth. Some particles are moved at lesser water-motion amplitudes than those listed in TABLE III. The first motion is a rocking motion of some particles that are perched in an unstable position. With a slight increase in amplitude, these particles roll into more stable positions on the surface of the bed. The first

movement of particles after the initial readjustment of the bed surface appears to be of the larger-sized particles. Initial movement of surface particles appeared to occur at about the time of maximum velocity. The reader is cautioned that the observations related above are not precise but are subject to the judgment of the observer.

3. Deformed-bed incipient motion

Dune systems will develop and will propagate away from a flow disturbance placed on the bed with water-motion amplitudes considerably less than amplitudes at which a dune system will spontaneously form on an initially flat bed. Run 62 was made for the purpose of determining the lowest water-motion amplitude at which a dune system would develop and would propagate away from the 1/2-in. diameter, half-round bar used as the flow disturber. The duration of Run 62 was 27 hours. At the end of the run, the leading crests were only 2.18 ft. and 2.70 ft. from the flow disturbance. At the time the run was terminated, nine dune crests appeared to be fully developed, that is, four on each side of the central crest which covered the bar. Both of the fourth crests from the central dune were 1.48 ft. from the crest of the central dune. Five partially developed dunes extended beyond the fourth crest on one side and three partially developed dunes extended beyond the fourth crest on the other. The only sand-grain movement appeared to be over the fourth crests. On the basis of the above observations, the water-motion amplitude of Run 62 was taken to be the lowest water-motion amplitude at which a dune system would develop and would propagate. Another connotation is that the water-motion amplitude of Run 62 is the amplitude at which surface-grain movement will cease with oscillatory flow over a two-dimensional dune system. The pertinent physical variables of Run 62 are listed in TABLE III.

4. Spontaneous appearance of ripples

If the water-motion amplitude, a, were greater than the values listed in TABLE III, ripples would spontaneously and simultaneously form all over the flat bed after a few cycles of oscillation. Prior to the onset of spontaneous ripples some of the surface grains would be moving back and forth practically in phase with the water velocity. At the onset of spontaneous ripples, the motion of the surface grains became restricted to transverse bands of grains moving essentially in phase with velocity. The bands of moving grains were separated by bands of stationary grains. The bands of moving grains became ripple crests and the stationary bands became ripple troughs. The ripple crests move back and forth nearly to the edges of the band of moving grains. The appreciable movement of the ripple crests in phase with the water motion might explain why no separation and vortex motion was observed in the lee of the crests. As the oscillation continues, ripple amplitude increases until separation occurs and vortices form, that is, a dune system is born. From this time until an equilibrium dune system is scoured into the bed, the bed-form pattern is very irregular as the shorter wave length ripple system is being replaced by the longer wave length dune system.

5. Work input (smooth flat immobile bed)

Work-input is evaluated from the work input on the water surface in the west leg of the U-tube. All of the external work to the oscillating tunnel required to maintain oscillation is pressure work applied to the free-water surface in the west leg of the U-tube. The work input per cycle in the west leg is

$$WI = \int_{-T/2}^{T/2} P \, dt \tag{1}$$

in which WI is the work input per cycle, T is the period of oscillation, P is power, and t is time. By definition

$$P = F \, v \tag{2}$$

in which F is the pressure force on the water surface and v is the velocity of the water surface. Further

$$F = p \, A \tag{3}$$

in which p is the measured pressure in the air above the water surface and A is the area of the water surface in the west leg of the U-tube. Since the water motion within the water tunnel is simple harmonic

$$v = \frac{2\pi a}{T} \cos \frac{2\pi t}{T} \tag{4}$$

in which $2a$ is the total amplitude of the water motion in the west leg of the U-tube and T is the period of the motion. Because the cross sectional area of the west leg, test section, and east leg are equal (1 ft. by 4 ft. in dimensions), the value of $2a$ which is measured in the east leg is equal to the total water-motion amplitude in the west leg. As a further consequence of the equality of cross sectional areas the maximum mean velocity in the test section, $U_m$ is simply $(2a)(\pi/T)$. Combining equations 1, 2, 3, and 4,

$$WI = A\,a \int_{-\pi}^{\pi} p \cos \frac{2\pi t}{T} \, d\left(\frac{2\pi t}{T}\right) \tag{5}$$

Work input to maintain oscillation was evaluated by numerical integration of equation 5 from the recorded data shown in figure 3. The water-motion record (upper trace in figure 3) was used to establish the relation between the measured value of p (middle trace in figure 3) and $2\pi t/T$. Values of the pressure were determined at every millimeter along the strip chart. The complete cycle in figure 3 is 87 mm in length of chart. Using the trapezoidal rule for numerical integration of equation 5, the total integral would be approximated by the summation 86 equal-width trapezoids in figure 3. The numerical computations were done by means of an electronic computer from punched-card data.

Equation 5 is the work input into the water tunnel. The work input is equal to the energy dissipation provided that the total water-motion amplitude, 2a, is constant. On the other hand if the amplitude, 2a, is increasing, part of the work input is used to increase the energy of the oscillating water mass. In this case, energy dissipation per cycle would be the work input per cycle minus the energy increase per cycle. Conversely if the amplitude, 2a, is decreasing, energy dissipation is the sum of the work input and the energy decrease per cycle. The energy of the oscillating water mass can be conveniently evaluated either when the kinetic energy is a maximum and the potential energy is zero or when the potential energy is a maximum and the kinetic energy is zero. When the kinetic energy is zero, the potential energy, PE, is as follows

$$PE_{max} = \gamma A a^2 \tag{6}$$

in which $\gamma$ is the specific weight of the water. The change in energy, E, of the oscillating mass between cycle, i + 1, and cycle, i, is as follows

$$E_{i+1} - E_i = \gamma A \left( a^2_{(i+1)} - a^2_{(i)} \right) \approx \frac{\gamma A}{2} (2a)(\Delta\, 2a) \qquad (7)$$

in which $\Delta\, 2a$ is the change in total water-motion amplitude per cycle. A convenient method of determining $\Delta\, 2a$ is to plot 2a versus the integer, i, and then to determine the slope graphically at the value of i of interest.

The work inputs with a smooth flat immobile bed determined from experimental measurements are listed in TABLE IV.

The results are graphically shown in figure 4 in which energy dissipation per cycle for the entire water mass is plotted as a function of total water-motion amplitude, 2a. The straight-line functions were visually fitted to the measured points.

## B. Regular runs

### 1. Evolution of a duned bed

#### a. Induced

If the water-motion amplitude, a, were less than that required for the spontaneous appearance of ripples (TABLE III), a dune system could be induced to form by placing a two-dimensional disturbance (II.C.1) on the bed. Upon starting the oscillation an embryo dune is formed on each side of the disturbance. This pair of dunesgrows in wave length and amplitude. At some stage in the development, the first dunes act as a disturbance thereby inducing a second pair of dunes, and so one. Position of the dune crests was repeatedly measured by noting the crest position in relation to a coordinate scale marked on the test section wall. During runs with a very low amplitude,

the scouring process was slow enough for the dunes to develop in an orderly manner; that is, the increase in wave length was accomplished by continuous outward movement of the more recently formed dunes. An example of an orderly development of dunes is shown in figure 5. For runs in which the amplitude of oscillation is greater, scour occurs rapidly with the result that the older dunes overtake some of the newer dunes. In these runs, the evolving dune system is disorderly. In spite of this interim disorderliness, the dune system developed into a regular pattern at equilibrium.

The formation of a new dune was noticed by the movement of sand grains some distance beyond the most advanced dune. This band of moving grains became the crest of the new dune. The wave length of the dune at the time of formation was always less than the wave length of an equilibrium dune. Because of the low order of accuracy of measurement no attempt is made to present numerical values for the initial wave length except to state that the initial wave length appeared to be one-half or less of the equilibrium wave length.

The large mass of data about the developing dune system is condensed in figure 6. Figure 5 is a complete space-time graph of dune positions. Each part of figure 6 is a space-time graph of the leading crests only. Because the dune system propagates in both directions from the disturbance, two sets of data are shown in the figure 6. The third function shown in each graph is the total water-motion amplitude, 2a. Since energy dissipation increases as the duned bed develops, the amplitude of the water motion tends to decrease unless the blower speed is adjusted manually.

b. Spontaneous

If the water motion amplitude, a, were greater than that required for the spontaneous appearance of ripples (TABLE III), a dune system would

evolve by scouring all over the bed. Just prior to the appearance of ripples some of the surface grains would be moving back and forth apparently in phase with the water velocity. Soon the motion of the surface grains become restricted to transverse bands of grains moving essentially in phase with the water velocity. The bands of moving grains were separated by bands of stationary grains. The bands of moving grains became ripple crests and the stationary bands became ripple troughs. In the beginning, the ripple crests moved back and forth nearly to the edge of the moving grains. As the oscillation continues, ripple amplitude increases and crest motion appears to decrease. Vortices in the lee of the crests become noticeable by the sand grain motion. From this time until an equilibrium dune system is scoured into the bed, the bed-form pattern is very irregular because many of the initial ripples must be obliterated as dunes develop having a longer wavelength. Data in this transitory stage was limited to the observations given above.

2. Bed geometry

Selected photographs of the equilbrium dunes as viewed through the side of the test section are shown in figure 7 and figure 8. The bed material is medium sand in figure 7 and coarse sand in figure 8. Topographic maps of the duned beds developed with the fine sand are shown in figure 9. The flow conditions for all runs are listed in TABLE II.

Dimensionless geometric and flow variables listed in TABLES V, VI, and VII and are summarized in figures 10, 11, and 12. The dependent variables of dune geometry are amplitude $\eta$ and wave length $\lambda$. The fluid-property variables are fluid density $\rho$ and the fluid specific weight. The fluid specific weight, $\gamma$, is a variable because the stabilizing force on the bed particles is a function of the submerged weight which is proportional to $\gamma_s - \gamma$ or $\Delta\gamma$ in which $\gamma_s$ is the specific

weight of the sediment. The fluid viscosity has been omitted as a variable by virtue of the negligible boundary layer thickness anticipated in the flow occurring over dunes. The fluid flow variables would be any two of the following three variables: the maximum velocity $U_m$ a short distance above the dune crests, the period T of the oscillatory motion, and the amplitude a of the water motion a short distance above the dune crests. The sediment-property variables are mean diameter $D_g$, geometric standard deviation $\sigma_g$ with regard to size, particle shape, and specific weight of the sediment $\gamma_s$. The omission of the sediment density $\rho_s$ is founded upon the idea that the inertial reaction of the sediment particles is insignificant in the movement of the bed grains. Since the two specific weights are involved in a known way, that is, by submerged weight, $\gamma$ and $\gamma_s$ can be replaced with a single variable $\Delta\gamma$. Thus

$$\eta \text{ or } \lambda = f\,(U\,, T\,, \rho, \Delta\gamma, D_g, \sigma_g, \text{particle shape}) \tag{8}$$

or

$$\eta \text{ or } \lambda = f\,(T\,, a, \rho, \Delta\gamma, D_g, \sigma_g, \text{particle shape}) \tag{9}$$

In dimensionless form the first combination is

$$\frac{\eta}{D}\,,\ \frac{\lambda}{D_g},\ \text{or}\ \frac{\eta}{\lambda} = f\left(T\sqrt{\frac{(s-1)g}{D_g}}\,,\ \frac{U_m}{\sqrt{(s-1)gD_g}}\,,\ \sigma_g,\ \text{particle shape}\right) \tag{10}$$

and the second is

$$\frac{\eta}{D},\ \frac{\lambda}{D_g},\ \text{or}\ \frac{\eta}{\lambda} = f\left(\frac{a}{D_g}, T\sqrt{\frac{(s-1)g}{D_g}}\,,\ \sigma_g,\ \text{particle shape}\right) \tag{11}$$

Values of the dimensionless parameters, which are listed in TABLES VI and VII, were computed from dimensions scaled from photographs - - samples of which are shown in figures 7 and 8. Variability of the dune amplitude, $\eta$, and the dune wave length, $\lambda$, is apparent in each of the photographs of figures 7 and 8. Wave length, of course, is simply the distance between successive crests. Amplitude was obtained by averaging the elevation of two successive crests and then subtracting the elevation of the intervening trough. Mean values are shown in TABLES V, VI, and VII with the number of observations used in the averaging being shown in the second column of the tables. For the fine sand, TABLE V, the data consisted of tabulated elevations (point-gage readings) taken along lines parallel to the axis of the test section.

3. Work input

Measurements from which to calculate work input into the tunnel were made with a flat sand bed and with a duned bed. Work-inputs were calculated from data such as shown in figure 3 by the method described in III.A.5.

Flat-sand-bed data were of two types. If the water-motion was less than that at incipient motion, the initially flat bed would remain flat. An example of a run of this type is Run No. 108 (TABLE II). If the water motion were greater than that for spontaneous formation of ripples (TABLE III), data had to be obtained immediately after the start of a run before the bed had become deformed. The two types are distinct in the sense that the first is a flat, immobile, sand bed whereas the second is a flat, mobile, sand bed. Work inputs with a flat sand bed determined from experimental measurements are given in TABLE VIII.

Measurements from which to calculate work input into the tunnel with a duned sand bed were made after the dunes had attained an equilibrium profile. Work inputs determined from experimental measurements are given in TABLE IX.

## 4. Energy dissipation within the test section

Energy dissipation within the test section could be evaluated from data such as shown in figure 13 which was obtained by means of the apparatus shown in figure 2. Energy dissipation is evaluated by using the experimental data to calculate the other terms in the work-energy equation.

The work-energy equation in the power form for the horizontal control volume shown in figure 14 is as follows

$$-(\text{rate of energy dissipation}) + \iint_{A_1} p_1 \, dQ - \iint_{A_2} p_2 \, dQ$$

$$= \frac{\partial}{\partial t} \iiint_{c.v.} \left(\frac{\rho u^2}{2}\right) d\forall + \iint_{A_2} \frac{\rho u^2}{2} \, dQ - \iint_{A_1} \frac{\rho u^2}{2} \, dQ \qquad (12)$$

Since the test section is a uniform flow zone and since $\rho$ is constant

$$\iint_{A_2} \frac{\rho u^2}{2} \, dQ - \iint_{A_1} \frac{\rho u^2}{2} \, dQ = 0 \qquad (13)$$

Since the test section is a uniform flow zone, the pressure work terms can be simplified as follows

$$\iint_{A_1} p \, dQ - \iint_{A_2} p \, dQ = (p_1 - p_2)Q = (p_1 - p_2)A \, U \qquad (14)$$

Substituting equations 14 and 15 into equation 12

$$-\left(\begin{matrix}\text{rate of energy dissipation}\\ \text{within the control volume}\end{matrix}\right) + (p_1 - p_2)A\,U = \frac{\partial}{\partial t}\iiint_{c.v.} \frac{\rho u^2}{2}\, d\forall \qquad (15)$$

The experimental data can be more conventiently handled by changing equation 15 from a rate equation by multiplying each term by dt and then integrating through a cycle. After multiplying by dt, the right side of equation 15 is a perfect differential. The integral of this perfect differential is simply the change in kinetic energy within the control volume during that cycle.

$$\underline{\text{energy dissipation within c.v.}}_{\text{cycle}} = \int_t^{t+T} (p_1 - p_2)A\,U\,dt - \underline{\Delta\,(\text{kinetic energy})}_{\text{cycle}} \qquad (16)$$

If the water-motion amplitude (figure 13) were constant at the time the data were taken, the change in kinetic energy during a cycle would be zero. If the water-motion amplitude were changing, the last term of equation 16 can be approximated as follows. Because of the negligible boundary-layer thickness, the velocity, U, can be considered to be the mean velocity, U, throughout the test section, as follows

$$u = U = \frac{2a\pi}{T}\cos\frac{2\pi t}{T} \qquad (17)$$

The mean kinetic energy within the test section during the $\underline{i}$th cycle

$$KE_{mean} = \frac{1}{T}\int_o^T KE\,dt = \frac{1}{2}\left[\frac{\rho\,AL\,a^2}{2}\left(\frac{2\pi}{T}\right)^2\right] \qquad (18)$$

Any change in the mean kinetic energy, equation 18, between the $\underline{i}$th and $\underline{i+1}$ th cycle enters into the evaluation of energy dissipation in accordance

with equation 16. Evaluating the change

$$\frac{\Delta \text{ KE}}{\text{cycle}} = \frac{\rho \text{ AL } \pi^2}{T^2} (a^2_{i+1} - a^2_i) \approx \frac{\rho \text{ AL } \pi^2}{2T^2} (2a)(\Delta 2a) \qquad (19)$$

in which 2a is the total water-motion amplitude. A convenient method of determining $\Delta$ 2a in a cycle is to plot 2a versus the integer, i, and then to determine the slope graphically at the value of i of interest.

Since the motion is simple harmonic, the pressure-work-input integral is

$$Aa \int_0^{2\pi} (p_1 - p_2) \cos \frac{2\pi t}{T} \, d\left(\frac{2\pi t}{T}\right) \qquad (20)$$

Work input per cycle was evaluated by numerical integration of the above equation. Numerical integration was by means of the trapezoidal rule using small increments of $\Delta(t/T)$. Great care has to be exercised in determining the location of t/T = 0 on the strip-chart record of float position, figure 13. In order to increase accuracy, actual determinations are made on a chart where a 1-sec interval is 100 mm long.

Values of energy dissipation within the 38-inch long section of the test section are tabulated in TABLE X.

# IV. ANALYSIS OF RESULTS

## A. Incipient motion

Incipient motion of the protruding surface particles occurs when the hydrodynamic forces on the protruding particles are sufficient to roll these surface particles over the bed. Early in the study, experiments revealed that incipient motion would occur at different values of water-motion amplitude depending upon whether the bed was flat or was deformed. Obviously the difference in the two situations is in the magnitude of the fluid velocity in the vicinity of the protruding particles. Not quite so obvious, is the desirability of formulation of an incipient-motion criterion which is in terms of the velocity in the vicinity of the protruding grains. The advantage of this kind of incipient-motion criterion is that the determination of the velocity in the vicinity of the protruding grains becomes a separate problem. In other words, an incipient-motion criterion which is formulated in terms of flow, fluid, and geometric variables in the vicinity of the protruding grain should be quite universal.

The analysis is based upon the hydrodynamic surface forces of drag, $F_D$, and lift, $F_L$, and the submerged weight, W, on a typical protruding particle. Additional surface forces arising from inertial reaction of the particles and of the fluid around the particles are not included because the surface particles at the crest of Run 62 were observed to move only when the velocity was near maximum, that is, when the acceleration in the flow is negligible. In other words, the lift and drag force on a typical protruding particle are considered to be quasi-steady in the following analysis.

The simplest case of incipient motion is illustrated in figure 15 in which submerged weight is the only force other than adjacent particle reactions.

If the bed is inclined at the angle of repose, $\phi$, some of the protruding surface particles will be at the incipient-motion condition. As shown in figure 15, the instability limit is

$$\tan \phi = F_T / F_N \tag{21}$$

in which $F_T$ and $F_N$ are the summation of the external forces on the particle which are tangential and normal to the bed, respectively. The angle of repose, $\phi$, can be determined in the laboratory. The angle of repose, $\phi$, is a function of particle size, angularity, and porosity. Typical values of $\phi$ are given by Simons and Albertson 13/ showing the relationship between $\phi$, particle size, and angularity for an unspecified porosity.

A more complex force system is illustrated in figure 16 in which $F_D$ and $F_L$ are hydrodynamic drag and lift forces, respectively, W is the submerged weight, and $\alpha$ is the inclination of the bed from horizontal. Substituting the forces shown in figure 16 into equation 21,

$$\tan \phi = \frac{F_D - W \sin \alpha}{W \cos \alpha - F_L} \tag{22}$$

The drag and lift forces can be written in the conventional form

$$F_D = C_D k_1 D_g^2 \frac{\rho u^2}{2} \tag{23}$$

and

$$F_L = C_L k_2 D_g^2 \frac{\rho u^2}{2} \tag{24}$$

in which $C_D$ and $C_L$ are coefficients of drag and lift, respectively, $k_1$ and $k_2$ are particle-shape coefficients, $D_g$ is mean size of particle, $\rho$

is fluid density, and u is fluid velocity at the level of the protruding particle. The submerged weight, W, can be written as

$$W = k_3 (\gamma_s - \gamma) D_g^3 \tag{25}$$

in which $\gamma_s$ and $\gamma$ are the specific weights of the bed particles and the fluid, respectively, and $k_3$ is another particle-shape coefficient. Substituting equations 23, 24, and 25 into equation 22, and rearranging,

$$\frac{u_c^2}{(s-1)g\, D_g} = \left[\frac{2k_3 (\tan \phi \cos \alpha + \sin \alpha}{k_1 + k_2 (C_L/C_D) \tan \phi}\right]\left[\frac{1}{C_D}\right] \tag{26}$$

in which s is the specific-weight ratio, $\gamma_s/\gamma$, and $u_c$ is the initial-motion value of the bottom velocity. Chepil 14/ measured the lift and drag on a hemisphere placed on a plane boundary. He found that $C_L$ was about 0.8 $C_D$. Since the protruding particles under consideration probably protrude further from the bed than the hemisphere and since the pressure condition under a protruding particle is unknown and variable depending upon the configuration of the flow passages under the particle, a value of unity for the ratio, $C_L/C_D$, is taken as a reasonable average value. In addition, the assumption is made that the particle-shape coefficients, $k_1$ and $k_2$, are equal. Also the assumption is made that the value of $C_D$ for the protruding particle is proportional to $C_D^1$ for the freely falling particle at the same particle Reynold number, that is

$$C_D = k_4 C_D^1 \tag{27}$$

Values of $C_D^1$ for free-falling sand grains with a shape factor of 0.7 are given by Albertson, Barton, and Simons 15/.

Substituting the above simplifications into equation 26,

$$\frac{u_c^2}{(s-1)gD_g} = \frac{\tan\phi\cos\alpha + \sin\alpha}{1 + \tan\phi} \quad \frac{K}{C_D^1} \tag{28}$$

in which K is equal to $2k_3/k_1k_4$ Since the constant, K, involves only particle-shape coefficients and a proportionality factor relating $C_D$ and $C_D^1$, the constant, K, is independent of the orientation of the gravity force

Flow over a duned bed under oscillatory flow as sketched in figure 17 is an ideal flow situation for the determination of the constant, K, in equation 28 principally because the boundary-layer thickness is negligible on the upstream face of the dune. First, the boundary layer of an oscillatory flow must be reformed and grow twice each cycle with insufficient time for the development of a thick boundary layer. Second, the pattern of separation of the flow at the crest, reattachment in the trough, and converging flow along the upstream face are flow conditions under which boundary-layer development is suppressed even under steady flow conditions. As a further precaution to insure a neglibible effect of a boundary layer, the coarse sand was used in the experiment, Run 62, for the determination of the deformed-bed incipient-motion condition.

Since the boundary-layer thickness is negligible along the upstream face of a dune (at least for coarse sand), the distribution of the velocity, u, can be determined from a solution for irrotational flow. The measured profile of the dunes, figure 18, was closely approximated in the irrotational flow solution shown in figure 19(a). The velocity shown in figure 19(b) at the crest is 1.2 U in which U is the velocity in the mainstream a short distance above the dune crests. The straight-line approximation shown in figure 19(b)

can be expressed as

$$\frac{u}{U_m} = 2.4 \ \frac{x}{\lambda} \ \cos \ \frac{2\pi t}{T} \qquad (29)$$

for the velocity distribution along the upstream face of a dune. The maximum velocity, $U_m$, above the dunes in Run 62 was 0.473 fps. Hence the maximum velocity at the crest would be 1.2 times 0.473 or 0.567 fps. Using the velocity, $u_c$, of 0.567 fps to compute the particle Reynolds number, the value of $C_D^1$ is found in reference 15/ to be 1.6 for particles with a shape factor of 0.7.

Flow over a dune under oscillatory flow is illustrated in figure 17. The water motion at the instant of illustration is from left to right in figure 17. The flow separates from the bed at the dune crest forming a vortex in the lee of the crest. The flow reattaches to the bed in the trough. The velocity at protruded-particle height is zero in the trough and increases continuously up the face of the dune to attain a maximum value at the crest. Sand grains experiencing bed-load movement are rolled along the upstream face of the dune and are dumped into the vortex in the lee of the crest. By virtue of the directions of the velocity, the angle of the bed $\alpha$ at the crest tends to be less than $\phi$ on the upstream face and to be greater than $\phi$ on the downstream face. The magnitude of the periodic fluctuations of $\alpha$ to values greater than $\phi$ and to values less than $\phi$ are proportional to the quantity of bed material moved over the crest in one-half cycle. Since the quantity moved over the crest is negligible at the initial-motion condition or at the cessation-of-motion condition,

$$\alpha \ (\text{crest}) \approx \phi \qquad (30)$$

The value of $\phi$ for the coarse sand used in Run 62 is 29.4 degrees according to Simons and Albertson 13/ for very rounded non-cohesive material. The 29.4 degree value for $\phi$ appeared to be quite reasonable from the dune slopes shown in figure 8.

Substituting the following values of Run 62

$u_c$ = 0.567 fps,

$s$ = 2.66,

$g$ = 32.14 ft/sec$^2$,

$\alpha$ = $\phi$ = 29.4 degrees,

$D_g$ = 0.585 mm, and

$C_D^1$ = 1.6,

into equation 28, the value of the constant K is found to be 8.2. Hence the universal incipient-motion criterion is

$$\frac{u_c^2}{(s-1)\, g\, D_g} = \left(\frac{\tan\phi \cos\alpha + \sin\alpha}{1 + \tan\phi}\right)\left(\frac{8.2}{C_D^1}\right) \qquad (31)$$

There are two significant points in equation 31 which deserve to be emphasized. First, the left-hand side of equation 31 is a sediment Froude number being derived from the hydrodynamic surface forces on the sediment to the submerged weight of the sediment. Second, the coefficient of drag, $C_D^1$, includes a Reynolds-number effect inasmuch as the velocity, $u_c$, is used to evaluate the Reynolds number in the determination of $C_D^1$. The use of the parameter, settling veloctiy, is tenuous in any incipient-motion criterion primarily because an incorrect Reynolds number is implicitly involved.

The incipient-motion criterion, equation 31, is deficient for use in analyzing incipient motion of protruding surface particles in which the particles

are submerged within a boundary layer. In this case the velocity gradient at particle level is large thereby requiring a more precise definition of the height, y, above the bed at which $u_c$ is to be evaluated.

Experimentally determined values of incipient motion of the three sands with a flat bed can be used to calculate the height, y, at which $u_c$ should be evaluated. The mathematical equation for the velocity distribution within a laminar boundary layer for oscillatory flow over a flat smooth bed is:

$$\frac{u}{U_m} = \sin \frac{2\pi t}{T} - e^{-y\sqrt{\pi/\nu T}} \sin \left( \frac{2\pi t}{T} - y \sqrt{\frac{\pi}{\nu T}} \right) \qquad (32)$$

in which

$u$ = fluid velocity,

$U_m$ = maximum velocity above the boundary layer,

$T$ = period of the oscillatory flow,

$y$ = vertical distance above the bed, and

$\nu$ = kinematic viscosity of the oscillating fluid

Differentiating equation 32 with respect of $2\pi/T$ and equating the derivative to zero yields a transcendental function from which the time in the cycle which the velocity is a maximum at various values of y can be determined. Using the measured physical variables of the incipient-motion runs, (TABLE III) and using equations 31 and 32, the height, y, above the bed for the evaluation of $u_c$ was calculated to be $0.55D_g$, $0.60\ D_g$, and $0.59D_g$ for the fine, medium, and coarse sand, respectively. The reasonable values of the height, y, and the close agreement of the values for the three sand sizes is interpreted by the writers to substantiate the entire analysis based upon forces. Therefore, on the basis of this study, the writers are proposing equation 31 as a universal incipient-

motion criterion with the velocity, $u_c$, being at a position $0.6D_g$ above the bed for bed materials in which the geometric standard deviation is small, say less than 1.3.

This modest theory permits the incipient-motion condition to be extrapolated to other wave periods as shown in figure 20. The lowest curve is for incipient motion either for the beginning of motion on a residual dune system or for the incipient motion of particles on a flat bed for wave periods, of 3, 6, and 9 seconds. The abscissa of figure 20 is geometric-mean diameter, $D_g$. The ordinate of figure 20 is the critical sediment number, $N_{sc}$, defined as:

$$N_{sc} = \frac{U_{mc}}{\sqrt{(s-1)g\ D_g}} \qquad (33)$$

in which $U_{mc}$ is the maximum value of the velocity a short distance above the dune crest at the incipient-motion condition In preparing figure 20, the bed material was assumed to have a shape factor of 0.7, the angle of repose was assumed to be 30 degrees, and the water temperature was assumed to be 60-degrees Fahrenheit.

As shown in figure 20, the flat-bed incipient-motion condition and the deformed-bed incipient motion differ in two respects. First the value of the critical sediment number, $N_{sc}$, is independent of the wave period on a duned bed, but is dependent on a wave period on a flat bed. Because the boundary layer is negligible on a duned bed, the velocity, $u_c$, at the crest at a y of $0.6\ D_g$ is simply $1.2\ U_{mc}$ regardless of the wave period Conversely, on a flat bed, the velocity ratio, $u_c/U_{mc}$ is dependent on the boundary-layer thickness with the boundary-layer thickness increasing with time for development, that is, wave period. Second the value of $N_{sc}$ increases with $D_g$ on a

duned bed but decreases on a flat bed. The increase with $D_g$ on a duned bed is simply the consequence of the decreasing values of $C_D^1$ in equation 31 with increasing particle Reynolds number. The coefficient of drag, $C_D^1$ approaches a minimum value of 1.12 at a particle Reynolds number of about 600 corresponding to $D_g$ of about 1.7 mm and to a maximum value of $N_{sc}$ of about 2.1. The decrease in $N_{sc}$ with decreasing $D_g$ on a flat bed is that the effect of the protusion of the particles into the boundary layer is greater than the effect of the decreasing $C_D^1$.

The generality of the incipient-motion criterion, equation 31, will be demonstrated by application to two-dimensional open-channel flow over a flat bed. In order to apply equation 31, the velocity distribution must be known in order to obtain the value of u at y equal to 0.6 $D_g$. Because the velocity distribution is known in the hydraulically smooth and in the hydraulically rough regions, solutions of equation 31 can be obtained in these regions but not in the transition region. Since the traditional criterion of incipient motion for two-dimensional open-channel flow is the Shields' parameter 16/, solutions for the Shields' parameter, $\tau_c/\gamma(s-1)D_g$ will be obtained from equation 31.

With fully developed turbulent flow over a rough wall the velocity is nearly logarithmic 17/ as follows

$$\frac{u}{\sqrt{\tau/\rho}} = 5.75 \log_{10} \frac{y}{k} + 8.5 \qquad (34)$$

in which $\tau$ is the boundary shear stress and in which k is the Nikuradse sand roughness height. With the flat sand bed, k is simply $D_g$ and y is $0.6D_g$ as previously discussed. Substituting these values in equation (34)

$$\frac{u_c}{\sqrt{\tau_c/\rho}} = 7.22 \qquad (35)$$

in which $\tau_c$ is the critical value of the boundary-shear stress. Noting that $\alpha$ is zero, eliminating $u_c$ from equation 31 by means of equation 35, and solving for the Shields' parameter

$$\frac{\tau_c}{\gamma\,(s-1)\,D_g} = \left(\frac{\tan\phi}{1+\tan\phi}\right)\frac{0.158}{C_D^1} \tag{36}$$

With fully developed turbulent flow over a smooth wall, the velocity distribution within the laminar sublayer is nearly linear 17/ as follows

$$\frac{u}{\sqrt{\tau/\rho}} = \frac{y\sqrt{\tau/\rho}}{\nu} \tag{37}$$

Substituting y of $0.6\,D_g$ into equation 34,

$$\frac{u_i}{\sqrt{\tau_c/\rho}} = \frac{0.6\,D_g\sqrt{\tau_c/\rho}}{\nu} \tag{38}$$

Noting that $\alpha$ is zero, eliminating $u_c$ from equation 31 by means of equation 38, and solving for the Shields' parameter,

$$\frac{\tau_c}{\gamma(s-1)\,D_g} = \left(\frac{\tan\phi}{1+\tan\phi}\right)\frac{13.7}{C_D^1}\,\frac{\nu}{D_g\sqrt{(s-1)g\,D_g}} \tag{39}$$

Equations 36 and 39 are the desired solutions for the Shields' parameter for the hydraulically rough boundary and the hydraulically smooth boundary, respectively. These functions have been evaluated and are shown in figure 21 in which Shields' parameter is a function $D_g$ assuming that the fluid is water at 60°F and that the particles are well rounded with a shape factor of 0.7 and a specific gravity of 2.65. The lower limit of the hydraulically rough condition was taken 18/ as

$$\frac{y\sqrt{\tau / \rho}}{\nu} = 70 \qquad (40)$$

and the upper limit of the smooth condition as

$$\frac{y\sqrt{\tau / \rho}}{\nu} = 5 \qquad (41)$$

These limits occur at 0.3 mm and 2 mm as shown in figure 21. Because the velocity distribution is unknown in the transition region between the smooth boundary flow and the rough boundary flow, equation 31 could not be related to the Shields' parameter in this region. The dashed lines are simply extrapolations of equations 36 and 39. A faired curve joining the functions from 0.3 mm to 2 mm would exhibit a dip, characteristic of the Shields' curve as determined from experiments 16/. The derived curves in both hydraulically rough range and the hydraulically smooth range are very reasonable representations of experimentally determined values particularly in the hydraulically rough range.

B. Evolution of a duned bed

Descriptions of the process by which a duned bed evolves from an initially flat bed have been presented in III.B.1.a. and III.B.1.b. Experimental data obtained during the initial stages of development of an induced dune system are shown in figures 5 and 6.

Celerities of the advancing dune systems are proportional to the slopes of the displacement-time curves of figure 6. In general the celerity, c, appears to decrease as the dune system develops, that is, the displacement-time curves tend to be concave downward. Some decrease in celerity would be expected during the runs in which the total water-motion amplitude, 2a, was allowed to diminish while the dunes developed (resistance to motion increased) as, for example, during Run 55 as shown in figure 6(k). However during Run 62, figure 6(l), the blower speed was manually adjusted so as to maintain a nearly constant amplitude but the displacement-time curve is still concave downward. On the other hand, during Run 85, figure 6(p), and Run 114, figure 6(s), both the water-motion amplitude, 2a, and the dune system celerity, c, were nearly constant. Because of this confusion about the changing celerity, the writers have defined a mean celerity based upon the time for the advancing dune system to reach the extremities of the bed, which are three feet from the location of the starting line (half-round bar).

The conditions during which a dune system will propogate with a finite celerity are limited as follows

$$0 < c < \infty \qquad \text{if} \qquad a_c < a < a_s \tag{42}$$

in which $a_c$ is the water-motion amplitude associated with the deformed-bed incipient-motion condition and $a_s$ is the water-motion amplitude at which ripples form spontaneously all over the bed.

The lower limit of ripple propagation, $a_c$, can be determined from equation 33 as follows

$$\frac{a_c}{D_g} = \frac{N_{scd}}{2\pi} \quad T\sqrt{\frac{(s-1)g}{D_g}} \tag{43}$$

in which $N_{scd}$ is the deformed-bed critical sediment number. As discussed in IV.A., the value of $N_{scd}$ is independent of wave period and is essentially a function of particle size as shown in figure 20.

The upper limit of ripple propagation, $a_s$, is at an amplitude slightly larger than the amplitude for flat-bed incipient-motion. Neglecting the small lag between spontaneous formation of ripples and flat-bed incipient-motion, the upper limit of ripple propagation can be determined from equation 33 as follows

$$\frac{a_s}{D_g} = T\sqrt{\frac{(s-1)g}{D_g}} \quad \frac{N_{scf}}{2\pi} \tag{44}$$

in which $N_{scf}$ is the flat-bed critical sediment number. The method for calculating $N_{scf}$ was discussed in IV.A. Some representative values are shown in figure 20.

Since the celerity function is confined to the limits defined by equations 43 and 44 regardless of the other variables, the amplitude parameter can be judiciously chosen to incorporate these limits as follows

$$\frac{c}{\sqrt{(s-1)g\,D_g}} = f\left( \frac{a/a_c - 1}{a_s/a_c - 1} \;,\; T\sqrt{\frac{(s-1)\,g}{D_g}} \;,\; \sigma_g, \text{ particle shape} \right) \tag{45}$$

The amplitude parameter, $(a/a_c - 1) / (a_s / a_c - 1)$, varies between 0 and 1 regardless of the values of the other independent parameters. The additional parameter which has been introduced, that is, $a_s/a_c$ can be determined independently from equations 43 and 44 as follows

$$\frac{a_s}{a_c} = \frac{N_{scf}}{N_{scd}} \tag{46}$$

Dune propagation celerities as determined from the results shown in figure 6 are shown in figure 22 in the form indicated by equation 45.

C. Dune geometry

The principal feature of dune geometry is the two-dimensional character of the dunes at low amplitudes and the destruction of the two-dimensional dunes with increasing amplitude. The series of topographic maps, figure 9, show the nature of the dunes at various amplitudes. In figure 10, the dune amplitude is shown to increase until $a/D_g$ is approximately 775. The range of two-dimensional dunes is as follows

$$\frac{a_c}{D_g} < \frac{a}{D_g} < 775 \tag{47}$$

The range given in equation 47 is verified by visual observations, figures 7 and 8. In figure 10, the dune amplitude is shown to decrease for amplitudes greater than $a/D_g$ of 775. Dunes in this range are three-dimensional in character. The range of three-dimensional dunes is as follows

$$775 < \frac{a}{D_g} < 1700 \tag{48}$$

At the upper limit the dunes have disappeared and the bed is flat. The range of a flat sand bed is as follows

$$\frac{a}{D_g} > 1700 \qquad (49)$$

Using the criterion for two-dimensional dunes, equation 47, the ratio, $\eta/\lambda$, is shown in figure 12 to be in the range from 2/13 to 1/5. In other words, the wave lengths of two-dimensional dunes are 5 to 6.5 times the dune amplitude.

With three-dimensional dunes, equation 48, dune amplitude $\eta$ is shown in figure 10 to decrease linearly with water-motion amplitude a to a zero value at the flat bed condition, equation 49. In contrast, the wave length $\lambda$ is nearly independent of the water-motion amplitude a as shown in figure 11.

The experimental results as shown in figures 10, 11, and 12 tend to verify the analysis leading to equation 11 with the added bonus that the effect of the parameter, $T\sqrt{(s-1)g/D_g}$, is practically insignificant in regard to dune geometry. In the array of variables, equation 9, viscosity was omitted on the premise that the scouring action occurred on the upstream face of the dunes where the boundary-layer thickness is negligible. In the writers' opinion, the experimental results have justified the omission of viscosity in equation 9.

On the other hand, in regard to the question of whether dunes will form by propagation or will form spontaneously, viscosity is an important variable. The value of $a_s/D_g$ which is the limit between propagation and spontaneous formation, equation 44, is a function of the boundary-layer thickness on a flat bed, equation 32. Even in this case, the effect of viscosity can be accounted for by the supplementary calculations for $N_{scf}$. Viscosity

is of lesser importance in the determination of $a_c/D_g$, equation 43, in which boundary-layer thickness is negligible but in which viscosity enters into the value of $C_D^1$, equation 31, for the determination of $N_{scd}$. In any event, the effect of viscosity must be considered both in the velocity distribution and in the value of the coefficient of drag on a surface particle. The separation of these two effects by the writers is considered to be a significant contribution as opposed to the combined treatment in the use of the Shields' parameter which is limited to a particular flow situation. The Shields' parameter is commonly used for two-dimensional, fully developed, steady, turbulent flow over a flat bed.

Neither the incipient-motion condition, $a_c/D_g$, nor the upper limit of propagating ripples, $a_s/D_{gs}$ appears to have any effect upon the geometry of equilibrium dunes. The amplitude $\eta$ and wave length $\lambda$, shown in figures 10 and 11, start at finite values just beyond the deformed-bed incipient-motion condition, $a_c/D_g$. The irrelevance of $a_c/D_g$ and $a_s/D_g$ was observed during the experiments in that the wave length of the initial ripples was always much less than the equilibrium wave length and in that confused developing dune patterns when an older dune overtook a newer dune did not appear to be significant in the equilibrium dune pattern except for the additional time required to scour out the inhomogeneity at the mixup. The irrelevancy of $a_c/D_g$ and $a_s/D_g$ in regard to geometry of equilibrium dunes is added confirmation of the prudent omission of viscosity as a significant variable in equation 9.

D. Energy dissipation

Dunes on the sea bed quite obviously increase the energy dissipation within the water by virtue of the generation of vortices in the lee of dune crests. Vortices are generated twice in an oscillatory cycle. These vortices are moved out and up into the main stream at about the time of flow reversal. The energy required to produce the energy stored within these vortices is ultimately dissipated as heat.

Two methods of evaluation of energy dissipation were attempted. The first method involves determining the energy dissipation within the entire tunnel from simultaneous measurements of the pressure over and the velocity of the driving piston which is the water surface in one of the vertical legs. The second method involves determining the energy dissipation within the test section from simultaneous measurements of the pressure gradient and the mean velocity within the test section.

1. First method of determination

The method of calculating the energy dissipation within the entire water tunnel is discussed in III.A.5 and in III.B.3. Energy dissipation per cycle with a smooth flat immobile bed, bed condition s, is presented in TABLE IV and in figure 4. Energy dissipation per cycle with a flat sand bed, bed condition f, is presented in TABLE VIII. Energy dissipation per cycle with a duned sand bed, bed condition d, is presented in TABLE IX. Since the oscillation frequency was essentially constant, the difference in energy dissipation at the same amplitude is the difference in energy dissipation within the test section inasmuch as the remainder of the flow passage is invariant regardless of the bed condition. In fact, only the bed of the test section

differs between runs with bed condition d and bed condition s or with bed condition f and bed condition s. Using the smooth flat immobile bed as a reference condition, the additional energy dissipation involved in flow over a flat sand bed and over duned sand can be evaluated.

The traditional hydraulic scheme of expressing the rate of energy dissipation in terms of a unit mass, weight, or volume of flowing fluid is inappropriate for oscillatory flow over a duned bed which results from surface waves. The reason is simply that the form of the bed and the energy stored within the lee vortices is localized in the vicinity of the bed and thus is independent of the mass of water above the bed. The important flow variables are bottom velocity, U, and wave period, T. The obvious approach is to express the energy dissipation per cycle in terms of the bottom velocity, U, and in terms of a unit area of bed. The rationality of this approach is verified by the following analysis in which the energy dissipation per cycle per unit area of bed is expressed in terms of the boundary-shear stress and the velocity. The relationship between energy dissipation and boundary shear stress is established by means of the linear momentum and energy equations.

The fluid control volume for which the linear momentum equation is written is shown schematically in figure 14. The linear momentum equation in the x direction is

$$\Sigma F_{(ex)x} = \frac{\partial}{\partial t} \iiint_{c.v.} \rho u \, d\forall + \iint_{A_2} \rho u \, dQ - \iint_{A_1} \rho u \, dQ \qquad (50)$$

in which $\Sigma F_{(ex)x}$ is the summation of the external forces on the control volume; $\rho$ is fluid density, u is the x component of velocity; t is time; $d\forall$ is a volume element; and dQ is the volume rate of flow (discharge) through an element of area dA in the cross section.

Since the test section is a uniform flow zone and since $\rho$ is constant,

$$\iint_{A_2} \rho u \, dQ - \iint_{A_1} \rho u \, dQ = 0 \tag{51}$$

at any instant.

The term embodying the unsteadiness of the motion can be simplified by noting that $d\forall$ can be written as $LdA$. Thus

$$\frac{\partial}{\partial t} \iiint_{c.v.} \rho u \, d\forall = \rho L \frac{\partial}{\partial t} \iint_{A} u \, dA = \rho L \frac{dQ}{dt} = \rho LA \frac{dU}{dt} \tag{52}$$

in which U is the mean velocity in the test section.

The external forces are surface forces which are as follows

$$\Sigma F_{(ex)x} = + (p_1 - p_2)A - \tau_{or}(BL) - 2\tau_{ow}(CL) - \bar{\tau}_{ob}(BL) \tag{53}$$

in which p is the pressure at a cross section; $\tau_{or}$ is the boundary-shear stress at the roof; $\tau_{ow}$ is the boundary-shear stress at the walls; $\bar{\tau}_{ob}$ is the spatial mean value of the boundary-shear stress on the bed; and B, C, and L are the width, height, and length, respectively, of the control volume which is over the sediment container in the bed of the test section.

Substituting equations 51, 52, and 53 into equation 50 and solving for $(p_1 - p_2)A$,

$$(p_1 - p_2)A = \tau_{or}(BL) + 2\tau_{ow}(CL) + \bar{\tau}_{ob}(BL) + \rho LA \frac{dU}{dt} \tag{54}$$

Multiplying each term of equation 54 by U dt and integrating throughout a cycle,

$$\int_t^{t+T} (p_1 - p_2) AU \, dt = BL \int_t^{t+T} \tau_{or} U \, dt + 2CL \int_t^{t+T} \tau_{ow} U \, dt + BL \int_t^{t+T} \bar{\tau}_{ob} U \, dt + \int_t^{t+T} \frac{d}{dt}\left(\frac{\rho LAU^2}{2}\right) dt \tag{55}$$

The magnitude of the last term of equation 55 is seen to be equal to the last term of the work-energy equation, equation 16.

Substituting equation 55 into equation 16,

$$\underset{\text{cycle}}{\text{energy dissipation within c.v.}} = BL\int_{t}^{t+T} \tau_{or}\, U\, dt + 2CL\int_{t}^{t+T} \tau_{ow}\, U\, dt + BL\int_{t}^{t+T} \bar{\tau}_{ob}\, U\, dt \qquad (56)$$

The difference in energy dissipation within the entire tunnel (for equal-amplitude runs) is simply the difference in energy dissipation within the control volume which extends over the sediment container in the test section. Furthermore, a reasonable assumption is that the boundary-shear stress on the smooth roof and smooth sidewalls is the same for equal-amplitude runs. In other words, the difference in energy dissipation is totally in the changed flow conditions at the bed. This assumption is quite reasonable because the boundary layers which form on the smooth boundaries of the roof and sidewalks reform twice each cycle and are very thin even at maximum development. Employing these concepts for two equal-amplitude runs,

$$\left(\frac{\text{energy dissipation in the tunnel}}{\text{cycle}}\right)_d - \left(\frac{\text{energy dissipation in the tunnel}}{\text{cycle}}\right)_s = \left[BL\int_{t}^{t+T} \bar{\tau}_{ob}\, U\, dt\right]_d - \left[BL\int_{t}^{t+T} \bar{\tau}_{ob}\, U\, dt\right]_s \qquad (57)$$

in which the subscripts de and s refer to duned sand bed and to smooth flat immobile bed, respectively. Values of the first term of equation 57 are listed in the last column of TABLE IX. Of course, runs with a flat-sand bed can also be analyzed in this way by utilizing the results listed in the last

column of TABLE VIII. The second term of equation 57 can be determined from the graph, figure 4, using the same amplitude. Values of the first term are listed in the second column of TABLES XI and XII; values of the second term are listed in the third column; and the difference which is the added energy dissipation is listed in the fourth column. In other words, the fourth column of TABLES XI and XII is a listing of the numerical values of the left side of equation 57.

The spatial mean values of the boundary-shear stress on the bed, $\overline{\tau_{ob}}$, can be expressed in the traditional form involving a boundary-drag coefficient. Assuming that the boundary shear force is $\pi$ radians out of phase with the velocity, the magnitude of $\overline{\tau_{ob}}$ can be expressed as follows

$$\overline{\tau}_{ob} = \frac{\overline{f}\,\rho\,U^2}{8} \tag{58}$$

in which $\overline{f}$ is a spatial mean value of the boundary-drag coefficient. This definition of the boundary-drag coefficient is consistent with the drag coefficient used in river hydraulics 19/ even though the drag force is principally form drag rather than surface drag in flow over a duned bed. For calculations of energy dissipation in oscillatory flow, a time mean value of the boundary-drag coefficient is desirable. A mean value in both space and time is defined as follows,

$$\int_t^{t+T} \overline{\tau}_{ob}\, U\, dt = \int_t^{t+T} \frac{\overline{f}\;\rho|U^3|dt}{8} = \overline{\overline{f}} \int_t^{t+T} \frac{\rho|U^3|dt}{8} \tag{59}$$

Using this definition equation, the right side of equation 57 can be written,

$$\left[BL\int_{t}^{t+T} \bar{\tau}_{ob}\, U\, dt\right]_d - \left[BL\int_{t}^{t+T} \bar{\tau}_{ob}\, U\, dt\right]_s$$

$$= (\bar{\bar{f}}_d - \bar{\bar{f}}_s)\ BL\int_{t}^{t+T} \frac{\rho|U^3|dt}{8} \qquad (60)$$

Since the motion is simple harmonic, equation 17, the right side of equation 60 can be expressed in terms of the total water-motion amplitude, 2a, and the period, T, as follows

$$(\bar{\bar{f}}_d - \bar{\bar{f}}_s)\ BL\int_{t}^{t+T} \frac{\rho|U^3|dt}{8} = \frac{(\bar{\bar{f}}_d - \bar{\bar{f}}_s)(BL)\ \pi^2\ \rho\ (2a)^3}{6T^2} \qquad (61)$$

Equation 61 is the right side of equation 57. Numerical values of the left side of equation 57 are listed in the fourth column of TABLE XI and XII. Computed values of the drag-coefficient difference, $\bar{\bar{f}}_d - \bar{\bar{f}}_s$, are listed in the last column of TABLE XII. Similarly the values of $\bar{\bar{f}}_f - \bar{\bar{f}}_s$ are in the last column of TABLE XI. Values of both $\bar{\bar{f}}_d - \bar{\bar{f}}_s$ and $\bar{\bar{f}}_f - \bar{\bar{f}}_s$ are shown in figure 23.

The trends of the results shown in figure 23 appear to be reasonable. The value of $\bar{\bar{f}}_d - \bar{\bar{f}}_s$ decreases with increasing values of $a/D_g$. The experimentally determined values of $\bar{\bar{f}}_d - \bar{\bar{f}}_s$ appear to be equal to the experimentally determined values of $\bar{\bar{f}}_f - \bar{\bar{f}}_s$ for values of $a/D_g$ greater than 1500. Referring to figure 12, the ratio of dune amplitude to wave length is seen to be less than 0.04 in this range. The values of $\bar{\bar{f}}_f - \bar{\bar{f}}_s$ are greater for a flat sand mobile bed than for a flat sand immobile bed. The two horizontal curves indicate this difference. The change from an immobile bed to a mobile bed occurs at the flat-bed incipient

motion condition. The two vertical curves are located at the amplitude for flat-bed incipient motion of the medium and fine sand. The experimentally determined values of $\bar{\bar{f}}_f - \bar{\bar{f}}_s$ with an immobile, flat, fine sand are negative. Since the value of $\bar{\bar{f}}_f - \bar{\bar{f}}_s$ can not be negative, the deviation from reality is an overall measure of accuracy. The accuracy of the results is considerably poorer with low amplitudes as evidenced by the scatter of all results at values of $a/D_g$ less than 500.

Even though the trends of the results shown in figure 23 are quite reasonable, the magnitude of the differences $\bar{\bar{f}}_d - \bar{\bar{f}}_s$ and $\bar{\bar{f}}_f - \bar{\bar{f}}_s$ appear to be shockingly high in comparison to the values for a duned bed in unidirectional flow 19/. There are three possible reasons the experimentally determined values of $\bar{\bar{f}}_d - \bar{\bar{f}}_s$ being an order of magnitude larger than anticipated. First, the dunes are more closely spaced under oscillatory flow than under unidirectional flow. Second, the oscillatory velocity used in determining the drag-coefficient difference is that at a small distance above the dunes, say one dune height, whereas, the mean velocity was used in the unidirectional flow determination 19/. Third, energy in the vortices in the lee of the crests is completely dissipated in the main stream of the oscillatory flow; whereas, in unidirectional flow the main vortex in the lee of a crest continues to exist.

Of the three possible reasons listed above for the large values of f, the effect of the velocity used in calculating the drag coefficient is easily demonstrated. An important difference between steady unidirectional flow and oscillatory flow over a rough bed is that of velocity distribution in the flow.

With steady unidirectional flow, the boundary force retards the entire flow with the maximum velocity being at the streamline furthest from the boundary.

Velocity distributions of such flows are closely approximated by the logarithmic velocity distribution in which the velocity is proportional to the logarithm of the distance from the boundary. In spite of the fact that the energy transferred to vortices in the lee of boundary deformations is directly related to the velocity of flow past the deformations, the practice is to evaluate the boundary-drag coefficient by using the mean velocity. By the convenient but irrational use of mean velocity, the velocity used to determine a boundary-drag coefficient from measurements is considerably larger than the velocity of flow past the deformation. As a consequence, the numerical values of the boundary-drag coefficients are low and the values are a function of the depth of flow. On the other hand, if the common usage were based upon the velocity of flow past the deformation, the boundary-drag coefficient would tend to be independent of the depth of flow (so-called relative roughness).

With oscillatory flow, flow past bed deformations has a negligible effect upon the velocity distribution in the main flow above the bed. Thus in the oscillatory flow tunnel the mean velocity U is also the velocity of flow past the deformations.

A large number of experiments were performed at the Waterways Experiment Station 20/ with exaggerated roughness elements. One form of roughness consisted triangular parallel ridges placed perpendicular to the axis of the rectangular flume. These ridges were continuous across the bottom and up the sidewalls. The upstream face of each ridge was vertical. The downstream face of each ridge was plane with a slope of 1 (vertical) on 2 (horizontal). The height of the ridges from the flume bottom corresponds to dune amplitude, $\eta$, and the longitudinal spacing corresponds to dune length, $\lambda$. In one series

of runs the ratio $\eta/\lambda$ was 1/6 which is in the range of two-dimensional dunes. Values of the boundary-drag coefficient, f, calculated from experimental data are shown in figure 24 as a function of $y_o/\eta$ in which $y_o$ is the depth of flow measured from the trough elevation. The mean velocity used in calculating the f-values was based upon the depth $y_o$. In this case the velocity used in the calculations is probably too low. In other words, the virtual bottom should be somewhere between the crest and the trough. Einstein and El-Samni 21/ deduced from experiments with flow over hemispheres that the virtual bottom should be 2/5 of the height from the channel floor to the top of the hemispheres measured from the top of the hemispheres. With this virtual bottom elevation, the depth of flow would be $y_o - 3\eta/5$ rather than $y_o$. Using this revised depth, the mean velocity used in calculating values of f would be increased. For example the maximum value of f shown in figure 24 is 4.07 when $y_o/\eta$ is 2.18. If the revised depth is used the value of f would be 2.46 rather than 4.07. In any event, the Waterways Experiment Station results are indicative that the large values of f obtained in the oscillatory flow tests may not be too high if the velocity used in calculating f is the velocity of flow past the bed deformation.

Motzfeld 22/ measured the flow characteristics past a deformed wall in a wind tunnel. The test section was 200 mm by 200 mm in cross section and 7.2 m long. Three walls were smooth. The other was wavy. One set of experiments was performed with a waviness consisting of circular arcs. The circular arcs were joined at pointed crests resembling the two-dimensional dunes which develop under oscillatory flow. The wave length was 150 mm and the amplitude from trough to crest was 20 mm. Motzfeld made velocity traverses

along six verticals along the wave. Pressures were measured along the boundaries. From his measurements, Motzfeld constructed a pattern of streamlines which is quite similar to the flow net shown in figure 19. From the pressure measurements he calculated the form drag which he converted to a spatially averaged form-drag coefficient. The value of f was calculated to be 0.078 for each of the four runs ranging in Reynolds number from 9.5 ($10^4$) to 2.67 ($10^5$). Motzfeld used the maximum velocity in evaluating the drag coefficient. The measured velocity profiles at the six longitudinal stations are identical at a distance of three dune amplitudes measured from a virtual wall midway between the crest and the trough. By extropolating this velocity profile back to the virtual wall, the velocity of flow past the dune is found to be 0.35 of the maximum velocity. Using this velocity, which is more rational, the value of f is calculated to be 0.64--an order of magnitude quite consistent with the results shown in figure 23.

In summary, the large values of the drag coefficients which were determined from experimental measurements have been found to be quite reasonable. The apparent order-of-magnitude difference between these results with oscillatory flow and the results with unidirectional flow has been traced primarily to the reference velocity used in defining the drag coefficient. In the oscillatory flow results, a reference velocity, which is the velocity of flow past the dunes, is both convenient and rational. On the other hand, in unidirectional flow, the mean velocity is chosen as the reference velocity. The choice of the mean velocity is certainly convenient but is physically irrational since the mean velocity is not the velocity of flow past the obstruction on the boundary.

2. Second method of determination

The method of calculating energy dissipation within the test section is discussed in III.B.4. The results are presented in TABLE X. This scheme of determining energy dissipation was unsatisfactory primarily because of the difficulty of exactly establishing the time of maximum velocity from records such as shown in figure 13. Very small shifts in the time scale, t/T, results in large changes in the computed energy dissipation. Inherently, of course, the first method is preferable to the second because the measured work input into the entire tunnel is dissipated whereas in the second method most of the work input is utilized to accelerate and decelerate the water mass within the test section.

An error is contained in the results in TABLE X. Run 105 had to be stopped because the sheet-metal covering of the insert (C in figure 1) had broken loose and was noticeably rubbing against the float. The data were reviewed to determine when the sheet-metal had first broken loose from the supporting frame. After studying the work input into the water tunnel, the conclusion was that Runs 83-105, inclusive were suspect. Sliding contact between the float and the insert would certainly affect the total work input into the tunnel but was not expected to influence the measured values of work input into test section. However the calculated energy dissipation within the test section was considerably lower after the insert was repaired. For example, the amplitudes of Run 86 and 114A were nearly the same but the calculated energy dissipation in Run 86 is about five times that of Run 114A.

The results in TABLE X for runs performed after Run 105 are considered to be reliable. Unfortunately all of these runs were performed with a duned bed

with the result that no corresponding flat-bed values are available from which to determine the added energy dissipation.

# V. SUMMARY AND CONCLUSIONS

Various features of the bed forms which occur with oscillatory flow over a bed of uniform sand were studied experimentally in an oscillatory-flow water tunnel. The amplitude of the water motion was a controlled variable. Three sizes of bed material were used in otherwise duplicate experiments. The period of oscillation was essentially constant in all runs. A flat bed was the initial condition in all runs. Initial and final transients were eliminated from the water motion. The experiments were organized in order to study (a) incipient motion, (b) evolution of a duned bed, (c) geometry of equilibrium dunes, and (d) energy dissipation in the flow over a duned bed.

The incipient-motion condition was determined both on a duned bed and on a flat bed. The incipient-motion condition was analyzed by considering the lift, drag, and submerged weight forces on a typical particle on the surface of the bed. An analytical expression was derived for the critical velocity in terms of the ratio of the specific weights of bed material and fluid, mean size of particle, angle of repose of bed material, bed slope, and a coefficient of drag (the magnitude of the coefficient of drag depends upon the critical velocity, fluid viscosity, and particle size). This rational incipient-motion criterion proved to be quite satisfactory for the prediction of incipient motion under oscillatory flow both with a duned bed and flat bed. The incipient-motion criterion was applied to two-dimensional, turbulent, unidirectional flow over a flat bed with very reasonable agreement with experimental results of others. As a result of this analysis rational expressions were derived (for the first time to the writers knowledge) for the widely-used Shields diagram which is based upon experimental findings.

The manner in which an intially flat bed evolves into a duned bed was observed. A ripple system forms spontaneously all over the flat bed if the maximum velocity is greater than the critical velocity. A ripple system can be induced to form with lesser velocities by a disturbance which creates a non-uniform flow zone just above the bed. Ripples will form and grow into dunes with the earlier formed dunes being a disturbance from which a new ripple will form. Celerity of an induced dune system was determined from experimental measurements.

Geometry of equilibrium dunes was determined from side-elevation photographs and from point-gage traverses over the bed after a run. The ratio of dune amplitude to mean particle diameter and the ratio of dune amplitude to dune wave length were found to be unique functions of a single variable--ratio of water motion amplitude to mean particle diameter. If the amplitude-to-diameter ratio is less than 775, the dunes are two dimensional with essentially straight and level crests and troughs. If the amplitude-to-diameter ratio is greater than 1700 the bed is flat regardless of the initial condition. In the intermediate range from 775 to 1700 the dunes are three dimensional with ill-defined crests and troughs. Dune amplitude decreases almost linearly with increasing water-motion amplitude in the range of three-dimensional dunes.

The added energy dissipation with oscillatory flow over a duned bed as compared with oscillatory flow over a smooth flat bed was determined by measurements of the work input into the oscillatory-flow tunnel. The results were analyzed and presented in terms of the difference in boundary-drag coefficients between the duned bed and the smooth flat bed. The values of the drag-coefficients appeared to be abnormally large in comparison with

drag coefficients determined in other flow situations. The apparent discrepancy was traced to the existence of an essentially uniform velocity distribution above the bed in oscillatory flow in contrast to the non-uniform velocity distribution above the bed in unidirectional flow. The magnitude of boundary-drag coefficients computed from experimental measurements is obviously greatly influenced by the choice of a reference velocity. The conclusion is that a velocity in the vicinity of the bed deformation is a more rational reference than a velocity far from the bed such as the mean velocity in unidirectional flow.

## REFERENCES


1. John F. Kennedy, "The Mechanics of Dunes and Antidunes in Erodible-Bed Channels," Journal of Fluid Mechanics, Vol. 16, Part 4, pp. 521-544.

2. John F. Kennedy, "The Formation of Sediment Ripples in Closed Rectangular Conduits and in the Desert," Journal of Geophysical Research, Vol. 69, No. 8, April 15, 1964, pp. 1517-1524.

3. John F. Kennedy and Marco Falcon, Wave-Generated Sediment Ripples, Report No. 86, Hydrodynamics Laboratory, Massachusetts Institute of Technology, Cambridge, Mass., August 1965.

4. Douglas L. Inman, Wind-Generated Ripples in Nearshore Sands, Technical Memorandum, No. 100, Beach Erosion Board, Department of the Army, Corps of Engineers, October 1957.

5. Douglas L. Inman and Anthony J. Bowen, "Flume Experiments on Sand Transport by Waves and Currents," Proceedings of the Eighth Conference on Coastal Engineering, 1962, Mexico City, Mexico, pp. 137-150.

6. S. Yalin and R. C. H. Russell, "Similarity in Sediment Transport due to Waves," Proceedings of the Eighth Conference on Coastal Engineering, 1962, Mexico City, Mexico, pp. 151-167.

7. R. A. Bagnold, "Motion of Waves in Shallow Water--Interaction between Waves and Sand Bottoms," Proceedings of the Royal Society of London, Series A, Vol. 187, October 1946, pp. 1-18.

8. Madhav, Manohar, Mechanics of Bottom Sediment Movement due to Wave Action, Technical Memorandum No. 75, Beach Erosion Board, Department of the Army, Corps of Engineers, June 1955.

9. George Kalkanis, Transportation of Bed Material due to Wave Action, Technical Memorandum No. 2, U. S. Army Coastal Engineering Research Center, February 1964.

10. Vito A. Vanoni, Norman H. Brooks, and John F. Kennedy, Lecture Notes on Sediment Transportation and Channel Stability, Report No. KH-R-1, California Institute of Technology, Pasadena, California, January 1961, Appendix 3A, pp. 3-20.

11. "Sediment Transportation Mechanics: Introduction and Properties of Sediment," Proc, ASCE, Journal of the Hydraulics Division, Vol. 88, No. HY4, July 1962, p. 98.

12. John F. Kennedy and Robert C. Y. Koh, "The Relation between the Frequency Distributions of Sieve Diameters and Fall Velocities of Sediment Particles," Journal of Geophysical Research, Vol. 66, No. 12, December 1961, pp. 4233-4246.

REFERENCES (Concluded)


13. Daryl B. Simons and Maurice L. Albertson, "Uniform Water Conveyance Channels in Alluvial Materials," Transactions, American Society of Civil Engineers, Vol. 128, 1963, p. 97.

14. W. S. Chepil, "Use of Evenly Spaced Hemispheres to Evaluate Aerodynamic Forces on a Soil Surface," Transactions, American Geophysical Union, Vol. 39, No. 3, June 1958, pp. 397-404.

15. Maurice L. Albertson, James R. Barton, and Daryl B. Simons, Fluid Mechanics for Engineers, Prentice-Hall Inc., Englewood Cliffs, New Jersey, 1960, p. 399.

16. "Sediment Transportation Mechanics: Initiation of Motion," Journal of the Hydraulics Division, American Society of Civil Engineers, Vol. 92, No. HY2, March 1966, pp. 291-314.

17. Hunter Rouse, Elementary Mechanics of Fluids, John Wiley and Sons, 1946, pp. 191-196.

18. Hermann Schlichting, Boundary Layer Theory, translated by J. Kestin, Pergamon Press, 1955, p. 407.

19. A. M. Z. Alam, T. F. Cheyer, and John F. Kennedy, Friction Factors for Flow in Sand Bed Channels, Hydrodynamics Laboratory Report No. 78, Massachusetts Institute of Technology, Cambridge, Massachusetts, June 1966.

20. Roughness Standards for Hydraulic Models, Technical Memorandum No. 2-364, Waterways Experiment Station, U. S. Army, Corps of Engineers, Vicksburg, Mississippi, June 1953, 53 pages.

21. H. A. Einstein and El-Sayed Ahmed El-Samni, "Hydrodynamic Forces on a Rough Wall," Reviews of Modern Physics, Vol. 21, No. 3, July 1949, pp. 520-524.

22. Heinz Motzfeld, "Die turbulente Strömung an welligen Wänden," Zeitschrift für Angewandte Mathematik und Mechanik, Band 17, Heft 4, August 1934, pp. 193-212.

# APPENDIX A--FIGURES

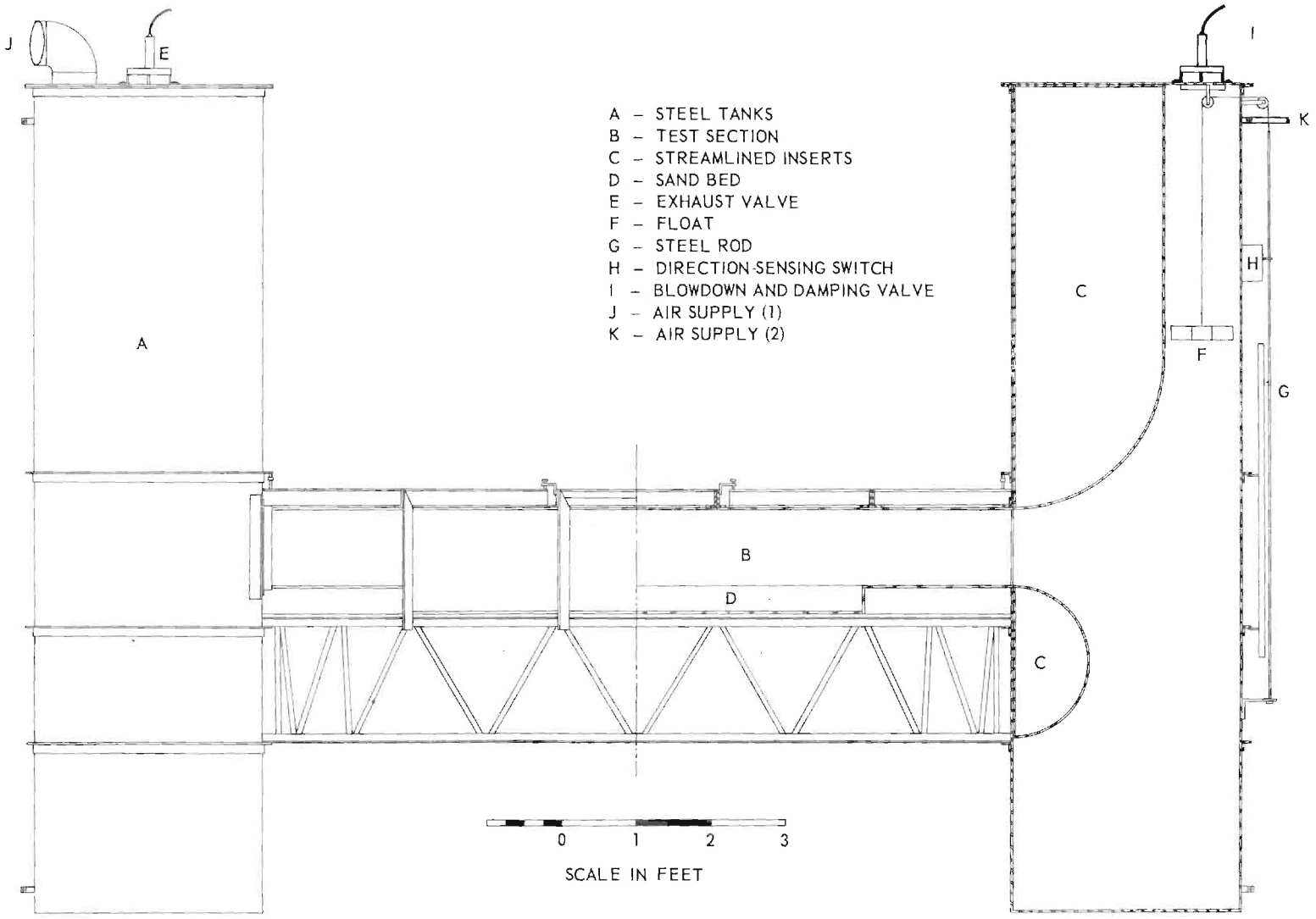


Figure 1. Oscillatory-flow Water Tunnel.

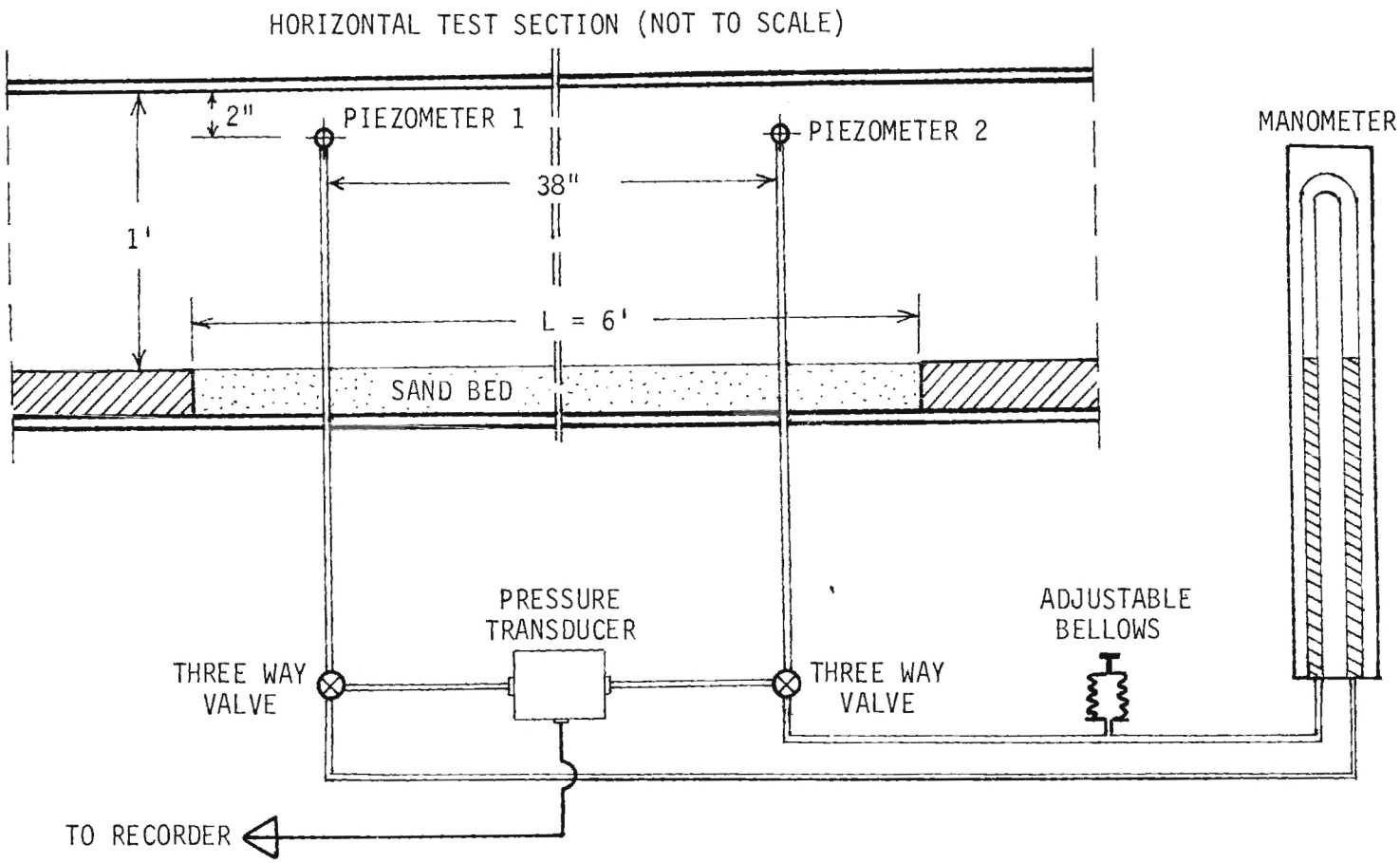


Figure 2. Arrangement for Measurement of the Pressure Gradient in the Test Section.

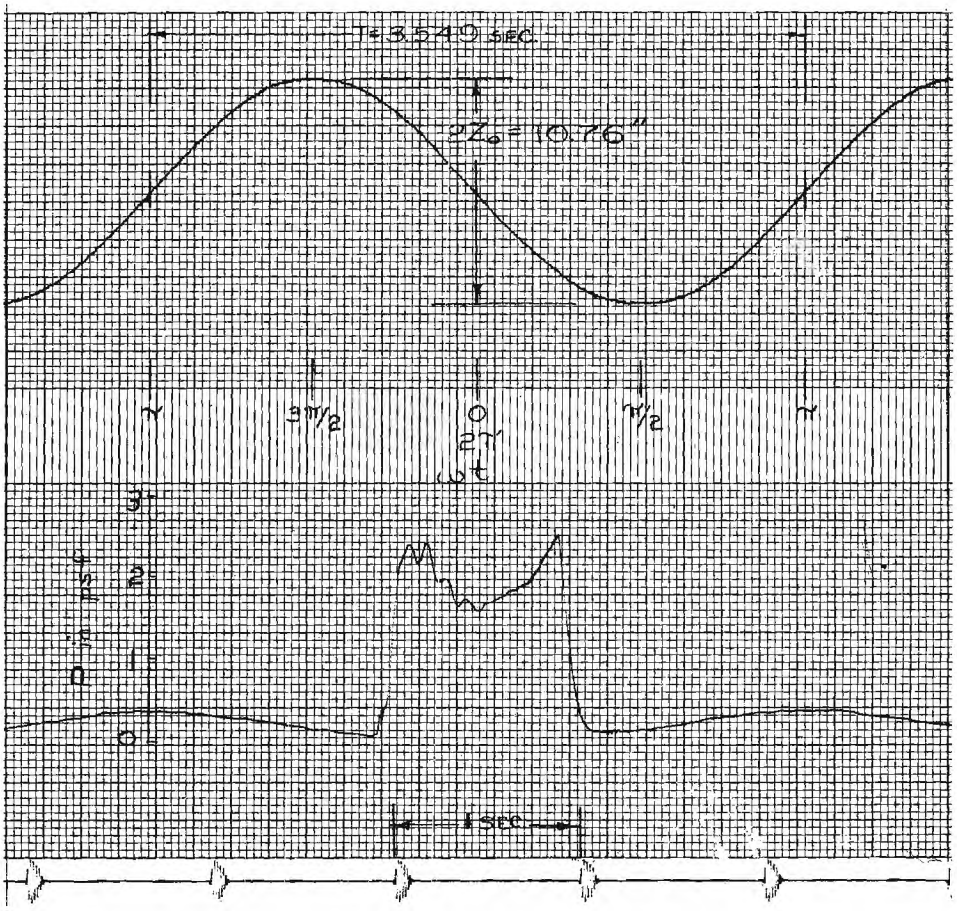


Figure 3. Record of Motion, Pressure Input, and Time.

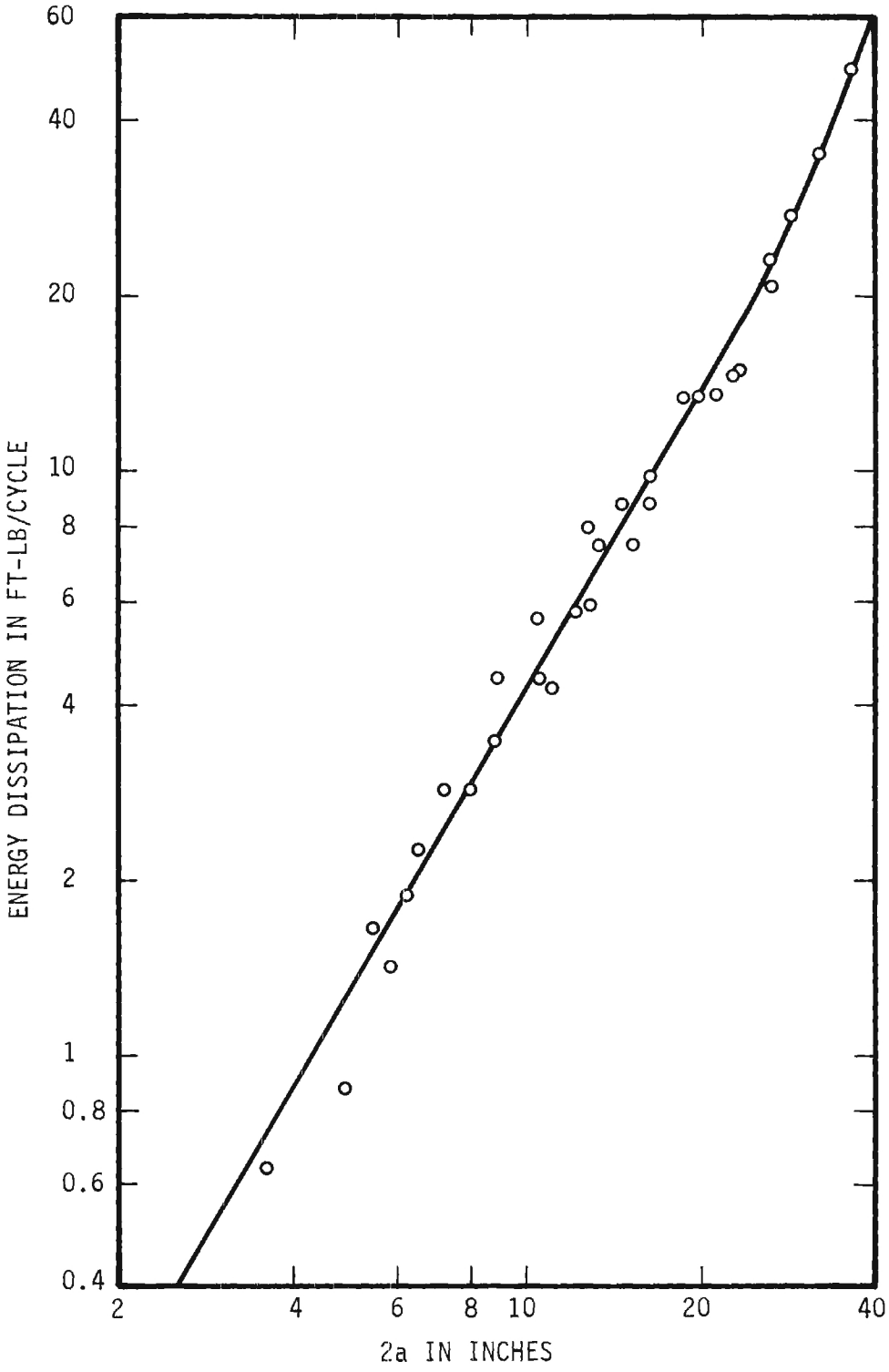


Figure 4. Energy Dissipation in the Water Tunnel with a Smooth Flat Immobile Bed.

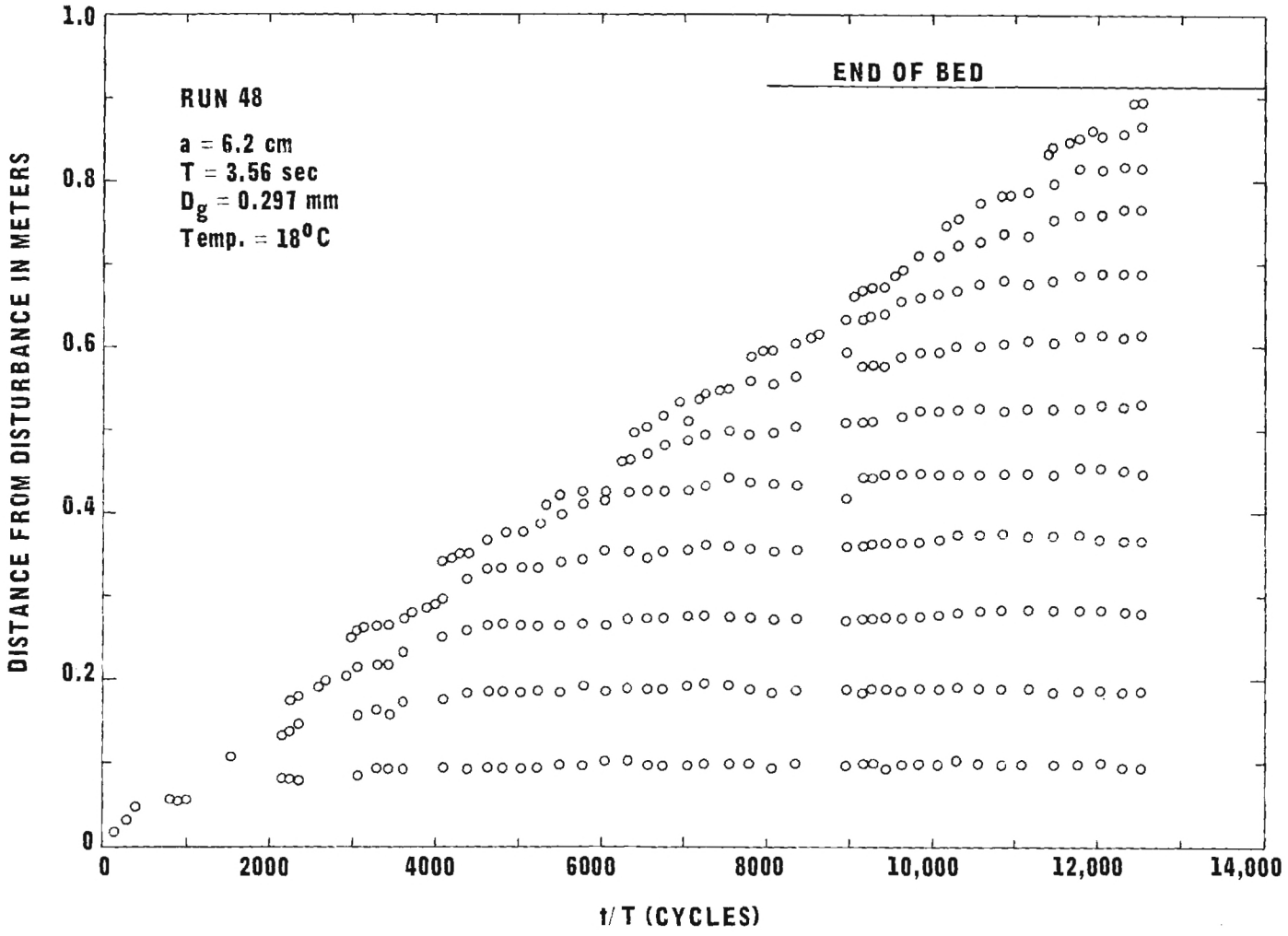


Figure 5. Dune Position as a Function of Time.

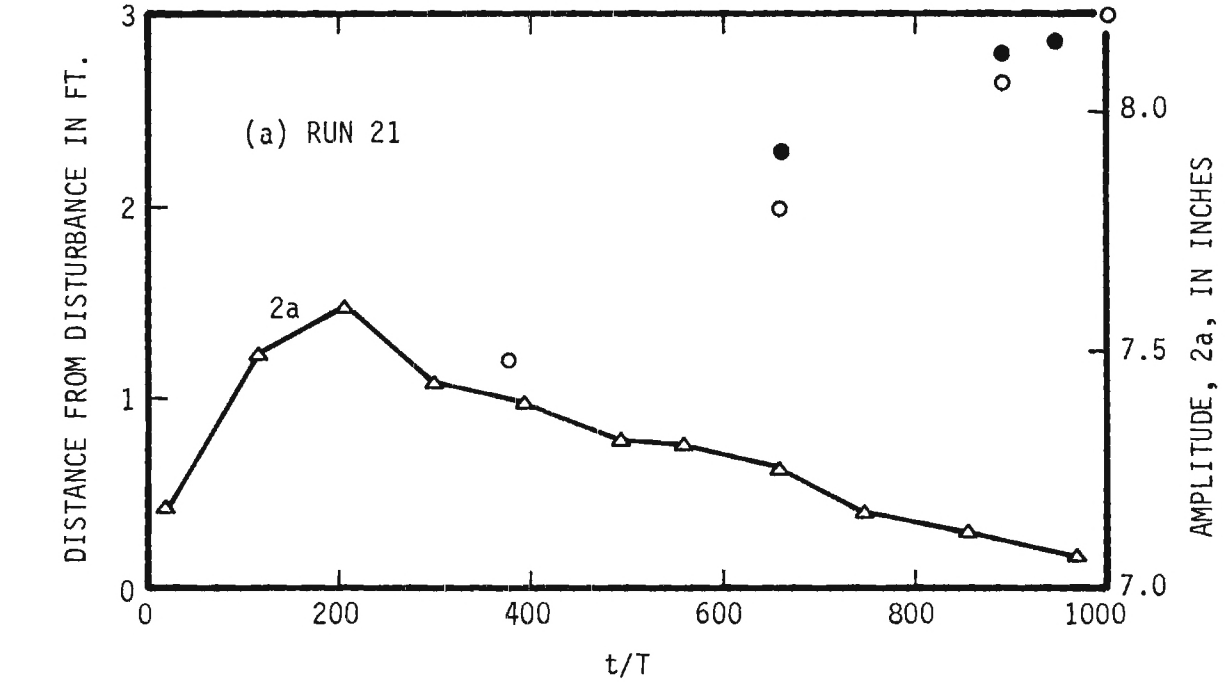


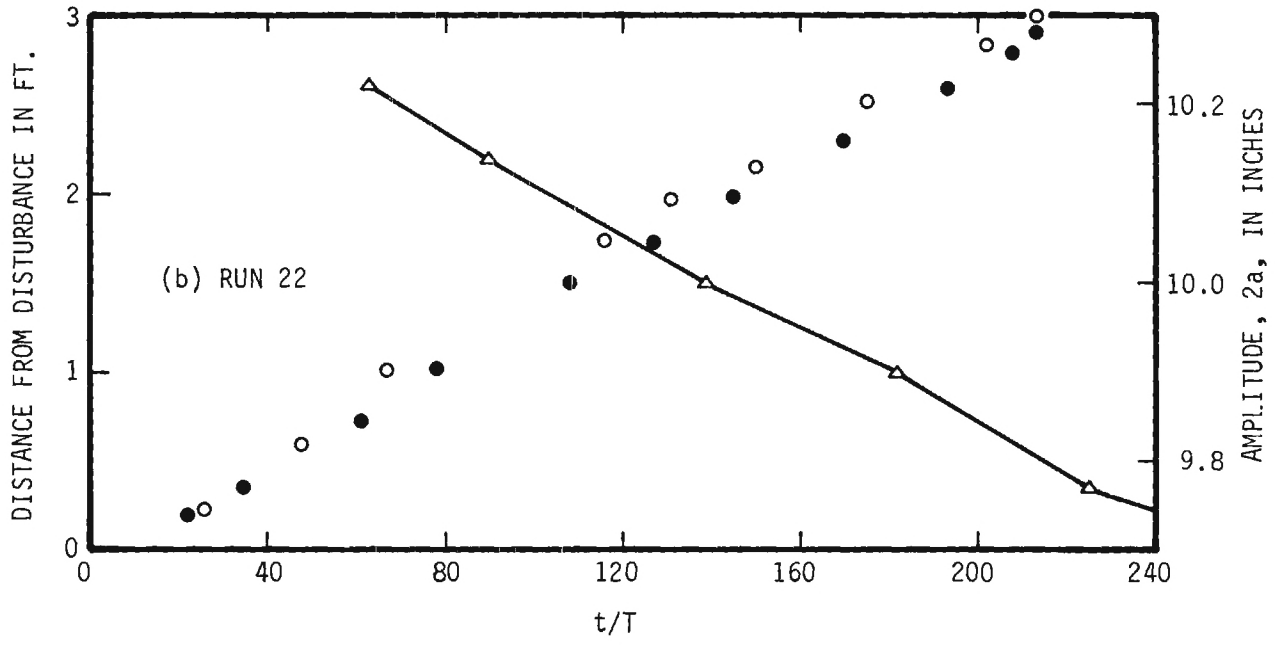


Figure 6. Position of Leading Dune as a Function of Time.

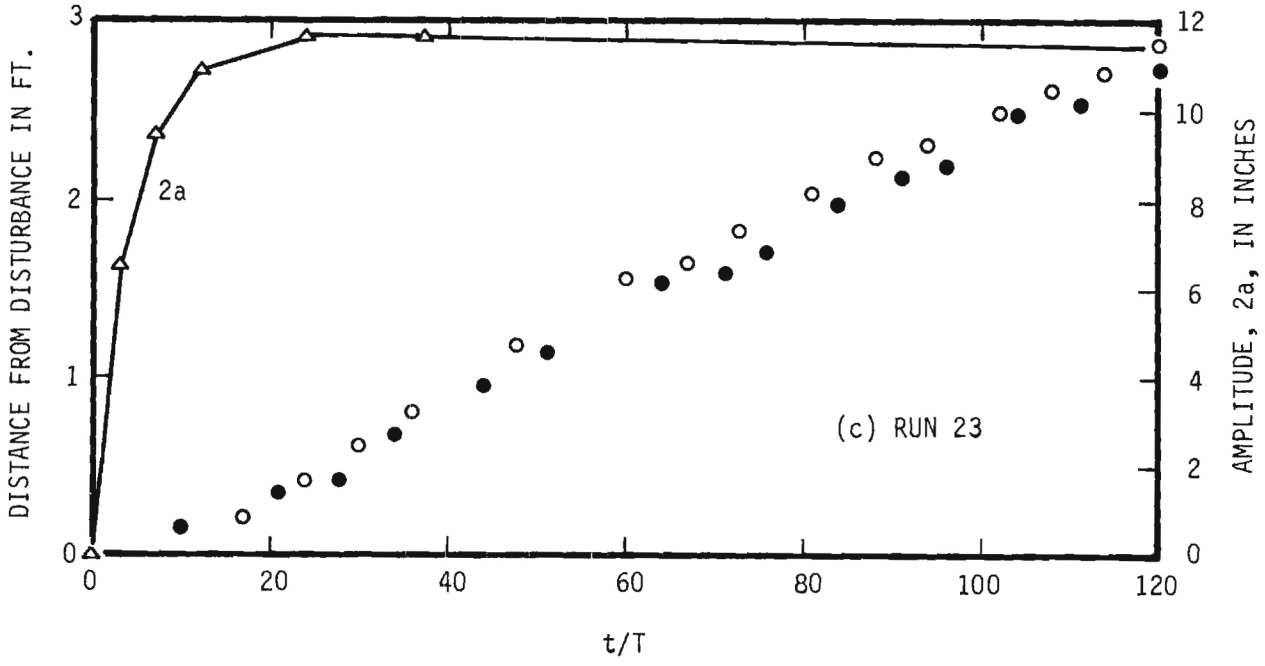


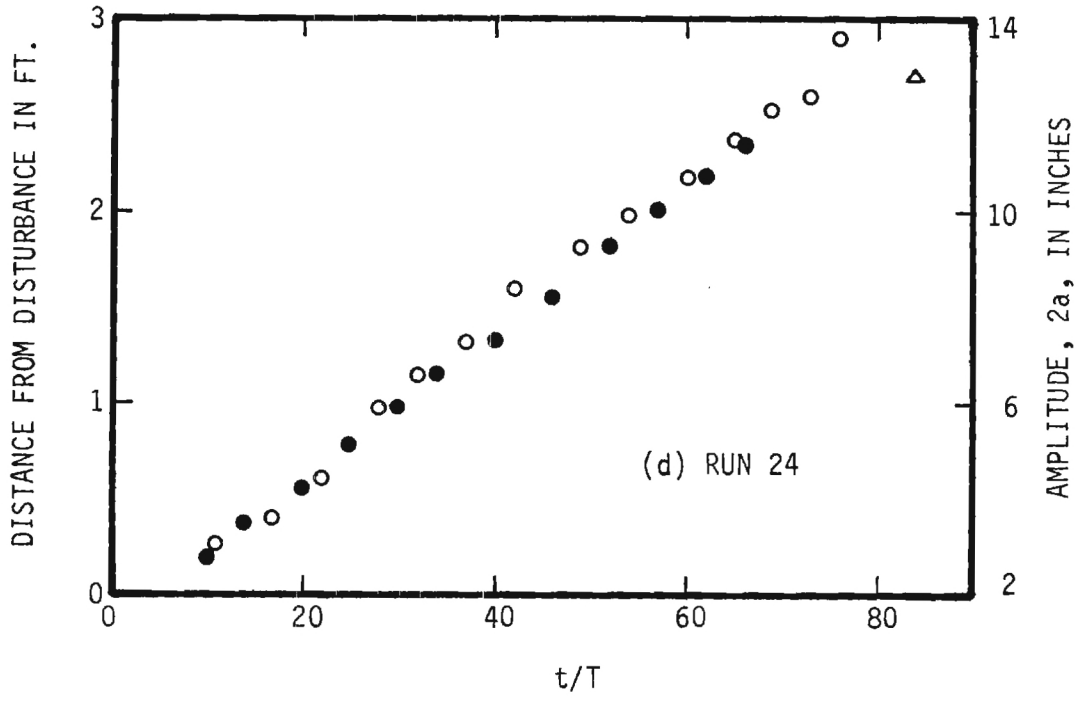


Figure 6. (Continued) Position of Leading Dune as a Function of Time.

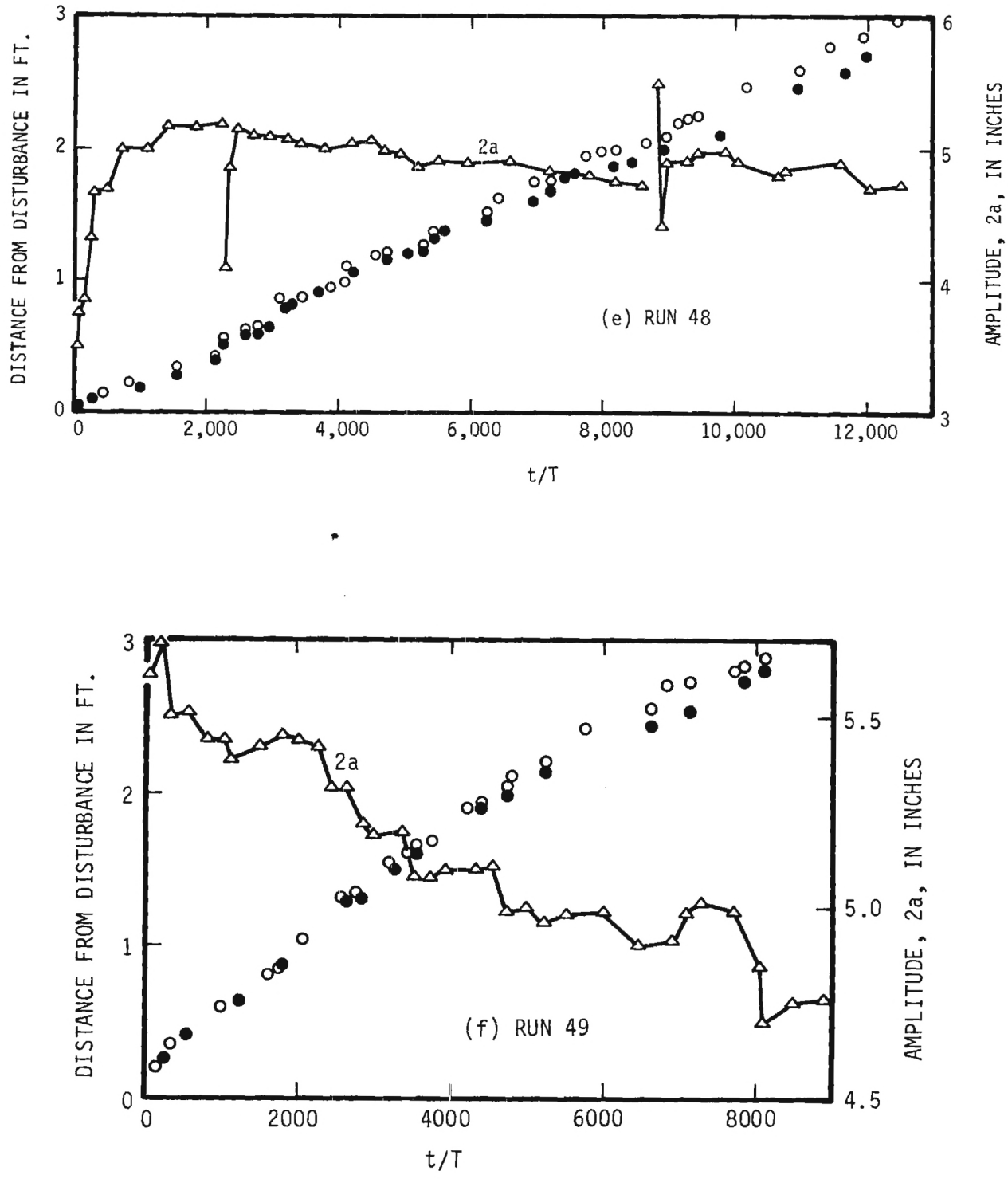


Figure 6. (Continued) Position of Leading Dune as a Function of Time.

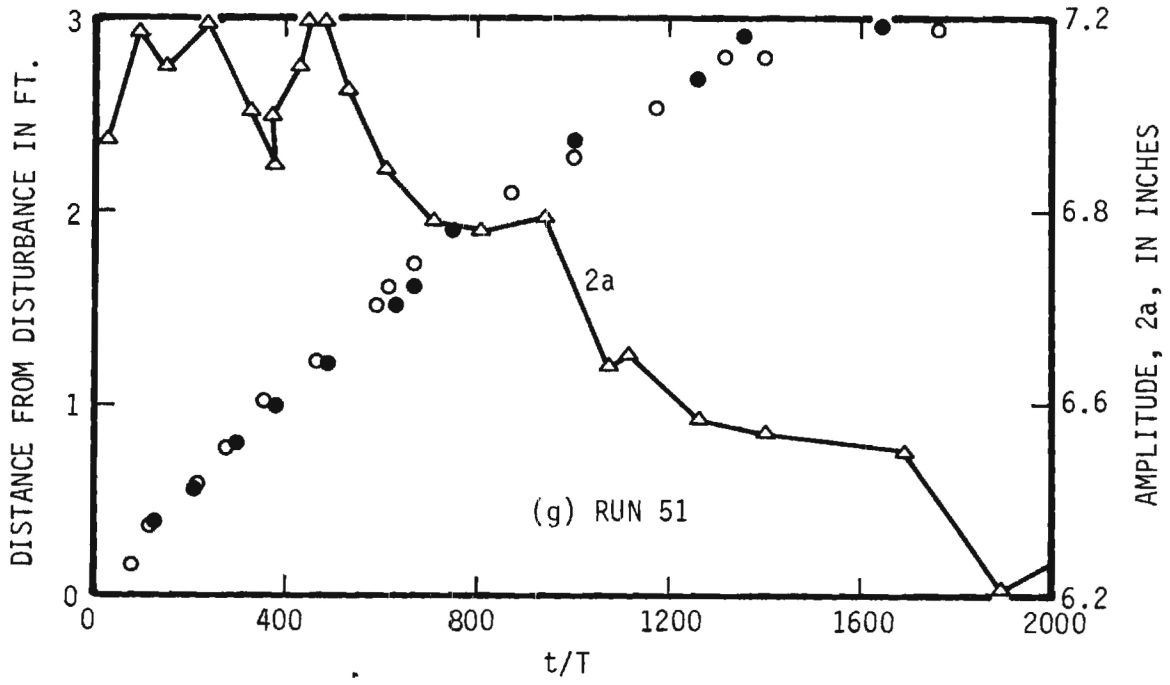


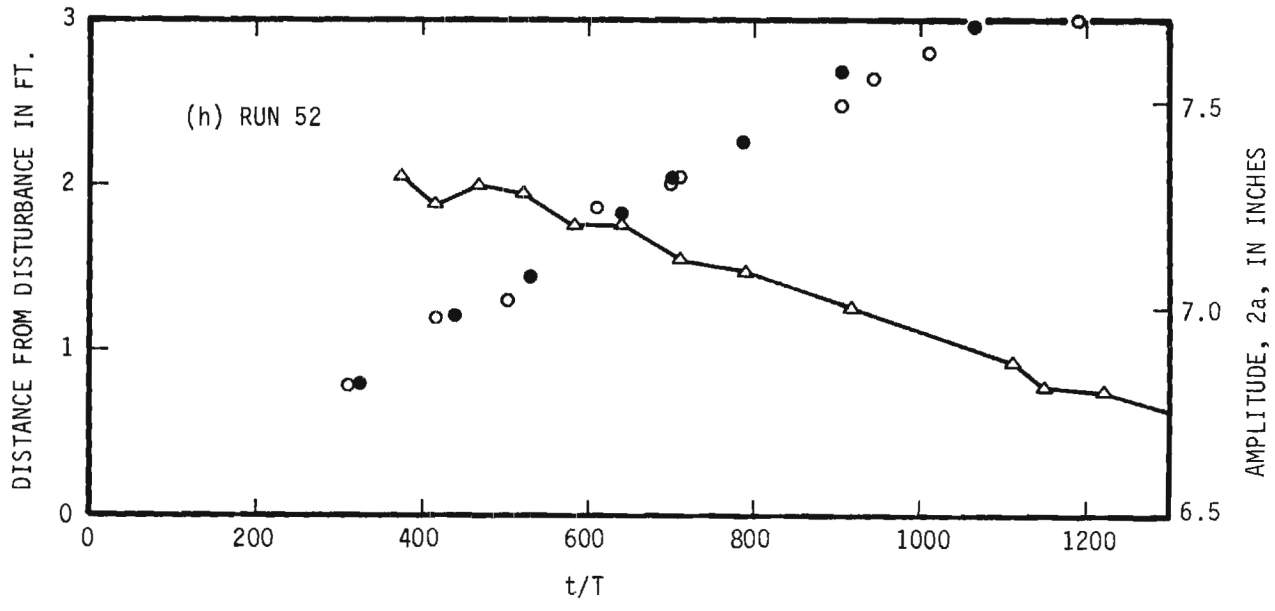


Figure 6. (Continued) Position of Leading Dune as a Function of Time.

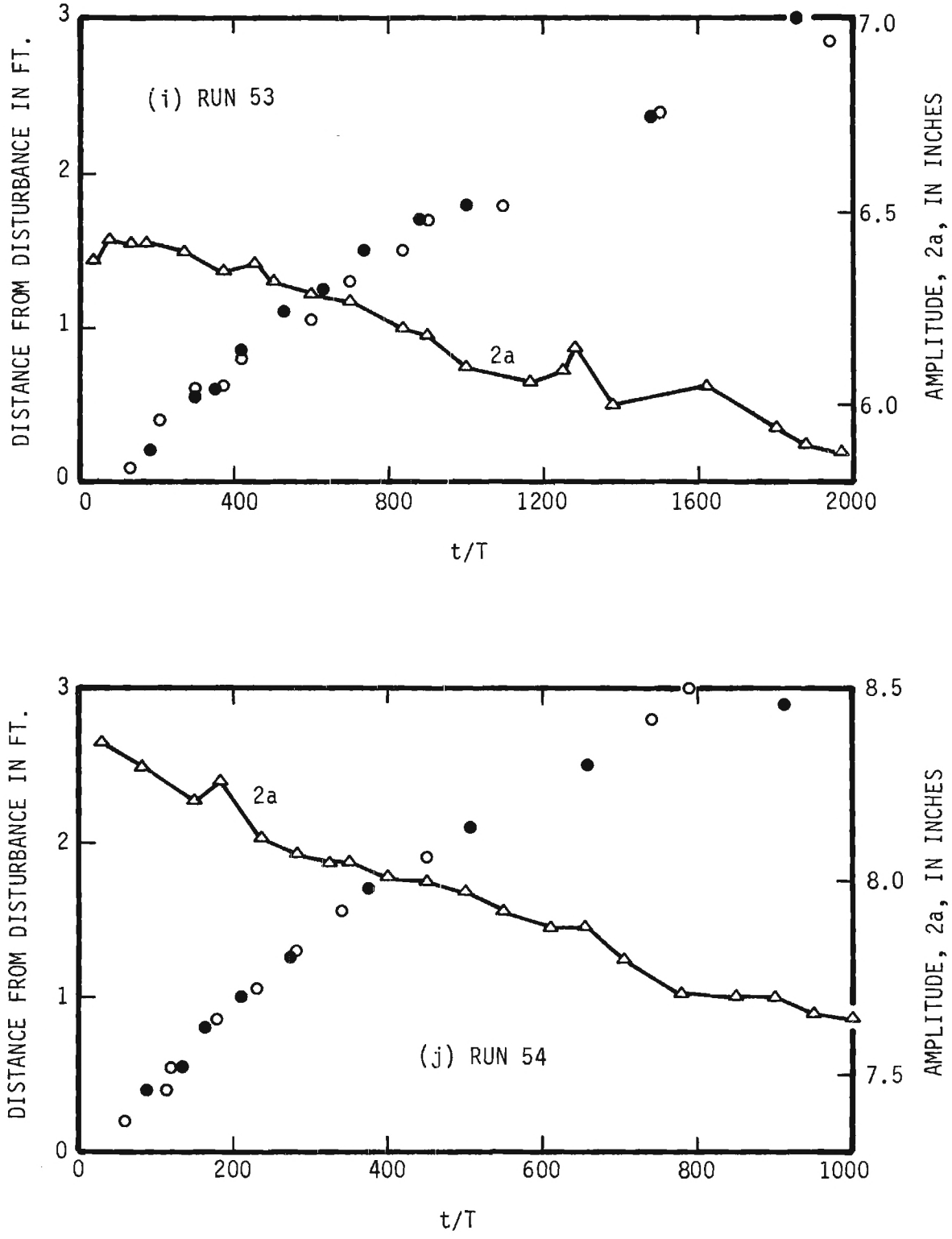


Figure 6. (Continued) Position of Leading Dune as a Function of Time.

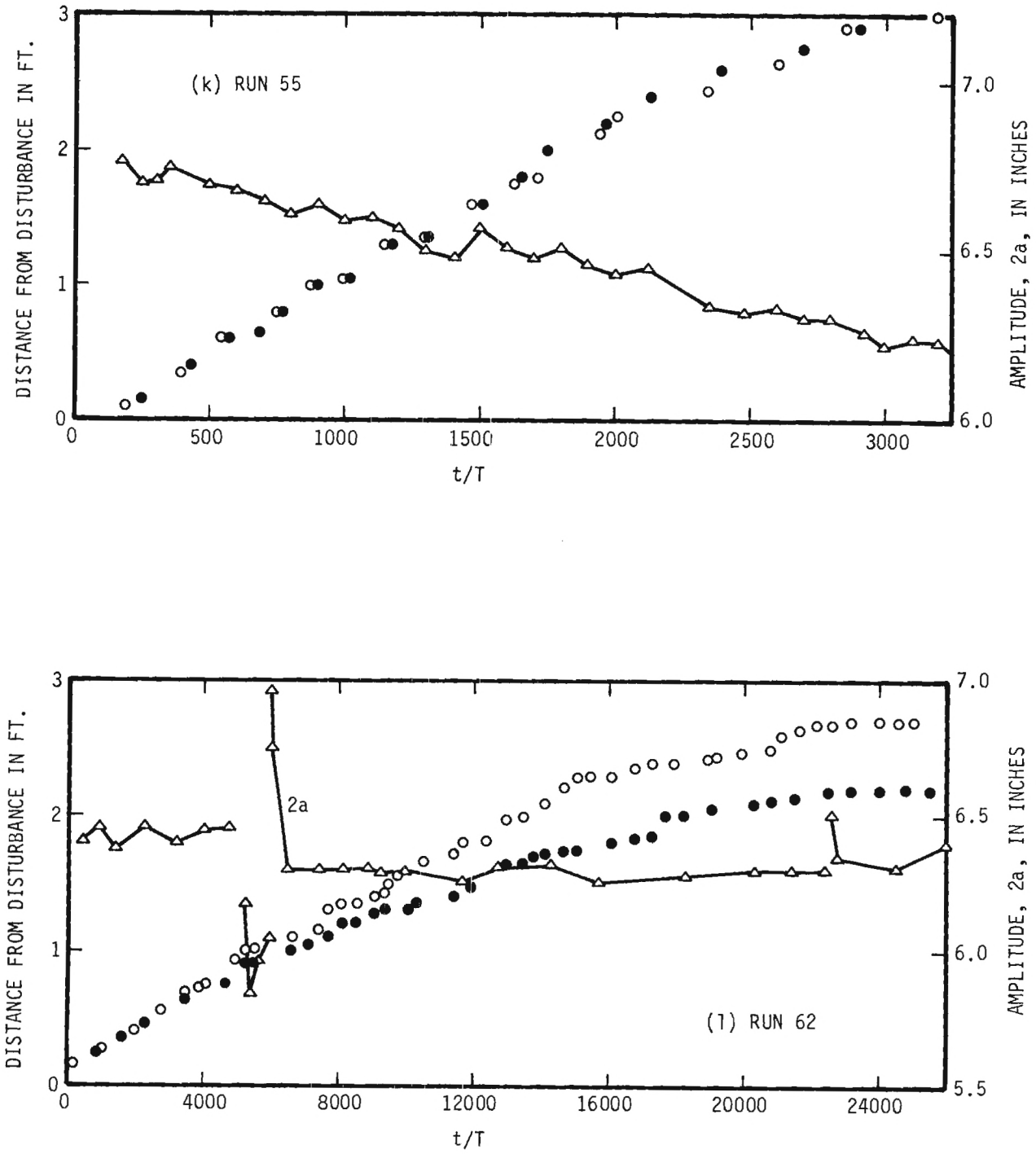


Figure 6. (Continued) Position of Leading Dune as a Function of Time.

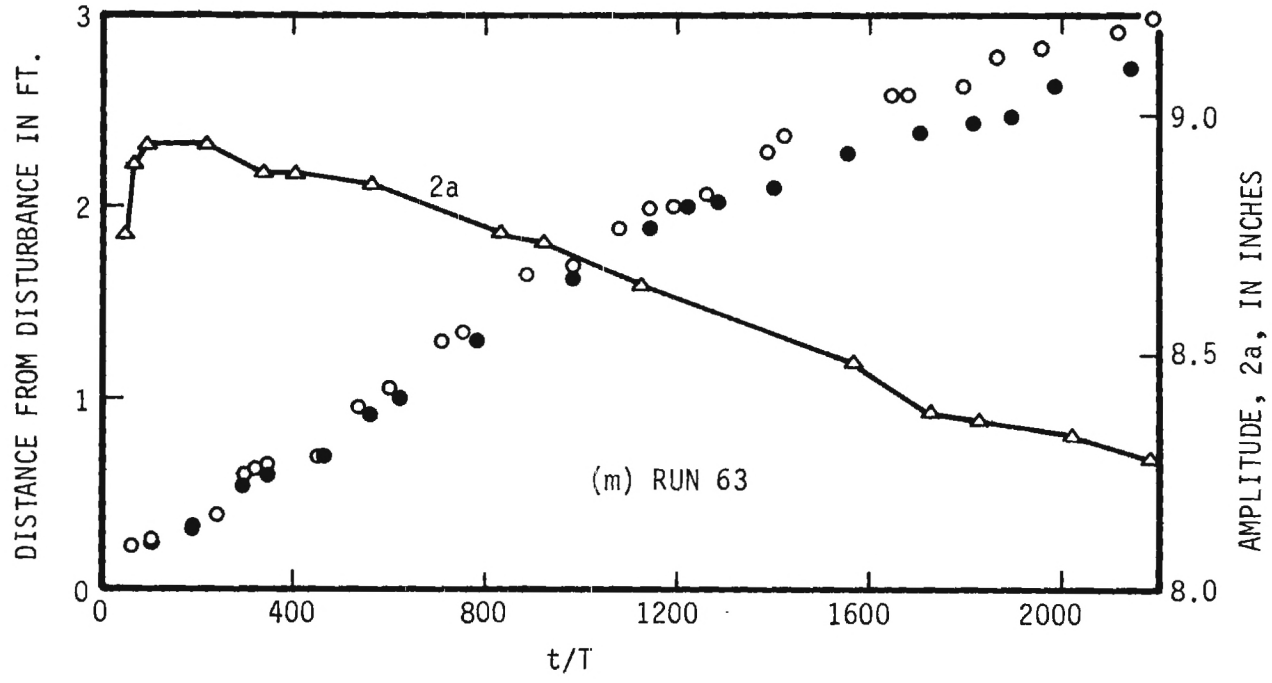


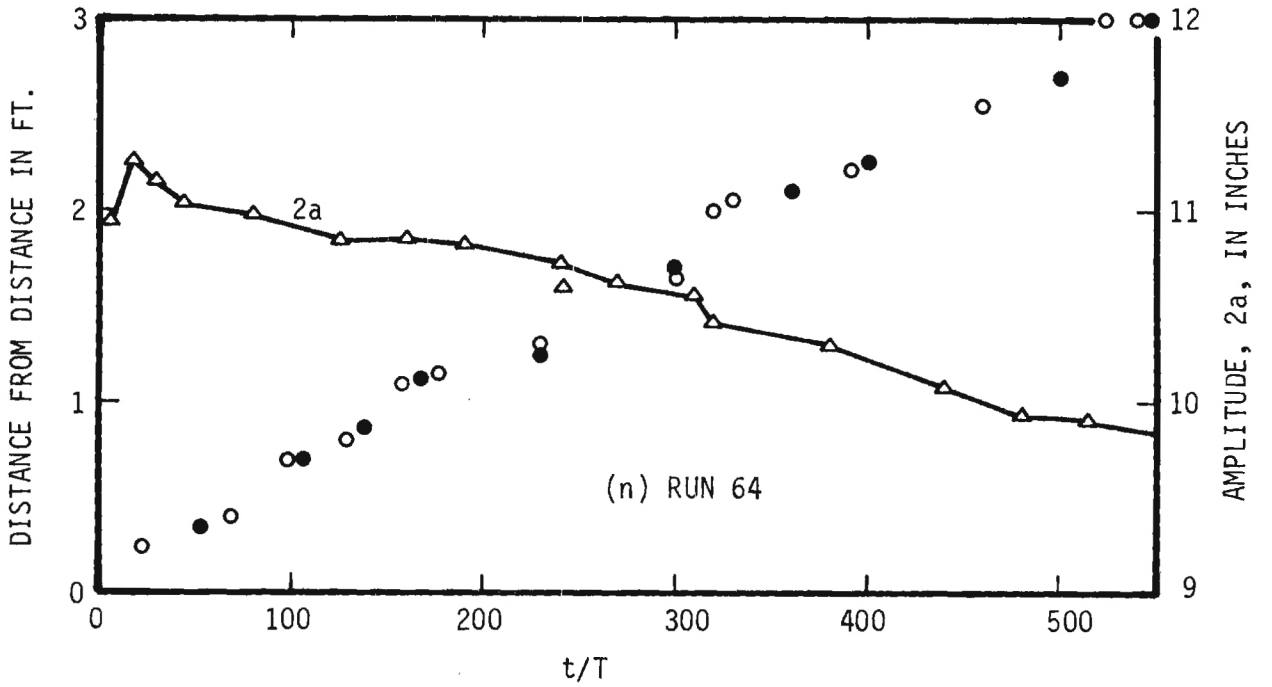


Figure 6. (Continued) Position of Leading Dune as a Function of Time.

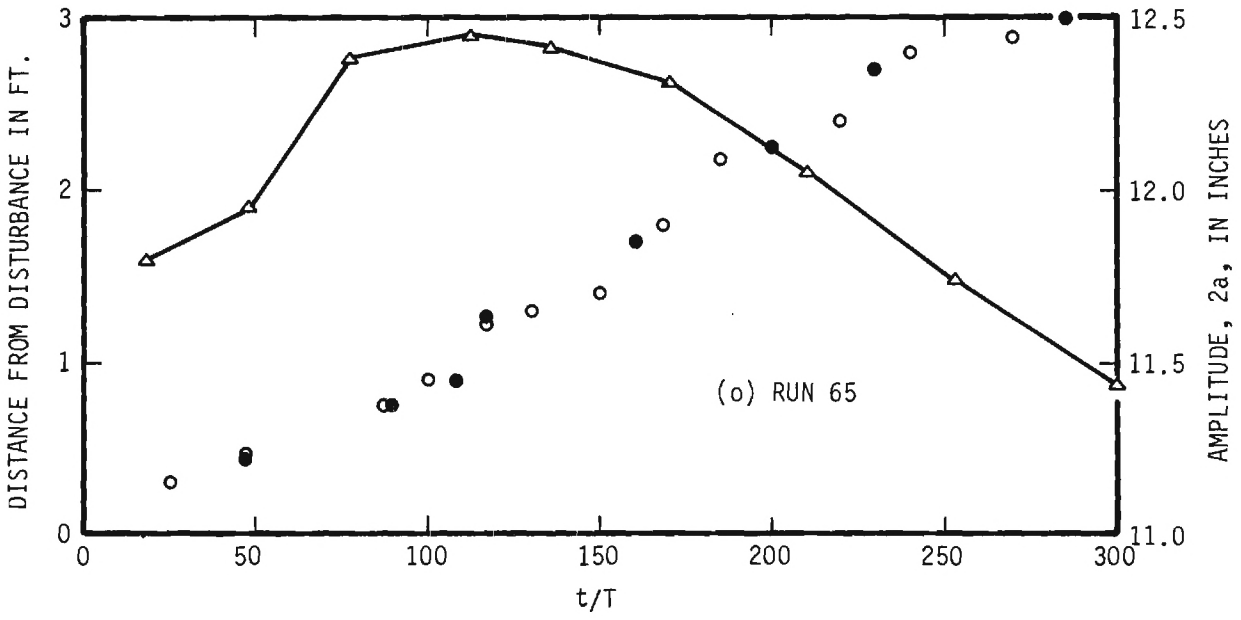


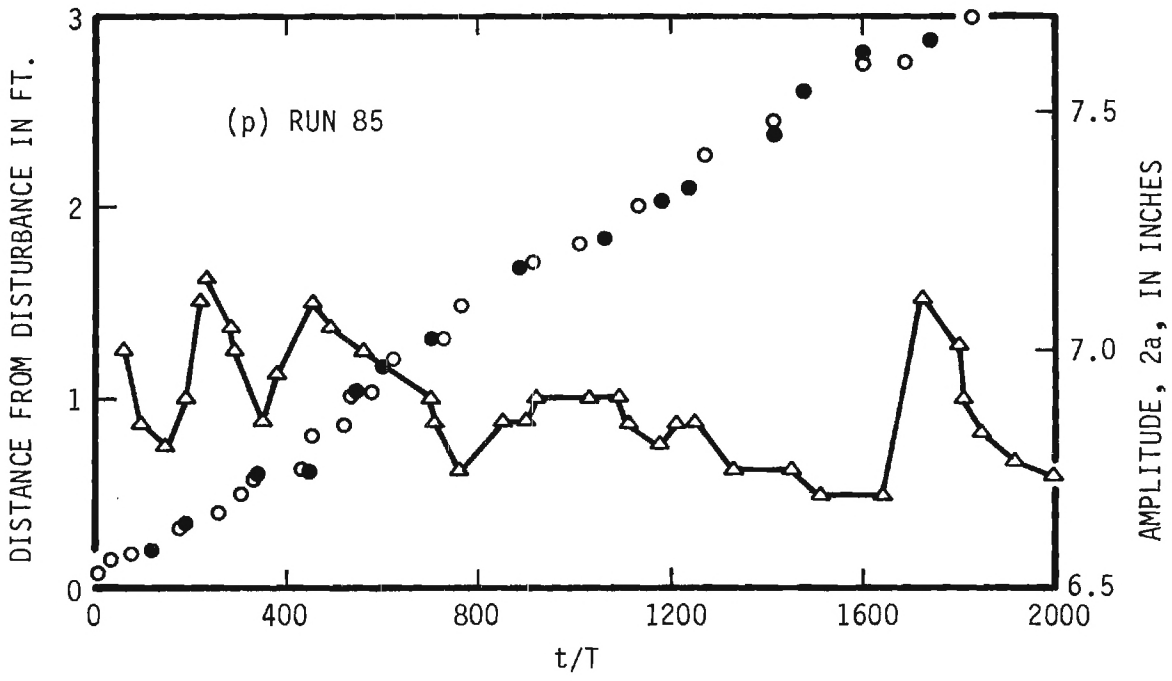


Figure 6. (Continued) Position of Leading Dune as a Function of Time.

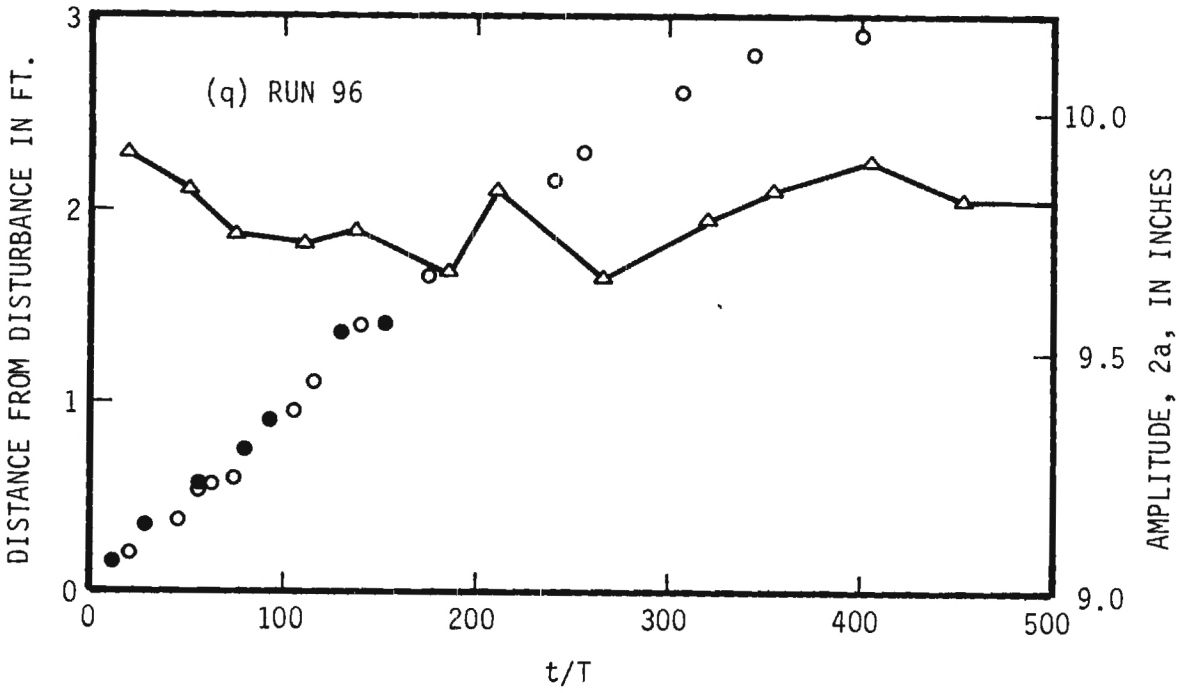


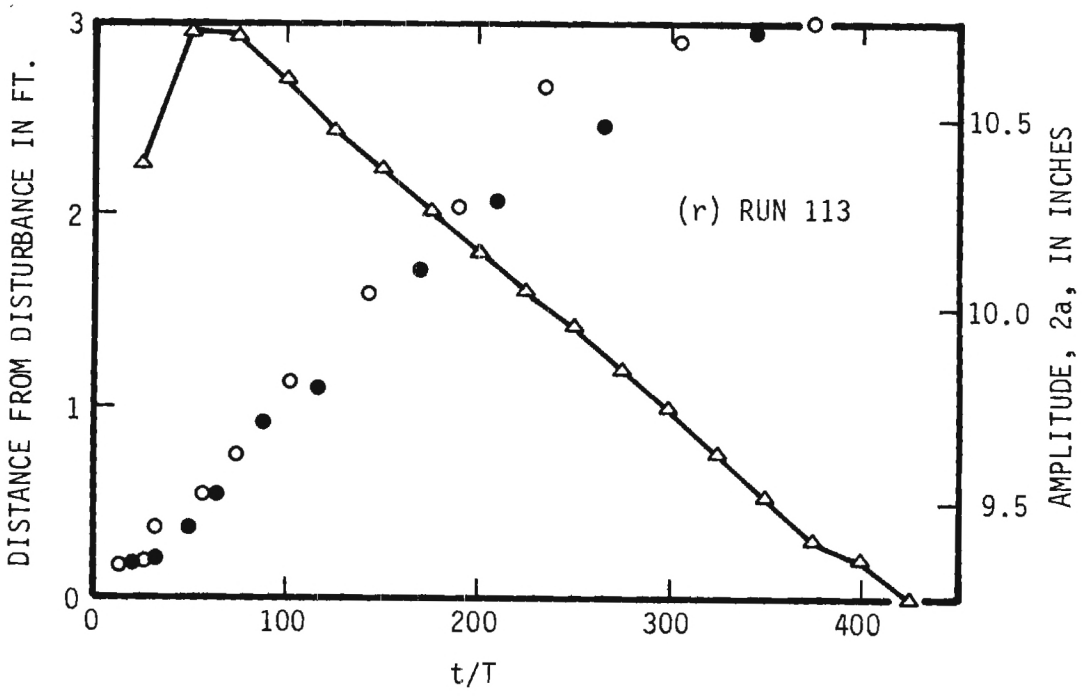


Figure 6. (Continued) Position of Leading Dune as a Function of Time.

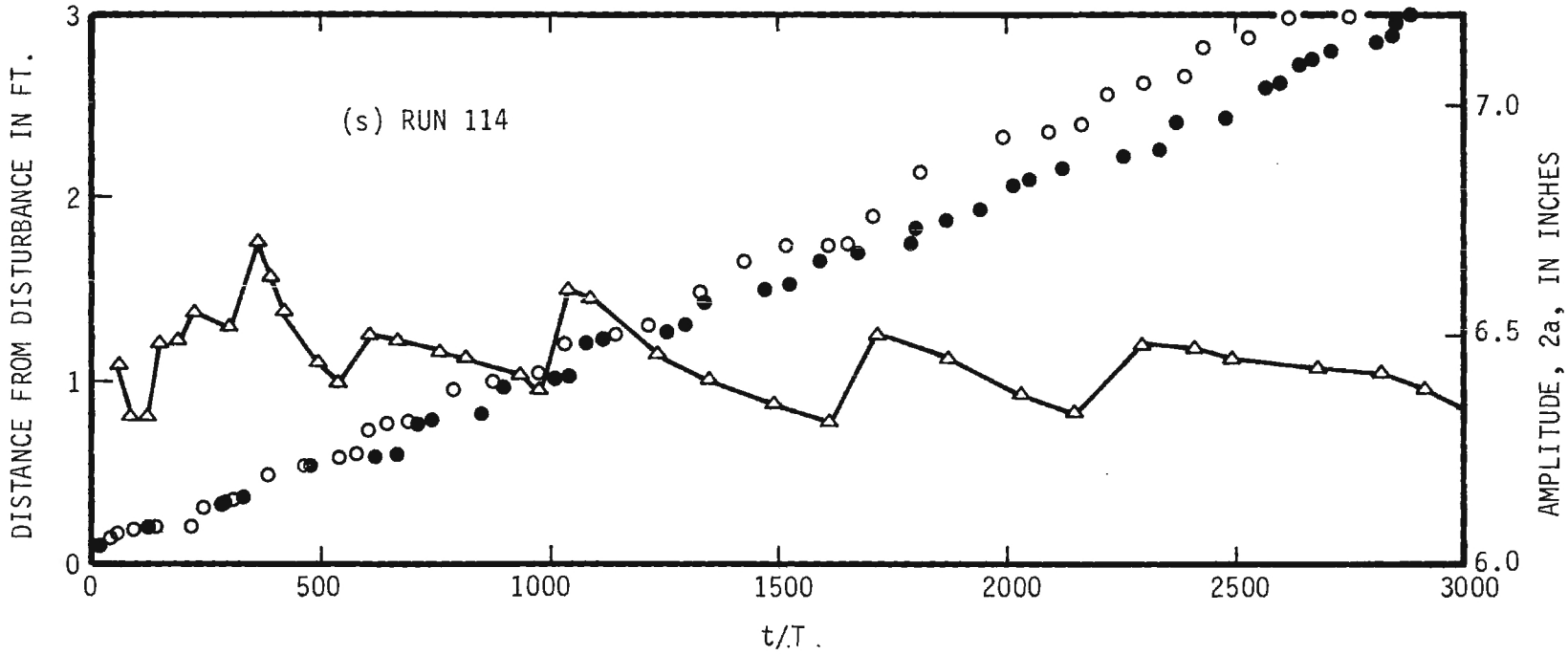


Figure 6. (Continued) Position of Leading Dune as a Function of Time.

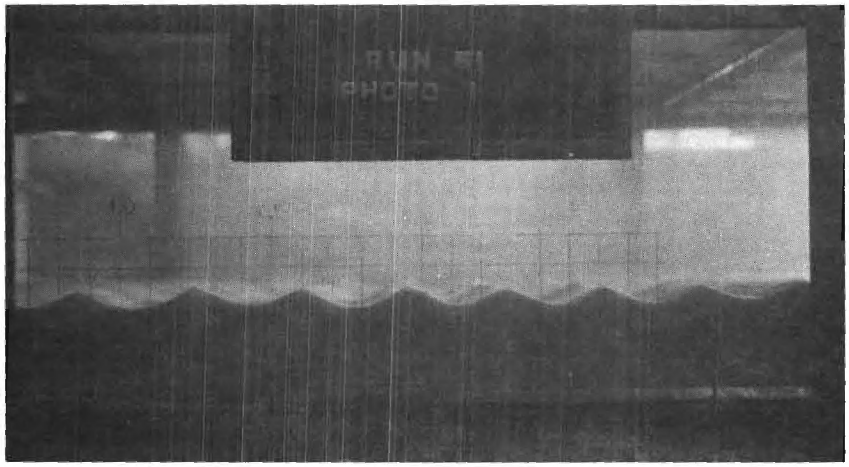

(a). Run 51 (a/Dg = 269)

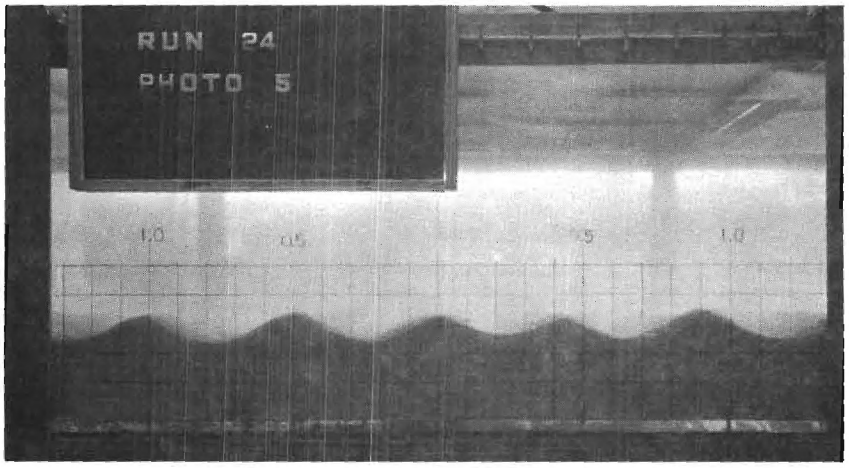


(b). Run 24 (a/Dg = 513)

Figure 7. Dune Geometry (Medium Sand).

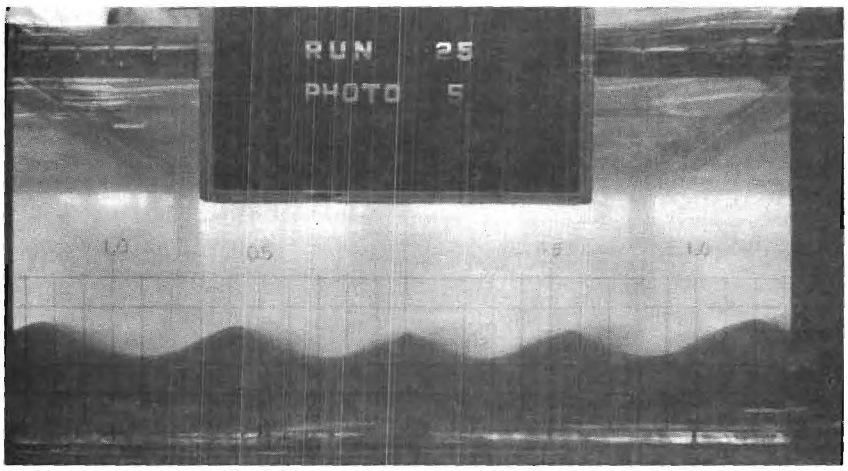


(c). Run 25 (a/Dg = 702)

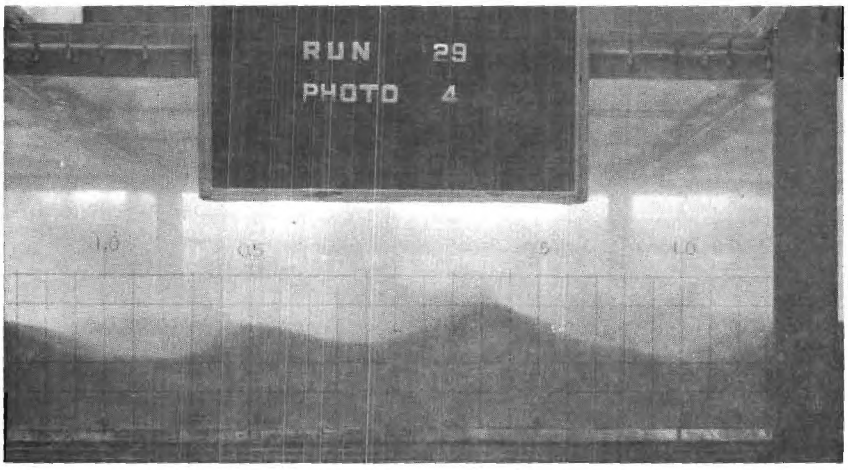


(d). Run 29 (a/Dg = 1075)

Figure 7. (Continued) Dune Geometry (Medium Sand).

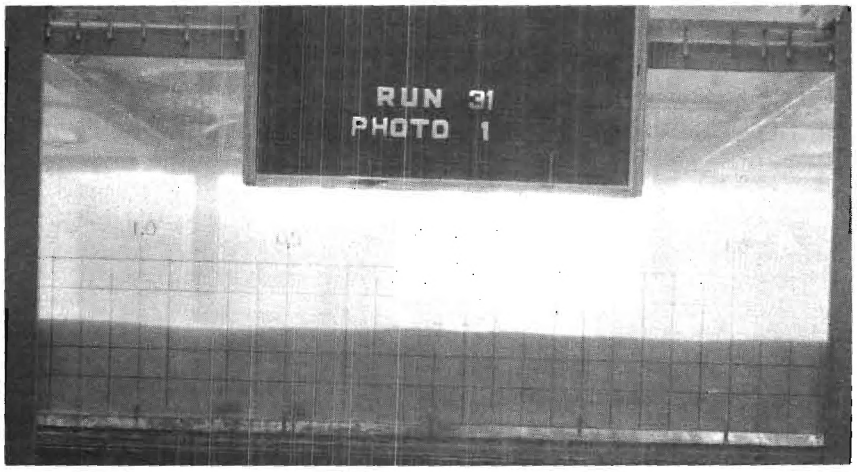


(e). Run 31 (a/Dg = 1501)

Figure 7. (Continued) Dune Geometry (Medium Sand).

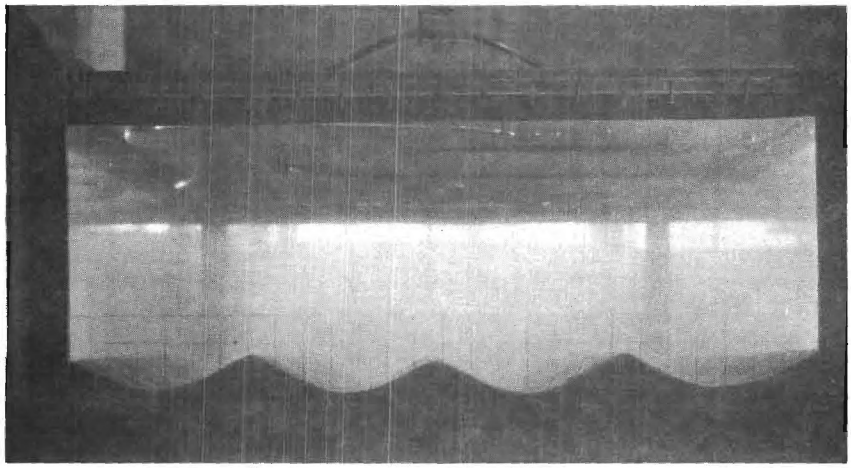

(a). Run 66 (a/Dg = 275)

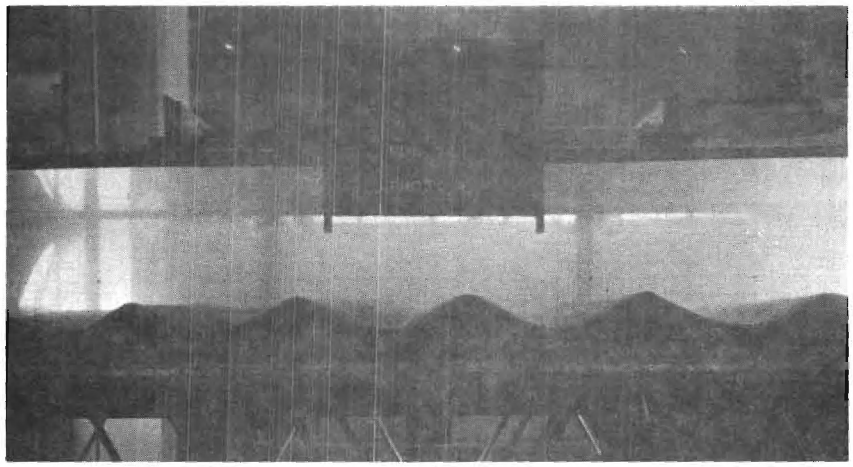

(b). Run 74 (a/Dg = 526)

Figure 8. Dune Geometry (Coarse Sand).

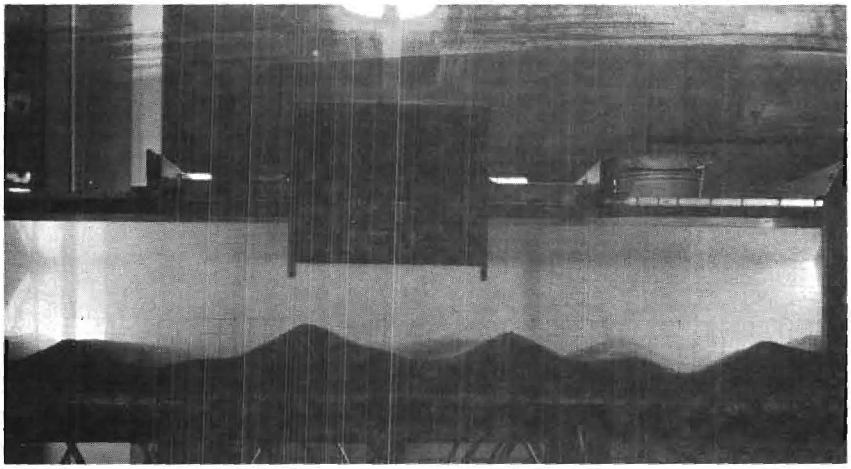

(c). Run 79 (a/Dg = 724)

Figure 8. (Continued) Dune Geometry (Coarse Sand).

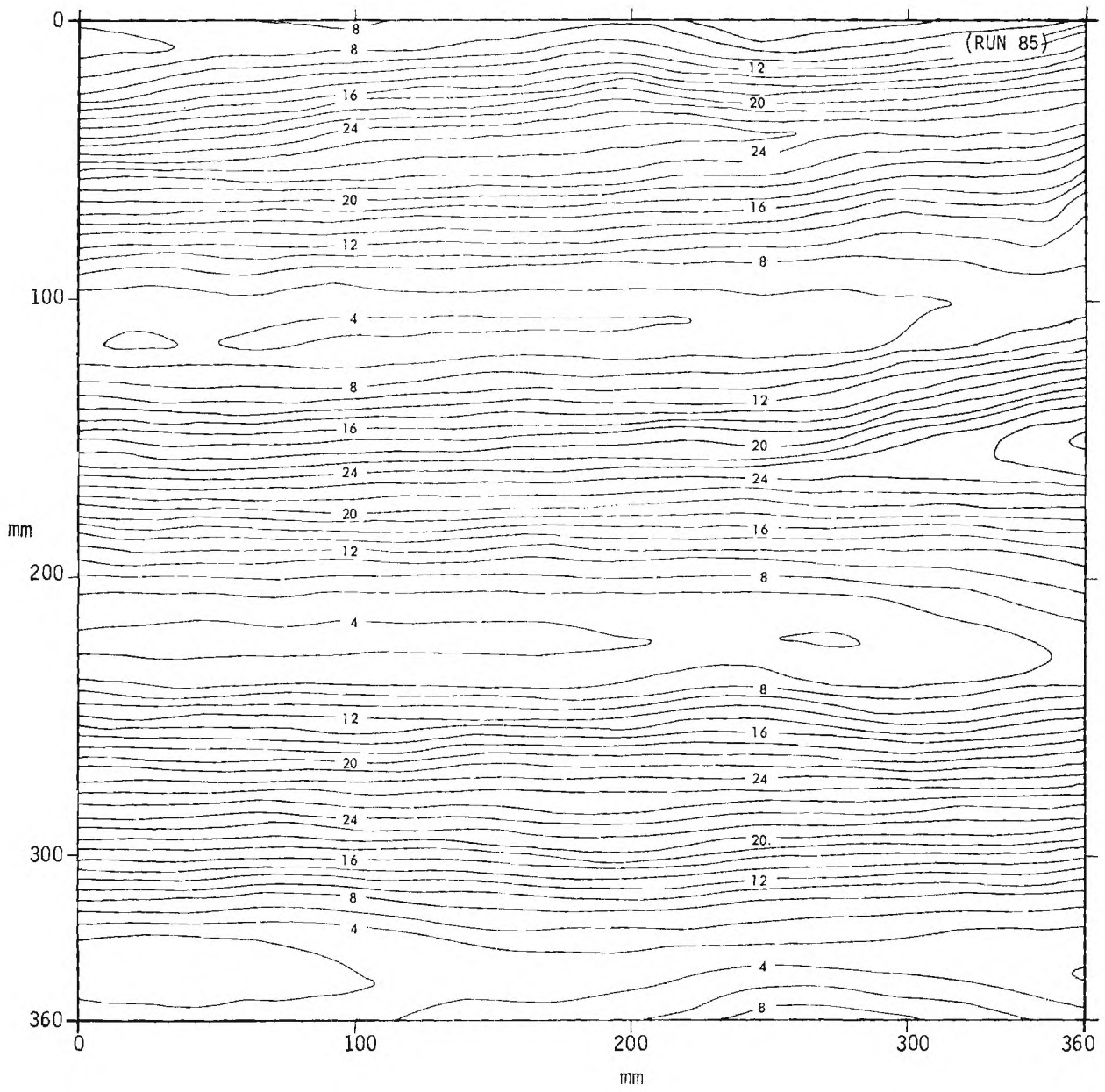


Figure 9. Topographic Map (Fine Sand).

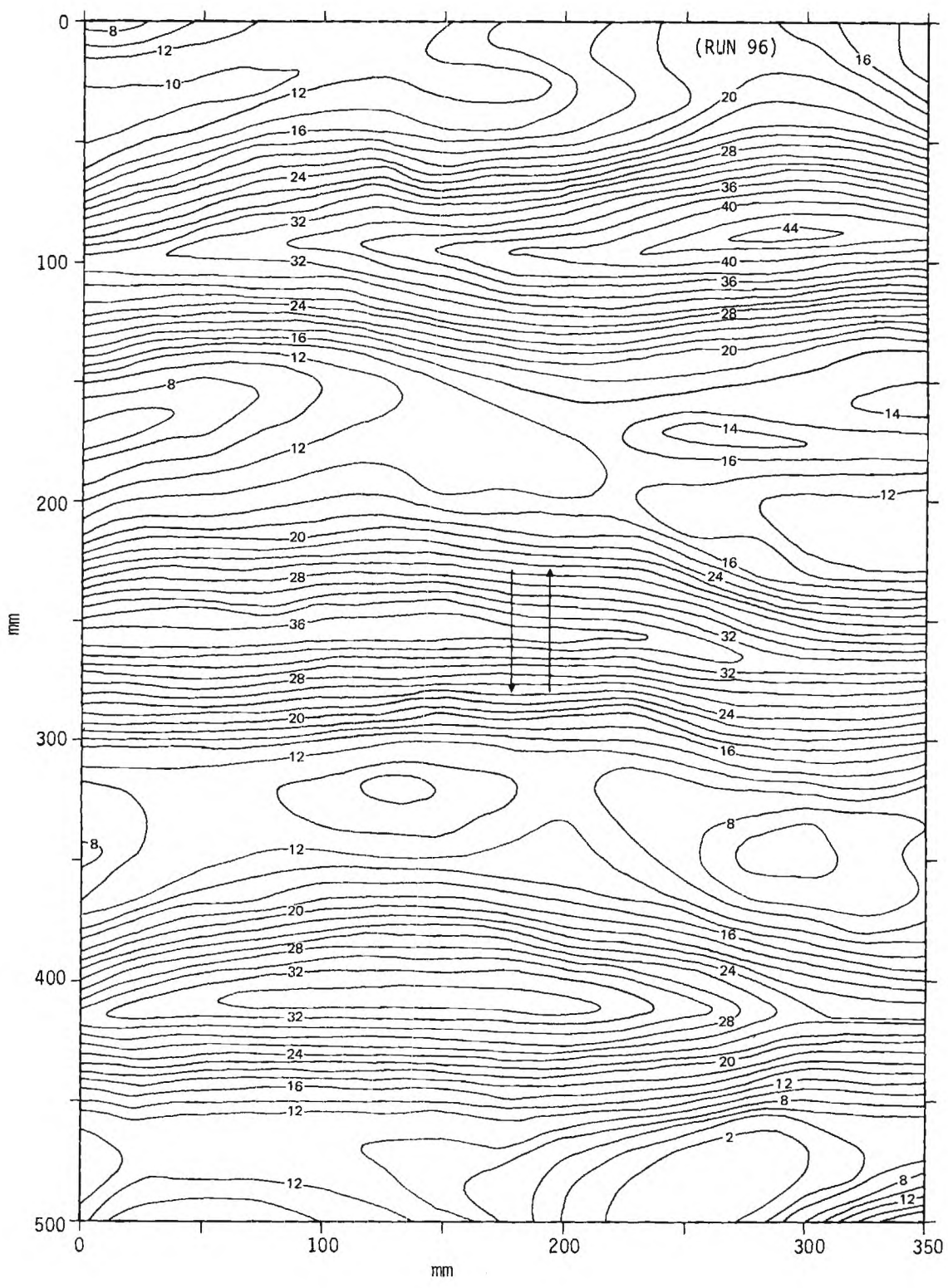


Figure 9. (Continued) Topographic Map (Fine Sand).

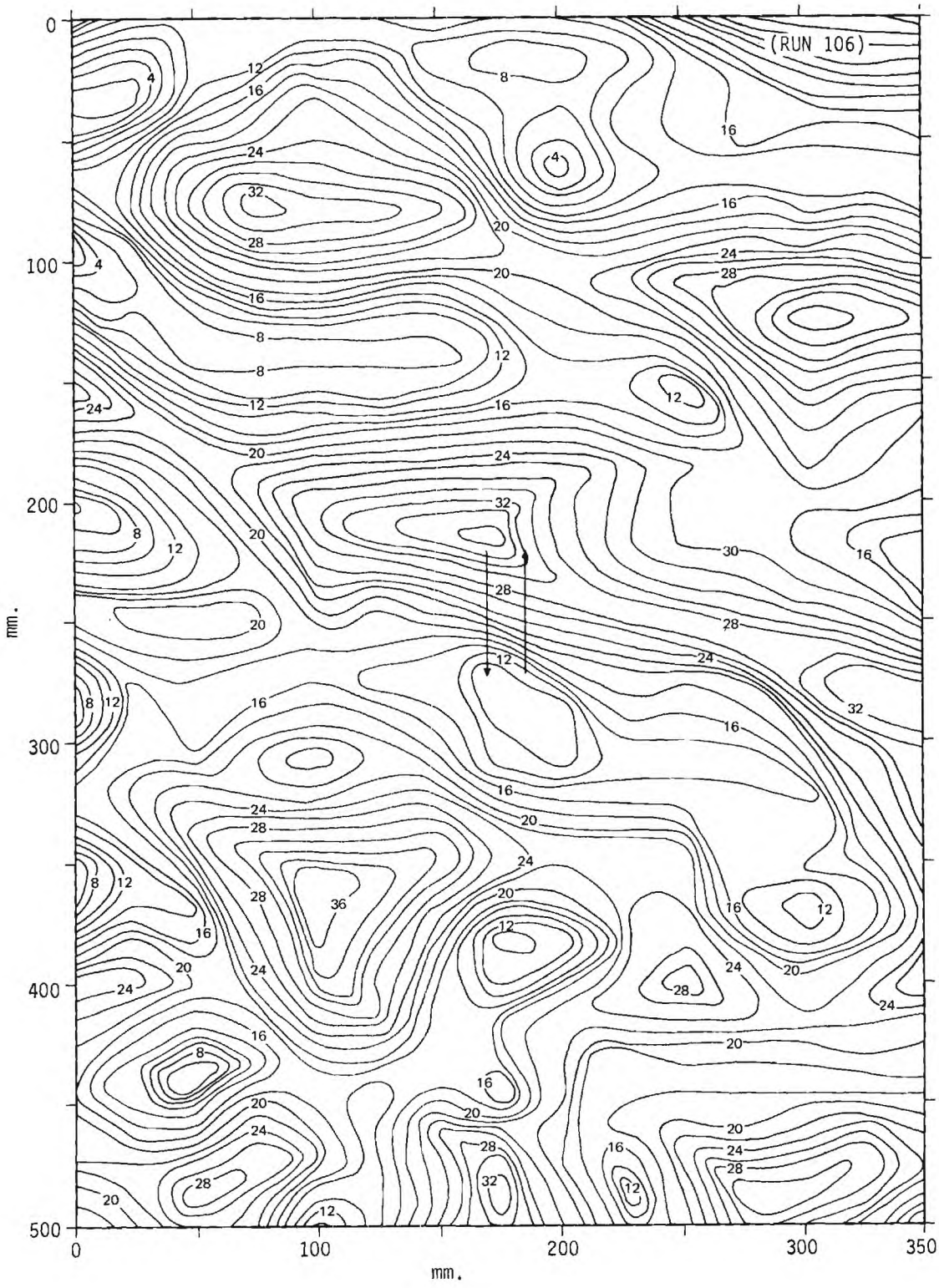


Figure 9. (Continued) Topographic Map (Fine Sand).

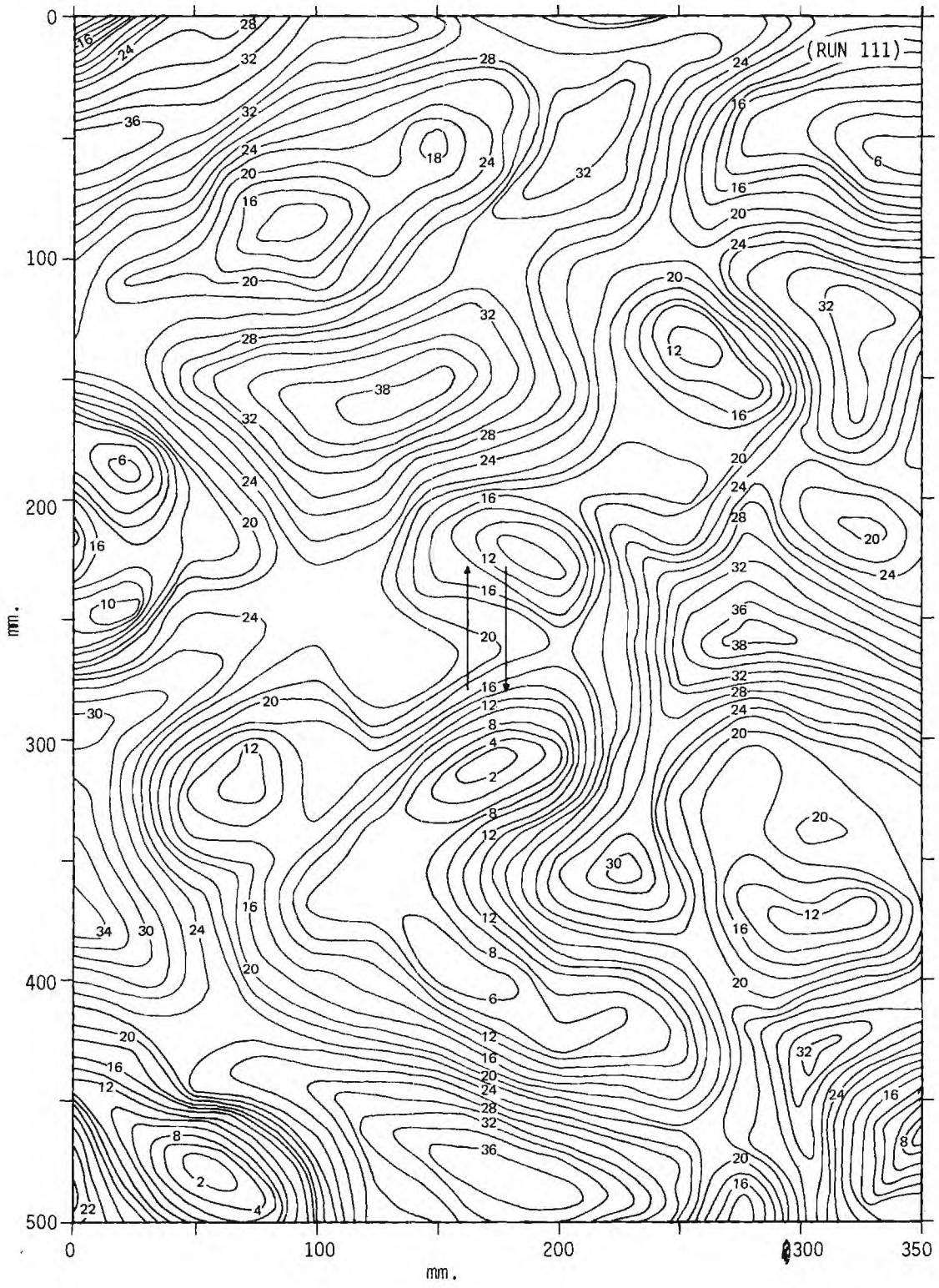


Figure 9. (Continued) Topographic Map (Fine Sand).

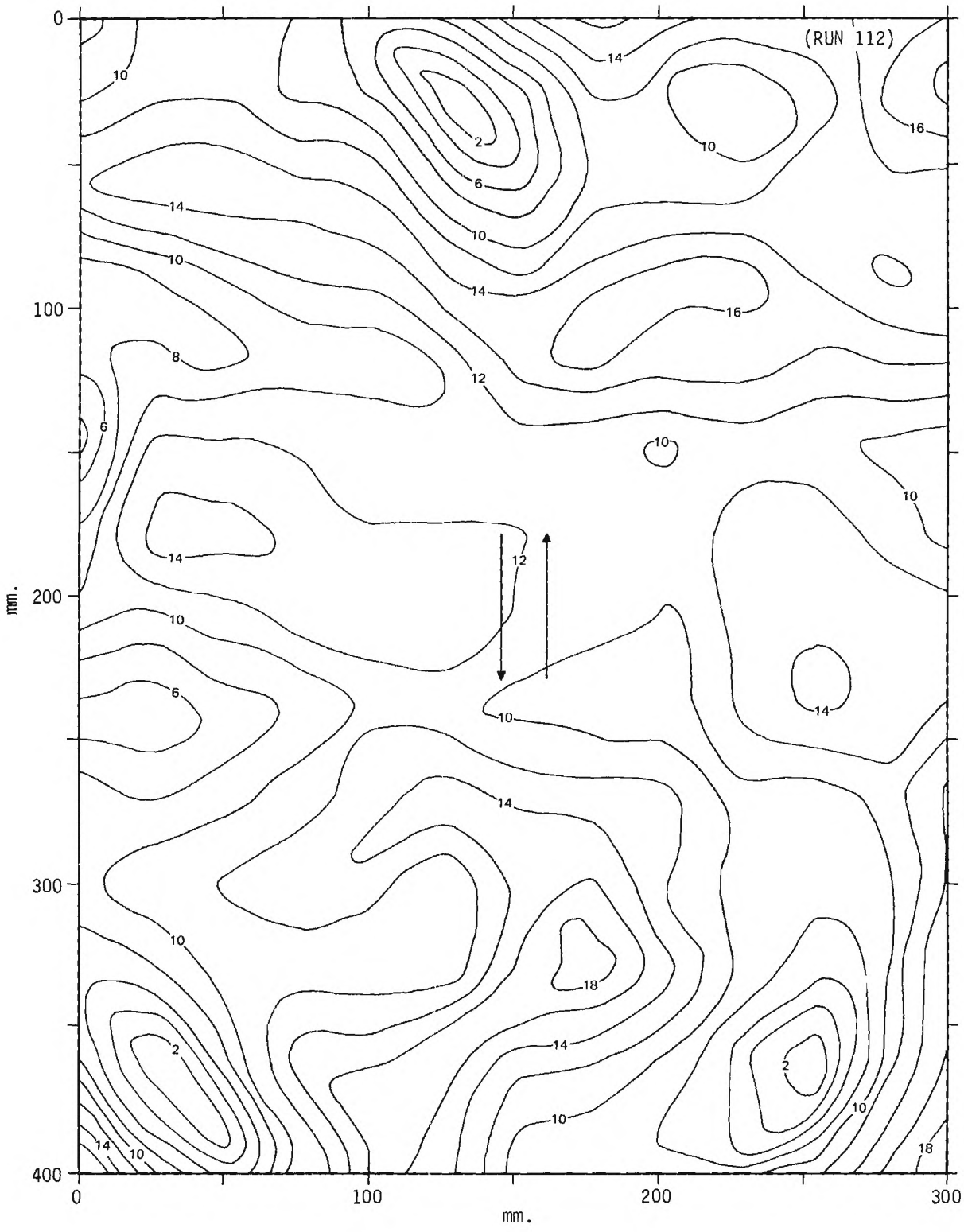


Figure 9. (Continued) Topographic Map (Fine Sand).

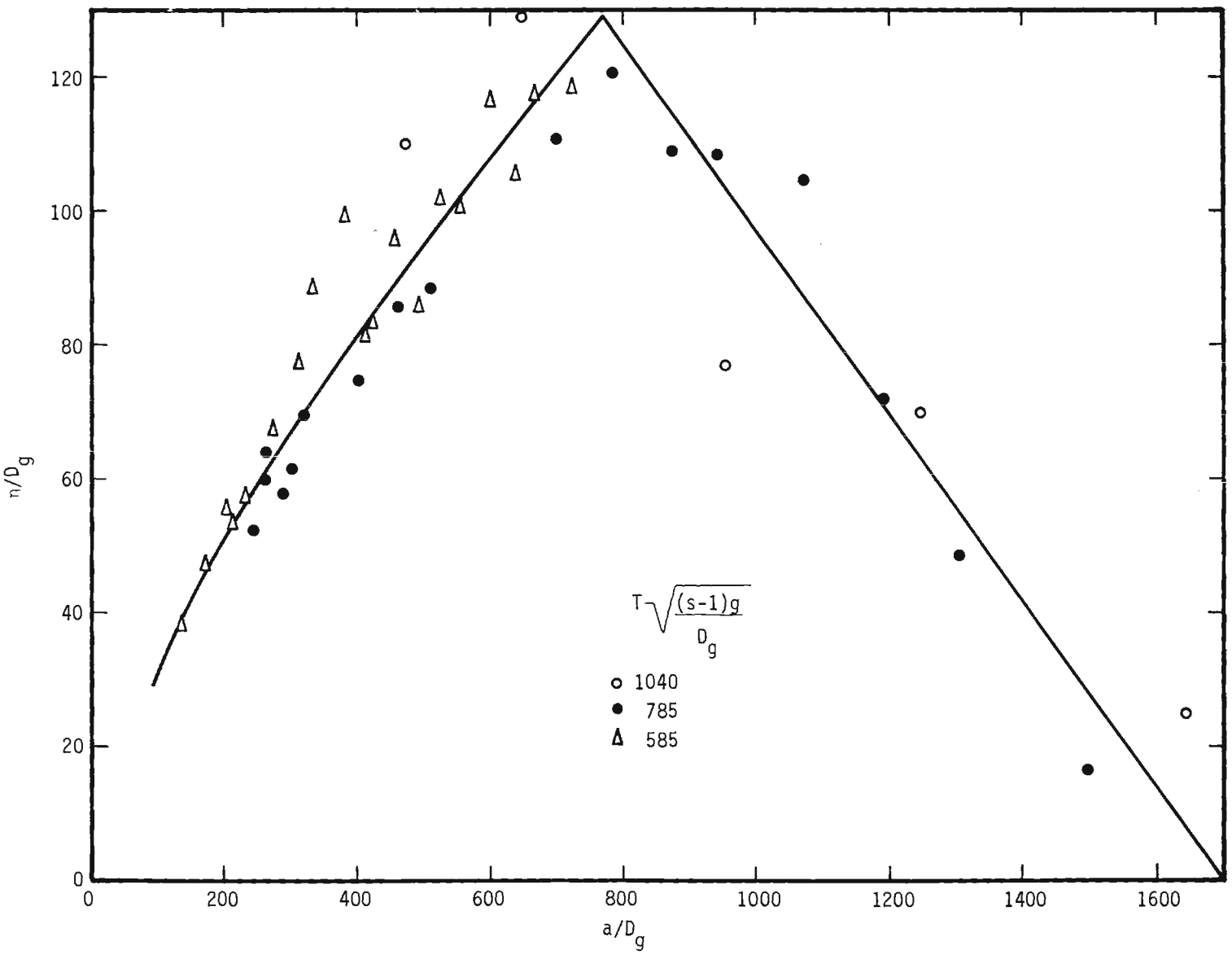


Figure 10. Dune Amplitude.

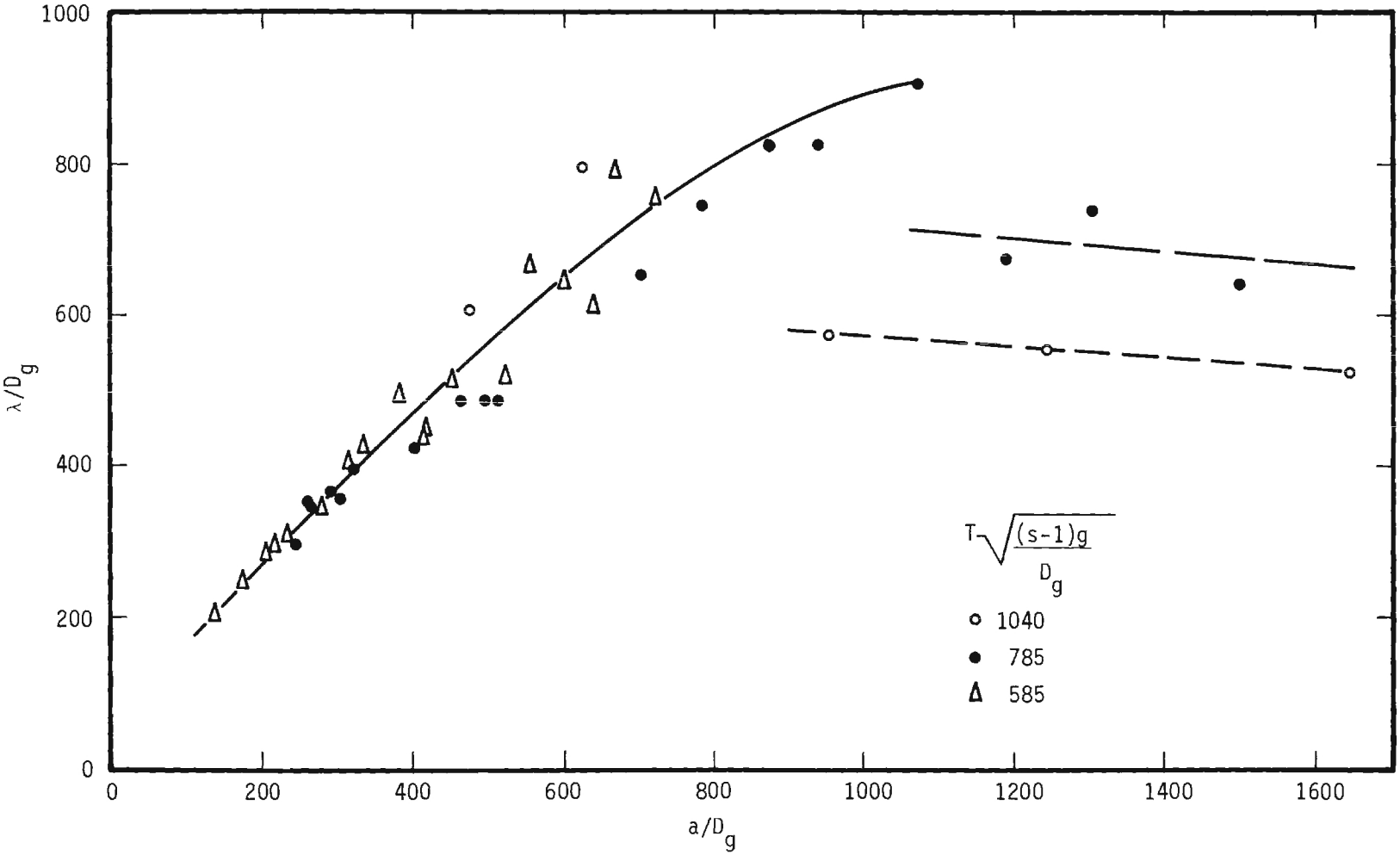


Figure 11. Dune Wave Length.

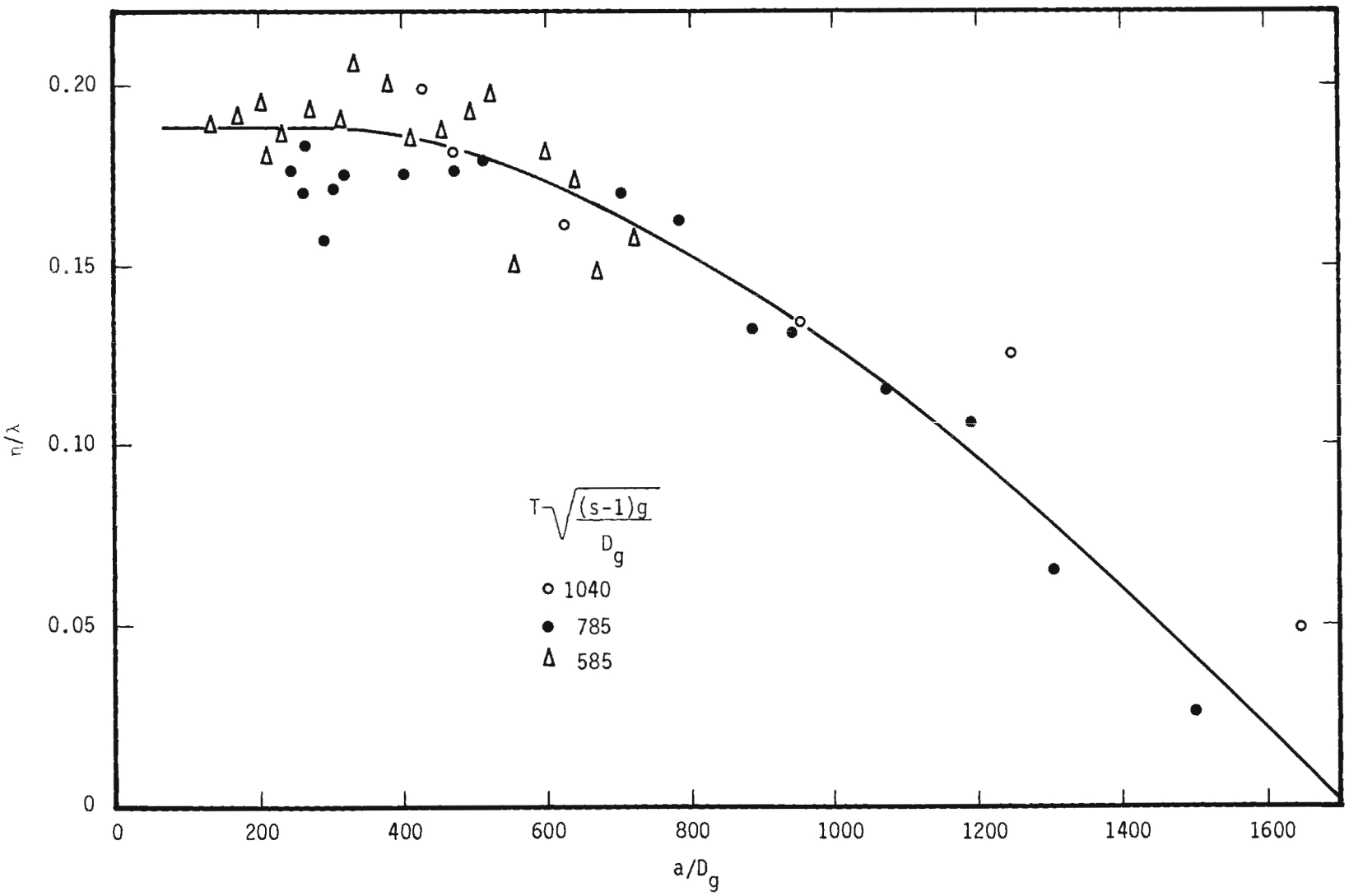


Figure 12. Ratio of Dune Amplitude to Dune Wave Length.

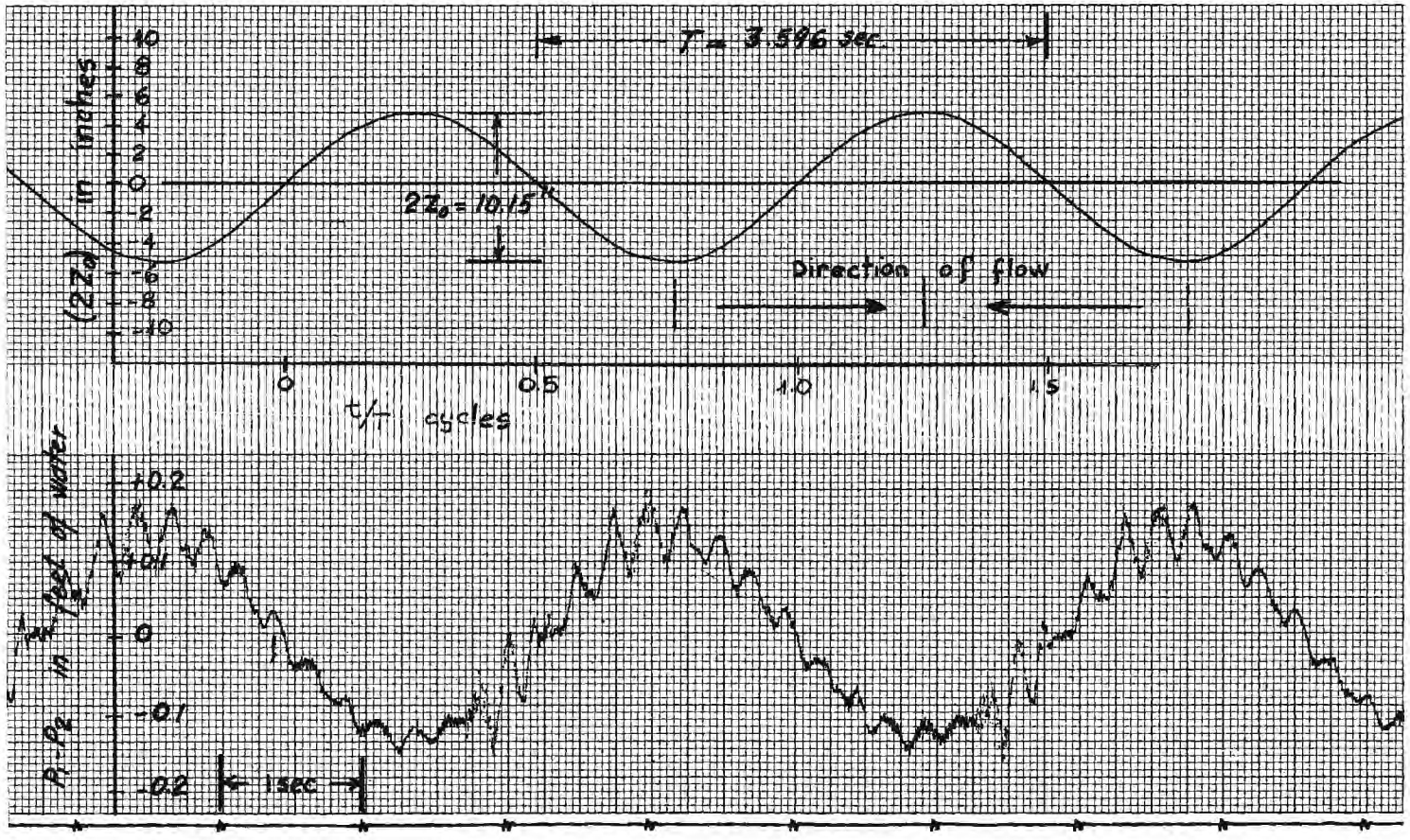


Figure 13. Strip-Chart Data (Run 95).

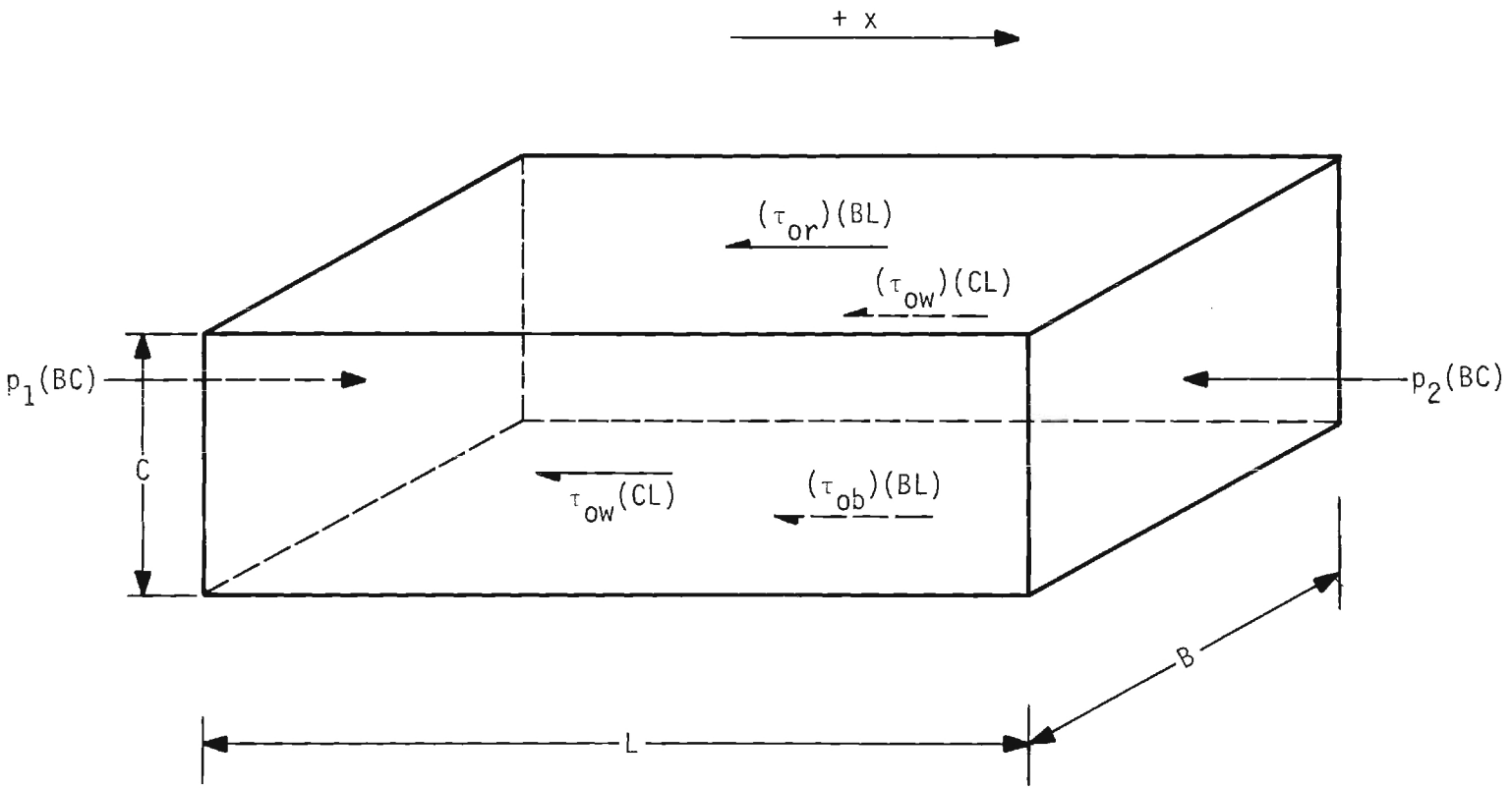


Figure 14. Control Volume Within Test Section.

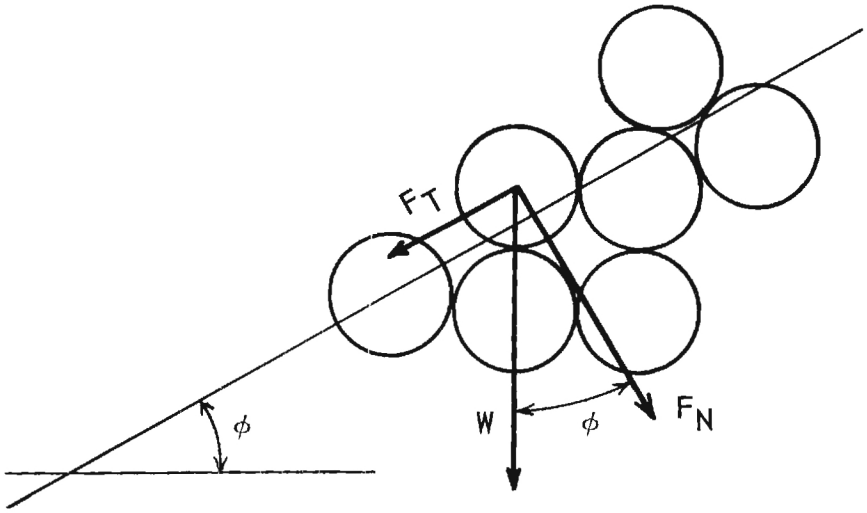


Figure 15. Gravity Forces on Bed Particles.

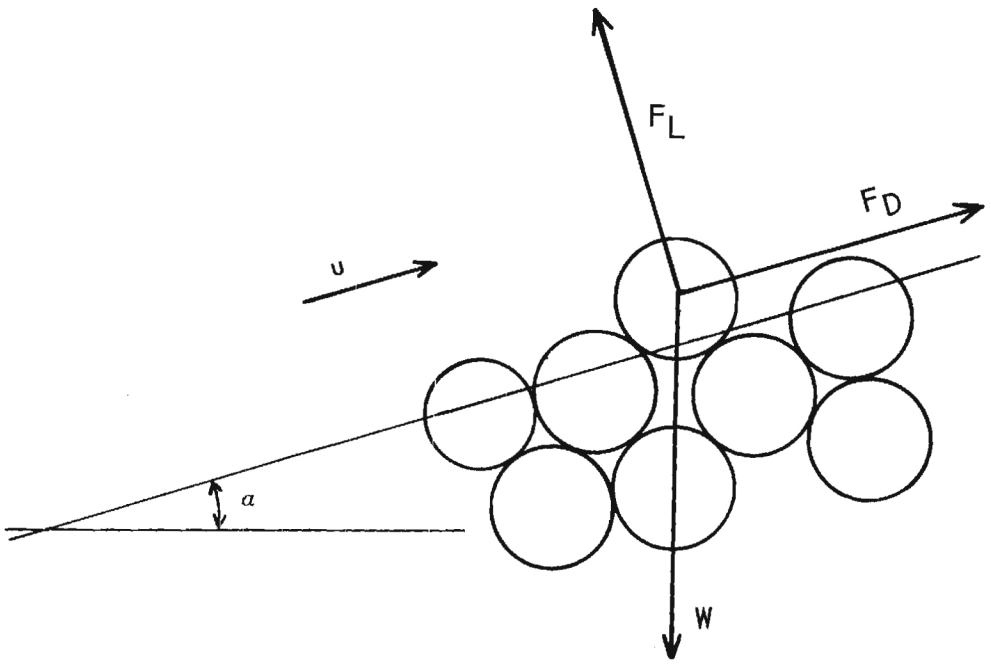


Figure 16. Forces on a Bed Particle.

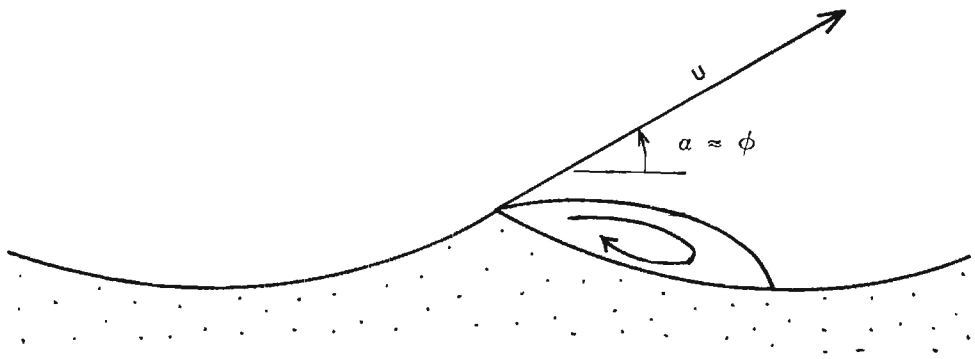


Figure 17. Velocity at the Crest of a Dune in Oscillatory Flow.

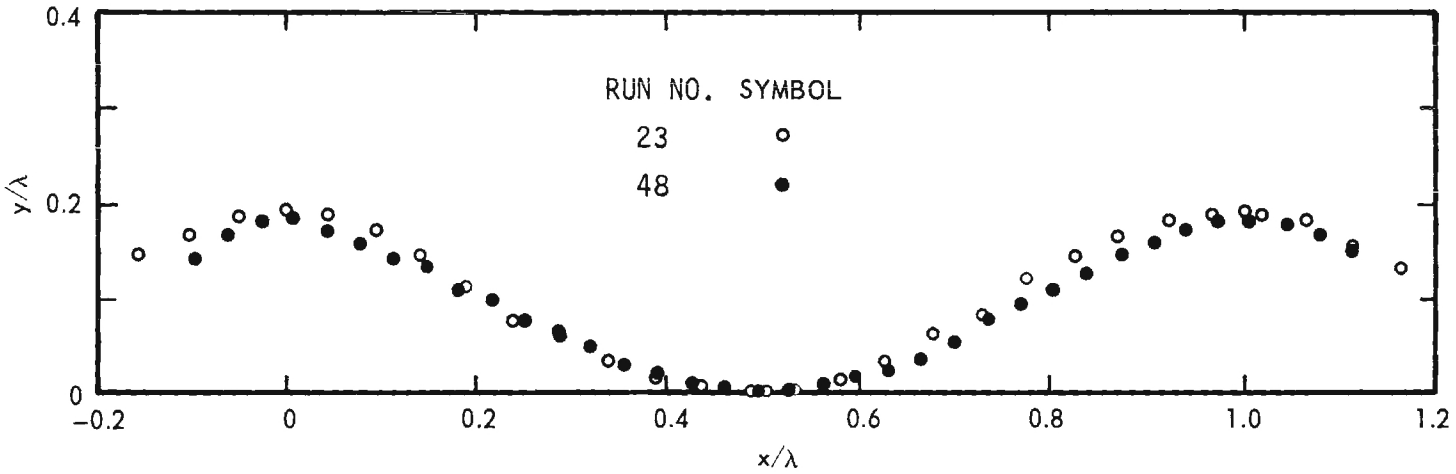


Figure 18. Dune Profiles.

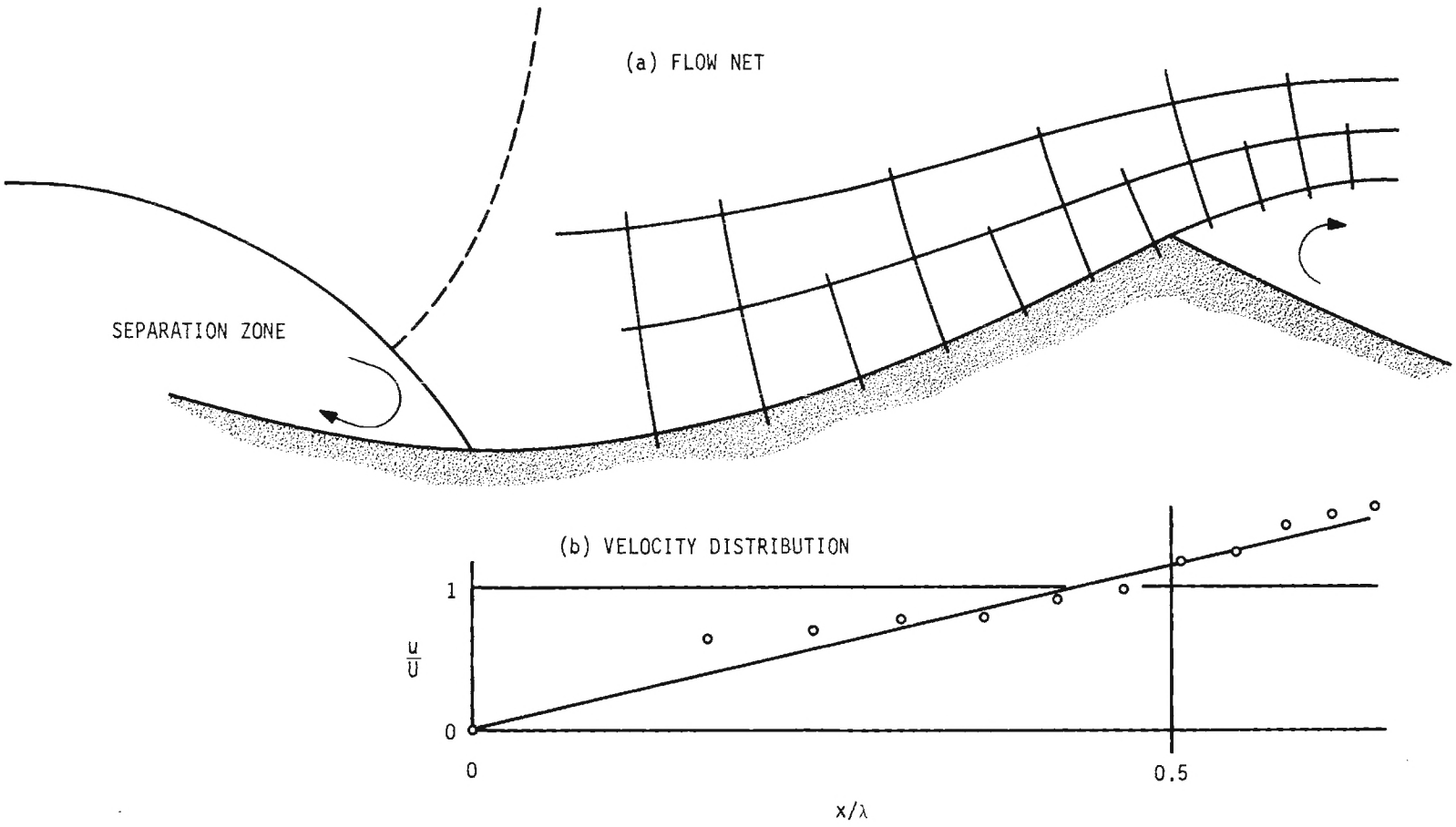


Figure 19. Velocity Distribution along Face of Dune.

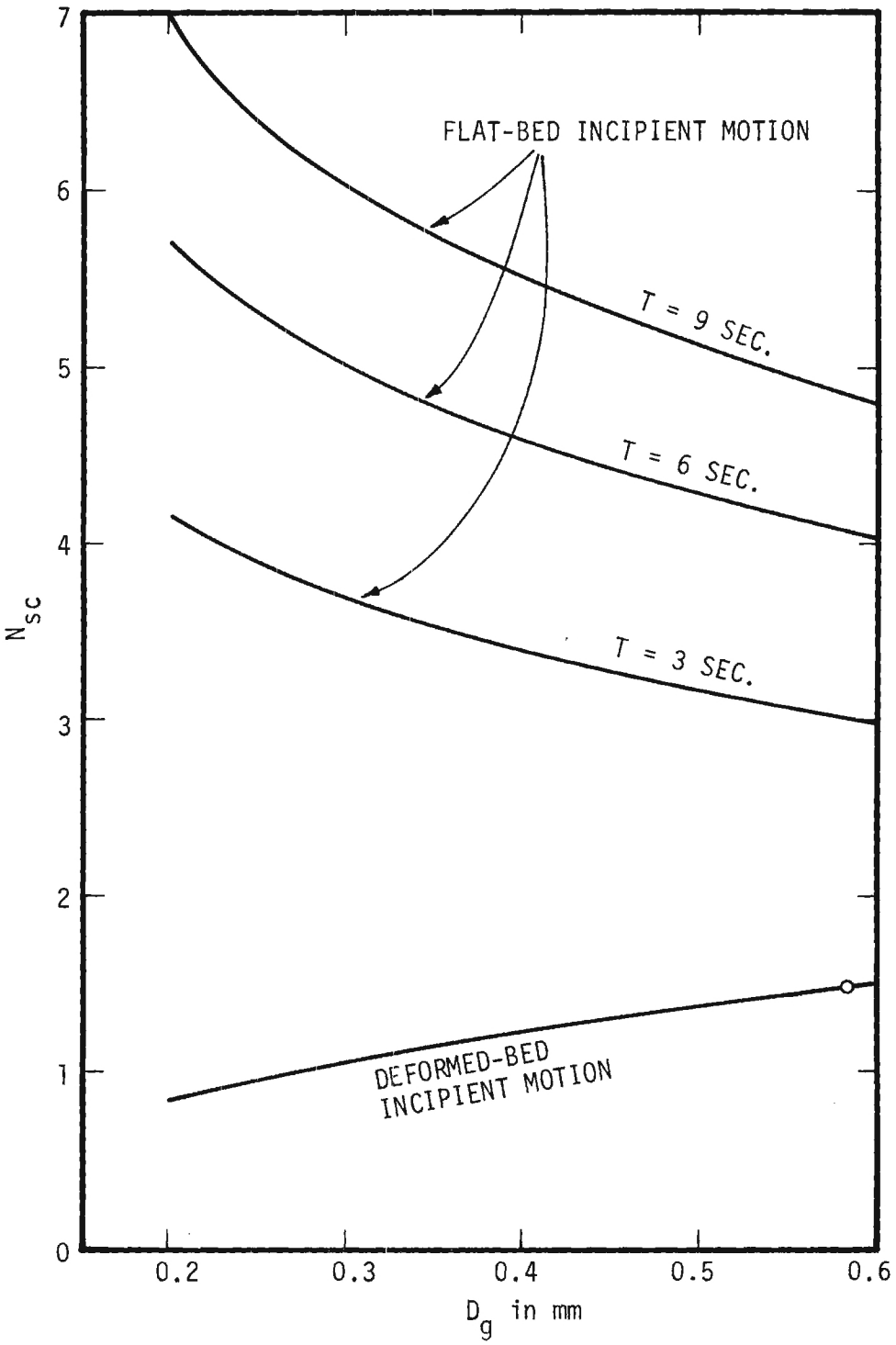


Figure 20. $N_{sc}$ at Incipient Motion for Oscillatory Flow (Water at 60°F, s.f. = 0.7, $\Phi$ = 30°).

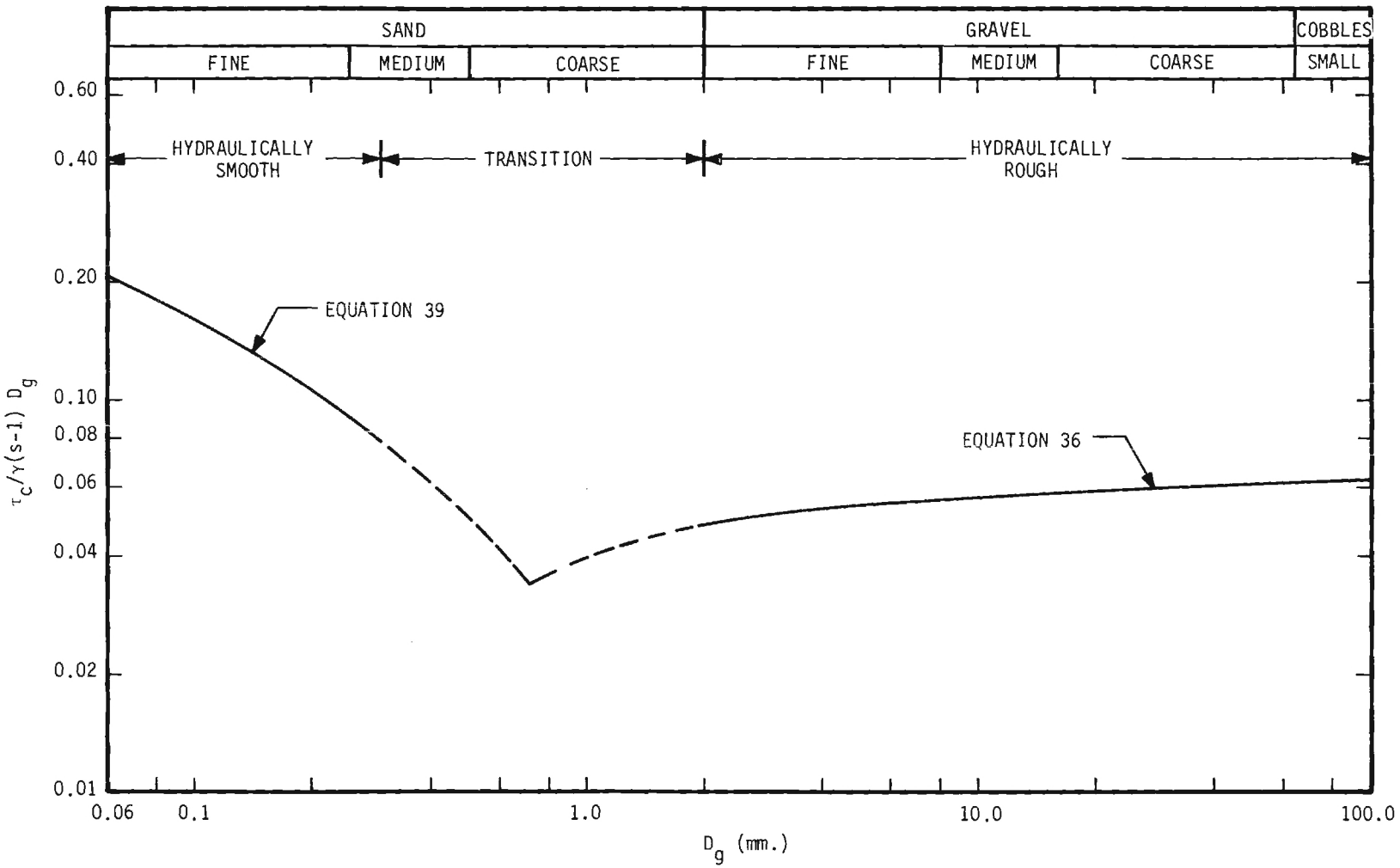


Figure 21. Shields' Parameter Computed from Equation 31 with y = 0.6 $D_g$ for Two-Dimensional, Steady, Uniform, Turbulent Flow.

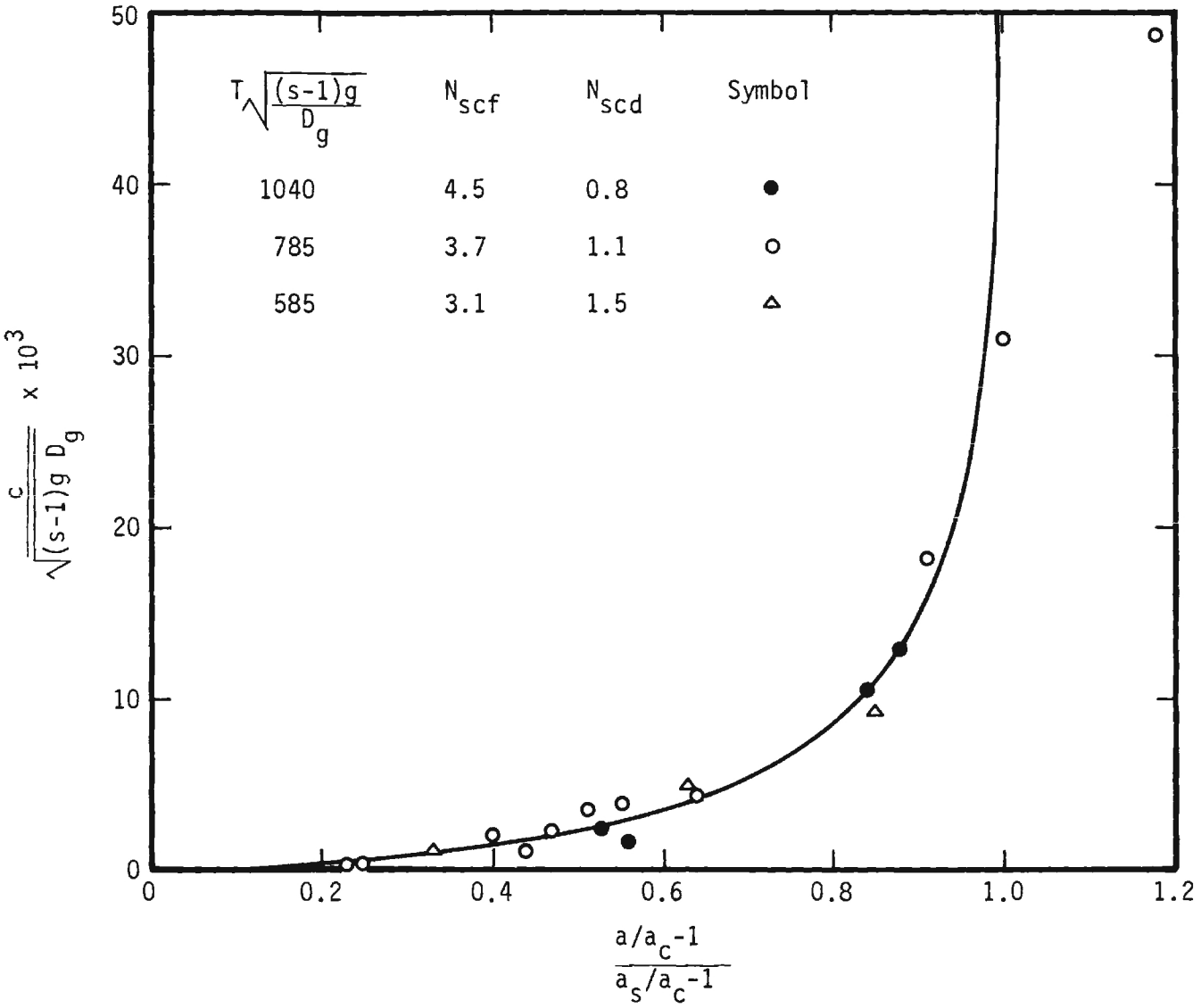


Figure 22. Rate of Propagation of a Dune System.

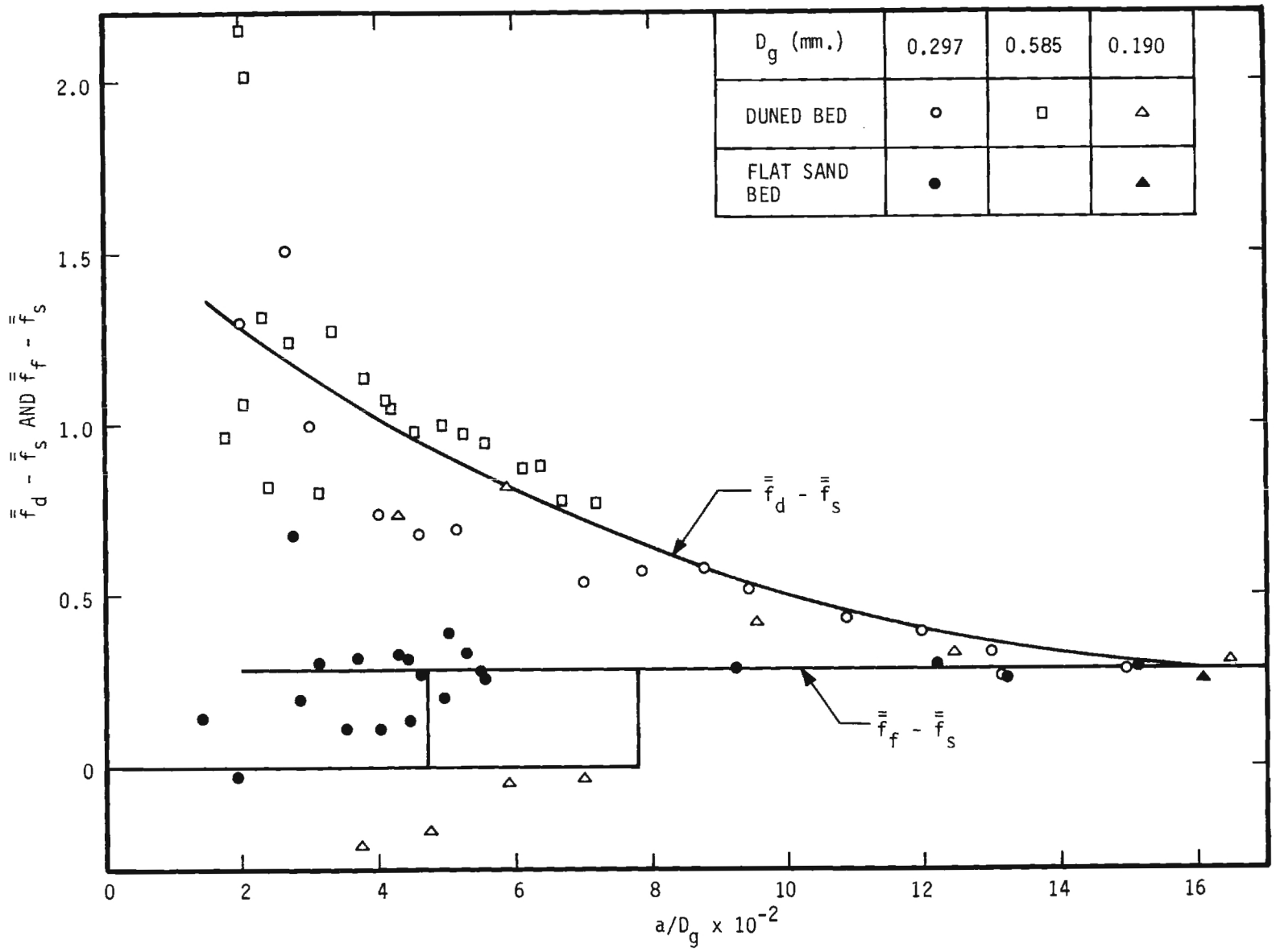


Figure 23. Drag Coefficients.

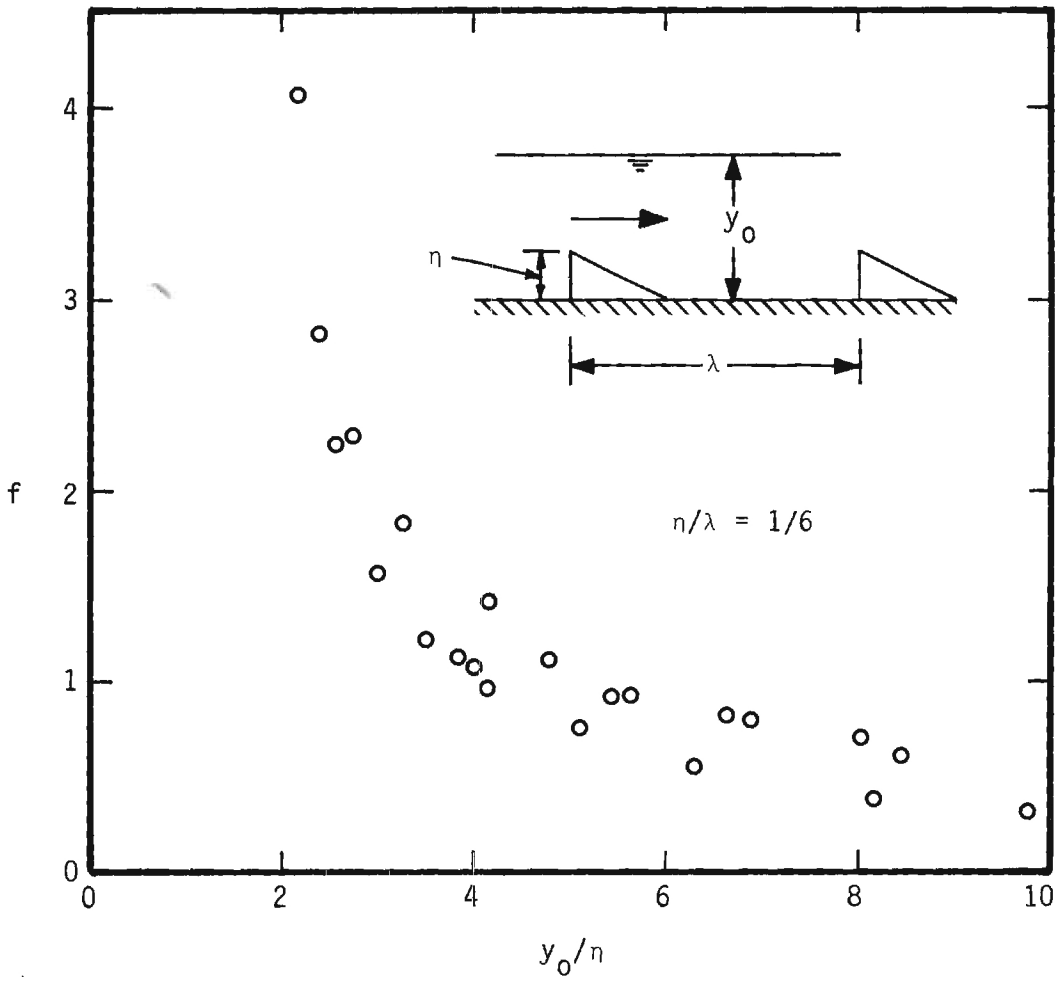


Figure 24. Drag Coefficient of Dune-like Roughness Ridges 20.

# APPENDIX B--TABLES

TABLE I

PROPERTIES OF SANDS

| Sand | Geometric mean diameter, $D_g$ (mm) | Geometric std. deviation, $\sigma_g$ | Specific gravity, s |
|---|---|---|---|
| Ottawa (Banding) | 0.190 | 1.35 | 2.66 |
| Glass Beads | 0.297 | 1.06 | 2.47 |
| Ottawa (Flint Shot) | 0.585 | 1.16 | 2.62 |

TABLE II

BED CONDITIONS AND PURPOSE OF EACH RUN

| Run No. | Period T (Sec) | Amplitude 2a (in) | Water Temp °F | Conditions (See key at the end of TABLE II) | Purpose |
|---|---|---|---|---|---|
| 13 A | 3.565 | 6.21 | 79 | 1, 13, 24 | 53 |
| 13 B | 3.552 | 8.05 | 79 | 1, 13, 24 | 53 |
| 13 C | 3.550 | 11.12 | 79 | 1, 13, 24 | 53 |
| 13 D | 3.549 | 12.97 | 79 | 1, 13, 24 | 53 |
| 13 E | 3.549 | 15.31 | 79 | 1, 13, 24 | 53 |
| 14 A | 3.554 | 5.52 | 80 | 1, 13, 24 | 53 |
| 14 B | 3.562 | 6.28 | 80 | 1, 13, 24 | 53 |
| 14 C | 3.564 | 7.29 | 80 | 1, 13, 24 | 53 |
| 14 D | 3.554 | 8.92 | 80 | 1, 13, 24 | 53 |
| 14 E | 3.557 | 10.61 | 80 | 1, 13, 24 | 53 |
| 15 A | 3.538 | 8.99 | 80 | 1, 13, 24 | 53 |
| 15 B | 3.553 | 10.48 | 80 | 1, 13, 24 | 53 |
| 15 C | 3.557 | 13.28 | 80 | 1, 13, 24 | 53 |
| 15 D | 3.558 | 14.87 | 80 | 1, 13, 24 | 53 |
| 16 A | 3.551 | 12.86 | 79 | 1, 13, 24 | 53 |
| 16 B | 3.553 | 16.32 | 79 | 1, 13, 24 | 53 |
| 16 C | 3.552 | 19.92 | 79 | 1, 13, 24 | 53 |
| 16 D | 3.551 | 24.40 | 79 | 1, 13, 24 | 53 |
| 16 E | 3.548 | 22.72 | 79 | 1, 13, 24 | 53 |
| 16 F | 3.548 | 21.23 | 79 | 1, 13, 24 | 53 |
| 17 A | 3.55 | 12.17 | 80 | 1, 13, 24 | 53 |
| 17 B | 3.553 | 16.34 | 80 | 1, 13, 24 | 53 |
| 17 C | 3.551 | 23.33 | 80 | 1, 13, 24 | 53 |
| 17 D | 3.548 | 26.33 | 80 | 1, 13, 24 | 53 |
| 17 E | 3.540 | 28.78 | 80 | 1, 13, 24 | 53 |
| 18 A | 3.55 | 18.78 | 80.2 | 1, 13, 24 | 53 |
| 18 B | 3.546 | 26.35 | 80.2 | 1, 13, 24 | 53 |
| 18 C | 3.539 | 32.00 | 80.2 | 1, 13, 20 | 53 |
| 18 D | 3.534 | 36.16 | 80.2 | 1, 13, 20 | 53 |
| 19 A | 3.555 | 3.60 | 80.2 | 1, 13, 20 | 53 |
| 19 B | 3.559 | 4.94 | 80.2 | 1, 13, 20 | 53 |
| 19 C | 3.560 | 5.87 | 80.2 | 1, 13, 20 | 53 |
| 20 A | 3.555 | 3.41 | 77 | 1, 11, 20 | 53 |
| 20 B | 3.552 | 4.62 | 77 | 1, 11, 20 | 53 |
| 20 C | 3.555 | 6.71 | 77 | 1, 11, 20 | 53 |
| 20 D | 3.547 | 8.31 | 77 | 1, 11, 20 | 53 |
| 20 E | 3.549 | 9.49 | 77 | 1, 11, 20 | 53 |
| 20 F | 3.548 | 10.51 | 77 | 1, 11, 20 | 53 |

(Continued)

TABLE II (Continued)

BED CONDITIONS AND PURPOSE OF EACH RUN

| Run No. | Period T (Sec) | Amplitude 2a (in) | Water Temp °F | Conditions | Purpose |
|---|---|---|---|---|---|
| 21 | 3.557 | 7.02 | 79 | 2, 11, 21 | 51, 52, 53 |
| 22 | 3.555 | 9.44 | 76 | 2, 11, 21 | 51, 52, 53 |
| 23 | 3.549 | 10.76 | 75 | 2, 11, 21 | 51, 52, 53 |
| 24 | 3.551 | 12.10 | 77 | 2, 11, 21 | 51, 52, 53 |
| 25 | 3.552 | 16.42 | 73 | 2, 11, 21 | 51, 53 |
| 26 | 3.551 | 18.42 | 73 | 2, 11, 21 | 51, 53 |
| 27 | 3.528 | 20.56 | 73 | 2, 11, 21 | 51, 53 |
| 28 | 3.510 | 21.67 | 69.5 | 1, 11, 20 | 53 |
| 29 A | 3.537 | 26.25 | 72.5 | 1, 11, 20 | 53 |
| 29 B | 3.544 | 25.50 | 73 | 2, 11, 20 | 51, 53 |
| 30 A | 3.525 | 28.56 | 72 | 1, 11, 20 | 53 |
| 30 B | 3.522 | 28.03 | 72 | 2, 11, 20 | 51, 53 |
| 31 A | 3.517 | 35.41 | 72 | 1, 11, 20 | 53 |
| 31 B | 3.521 | 35.04 | 72 | 2, 11, 20 | 51, 53 |
| 32 A | 3.551 | 30.90 | 71.5 | 1, 11, 20 | 53 |
| 32 B | 3.534 | 30.75 | 71.5 | 2, 11, 20 | 51, 53 |
| 33 | 3.544 | 12.90 | 73.5 | 1, 11, 20 | 53 |
| 34 A | 3.555 | 11.79 | 73.5 | 1, 11, 20 | 53 |
| 34 B | 3.554 | 12.41 | 73.5 | 1, 11, 20 | 53 |
| 34 C | 3.546 | 12.90 | 73.5 | 1, 11, 20 | 53 |
| 35 | 3.550 | 15.23 | 73.5 | 1, 11, 20 | 53 |
| 36 | 3.553 | 22.11 | 73 | 2, 11, 20 | 51, 53 |
| 37 | 3.552 | 7.42 | 68.5 | 1, 11, 20 | 53, 54 |
| 38 | 3.546 | 8.67 | 69 | 1, 11, 24 | 53, 54 |
| 39 | 3.548 | 10.10 | 69 | 1, 11, 24 | 53, 54, 55 |
| 40 | 3.540 | 10.44 | 69 | 1, 11, 24 | 53, 54 |
| 41 | 3.545 | 10.85 | 69 | 1, 11, 24 | 53, 54 |
| 42 | 3.55 | 11.18 | 69 | 1, 11, 24 | 55, 55 |
| 43 | 3.55 | 11.50 | 69 | 1, 11, 24 | 55, 55 |
| 44 | 3.55 | 11.59 | 69 | 1, 11, 24 | 55 |
| 45 | 3.550 | 11.62 | 67 | 1, 11, 24 | 53, 54, 55 |
| 46 | 3.550 | 11.11 | 67 | 1, 11, 24 | 53, 54, 55 |
| 47 | 3.55 | 10.90 | 63.5 | 2, 11, 21 | 51, 53, 56 |
| 48 | 3.55 | 4.70 | 64.1 | 2, 11, 21 | 51, 52 |
| 49 | 3.560 | 4.70 | 70 | 2, 11, 22 | 51, 52, 53 |
| 50 | 3.550 | 30.37 | 65 | 2, 11, 24 | 51, 53 |

(Continued)

TABLE II (Continued)

BED CONDITIONS AND PURPOSE OF EACH RUN

| Run No. | Period T (sec) | Amplitude 2a (in) | Water Temperature (°F) | Conditions | Purpose |
|---|---|---|---|---|---|
| 51 | 3.579 | 6.30 | 75 | 2, 11, 21 | 51, 52, 53 |
| 52 | 3.434 | 6.80 | 75 | 2, 11, 21 | 51, 52, 53 |
| 53 | 3.309 | 5.79 | 74 | 2, 11, 21 | 51, 52, 53 |
| 54 | 3.681 | 7.50 | 73 | 2, 11, 21 | 51, 52, 53 |
| 55 | 3.790 | 6.11 | 75.5 | 2, 11, 21 | 51, 52, 53 |
| 56 | 3.295 | 6.52 | 76 | 1, 11, 24 | 53 |
| 57 | 3.430 | 6.52 | 76 | 1, 11, 24 | 53 |
| 58 | 3.594 | 6.50 | 76 | 1, 11, 24 | 53 |
| 59 | 3.655 | 6.53 | 75 | 1, 11, 24 | 53 |
| 60 | 3.764 | 6.55 | 75 | 1, 11, 24 | 53 |
| 61 | ~3.56 | 6.5 | 77 | 2, 11, 21 | 52 |
| 62 | 3.55 | 6.40 | 81 | 2, 11, 21 | 52, 55 |
| 63 | 3.568 | 7.96 | 78.5 | 2, 12, 21 | 51, 52, 53 |
| 64 | 3.552 | 9.46 | 78 | 2, 12, 21 | 51, 52, 53 |
| 65 A | 3.543 | 10.84 | 76 | 2, 12, 21 | 51, 52, 53 |
| 65 B | 3.531 | 11.12 | 76.5 | 2, 12, 21 | 53 |
| 66 | 3.554 | 12.65 | 75 | 2, 12, 21 | 51, 52, 53 |
| 67 | 3.540 | 14.60 | 77 | 2, 12, 21 | 51, 53 |
| 68 | 3.568 | 15.47 | 76 | 2, 12, 21 | 51, 53 |
| 69 | 3.556 | 17.60 | 77 | 2, 12, 21 | 51, 53 |
| 70 | 3.543 | 19.05 | 77 | 2, 12, 24 | 51, 53 |
| 71 | 3.530 | 19.50 | 77 | 2, 12, 24 | 51, 53 |
| 72 | 3.532 | 20.98 | 72 | 2, 12, 24 | 51, 53 |
| 73 | 3.547 | 22.90 | 73 | 2, 12, 24 | 51, 53 |
| 74 | 3.560 | 24.25 | 73 | 2, 12, 24 | 51, 53 |
| 75 | 3.554 | 25.73 | 73 | 2, 12, 24 | 51, 53 |
| 76 | 3.531 | 27.70 | 73 | 2, 12, 24 | 51, 53 |
| 77 | 3.545 | 29.47 | 73 | 2, 12, 24 | 51, 53 |
| 78 | 3.474 | 30.88 | 73 | 2, 12, 24 | 51, 53 |
| 79 | 3.555 | 33.35 | 74 | 2, 12, 24 | 51, 53 |
| 80 A | 3.540 | 9.80 | 73 | 2, 12, 24 | 51, 53 |
| 80 B | 3.580 | 9.65 | 73 | 2, 12, 24 | 53 |
| 81 | ~3.56 | 13.60 | 72 | 2, 12, 24 | 51 |
| 82 | ~3.56 | 14.8-15.2 | | 2, 12, 24 | 52 |

(Continued)

TABLE II (Continued)

BED CONDITIONS AND PURPOSE OF EACH RUN

| Run No. | Period T (sec) | Amplitude 2a (in) | Water Temperature ($^{o}$F) | Conditions | Purpose |
|---|---|---|---|---|---|
| 83 A | ~3.56 | 4.90 | 69.5 | 1, 10, 24 | 55 |
| 83 B | ~3.56 | 5.00 | 69.5 | 1, 10, 24 | 55 |
| 83 C | ~3.56 | 6.70 | 69.5 | 1, 10, 24 | 55 |
| 83 D | ~3.56 | 8.15 | 69.5 | 1, 10, 24 | 55 |
| 83 E | ~3.56 | 9.85 | 69.5 | 1, 10, 24 | 55 |
| 83 F | ~3.56 | 11.55 | 69.5 | 1, 10, 24 | 55 |
| 83 G | ~3.56 | 11.78 | 69.5 | 1, 10, 24 | 55 |
| 83 H | ~3.56 | 12.33 | 69.5 | 1, 10, 24 | 55 |
| 83 I | ~3.56 | 12.65 | 69.5 | 1, 10, 24 | 55 |
| 85 | 3.611 | 7.09 | 63 | 2, 10, 21 | 52, 58 |
| 86 | 3.598 | 6.86 | 68.5 | 2, 10, 21 | 57 |
| 88 | 3.590 | 4.03 | 64 | 1, 10, 24 | 57 |
| 89 | 3.590 | 5.48 | 64 | 1, 10, 24 | 57 |
| 90 | 3.591 | 7.69 | 63.5 | 1, 10, 24 | 57 |
| 91 | 3.605 | 9.66 | 63.5 | 1, 10, 24 | 57 |
| 93 | 3.596 | 6.35 | 68.4 | 1, 10, 24 | 57 |
| 95 | 3.576 | 10.24 | 69 | 1, 10, 24 | 57 |
| 96 A | 3.584 | 9.35 | 77.5 | 2, 10, 21 | 52, 58 |
| 96 B | 3.585 | 9.79 | 77.7 | 2, 10, 21 | 57 |
| 106 A | 3.542 | 14.30 | 79.2 | 2, 10, 24 | 53, 58 |
| 106 B | 3.545 | 14.28 | 79.5 | 2, 10, 24 | 57 |
| 107 | 3.546 | 5.62 | 75.7 | 1, 10, 24 | 53 |
| 108 | 3.544 | 7.12 | 76 | 1, 10, 24 | 53 |
| 109 | 3.539 | 8.84 | 76.1 | 1, 10, 24 | 53 |
| 110 | 3.530 | 10.64 | 76 | 1, 10, 24 | 53 |
| 111 A | 3.533 | 18.66 | 76.7 | 2, 10, 24 | 53, 58 |
| 111 B | 3.534 | 18.62 | 76.7 | 2, 10, 24 | 57 |
| 112 A | 3.536 | 24.1 | 75 | 1, 10, 24 | 53 |
| 112 B | 3.533 | 24.67 | 75 | 2, 10, 24 | 53, 58 |
| 112 C | 3.531 | 24.15 | 75 | 2, 10, 24 | 57 |
| 113 A | 3.542 | 8.84 | 75 | 2, 10, 21 | 52, 53 |
| 113 B | 3.544 | 8.80 | 75 | 2, 10, 21 | 57 |
| 114 A | 3.551 | 6.44 | 76 | 2, 10, 21 | 51, 52, 53 |
| 114 B | 3.551 | 6.41 | 76 | 2, 10 21 | 57 |

(Continued)

TABLE II (Concluded)

BED CONDITIONS AND PURPOSE OF EACH RUN

Key to symbols

1 - flat bed

2 - duned bed

10 - bed particles, 0.190 mm - diameter Ottawa sand

11 - bed particles, 0.297 mm - diameter glass beads

12 - bed particles, 0.585 mm - diameter Ottawa sand

13 - smooth flat immobile bed, aluminum sheet

21 - $\frac{1}{2}$-in diameter, half-round, disturbance element

22 - 1-in diameter, half-round, disturbance element

23 - $1\frac{1}{2}$-in diameter, half-round, disturbance element

24 - no disturbance element

51 - dune geometry (photographs)

52 - evolution of dunes

53 - work input into tunnel

54 - boundary-layer transition

55 - incipient motion

56 - motion pictures

57 - energy dissipation within test section

58 - dune geometry (maps)

TABLE III

RESULTS OF SPECIAL STUDIES

| Occurrence | $D_g$ (mm) | Period T (sec) | Water Temperature (°C) | Amplitude a (cm) |
|---|---|---|---|---|
| Beginning of boundary-layer transition | 0.297 | 3.56 | 21.0 | 11.0 |
| | smooth | 3.58 | 22.4 | 14.7 |
| Fully turbulent boundary layer | smooth | 3.63 | 22.4 | 23.8 |
| Flat-bed incipient motion | 0.190 | 3.57 | 20.8 | 14.8 |
| | 0.297 | 3.56 | 19.4 | 14.0 |
| | 0.585 | 3.58 | 22.2 | 16.6 |
| Deformed-bed incipient motion | 0.585 | 3.55 | 27.2 | 8.13 |
| Spontaneous appearance of ripples | 0.190 | 3.57 | 20.8 | 15.0 |
| | 0.297 | 3.55 | 22.8 | 18.3 |
| | 0.585 | 3.55 | 23.9 | 18.8 |

TABLE IV

WORK INPUT WITH SMOOTH FLAT IMMOBILE BED

| Run No. | Work Input $\left(\frac{\text{ft-lb}}{\text{cycle}}\right)$ | Energy Increase $\left(\frac{\text{ft - lb}}{\text{cycle}}\right)$ | Energy Dissipation $\left(\frac{\text{ft - lb}}{\text{cycle}}\right)$ |
|---|---|---|---|
| 13 A | 1.85 | 0 | 1.85 |
| 13 B | 2.81 | 0 | 2.81 |
| 13 C | 4.20 | 0 | 4.20 |
| 13 D | 5.90 | 0 | 5.90 |
| 13 E | 7.44 | 0 | 7.44 |
| 14 A | 1.63 | 0 | 1.63 |
| 14 B | 2.23 | 0 | 2.23 |
| 14 C | 2.83 | 0 | 2.83 |
| 14 D | 3.41 | 0 | 3.41 |
| 14 E | 4.39 | 0 | 4.39 |
| 15 A | 4.40 | 0 | 4.40 |
| 15 B | 5.59 | 0 | 5.59 |
| 15 C | 7.41 | 0 | 7.41 |
| 15 D | 8.74 | 0 | 8.74 |
| 16 A | 7.96 | 0 | 7.96 |
| 16 B | 9.72 | 0 | 9.72 |
| 16 C | 13.4 | 0 | 13.4 |
| 16 E | 14.5 | 0 | 14.5 |
| 16 F | 13.5 | 0 | 13.5 |
| 17 A | 5.66 | 0 | 5.66 |
| 17 B | 8.69 | 0 | 8.69 |
| 17 C | 14.8 | 0 | 14.8 |
| 17 D | 20.8 | 0 | 20.8 |
| 17 E | 27.5 | 0 | 27.5 |
| 18 A | 13.2 | 0 | 13.2 |
| 18 B | 23.1 | 0 | 23.1 |
| 18 C | 35.0 | 0 | 35.0 |
| 18 D | 49.0 | 0 | 49.0 |
| 19 A | 0.639 | 0 | 0.639 |
| 19 B | 0.870 | 0 | 0.870 |
| 19 C | 1.40 | 0 | 1.40 |

TABLE V

DUNE GEOMETRY (FINE SAND)

| Run No. | No. of Observations | $\frac{\eta}{D_g}$ | $\frac{\lambda}{D_g}$ | $\frac{\eta}{\lambda}$ | $\frac{a}{D_g}$ | $\frac{U_m}{\sqrt{(s-1)gD_g}}$ | $T\sqrt{\frac{(s-1)g}{D_g}}$ |
|---|---|---|---|---|---|---|---|
| 85 | 16 | 110 | 610 | .181 | 474 | 2.82 | 1056 |
| 96 A | 12 | 129 | 799 | .161 | 625 | 3.74 | 1048 |
| 106 A | 23 | 77 | 573 | .134 | 956 | 5.79 | 1036 |
| 111 A | 22 | 70 | 556 | .125 | 1247 | 7.58 | 1033 |
| 112 B | 14 | 25 | 528 | .048 | 1649 | 10.02 | 1033 |
| 114 A | 18 | 109 | 548 | .199 | 430 | 2.60 | 1039 |

TABLE VI

DUNE GEOMETRY (MEDIUM SAND)

| Run No. | No. of Observations | $\frac{\eta}{D_g}$ | $\frac{\lambda}{D_g}$ | $\frac{\eta}{\lambda}$ | $\frac{a}{D_g}$ | $\frac{U_m}{\sqrt{(s-1)gD_g}}$ | $T\sqrt{\frac{(s-1)g}{D_g}}$ |
|---|---|---|---|---|---|---|---|
| 21 | 7 | 61.2 | 358 | 0.171 | 304 | 2.43 | 785 |
| 22 | 9 | 74.7 | 428 | 0.175 | 403 | 3.23 | 785 |
| 23 | 8 | 85.8 | 489 | 0.176 | 463 | 3.72 | 782 |
| 24 | 12 | 87.1 | 487 | 0.179 | 513 | 4.12 | 782 |
| 25 | 4 | 110.8 | 653 | 0.170 | 702 | 5.64 | 782 |
| 26 | 4 | 120.4 | 745 | 0.162 | 787 | 6.32 | 782 |
| 27 | 4 | 108.9 | 825 | 0.132 | 878 | 7.09 | 778 |
| 29 B | 5 | 104.5 | 910 | 0.115 | 1075 | 8.66 | 780 |
| 30 B | 5 | 72.0 | 677 | 0.106 | 1191 | 9.64 | 776 |
| 31 B | 4 | 16.4 | 643 | 0.026 | 1501 | 12.16 | 776 |
| 32 B | 2 | 48.2 | 740 | 0.065 | 1304 | 10.53 | 782 |
| 36 | 5 | 108.2 | 825 | 0.131 | 942 | 7.57 | 782 |
| 51 | 5 | 64.0 | 349 | 0.183 | 269 | 2.15 | 789 |
| 52 | 4 | 57.5 | 367 | 0.157 | 291 | 2.42 | 756 |
| 53 | 5 | 52.1 | 297 | 0.176 | 248 | 2.13 | 730 |
| 54 | 6 | 69.6 | 398 | 0.175 | 321 | 2.48 | 811 |
| 55 | 6 | 59.8 | 352 | 0.170 | 261 | 1.97 | 835 |

TABLE VII

DUNE GEOMETRY (COARSE SAND)

| Run No. | No. of Observations | $\frac{\eta}{D_g}$ | $\frac{\lambda}{D_g}$ | $\frac{\eta}{\lambda}$ | $\frac{a}{D_g}$ | $\frac{U_m}{\sqrt{(s-1)gD_g}}$ | $T\sqrt{\frac{(s-1)g}{D_g}}$ |
|---|---|---|---|---|---|---|---|
| 62 | 4 | 38.2 | 202 | 0.189 | 139 | 1.49 | 585 |
| 63 | 4 | 47.6 | 250 | 0.191 | 173 | 1.85 | 588 |
| 64 | 4 | 55.7 | 285 | 0.195 | 205 | 2.20 | 586 |
| 65 A | 4 | 57.4 | 309 | 0.186 | 235 | 2.53 | 584 |
| 66 | 2 | 67.3 | 348 | 0.193 | 275 | 2.94 | 586 |
| 67 | 2 | 77.6 | 408 | 0.190 | 317 | 3.41 | 584 |
| 68 | 2 | 88.7 | 430 | 0.206 | 336 | 3.59 | 588 |
| 69 | 4 | 99.3 | 496 | 0.200 | 382 | 4.09 | 586 |
| 70 | 5 | 81.4 | 440 | 0.185 | 414 | 4.45 | 584 |
| 71 | 4 | 83.4 | 451 | 0.185 | 423 | 4.57 | 582 |
| 72 | 4 | 95.7 | 512 | 0.187 | 455 | 4.91 | 582 |
| 73 | 5 | 85.9 | 448 | 0.192 | 497 | 5.34 | 585 |
| 74 | 5 | 102.0 | 519 | 0.197 | 526 | 5.64 | 587 |
| 75 | 2 | 100.5 | 669 | 0.150 | 559 | 5.99 | 586 |
| 76 | 2 | 116.8 | 646 | 0.181 | 601 | 6.49 | 582 |
| 77 | 3 | 105.6 | 611 | 0.173 | 640 | 6.88 | 584 |
| 78 | 3 | 117.4 | 792 | 0.148 | 670 | 7.35 | 573 |
| 79 | 2 | 118.4 | 754 | 0.157 | 724 | 7.76 | 586 |
| 80 A | 4 | 53.5 | 297 | 0.180 | 211 | 2.26 | 587 |

TABLE VIII

WORK INPUT WITH A FLAT SAND BED

| Run No. | Work Input $\left(\frac{\text{ft-lb}}{\text{cycle}}\right)$ | Energy Increase $\left(\frac{\text{ft - lb}}{\text{cycle}}\right)$ | Energy Dissipation $\left(\frac{\text{ft - lb}}{\text{cycle}}\right)$ |
|---|---|---|---|
| 20 A | 0.720 | 0 | 0.720 |
| 20 B | 1.15 | 0 | 1.15 |
| 20 C | 2.37 | 0 | 2.37 |
| 20 D | 3.33 | 0 | 3.33 |
| 20 E | 4.23 | 0 | 4.23 |
| 20 F | 5.22 | 0 | 5.22 |
| 28 | 26.4 | 0 | 26.4 |
| 30 A | 52.7 | 0 | 52.7 |
| 31 A | 93.9 | 0 | 93.9 |
| 32 A | 60.9 | 0 | 60.9 |
| 33 | 7.24 | -1.30 | 8.54 |
| 34 A | 9.55 | 1.71 | 7.84 |
| 34 B | 9.61 | 1.29 | 8.32 |
| 34 C | 9.05 | 0.90 | 8.15 |
| 37 | 2.99 | 0 | 2.99 |
| 38 | 4.07 | 0 | 4.07 |
| 39 | 5.31 | 0 | 5.31 |
| 40 | 5.77 | 0 | 5.77 |
| 41 | 6.05 | 0 | 6.05 |
| 45 | 6.55 | 0 | 6.55 |
| 58 | 2.68 | 0 | 2.68 |
| 107 | 1.46 | 0 | 1.46 |
| 108 | 2.17 | 0 | 2.17 |
| 109 | 3.33 | 0 | 3.33 |
| 110 | 4.60 | 0.05 | 4.55 |
| 112 A | 34.7 | 2.6 | 32.1 |

TABLE IX

WORK INPUT WITH A DUNED SAND BED

| Run No. | Work Input $\left(\frac{\text{ft-lb}}{\text{cycle}}\right)$ | Energy Increase $\left(\frac{\text{ft - lb}}{\text{cycle}}\right)$ | Energy Dissipation $\left(\frac{\text{ft - lb}}{\text{cycle}}\right)$ |
|---|---|---|---|
| 21 | 3.53 | 0 | 3.53 |
| 22 | 5.99 | 0 | 5.99 |
| 23 | 7.80 | 0 | 7.80 |
| 24 | 10.1 | 0 | 10.1 |
| 25 | 18.0 | 0 | 18.0 |
| 26 | 24.9 | 0 | 24.9 |
| 27 | 32.7 | 0 | 32.7 |
| 29B | 45.5 | -0.8 | 46.3 |
| 30B | 57.7 | -1.0 | 58.7 |
| 31B | 89.4 | 0 | 89.4 |
| 32B | 59.6 | 0 | 59.6 |
| 36 | 35.7 | 0 | 35.7 |
| 49 | 1.63 | 0 | 1.63 |
| 50 | 65.4 | 0 | 65.4 |
| 51 | 3.17 | 0 | 3.17 |
| 63 | 4.56 | 0 | 4.56 |
| 64 | 7.06 | 0 | 7.06 |
| 65A | 10.8 | 0 | 10.8 |
| 65B | 9.12 | 0 | 9.12 |
| 66 | 15.1 | 0 | 15.1 |
| 67 | 16.8 | 0 | 16.8 |
| 68 | 25.2 | 0 | 25.2 |
| 69 | 32.8 | 0 | 32.8 |
| 70 | 38.8 | -0.1 | 38.9 |
| 71 | 40.7 | 0 | 40.7 |
| 72 | 47.1 | -0.1 | 47.2 |
| 73 | 59.4 | -0.2 | 59.6 |
| 74 | 68.9 | -0.1 | 69.0 |
| 75 | 78.0 | -0.4 | 78.4 |
| 76 | 91.8 | 0 | 91.8 |
| 77 | 109 | 0 | 109 |
| 78 | 118 | 0 | 118 |
| 79 | 141 | - | 141 |
| 80A | 10.8 | 0 | 10.8 |
| 80B | 10.9 | 0 | 10.9 |
| 106A | 12.1 | 0.1 | 12.0 |
| 111A | 19.8 | -0.1 | 19.9 |
| 112B | 36.2 | -0.2 | 36.4 |
| 113A | 5.41 | 0 | 5.41 |
| 114A | 2.71 | 0 | 2.71 |

TABLE X

ENERGY DISSIPATION WITHIN THE TEST SECTION

| Run No. | Pressure Work $\left(\frac{\text{ft-lb}}{\text{cycle}}\right)$ | Kinetic Energy increase $\left(\frac{\text{ft-lb}}{\text{cycle}}\right)$ | Energy dissipation $\left(\frac{\text{ft-lb}}{\text{cycle}}\right)$ |
|---|---|---|---|
| 86 | 1.26 | 0 | 1.26 |
| 88 | 0.080 | 0 | 0.08 |
| 89 | 0.48 | 0 | 0.48 |
| 90 | 0.88 | 0 | 0.88 |
| 91 | 1.39 | 0 | 1.39 |
| 93 | 0.77 | 0 | 0.77 |
| 95 | 2.05 | 0 | 2.05 |
| 96B | 3.82 | 0 | 3.82 |
| 106B | 1.00 | 0 | 1.00 |
| 111B | 2.62 | 0 | 2.62 |
| 112C | 2.22 | +0.17 | 2.05 |
| 113B | 0.69 | +0.02 | 0.67 |
| 114B | 0.25 | 0 | 0.25 |

TABLE XI

ADDED ENERGY DISSIPATION
FLAT SAND BED

| Run No. | Energy dissipation in tunnel: Flat sand $\left(\frac{\text{ft-lb}}{\text{cycle}}\right)$ | Energy dissipation in tunnel: Smooth immobile $\left(\frac{\text{ft-lb}}{\text{cycle}}\right)$ | Added energy dissipation $\left(\frac{\text{ft-lb}}{\text{cycle}}\right)$ | $\bar{f}_f - \bar{f}_s$ |
|---|---|---|---|---|
| 20A | 0.72 | 0.70 | 0.02 | 0.142 |
| 20B | 1.15 | 1.16 | -0.01 | -0.029 |
| 20C | 2.37 | 2.16 | 0.21 | 0.199 |
| 20D | 3.33 | 3.12 | 0.21 | 0.105 |
| 20E | 4.23 | 3.90 | 0.33 | 0.109 |
| 20F | 5.22 | 4.65 | 0.57 | 0.139 |
| 28 | 26.4 | 16.0 | 10.4 | 0.285 |
| 30A | 52.7 | 28.0 | 24.7 | 0.299 |
| 31A | 93.9 | 48.0 | 45.9 | 0.291 |
| 32A | 60.9 | 34.0 | 26.9 | 0.260 |
| 33 | 8.54 | 6.60 | 1.94 | 0.256 |
| 34A | 7.84 | 5.60 | 2.24 | 0.388 |
| 34B | 8.32 | 6.10 | 2.22 | 0.331 |
| 34C | 8.15 | 6.10 | 2.05 | 0.272 |
| 37 | 2.99 | 2.55 | 0.44 | 0.306 |
| 38 | 4.07 | 3.35 | 0.72 | 0.315 |
| 39 | 5.31 | 4.13 | 1.18 | 0.327 |
| 40 | 5.77 | 4.62 | 1.15 | 0.314 |
| 41 | 6.05 | 4.85 | 1.20 | 0.267 |
| 45 | 6.55 | 5.45 | 1.10 | 0.199 |
| 58 | 2.68 | 2.04 | 0.64 | 0.678 |
| 107 | 1.46 | 1.60 | -0.14 | -0.225 |
| 108 | 2.17 | 2.40 | -0.23 | -0.181 |
| 109 | 3.33 | 3.45 | -0.12 | -0.049 |
| 110 | 4.55 | 4.70 | -0.15 | -0.037 |
| 112A | 32.1 | 19.3 | 12.8 | +0.256 |

TABLE XII

ADDED ENERGY DISSIPATION
DUNED SAND BED

| Run No. | Energy dissipation in tunnel: Duned $\left(\frac{\text{ft-lb}}{\text{cycle}}\right)$ | Energy dissipation in tunnel: Smooth immobile $\left(\frac{\text{ft-lb}}{\text{cycle}}\right)$ | Added energy dissipation $\left(\frac{\text{ft-lb}}{\text{cycle}}\right)$ | $\bar{f}_d - \bar{f}_s$ |
|---|---|---|---|---|
| 21 | 3.53 | 2.33 | 1.20 | .992 |
| 22 | 5.99 | 3.82 | 2.17 | .738 |
| 23 | 7.80 | 4.85 | 2.95 | .675 |
| 24 | 10.1 | 5.83 | 4.3 | .692 |
| 25 | 18.0 | 9.8 | 8.2 | .534 |
| 26 | 24.9 | 12.1 | 12.7 | .572 |
| 27 | 32.7 | 14.6 | 18.1 | .579 |
| 29B | 46.3 | 21.2 | 25.1 | .427 |
| 30B | 58.7 | 27.8 | 30.9 | .392 |
| 31B | 89.4 | 46.3 | 43.1 | .280 |
| 32B | 59.6 | 33.0 | 26.6 | .258 |
| 36 | 35.7 | 16.6 | 19.1 | .514 |
| 49 | 1.63 | 1.17 | 0.46 | 1.294 |
| 50 | 65.4 | 32.4 | 33.0 | .333 |
| 51 | 3.17 | 1.90 | 1.27 | 1.501 |
| 63 | 4.56 | 2.88 | 1.68 | .963 |
| 64 | 7.06 | 3.90 | 3.16 | 1.061 |
| 65A | 10.8 | 4.9 | 5.9 | 1.316 |
| 65B | 9.12 | 5.15 | 3.97 | .802 |
| 66 | 15.1 | 6.3 | 8.8 | 1.241 |
| 67 | 16.8 | 8.0 | 8.8 | .801 |
| 68 | 25.2 | 8.9 | 16.3 | 1.271 |
| 69 | 32.8 | 11.1 | 21.7 | 1.139 |
| 70 | 38.9 | 12.8 | 26.1 | 1.070 |
| 71 | 40.7 | 13.2 | 27.5 | 1.048 |
| 72 | 47.2 | 15.1 | 32.1 | .979 |
| 73 | 59.6 | 17.6 | 42.0 | .995 |
| 74 | 69.0 | 19.4 | 49.6 | .997 |
| 75 | 78.4 | 22.0 | 56.4 | .942 |
| 76 | 91.8 | 26.0 | 65.8 | .868 |
| 77 | 109 | 30 | 79 | .877 |
| 78 | 118 | 34 | 84 | .779 |
| 79 | 141 | 41 | 100 | .770 |
| 80A | 10.8 | 4.1 | 6.7 | 2.017 |
| 80B | 10.9 | 4.2 | 6.7 | 2.157 |
| 106A | 12.0 | 7.8 | 4.2 | .420 |

(Continued)

TABLE XII (Concluded)

ADDED ENERGY DISSIPATION
DUNED SAND BED

| Run No. | Energy dissipation in tunnel | | Added energy dissipation | $\bar{f}_d - \bar{f}_s$ |
|---|---|---|---|---|
| | Duned $\left(\frac{\text{ft-lb}}{\text{cycle}}\right)$ | Smooth immobile $\left(\frac{\text{ft-lb}}{\text{cycle}}\right)$ | $\left(\frac{\text{ft-lb}}{\text{cycle}}\right)$ | |
| 111A | 19.9 | 12.3 | 7.6 | .331 |
| 112B | 36.4 | 20.0 | 16.4 | .308 |
| 113A | 5.41 | 3.42 | 1.99 | .817 |
| 114A | 2.71 | 2.02 | 0.69 | .736 |